DIRECTIONAL AMORPHOUS LACTOSE CRYSTALLIZATION

A thesis presented in partial fulfilment of the requirements for the degree
of Master of Engineering
In
Bioprocess Engineering

at Massey University, Manawatu,
New Zealand.

Nicholas Ibell-Pasley
2018

Abstract:

It was proposed that during industrial drying of lactose crystals a surface layer of amorphous lactose may be formed in a flash drier and then crystallized during fluid bed drying. This crystallization is hypothesized to occur in one of two directions depending on the conditions, inside-out resulting in a dry product, and outside-in trapping moisture. In the inside-out case the moisture is driven outside the product, in the outside in case this moisture would be contained by a surface layer of crystalline lactose. The trapped moisture from the outside-in case is proposed to slowly diffuse through the crystal layer during storage and cause handling problems, explaining observed differences between industrial products.

To investigate this scenario the crystallization of amorphous lactose was modelled, and crystallization trials were conducted to try and achieve inside-out and outside-in crystallization.

William-Landel-Ferry (WLF) and Arrhenius type kinetics were found to fit literature data for amorphous crystallization. Predictions made using these models showed that amorphous lactose crystallization under the high temperature conditions in a fluid bed dryer was possible.

A method for isolating the enthalpy change associated with crystallization of amorphous lactose from simultaneous thermal analysis data was developed. This method shows promise for observing the crystallization process, but it may not be suitable for amorphous lactose quantification.

Two methods were designed to achieve inside-out and outside-in crystallization of amorphous lactose. This required the temperature and water activity conditions to be precisely and independently controlled in lab trials. Simultaneous thermal analysis was used to monitor the crystallization of amorphous lactose samples under these conditions.

Following the simultaneous thermal analysis, the samples were monitored for moisture release. Both the inside-out and outside-in crystallized samples were observed to slowly release moisture, increasing the measured relative humidity above the expected equilibrium value. Afterwards the samples were analysed and found to still contain low levels of amorphous lactose. The source of the rise in relative humidity could not be definitively attributed to either trapped moisture or ongoing crystallization but would not be expected had crystallization not been induced.

Based on these findings it is recommended that a lactose crystal fluid bed drier is operated at conditions which would not allow for amorphous lactose crystallization. These conditions could be determined using the kinetic models fitted here.

Acknowledgements:

I am particularly grateful to my principal supervisor, Professor Tony Paterson, who gave me the opportunity to undertake this project, and for his steady guidance. He set me in the right direction many times and I feel very fortunate to have had him as my supervisor.

Thanks also to Dr. Georg Ripberger for his valuable insights and patiently training me to use the STA.

I would also like to thank Dr. Jim Q Chen who was always helpful when I ran into problems, and Sebastian Linnenkugel who provided valuable assistance and discussion.

I am grateful for all the technical advice and assistance provided by Ann-Marie Jackson, John Sykes, John Edwards, Steve Glasgow, and Ian Thomas. Thanks also to Professor Geoff Jameson and the institute of Fundamental Sciences for providing me the training and allowing access to conduct X-ray diffraction analysis.

Previous research, in particular that of Tony Paterson, John Bronlund, Georg Ripberger, Zachary Clark, and Paolo Dormeuil, was invaluable.

I would like to express my appreciation for the financial support provided by Hilmar Cheese and Volac.

Finally, thanks to my family and friends for their support and encouragement.

Table of Contents:

List of Figures:

List of Tables:

List of Equations:

1 Project Overview:

1.1 Lactose Drying Proposal

The drying process in the industrial production of lactose crystals is regarded as being a relatively simple operation and many dryers have been operated for years. Despite this, the effects of the process on the product are not well understood. Some industrial driers produce dried lactose crystal product that have a low water activity (<0.25) that stays low during subsequent storage and packaging. But other driers produce a product which starts at a low water activity of 0.2-0.25, which then climbs to 0.5-0.6 as the product is stored in a silo (A.Paterson, personal communication, August 7, 2017).

After crystallization, a crystal cake containing 3-12%wt concentrated lactose solution is fed into the first stage of drying, typically a flash drier (Paterson, 2017). The first stage of drying is rapid and has a low residence time by design; to prevent agglomeration of the particles. The rapid removal of moisture causes any remaining solution to become increasingly viscous; reducing the molecular freedom required for crystallization. For crystallization to occur in the solution the drying process must be relatively slow, the alternative is that drying continues producing an amorphous solid. Therefore, in successful drying operations it is likely that there is some amorphous lactose present during drying. This amorphous lactose is formed on the surface of the crystals and is estimated to make up 0.5-2%wt of the powder (Bronlund & Paterson, 2004; Durham, 2009; Paterson, 2017).

The presence of amorphous lactose is known to cause handling problems depending on the storage conditions (Carpin et al., 2017; Paterson, Brooks, Bronlund, & Foster, 2005). Crystallization of amorphous lactose can contribute to these handling problems and this occurs when the temperature exceeds the glass transition temperature (T_g) which depends on the moisture content (Dilworth, Buckton, Gaisford, & Ramos, 2004). For this reason attempts have been made to 'condition' amorphous lactose containing powders in fluid bed driers to obtain a fully crystalline product, with some success (O'Donnell, 1998; Yazdanpanah & Langrish, 2011).

The question that then arises is what then happens to the amorphous lactose layer during the existing drying process?

It has been proposed that if the amorphous layer has not dried sufficiently in the flash drier it is likely to crystallize during the fluid bed drying stage (Paterson, 2009). If the product is dried quickly to a low enough moisture content this should not occur, see Figure 1-1.

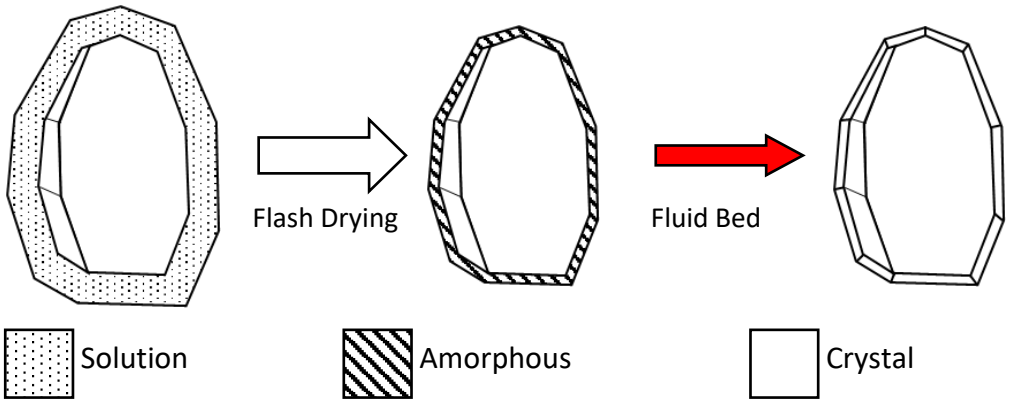

Figure 1-1: Theoretical solution phase changes during drying

During an amorphous lactose conditioning trial it was observed that following crystallization the product was difficult to dry; with the product continuing to display a water activity of approximately 0.5 over several hours (O'Donnell, 1998). Similarly Chavda (2009) recorded lower than expected changes in vapour pressure during crystallization. Together these results indicate that in some cases moisture may be trapped during the crystallization of amorphous lactose. This moisture would then be released gradually increasing the relative humidity of the product and potentially causing handling issues.

From these observations it is hypothesized that there are three cases for amorphous lactose formed during the drying process; no crystallization, outside-in crystallization, and inside-out crystallization, these cases are examined below.

1.1.1 No Crystallization:

The no crystallization case occurs when the amorphous lactose, once formed, continues to dry rapidly to a moisture content where the glass transition temperature remains above the drying temperatures and crystallization cannot occur. The resulting product would be dry, stable below 50% relative humidity (RH), and be unlikely to have handling issues if stored below 25%RH as recommended by Bronlund (1997) for powders with an amorphous content. Amorphous lactose has been detected in commercially produced α-lactose monohydrate powders (Bronlund & Paterson, 2004).

1.1.2 Outside-in Crystallization:

Outside-in crystallization is theorized to occur when the amorphous lactose layer formed is dried evenly. Due to the thinness of the amorphous layer it is possible for it to have quite an even moisture distribution. As the particle is heated through the fluid bed dryer a temperature gradient is formed in the amorphous layer. The higher temperature makes crystallization more favourable at or near the surface and it propagates from there. Due to the temperature of drying the crystalline product is anhydrous and crystallization releases moisture. The crystal layer slows external diffusion this moisture is driven inwards through the layer. The moisture reduces the glass transition temperature and crystallization continues through the entire layer. As the crystal formed is anhydrous this moisture is then trapped by the crystal layer from which it eventually diffuses causing an increase in humidity and handling issues unless it is dried. This scenario fits the observations of Chavda (2009) and O'Donnell (1998) as the product

would be hard to dry and during crystallization the amount of water expelled would be less than expected.

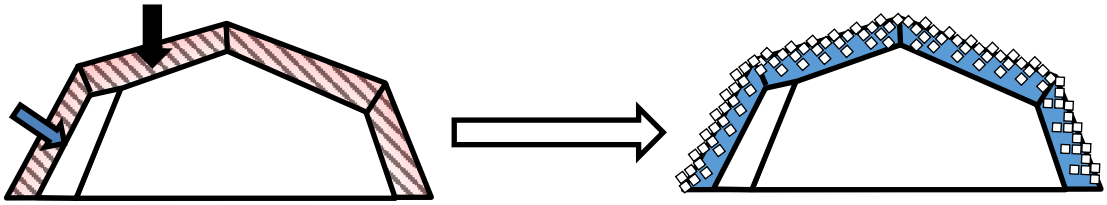

Figure 1-2: Outside-in crystallization; the black and blue arrows showing the direction of crystallization and moisture flow respectively, the red gradient indicates the temperature gradient in the amorphous layer, the diamonds show the grouping of the crystallized lactose and the blue background represents the trapped moisture.

1.1.3 Inside-out Crystallization:

Inside-out crystallization is theorized to occur when the crystals are dried rapidly in the first stage both forming amorphous lactose from the solution and then partially drying it. In this scenario the surface of the amorphous lactose is dry with an inward moisture gradient. The high T_g prevents crystallization at the surface, while it may still occur on the interior. Crystallization is induced near the amorphous-crystal interface as the temperature increases and moisture is driven outward from the anhydrous crystal formed. This moisture has a plasticising effect reducing the T_g in the amorphous lactose on the crystal front to the point that it too can crystallize. This process proceeds through the layer with the moisture expelled from the crystal resulting in a dry product. This product would be unlikely to have handling issues being non-hygroscopic and stable up to 80% relative humidity.

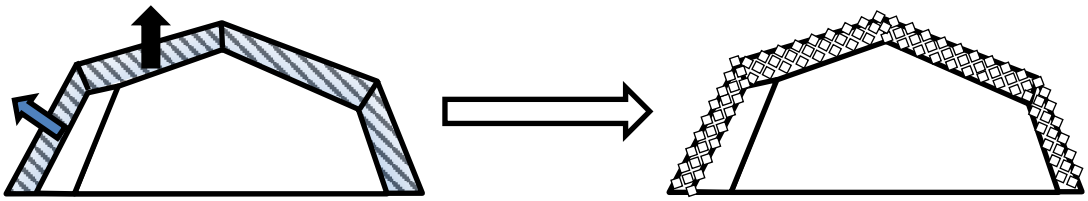

Figure 1-3: Inside-out crystallization; the black and blue arrows showing the direction of crystallization and moisture flow respectively, the blue gradient indicates the moisture gradient in the amorphous layer, the diamonds show the grouping of the crystallized lactose.

1.1.4 Areas to Investigate:

The aim of this study is to experimentally confirm or disprove the hypothesis of directional crystallization trapping moisture. To develop both the theory of how this occurs and an experimental method more information is required. It is important to review existing research on the crystallization kinetics of amorphous lactose and available techniques for recording the crystallization process. This kinetic information can then be applied to investigate the possibility of crystallization at the conditions present during fluid bed drying. As the amount of moisture and its location is a key component, the sorption behaviour of amorphous lactose must also be understood. The kinetics and sorption behaviour can then inform the experimental design using one of the techniques identified to observe the crystallization.

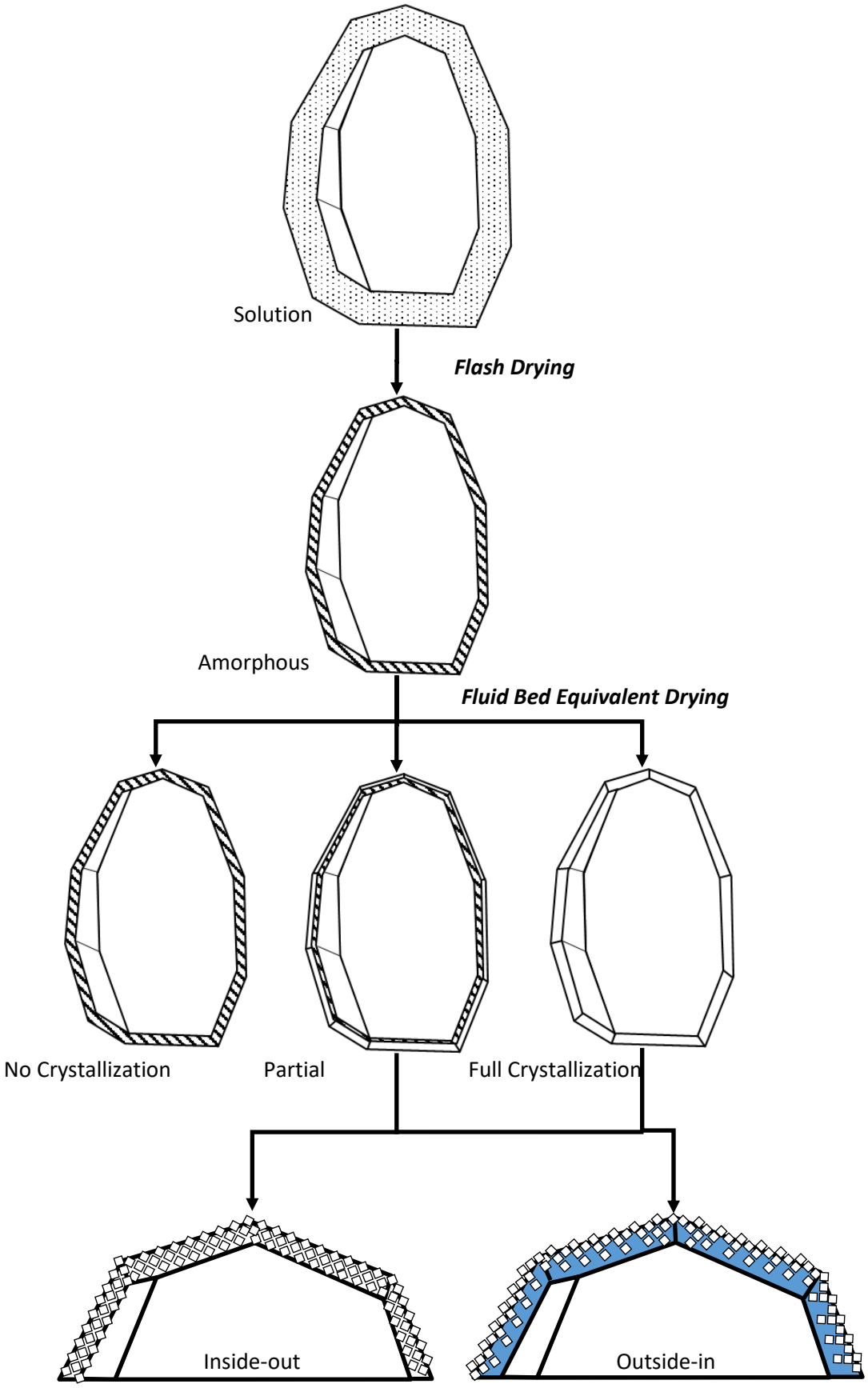

Figure 1-4: A flow-chart showing the theoretical changes and outcomes for the product during the drying process

2 Literature Review:

Lactose, sometimes referred to as “milk sugar”, is the chief carbohydrate of most mammalian milk. Lactose produced industrially is derived from the whey of cow’s milk. Cow’s milk contains between 4.4% and 5.2% lactose by weight, while human milk contains 7% on average (Gänzle, Haase, & Jelen, 2008).

Lactose is a disaccharide of glucose and galactose and has the molecular formula $C_{12}H_{22}O_{11}$. Two anomeric forms exist; α- and β-, differentiated by the orientation of the C-1 carbon of the glucose ring. Mutarotation between the α- and β- forms occurs spontaneously in solution with the two forms existing in equilibrium.

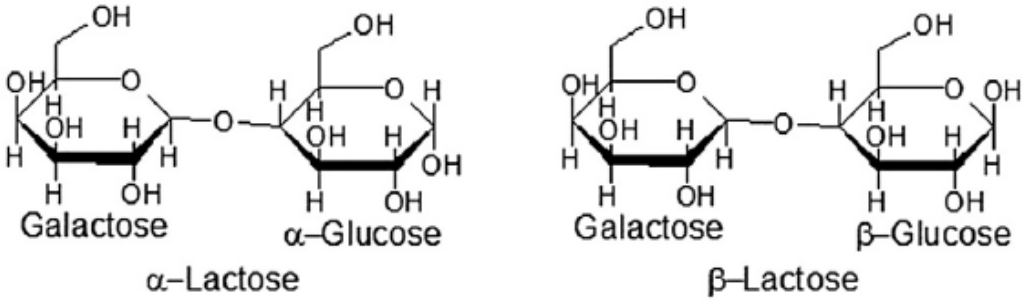

Figure 2-1: Molecular structures of α-(left) and β-(right) forms of lactose in chair conformation. Reproduced from (Ihli & Paterson, 2015)

The different anomers of lactose have very different physical properties shown in Table 2-1 below. The most important differences in properties of the anomers are in the solubility and specific optical rotation (Fox, 2009).

Table 2-1: Physical differences between the α- and β-Lactose anomers. Reproduced from (Kellam, 2005-2017).

Anomer:	α-Lactose:	β-Lactose:	Units:
Molecular Weight:	360.3*	342.3	Da
Melting Point:	202	252	°C
Density:	1.545	1.59	g/cm^3
Specific Optical Rotation:	+91.1	+33.5	α^{20}_{589}
Heat of Solution:	-50.24	-9.62	J/g
Solubility in Water at 20°C:	7.4	50.00	g/100ml

*for the monohydrate form, which is the most common α-lactose crystalline form

Lactose is a versatile substance with many uses in the production of foods and pharmaceuticals, Figure 2-2 shows a breakdown of lactose usage in Europe by Affertsholt-Allen (2007).

Food industry usage can be attributed to its low sweetness when compared with sucrose; important in confectionary, its ability to undergo the Maillard reaction, and energy content which is the key in infant formula where it is used to increase the energy value (Paterson, 2009).

In the pharmaceutical industry lactose is used as the main carrier or excipient for drugs due to its low sweetness, safety, availability in highly refined forms, and good tableting properties (Paterson, 2009).

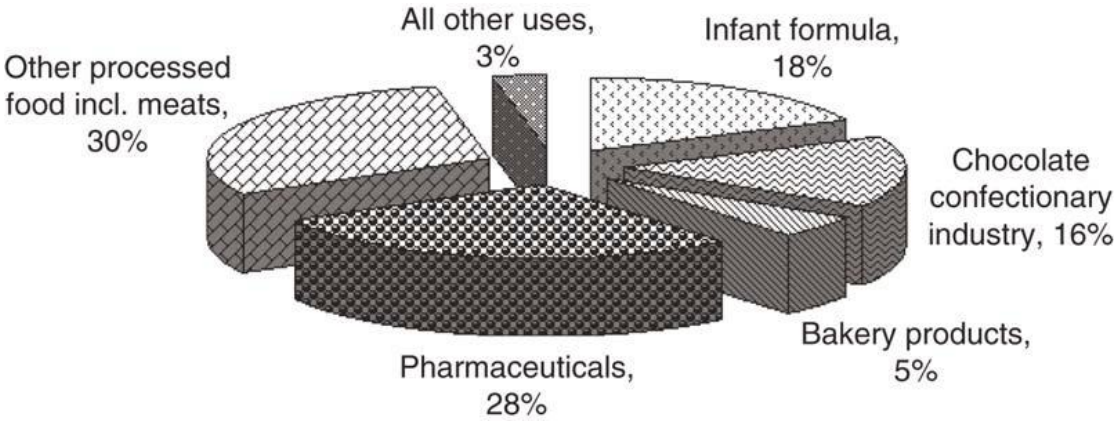

Figure 2-2: Market structure for lactose in 2005. Reproduced from (Paterson, 2009).

Lactose can exist in three different solid forms; crystalline, amorphous, and partially amorphous. The amorphous and partially amorphous forms will be explained in greater detail in section 2.1. Some mechanisms of transitions between different phases are shown in Figure 2-3.

Crystalline Lactose:
Crystalline systems are characterised by a highly ordered, repeating, three-dimensional arrangement of the constituent ions or molecules. They are one of the two basic supra-molecular structures (Palzer, 2010). The different known forms of lactose crystal are described below:

<u>α-Lactose Monohydrate:</u>

α-lactose monohydrate consists of lactose molecules each associated with a single water molecule. The standard water content of α-lactose monohydrate is therefore approximately 5% which may be removed by drying at 130°C (Pharma, 2017b).

It is commonly produced by crystallization from a super saturated solution; below 93.5°C α-lactose monohydrate is the sole product, with the shape of the crystal depending on the conditions of crystallization. Typical α-lactose monohydrate crystal shapes include “tomahawks” and prisms (Kellam, 2005-2017; Pharma, 2017b).

The isotherm produced by Bronlund (1997) showed very little moisture is adsorbed by α-lactose monohydrate below 0.85 water activity, and that no significant temperature dependency was observed between 12-37°C. Above 0.85 water activity rises rapidly and is attributed to capillary condensation.

α-Lactose Anhydrous:

Anhydrous α-lactose consists of α-lactose molecules with no associated water, formed after dehydration of α-lactose monohydrate by physical or chemical methods. Anhydrous α-lactose can exist in a stable form or a hygroscopic unstable form (Hourigan, Lifran, Vu, Listiohadi, & Sleigh, 2012).

β-Lactose Anhydrous:

β-lactose crystals are produced by crystallization from a super saturated solution at temperatures above 93.5°C with pure crystals having a kite-like shape. Free of bound moisture crystalline β-lactose is anhydrous. Industrially β-lactose is produced by roller drying a concentrated lactose solution, this product has a β-lactose content of approximately 80% with the balance being α-lactose (Kellam, 2005-2017; Pharma, 2017b).

An isotherm for β-lactose produced by Bronlund (1997) showed β-lactose absorbs very little moisture below 0.6 water activity. Beyond 0.6 water activity the increased mass gain was attributed to conversion to α-lactose monohydrate.

Compound α:β Anhydrous:

Compound crystals with α and β lactose in different molecular ratios (including α_1:β_1, α_5:β_3 and α_4:β_1) have been reported on the basis of x-ray diffraction results and nuclear magnetic resonance (Drapier-Beche, Fanni, Parmentier, & Vilasi, 1997; Earl & Parrish, 1983; Simpson, Parrish, & Nelson, 1982). These compound crystals have been proposed to be the result of isomorphous replacement of α-lactose in the anhydrous form by β-lactose (Simpson et al., 1982). Alongside the methods of production described in Figure 2-3, α:β 1:1 compound crystals have been produced from solution using super-heated steam (Clarke, 2002; Dhanjee & Paterson, 2000; Ecroyd, 2003). However compound crystals have not been recognised as distinct forms in all studies (Kirk, Dann, & Blatchford, 2007).

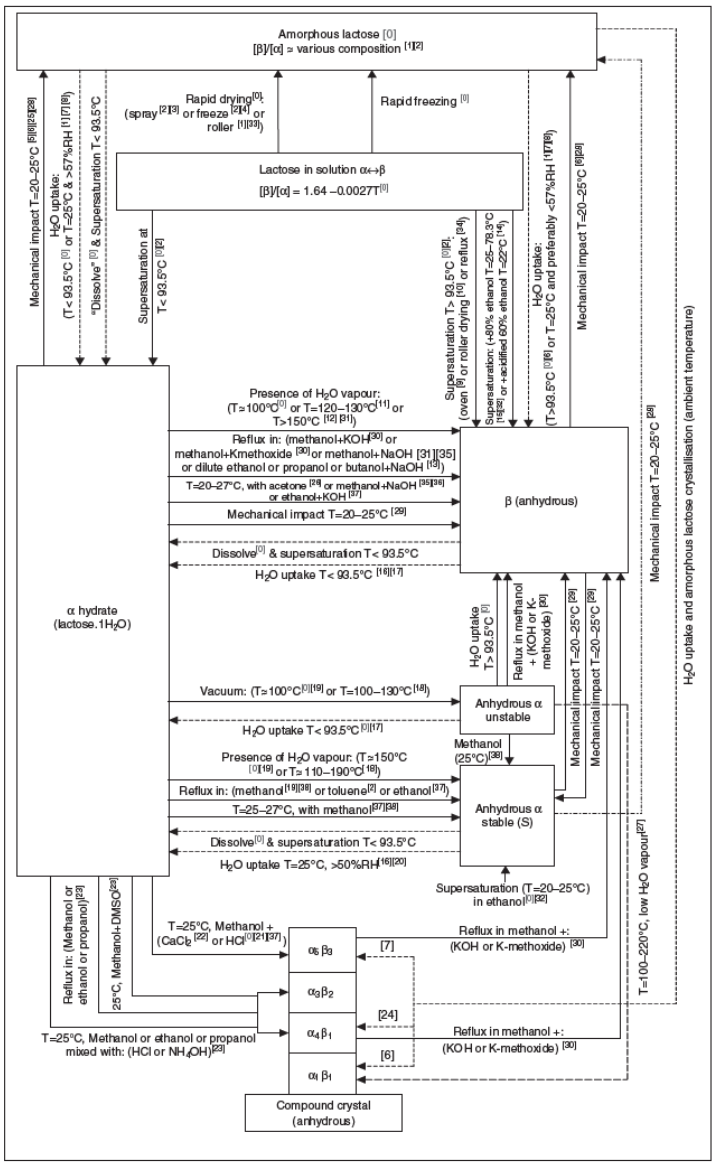

Citation	Reference
0	Walstra et al. (1999)—original data
1	Listiohadi et al. (2005b)
2	Holsinger (1988)
3	Sebhatu et al. (1994)
4	Kedward et al. (2000)
5	Newell et al. (2001a); Newell et al. (2001b)
6	Lerk et al. (1984)
7	Bushill et al. (1965)
8	Wursch et al. (1984)
9	Hudson (1908)
10	Bell (1930)
11	Sharp (1934)
12	Listiohadi (2000); Asano et al. (1978); Van Leverink (1981)
13	Olano (1978)
14	Singh and Shah (1992)
15	Lifran et al. (2001)
16	Listiohadi et al. (2008)
17	Cal et al. (1996)
18	Sharp (1943)
19	Buma and Wiegers (1967)

Citation	Reference
20	Figura and Epple (1995)
21	Hockett and Hudson (1931)
22	Domovs and Freund (1961)
23	Olano et al. (1977)
24	Jouppila et al. (1997)
25	Listiohadi et al. (2005c)
26	Garnier et al. (2002)
27	Kussendrager and Andreae (1986)
28	Otsuka et al. (1993)
29	Otsuka et al. (1991)
30	Parrish et al. (1980)
31	Olano et al. (1983)
32	Madj and Nickerson (1976)
33	Angberg et al. (1991)
34	Itoh et al. (1978)
35	Olano and Rios (1978)
36	Drapier-Beche et al. (1997)
37	Parrish and Brown (1982)
38	Lim and Nickerson (1973)

Figure 2-3: Lactose conversion diagram and citations. Reproduced from (Hourigan et al., 2012).

Amorphous Lactose:

Amorphous lactose lacks the organised molecular structure of crystalline lactose (Palzer, 2010). Pure samples of amorphous lactose are typically produced by one of two methods; spray drying and freeze drying of dissolved lactose solutions, the two paths of production are shown on Figure 2-4, and are discussed below. During spray drying water is removed from the solution quickly with the viscosity increasing without crystallization occurring, creating an amorphous structure (Pharma, 2017a). During freeze drying the disorder present in the solution is preserved by freezing it, preventing crystallization as water is removed by sublimation creating a dry glass (Pharma, 2017a). The two methods can produce a pure amorphous product, although the physical properties differ with freeze dried amorphous lactose having a higher porosity and diffusivity of water (Clark, 2012; Ripberger, 2010).

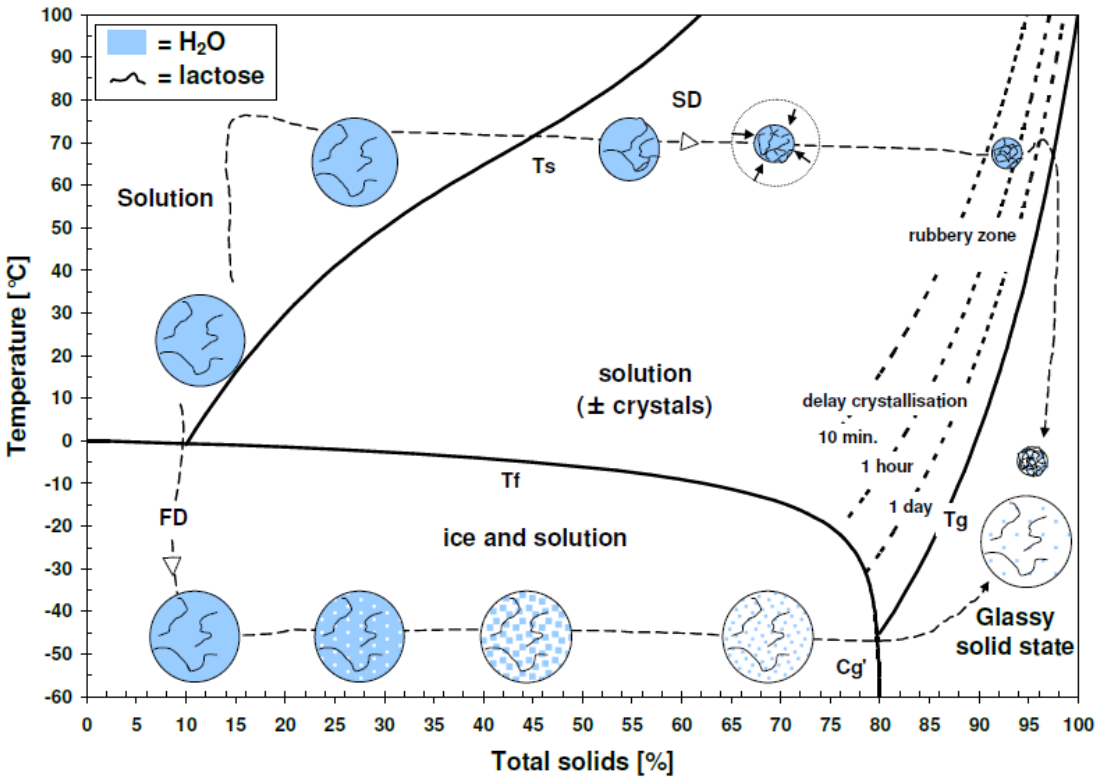

Figure 2-4: Phase diagram of lactose in water. Tf: freezing temperature, Tg: glass transition temperature, Ts: lactose solubility the two dotted lines show the path for amorphous lactose production by spray drying and freeze drying. Reproduced from (Pharma, 2017).

Partially Amorphous Lactose:

Partially amorphous lactose is formed during spray/freeze drying of a lactose crystal slurry or solution, drying of the centrifuged lactose crystal cake, or milling of spray dried or crystalline lactose. During spray drying water is rapidly removed from the crystal slurry which can cause the formation of amorphous regions as the viscosity increases rapidly, preventing complete crystallization from occurring. The amorphous portion exists as a matrix around crystalline fragments with the majority located in the centre (Darcy & Buckton, 1998a).

Partially amorphous lactose may also be formed as the lactose crystal cake is dried. The α-lactose monohydrate crystal cake from a centrifuge contains a small amount of lactose in solution (less than 12%wt of saturated lactose solution in the cake). This can form a thin layer, about 0.5-2%wt, of amorphous lactose on the crystal surface when the water is flashed off in a flash or spray dryer (Paterson, 2017).

Milling of crystalline lactose can also produce a layer of amorphous lactose on the surface of the particle (Pazesh, Gråsjö, Berggren, & Alderborn, 2017). This is thought to occur through two mechanisms; a vitrification or melting and solidifying process, and the creation of a critical density of crystal defects (Newman & Zografi, 2014). During ball milling it has been hypothesized that amorphisation occurs by vitrification during high shear stress conditions (Pazesh et al., 2017).

The aim of this project was to test the hypothesis of directional crystallization within an amorphous lactose layer. To achieve this, detailed information on the crystallization induction

conditions, crystallization kinetics, and moisture sorption properties of amorphous lactose are required.

2.1 Amorphous Lactose:

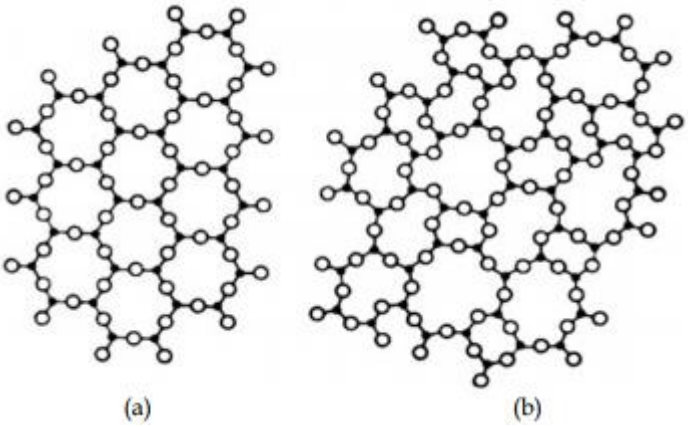

Figure 2-5: Schematic two-dimensional illustration of the atomic arrangement in (a) crystal and (b) glass. Reproduced from (Carter & Norton, 2007).

Amorphous systems are considered one of two basic supra-molecular structures, the other being crystalline systems (Palzer, 2010). Amorphous systems include liquids and gasses with amorphous solids considered metastable non-crystalline supercooled liquids (Roos, 2012). In an amorphous state of a substance is characterised by a disordered molecular structure, where no exact position can be defined for the molecules at a given time. Glasses are amorphous solids with a viscosity greater than 10^{12}Pa.s, enabling it to support its own weight. They exhibit glass transition (Downton, Flores-Luna, & King, 1982; Jones, 1956; Palzer, 2010; Roos, 2012). Figure 2-5 illustrates the difference in molecular arrangement between a glass and crystalline solid.

Glass Transition

When heated a glassy amorphous material transitions, or "collapses" from a "glassy" solid state into a "rubbery" viscous state, with a significant decrease in its viscosity. In the rubbery state molecular arrangements are relaxed; allowing greater molecular mobility and subsequently flow, collapse, and crystallization of the material (Downton et al., 1982; Palzer, 2010; Roos, 2012).

Amorphous lactose is an amorphous glass with a glass transition temperature below 25°C at 48% RH (Chidavaenzi, Buckton, Koosha, & Pathak, 1997) and a viscosity of $1.1*10^{14}$ Pa.s at the glass transition point (Paterson, Ripberger, & Bridges, 2015).Glass transition occurs over a temperature range after which the change in free volume with temperature increases as shown in Figure 2-7. The glass transitions temperature (T_g) has differing definitions including the temperature of the onset of glass transition, or the midpoint of the transition. Furthermore the derived value of T_g varies greatly with the method of analysis (Palzer, 2010).

Procedures for investigating glass transition include Differential Scanning Calorimetry, Dynamic Mechanical Thermal Analysis, and Nuclear Magnetic Resonance Spectroscopy (O'Donnell, 1998; Palzer, 2010). Water is well documented as having a plasticising effect on amorphous

lactose increasing the molecular mobility and reducing the T_g (Levine & Slade, 1986; Roos & Karel, 1991). The Gordon-Taylor equation (2-3), originally formulated for polymer blends, has been used to predict the glass transition temperature of amorphous sugars, including lactose, from the moisture content (Bronlund, 1997; Gordon & Taylor, 1952; Jouppila & Roos, 1994).

$$T_g = \frac{w_1 T_{g1} + k w_2 T_{g2}}{w_1 + k w_2} \quad (2\text{-}1)$$

- T_{g1} = Glass transition temperature of amorphous lactose (°C)
- T_{g2} = Glass transition temperature of water (°C)
- w_1 = Mass fraction of amorphous lactose (g/g total)
- w_2 = Mass fraction of water (g/g total)
- k = Constant

Table 2-2 provides constants fitted to the Gordon-Taylor equation for amorphous lactose by Brooks (2000) for data adjusted to include the effect of bound moisture and by Fan and Roos (2015) including values predicted for mixtures with whey protein isolate. Figure 2-6 shows that when the values predicted by Fan and Roos (2015) are also adjusted to include bound moisture they fit well with the Brooks predictions.

Table 2-2: Gordon-Taylor Equation Literature Parameters (Brooks, 2000; Fan & Roos, 2015)

Parameter:	Brooks (2000)	Fan and Roos (2015)
Amorphous lactose preparation:	Spray-dried and Freeze-dried	Freeze-dried
T_{g1}(Amorphous Lactose)	115°C	105°C
T_{g2}(Water)	-135°C	-135°C
k	6.9	8.1

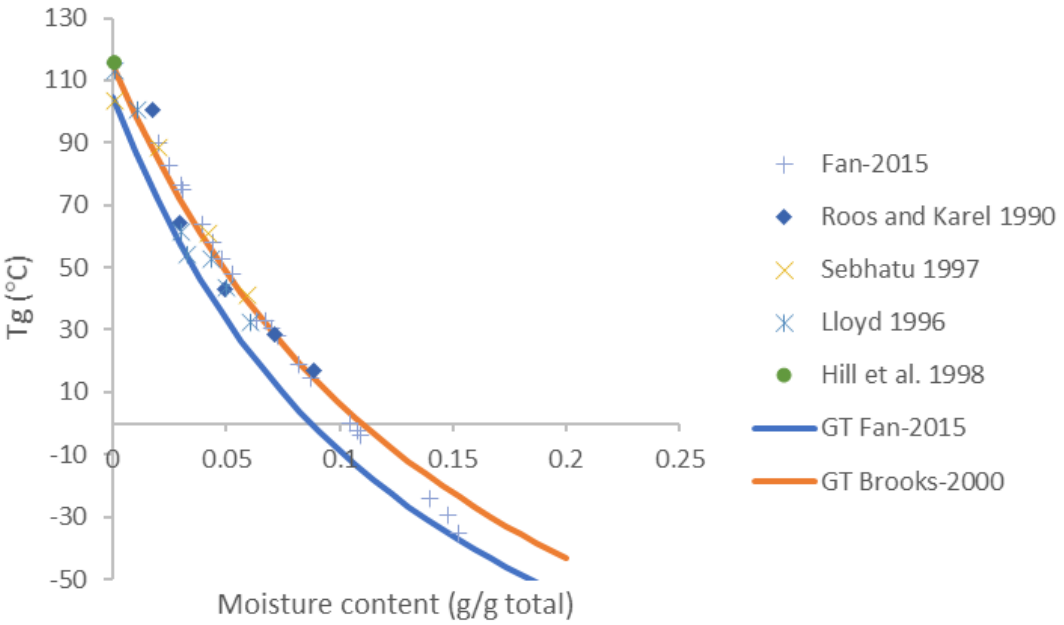

Figure 2-6: Plot of Gordon-Taylor equations of Fan and Roos (2015) and Brooks (2000) with literature data adjusted for bound moisture (Fan & Roos, 2015; J. Lloyd, Dong Chen, & B. Hargreaves, 2003; Roos & Karel, 1990; Sebhatu, Ahlneck, & Alderborn, 1997)

For calculating the T_g of amorphous lactose from a measured water activity (a_w) at a relative humidity below 57.5% equation (2-2) was fitted by Brooks (2000). This equation provided a better fit to literature data than the Gordon-Taylor equation combined with the isotherm (Brooks, 2000; Gordon & Taylor, 1952). However this equation does not have a theoretical basis.

$$T_g = -530.66\, a_w^3 + 652.06\, a_w^2 - 366.33\, a_w + 99.458 \qquad (2\text{-}2)$$

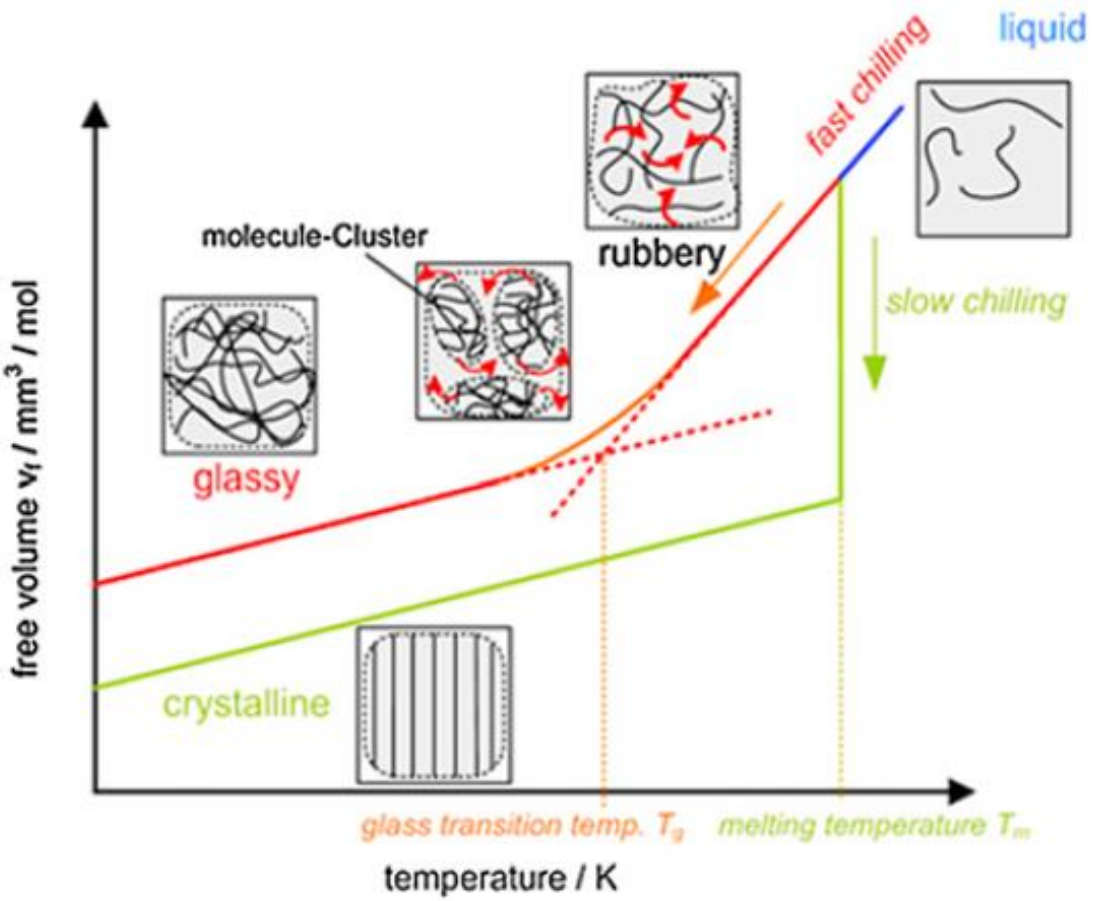

Figure 2-7: Free specific volume in crystalline and amorphous structures depending on temperature. Reproduced from (Palzer, 2010).

2.1.1 Moisture Sorption Isotherms of Amorphous Lactose

The Guggenheim, Anderson, de Boar (GAB) isotherm model, equation (2-3), has been shown to accurately predict the moisture content of amorphous lactose up to a water activity of 0.6, beyond which crystallization occurs at ambient temperatures (Bronlund, 1997; Bronlund & Paterson, 2004; Jouppila & Roos, 1994).

$$\frac{w'}{w'_m} = C\,K\frac{a_w}{(1-K\,a_w)(1+(C-1)K\,a_w)} \tag{2-3}$$

Where:

- w'= moisture content on a dry basis (g/g_{dry}),
- w'_m = the monolayer moisture content (g/g_{dry})
- C and K are constants.

Table 2-3: A Selection of GAB Isotherm Parameters (Bronlund, 1997; Brooks, 2000; Jouppila & Roos, 1994)

Parameter:	Bronlund (1997)	Jouppila and Roos (1994)	Brooks (2000)
Temperature:	15-40°C	24°C	15-40°C
Amorphous lactose preparation:	Spray dried and Freeze dried	Freeze dried	Spray dried and Freeze dried
w_m' (g H_2O/g dry lactose)	0.0488	0.0491	0.0627
K	1.16	1.18	1.01
C	3.23	4.33	2.81

The equilibrium moisture content of amorphous lactose was found to not be sensitive to temperature in the range between 15°C and 40°C Bronlund (1997).

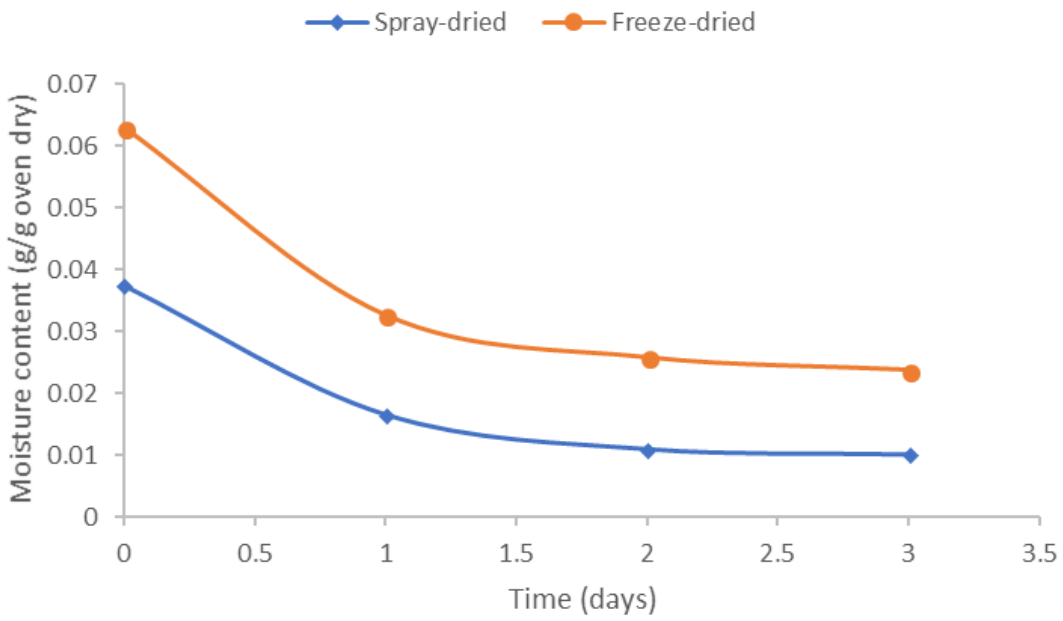

Figure 2-8: Plot of moisture content vs desiccation time, data from (Brooks, 2000).

Brooks (2000) investigated the residual moisture content of amorphous lactose during desiccation above phosphorous pentoxide at room temperature. After three weeks, as shown in Figure 2-8, a 0.01 g/g dry bound moisture remained in the spray-dried sample as determined by oven drying the sample at 120°C. The higher moisture content for the freeze-dried sample was attributed to contamination with α-lactose monohydrate. This bound moisture was used to correct literature data by Foster (2002) and produce an isotherm accounting for it, as shown in Figure 2-9. The bound moisture with Karl-Fischer titration determined moisture contents of J. Lloyd et al. (2003) and Hargreaves (1995) were not corrected.

Using the values for bound moisture and the isotherm parameters of Table 2-3, Ripberger (2010) showed that the sorption behaviour for spray and freeze dried lactose is very similar.

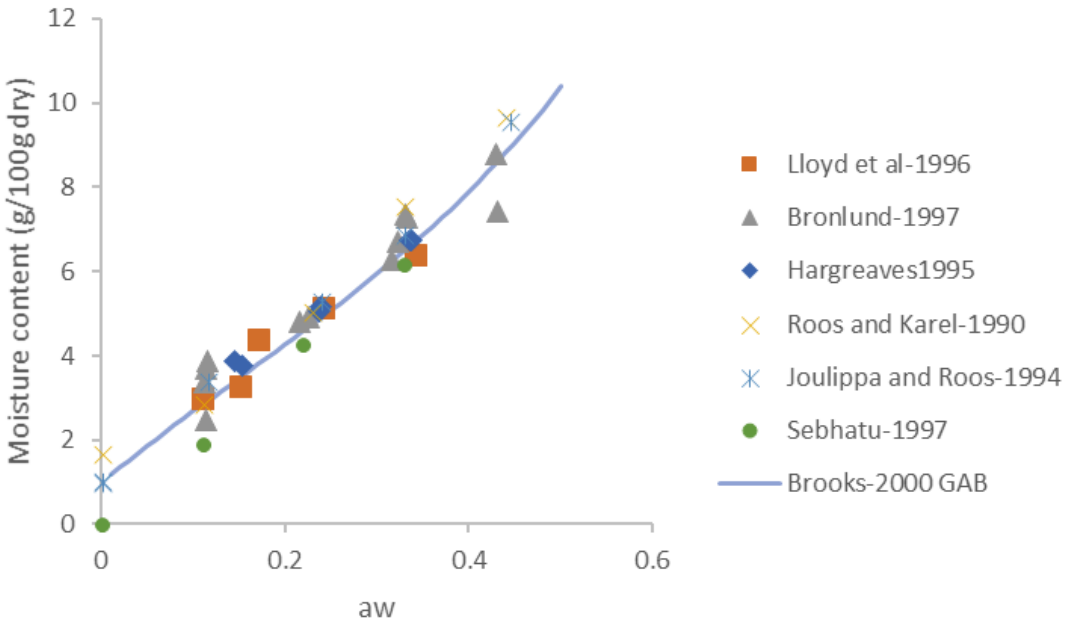

Figure 2-9: Amorphous lactose moisture sorption isotherm. Reproduced from (Foster, 2002).

A more recent study by Fan and Roos (2015) determined sorption isotherms (Figure 2-10) for freeze-dried amorphous lactose over saturated salt solutions at 25°C, 35°C, and 45°C. The dry mass was determined by desiccation above phosphorous pentoxide, so the results do not consider bound moisture. These isotherms were fitted with GAB models and extrapolated beyond the water activity at which crystallization occurs by using results for amorphous lactose and whey protein isolate mixtures. Contrary to the results of Bronlund and Paterson (2004) the isotherms show a significant decrease in the equilibrium moisture content with increasing temperature.

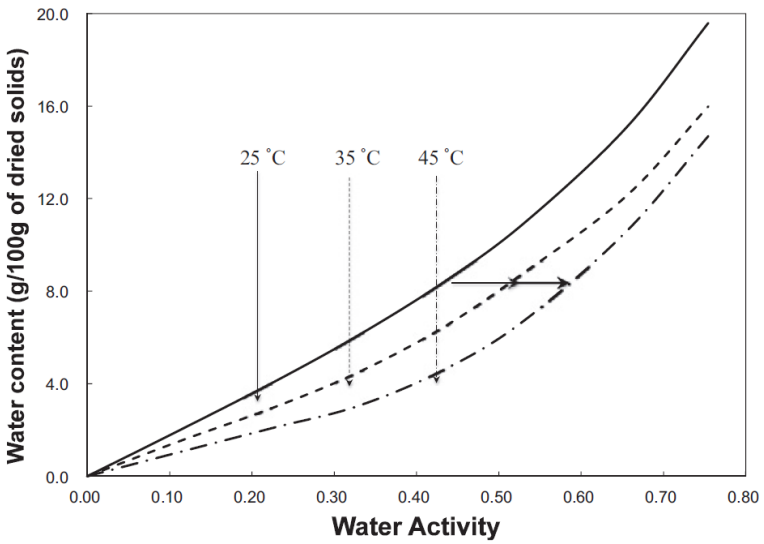

Figure 2-10: GAB sorption isotherms for non-crystalline lactose. Reproduced from (Fan & Roos, 2015).

Net Isosteric Heat of Sorption

The net isosteric heat of sorption is the difference between the specific latent heat of condensation or vaporization and the total observed change in enthalpy for a sorption process. The net isosteric heat of sorption depends strongly on the moisture content of a material and can be calculated from isotherms obtained at different temperatures using the Clausius Clapeyron equation (Hardy, Scher, & Banon, 2002; Rückold, Isengard, Hanss, & Grobecker, 2003; Tadapaneni, Yang, Carter, & Tang, 2017).

The properties of the amorphous lactose, especially the relationship between the sorption and glass transition behaviour, are important for identifying when crystallization may occur. To observe crystallization itself a method for measuring the amorphous lactose fraction over time is required.

2.1.2 Quantification Methods for Amorphous Lactose

A number of different methods have been applied to quantify the amount of amorphous lactose in a sample. These methods are detailed below and summarized in Table 2-5.

X-ray powder diffraction (XRPD)

X-ray powder diffraction (XRPD) relies on the difference in diffraction of x-rays between amorphous and crystalline material. The crystalline component produces sharp diffraction peaks which can be distinguished from the smoother baseline produced by the amorphous fraction. The diffraction angle of the peaks depends on the type of crystal (Barham & Hodnett, 2005; Haque & Roos, 2005; Nijdam, Ibach, Eichhorn, & Kind, 2007).

Barham and Hodnett (2005) as well as Nijdam et al. (2007) used standards of potassium chloride mixed in a known quantity with samples to correlate the increasing intensity of characteristic crystalline peaks with the proportion of the crystal. In this way they could track the crystallization of the sample over time. Table 2-4 collects some of the reported characteristic diffraction angles reported for Cu Kα radiation.

These peaks increase in intensity with crystallinity and can be used to estimate the amorphous content, with predictions improved by whole-pattern fitting. Whole pattern fitting requires that the crystalline component must be in the same polymorph as the reference (Chen, Bates, & Morris, 2001; Fix & Steffens, 2004; Lehto et al., 2006).

Table 2-4: Crystal Forms and Characteristic Peaks from Literature

Crystal Form:	Diffraction Angle (2θ):	Reference:
α-lactose Monohydrate	12.5°, 16.4° 20.0°	(Haque & Roos, 2005)
	20.1°	(K. Jouppila, J. Kansikas, & Y.H. Roos, 1997b)
	19.1°, 19.6°, 19.9°	(Barham & Hodnett, 2005)
Anhydrous β-lactose	10.5°, 20.1°	(Haque & Roos, 2005)
	21.0°	(Buma & Wiegers, 1967)
Anhydrous α:β 5:3	19.1°, 20.1°	(Simpson et al., 1982)
	20.0°	(Jouppila et al., 1997b)
	18.3°, 22.1°	(Barham & Hodnett, 2005)
Anhydrous α:β 4:1	19.5°	(Simpson et al., 1982)

Infra-Red Spectroscopy (IR)

IR spectroscopy relies on differences in the adsorption spectra of amorphous and crystalline samples. The quantity of a phase producing vibrational bands is proportional to their intensity. Calibration can be carried out using samples of a known amorphous content and correlating this content with wavelengths of the infra-red spectra. Accuracy of within ±1% can be obtained with this method (Buckton, Yonemochi, Hammond, & Moffat, 1998; Hogan & Buckton, 2001). Nieuwmeyer et al. (2007) collected near infra-red spectra and was able to correlate them by principle component analysis to predict the amorphous content of lactose granules during fluid bed drying.

Table 2-5 Amorphous lactose detection and quantification methods. Updated from Clark (2012).

Method:	XRPD	IR	Raman	TPS	ICG	DSC	TGA/STA	SS-DSC	Hyper-DSC	IMC	DVS	Isotherm	NMR	SC
Detection Limit:	0.27%-10%	<1%	1%	~1%[1]	<1%,~5%[3]	1-20%	1%	<1%	<1.5%	<0.5%	0.3-0.7%	0.1%	<0.5%	1%
Quantification Limit:			0.2-0.25%	~15%[2]	n/a[3]									
Analysis Time:	<1h	0.5-10	<0.5	~90s	5-8h	<1h	<1h	~1h	<0.5h	0.5-4h	1-5h	>3h	0.5-10h	<1h
Destructive:	Yes	No	No	No	Yes	Yes	Yes	Yes	Yes	Yes	Yes	No	No	Yes
Sample weight:	200-400mg	500-700	2000	400mg	200-300mg	3.5-4mg	5-15mg	1.6mg	1-3mg	20-300mg	50-150mg	800-1200mg	500-700mg	200-400mg
Reproducibility:	Good	Good	Good	Good (similar to IMC)	Good	Variable	Good	Good	Good	Good	Good	Good	Good	Good
Structural information provided:	Yes	Possible	No	Yes	Yes	No	No	No	No	No	No	No	Yes	No
Tracking crystallization:	Yes			Yes		Yes				Yes	Yes			No
Reference:	(Chen et al., 2001; Fix & Steffens, 2004; Lehto et al., 2006; Saleki-Gerhardt, Ahlneck, & Zografi, 1994)	(Fix & Steffens, 2004; Hogan & Buckton, 2001)	(Lehto et al., 2006; Pazesh, Lazorova, Berggren, Alderborn, & Gråsjö, 2016)	(Smith, Hussain, Bukhari, & Ermolina, 2015a, 2015b; Strachan et al., 2004; Strachan et al., 2005)	(Brum & Burnett, 2011; Newell, Buckton, Butler, Thielmann, & Williams, 2001)	(Fix & Steffens, 2004)	(Listiohadi, Hourigan, Sleigh, & Steele, 2009; Smith, Mannheim, & Gilbert, 1981)	(Lehto et al., 2006)	(Saunders, Podluii, Shergill, Buckton, & Royall, 2004)	(Dilworth et al., 2004; Gustafsson, Lennholm, Iversen, & Nyström, 1998; Lehto et al., 2006)	(Buckton & Darcy, 1995; Burnett, Malde, & Williams, 2009; Clark, 2012; Vollenbroek, Hebbink, Ziffels, & Steckel, 2010)	(Bronlund, 1997; Burnett et al., 2009; Vollenbroek et al., 2010)	(Gustafsson et al., 1998)	(Harjunen et al., 2004)

[1]Applied to other substances, [2]Experimental level quantified, not limit, [3]Quantification/detection of the surface amorphicity not in bulk

Raman Spectroscopy

Rama spectroscopy relies on Raman scattering of monochromatic light, typically from a laser, as the light interacts with excitations in the system being studied. Amorphous samples show reduced peak intensity and definition of the spectra. Calibration can be carried out using samples of a known amorphous content/crystal content and correlating this content with the intensity, by area/amplitude, of characteristic bands of the Raman spectra (Kirk et al., 2007; Niemelä et al., 2005; Pazesh et al., 2016).

Tetrahertz Pulsed Spectroscopy (TPS)

In terahertz pulsed spectroscopy (TPS) pulses are produced in the femtosecond time scale, between 0.1 and 3 THz. This provides information on crystal lattice and hydrogen bonding vibrations, which occur in this region. The intensity of the specific absorption peaks can be used to identify and quantify the crystallinity in a mixed phase system (Strachan et al., 2004; Strachan et al., 2005). Terahertz time domain spectroscopy has been applied to partially amorphous samples of milled α-lactose monohydrate and anhydrous β-lactose (Smith et al., 2015a, 2015b). The quantification of the crystallinity of the α-lactose monohydrate samples producing similar results to DSC (Smith et al., 2015a). Quantification of β-lactose crystallinity by TPS was considered less reliable than DSC (Smith et al., 2015b).

Solution Calorimetry (SC)

Solution calorimetry has been applied to partially amorphous samples measuring the enthalpy of solution in water. Solution calorimetry is isothermal microcalorimetry with the solution temperature maintained and the power required to do this recorded as the sample dissolves. From this data the enthalpy of solution is calculated. A strong correlation was found between a decreasing enthalpy of solution and increasing amorphous content. A similar correlation was found with the change in the enthalpy of solution when the samples of amorphous lactose were added to a saturated lactose solution (Harjunen et al., 2004).

Inverse Gas Chromatography (IGC)

Inverse gas chromatography (ICG) uses a carrier gas and probe vapours to investigate surface energies of materials. There is a difference in surface energy between crystalline and amorphous forms of a solid and ICG has been applied to investigate surface changes of amorphous lactose during collapse and crystallization (Newell et al., 2001), as well as to quantify the amorphous content of the surface (Newell et al., 2001). This method is not suitable for quantification of the bulk crystallinity but gives valuable information on the amorphous distribution at the surface.

Thermogravimetric analysis (TGA/STA)

Thermal gravimetric analysis is the measurement of the mass of a sample as the temperature changes. When combined with single differential calorimetry it is referred to as simultaneous thermal analysis providing the mass and energy changes over time. Thermogravimetric analysis was used to measure the amorphous content by the water of crystallinity mass loss in milled α-lactose samples by (Smith et al., 2015a). Simultaneous thermal analysis was used by Listiohadi et al. (2009) with the advantage of determining the surface water, water of crystallization, and amorphous lactose content simultaneously.

Differential Scanning Calorimetry (DSC)

Crystallization of lactose involves an exothermic enthalpy change (see section 2.3.4) and energy is released proportional to the mass crystallized. In DSC the sample is heated, above the glass transition temperature and crystallization is induced and the exothermic response is measured. The enthalpy change for the sample can be correlated to the amorphous content. DSC can also be used to record the change of the specific heat capacity which requires modulated temperature DSC and high-speed DSC (Fix & Steffens, 2004; Lehto et al., 2006; Smith et al., 2015b).

Isothermal Microcalorimetry (IMC)

Isothermal microcalorimetry is similar to differential scanning calorimetry but instead of inducing crystallization by changing the temperature it is induced by adsorption. The sample is sealed at a humidity condition reducing the glass transition temperature to below the experimental temperature which is maintained. The energy flow is measured by the power required to maintain this temperature. A thermal activity monitor can be used to make these measurements. The heat flow for crystallization is integrated and the enthalpy change for the sample is proportional to the amorphicity if the same conditions are used (Gustafsson et al., 1998; Lehto et al., 2006).

Dynamic Vapor Sorption (DVS)

Dynamic vapor sorption is an example of a gravimetric detection/quantification method. Similarly, with the isotherm methods these rely on the higher equilibrium moisture content of amorphous lactose when compared with the crystalline forms. Crystallization can be induced by exposing an amorphous lactose containing sample to high humidity. This crystallization process can subsequently be tracked by the characteristic mass loss from the adsorption peak as it proceeds to an equilibrium value. The amount of mass gained by the sample prior to crystallization as well as the amount released can be correlated to the amorphous content (Burnett, Thielmann, Sokoloski, & Brum, 2006; Clark, 2012; Lehto et al., 2006).

Nuclear Magnetic Resonance (NMR)

Solid-state nuclear magnetic resonance is a spectroscopic technique where the sample is placed in a magnetic field, excited by radio waves, and the resulting NMR signal recorded. Peaks in NMR spectra can be associated with crystalline forms of lactose and the absence of defined peaks in these regions can indicate amorphicity. Spectra collected for predefined mixtures of crystalline and amorphous lactose can be used to create a correlation for predicting the amorphous content in an unknown sample (Gustafsson et al., 1998) (Earl & Parrish, 1983).

Isotherm Method

This method involves first equilibrating a partially amorphous sample at a known relative humidity then measuring its free moisture content. The amorphous content can then be calculated from the equilibrium moisture contents of the crystal and amorphous components. The sample can also be equilibrated over a range of relative humidities and fitted with the isotherms combined additively. This approach relies on the type of crystal being known, or the crystal components having very similar equilibrium moisture contents (Bronlund, 1997). To fit results for the sample the BET isotherm model can also be used, especially for lower

amorphous contents, with the monolayer moisture constant correlating with amorphicity (Vollenbroek et al., 2010).

Of the methods available thermogravimetric analysis showed promise for tracking crystallization in real time by both mass and energy changes. Dynamic vapour sorption and isothermal microcalorimetry were used in this work for quantifying low levels of amorphous lactose in samples as both have a lower detection limit than TGA and conventional DSC. For identification of the crystalline forms present in a sample, X-ray powder diffraction was used due to the accessibility and wealth of reference patterns.

2.1.3 Handling Properties of Amorphous Lactose

Amorphous lactose has applications in the pharmaceuticals industry, however it also contributes to handling issues when present in bulk food powders. Spray dried pharmaceutical-grade lactose is used for tabletting in pharmaceuticals and the suitability for this is partially attributed to the amorphous content (Pharma, 2017b).

Lactose is a main component in dairy powders and is responsible for powder cohesion which is a major issue. It is described by two terms; sticking and caking. Caking is the unwanted agglomeration of powder particles into lumps then forming a clumped solid. Caking is a two-step process involving the formation of a liquid bridge between particles which then must solidify for caking to occur. Sticking is formation of these bridges between the particles (Carpin et al., 2017; Paterson et al., 2005).

Amorphous lactose can cause sticking when it transitions into the rubbery state with a lower viscosity allowing bridging to occur. Amorphous sticking can occur at high relative humidity due to the plasticization by water; this results in caking when the RH drops and the bridges solidify. This process is known as amorphous caking (Carpin et al., 2017).

Other recognised mechanisms of caking are humidity caking, and mechanical caking. Mechanical caking does not itself cause caking but describes the aggravating effect of mechanical pressure on sticking. Humidity caking occurs where water adsorbs to the surface of particles, solid dissolves into the water layer, and liquid bridges containing solute are formed by capillary action solidifying when the relative humidity is reduced (Carpin et al., 2017). Humidity caking due to temperature gradient induced moisture movement was found to be the cause of caking in bulk bags of α-lactose monohydrate by Bronlund (1997). Based on this it bags are now stored below 25% RH. The release of moisture from amorphous lactose upon crystallization could contribute to humidity caking (Dilworth et al., 2004).

2.2 Lactose Production

Lactose is produced industrially from whey, a by-product from cheese production. There are two common types of lactose produced; pharmaceutical-grade and food-grade (Kellam, 2005-2017; Paterson, 2009).

In food-grade lactose production first the whey is concentrated by evaporation, reverse osmosis, or a combination of the two. The concentrated whey is cooled into a supersaturated solution and held to crystallize. The crystals are then separated by a centrifuge or decanter before being washed, dried and packaged (Kellam, 2005-2017; Paterson, 2009). A process flow diagram is shown in Figure 2-11.

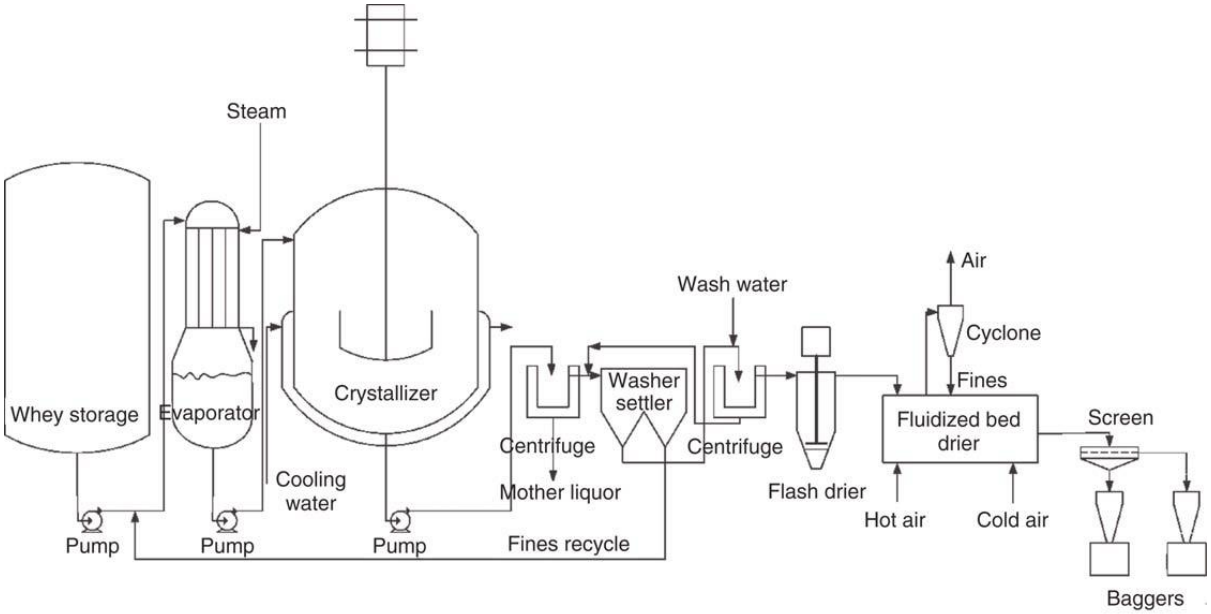

Figure 2-11: Process flow diagram of an edible grade alpha lactose monohydrate production plant. Reproduced from (Paterson, 2009)

For use in pharmaceuticals, lactose must meet more stringent standards regarding impurities (Paterson, 2009) than for food usage and requires additional processing. Pharmaceutical grade lactose is commonly produced using re-dissolving and purifying edible-grade lactose, before following the same processing steps used for edible-grade production (Kellam, 2005-2017). There is also the potential to produce pharmaceutical-grade lactose directly from purified whey (Durham, Hourigan, & Sleigh, 2007).

2.2.1 Lactose Drying

Drying is an important stage in lactose production as improper drying can result in humidity caking of the final product. The drying stage is also a process, during which amorphous lactose can be formed and also crystallized (Paterson, 2017). For the production of α-lactose monohydrate crystals the crystal cake is fed into the drier at 3-12%wt free moisture (Paterson, 2017), and is dried to 4.5-5.5%wt total moisture (Durham, 2009). Three main drying processes are used in lactose production; spray driers, flash driers, and fluid bed driers.

Spray Drying

In a spray drier, a liquid feed is dried by spraying fine droplets through heated air (van 't Land, 2011c). Spray dried lactose is typically produced to be used as an excipient in pharmaceutical tabletting (Durham, 2009). The amorphous content of spray dried lactose deforms with pressure, binding the tablet, and is usually considered to be desirable (Bolhuis, Kussendrager, & Langridge, 2004). A feed slurry of saturated aqueous lactose solution and α-lactose monohydrate crystals (Paterson, 2009), with up to 60% solids (Durham, 2009) is atomised in the spray drier. The product is spherical agglomerates with good flowing characteristics consisting of crystalline lactose in an amorphous lactose matrix with much of the amorphous content in the centre (Darcy & Buckton, 1998a). The product consists of 15-20% amorphous lactose with the rest being alpha lactose monohydrate crystals. The amorphous lactose typically contains about 60% beta lactose and 40 % alpha lactose (Bolhuis et al., 2004). Further conditioning drying is typically required, using a fluid bed drier and air of a low water activity to ensure product stability (Durham, 2009).

Flash Drying

In a flash drier small wet particulate solids are dried and transported by high velocity heated air (van 't Land, 2011b). Of the different flash drier designs spin-type driers have been applied in lactose production (Durham, 2009). A flash drier is used in most α-lactose monohydrate crystal production to receive the centrifuged crystal cake, with an inlet air temperature of 120-180°C (Paterson, 2009). The drier flashes off the moisture and creates a thin layer of amorphous lactose on the crystal surface making up 0.5-2%wt (Paterson, 2017). Flash drying is typically used prior to conditioning fluid bed drying.

Fluidised Bed Drying

In a fluidised bed drier a wet particulate feed is dried by a heated air stream blown through the material to maintain a fluidised state (van 't Land, 2011a). A fluidised bed drier can be used to receive the centrifuge crystal cake directly or is used as a conditioning step receiving already spray or flash dried lactose. It has two functions: to further dry the product, with a typical air temperature being 110°C and to then cool the product to a suitable packaging temperature, below 40°C (Durham, 2009; Paterson, 2009). If used to receive the crystal cake it is expected that amorphous lactose would be produced as in flash drying, although this is complicated by agglomeration. It is possible that crystallization of amorphous lactose formed during previous drying may occur during fluidised bed drying (Ranger, Paterson, & McLeod, 2017).

2.3 Amorphous Lactose Crystallization

Crystallization is a dramatic change in the structure and physiochemical properties of a material (Roos, 2012). In amorphous materials this occurs as the amorphous state is metastable and on a higher energetic level than the crystalline state. Amorphous materials above their glass transitions temperature become physically unstable and are likely to crystallize into a more thermodynamically stable form. This change of form is driven by a reduction in the Gibbs free energy (Burnett et al., 2009; Palzer, 2010).

The plasticising effect of water reduces the T_g with greater molecular mobility allowing for crystallization of amorphous lactose at room temperature and below. At a relative humidity (RH) of 48% T_g falls below 25°C (Chidavaenzi et al., 1997).

2.3.1 Products of Crystallization

The conditions for producing the different forms of lactose, including formation by chemical means, are shown in Figure 2-3. Bronlund (1997) has stated that at a low water activity (<0.55) α-lactose monohydrate will not form crystallize from amorphous lactose crystallization instead being anhydrous α-lactose, or β-lactose will form. At higher water activities (>0.55) α-lactose monohydrate can be formed as water is available to be incorporated into the structure. Where sufficient water is available α-lactose monohydrate is preferentially formed at lower crystallization temperatures (<93.5°C), with the β-lactose anomer preferred at higher temperatures (>93.5°C) (Bronlund, 1997; Jenness & Walstra, 1984; Nijdam et al., 2007). Both forms of α-lactose anhydrous can be formed by dehydration of α-lactose monohydrate, the unstable from will convert to anhydrous β-lactose with water uptake above 93.5°C (Buma & Wiegers, 1967; Walstra, 1999). All anhydrous lactose crystal forms will convert to α-lactose monohydrate with moisture uptake at room temperature and a sufficiently high water activity. Anhydrous β-lactose and α-lactose unstable will both convert below 93.5°C with water uptake (Listiohadi, Hourigan, Sleigh, & Steele, 2008; Walstra, 1999). Compound α:β crystals in the ratios of 1:1, 5:3, and 4:1 have been formed by moisture uptake at room temperature (Bushill, Wright, Fuller, & Bell, 1965; K. Jouppila, J. Kansikas, & Y. H. Roos, 1997a). Compound α:β 1:1 crystals produced using superheated steam are believed to have crystallized from an amorphous intermediary phase (Clarke, 2002; Dhanjee & Paterson, 2000; Ecroyd, 2003).

2.3.2 Adsorption and Diffusion

Adsorption of water plays a major role in the crystallization of amorphous lactose due to its plasticizing effect. This effect reduces the T_g and results in greater molecular freedom reducing the temperature at which crystallization can occur as discussed in section 2.1. In the case of a bed of amorphous lactose particles the rate of moisture adsorption into the bed is limited by adsorption to the particles and not the diffusion of humid air through the bed itself (Ripberger, 2010).

An investigation by Buckton and Darcy (1996) into sorption behaviour of amorphous lactose showed that adsorption behaviour differed at the relative humidities of 40% and 50%. At both relative humidities adsorption was observed to consist of two phases with different rates. This biphasic nature was much more pronounced at 40% RH where a region of slow adsorption is clearly distinguishable from preceding and succeeding exponential regions. Desorption was also investigated with desorption from the non-collapsed amorphous lactose observed as rapid

and proportional to the drying relative humidity. Following collapse or glass transition, desorption was slow and square root of time dependent.

Crystallisation at a high relative humidity often causes a concentration gradient through an amorphous lactose sample as water is adsorbed to the surface and takes time to diffuse through the solid (Bronlund, 1997; Buckton & Darcy, 1995). In an amorphous powder bed, absorption of water is thought to take place in two phases. These phases are; an initial phase where the surface is unsaturated as diffusion occurs more quickly than adsorption, and a second phase where adsorption exceeds diffusion.

Upon crystallization of amorphous lactose water is expelled from the crystalline structure and can saturate nearby amorphous lactose causing further crystallization (Buckton & Darcy, 1995). This effect was posited to be one of the mechanisms behind rapid crystallization by Clark (2012).

Table 2-6: List of published diffusion coefficients for amorphous and partially amorphous lactose.

Compound:	Coefficient of diffusion (±s.d.):	Reference:
Spray dried amorphous lactose (estimated)	2.33×10^{-14} m^2/s	(Bronlund, 1997)
Spray dried amorphous lactose, from 30%wtsolution	$3.4 \pm1.7\times10^{-14}$ m^2/s	(Paterson & Ripberger, 2011)
Spray dried amorphous lactose, from 10%wtsolution	$6.6 \pm0.7\times10^{-14}$ m^2/s	(Paterson & Ripberger, 2011)
Freeze dried amorphous lactose, from 20%wtsolution	$4.5 \pm2.5\times10^{-11}$ m^2/s	(Paterson & Ripberger, 2011)
Supertab, spray dried 6-12%wt amorphous lactose	$3.4 \pm1.9\times10^{-13}$ m^2/s	(Clark, 2012)
Spray dried amorphous lactose, from 10%wt, 30%wt solution	$1.4 \pm1.2\times10^{-14}$ m^2/s	(Clark, 2012)
Freeze dried amorphous lactose, from 10%wt, 30%wt solution	$7.6 \pm1.2\times10^{-12}$ m^2/s	(Clark, 2012)
Milled spray dried lactose, 1.1±0.4% amorphous lactose	$3.6 \pm2.3\times10^{-13}$ m^2/s	(Clark, 2012)

Table 2-6 presents the published diffusion coefficients for amorphous lactose. From this table it is clear that the diffusion coefficients differ between amorphous lactose prepared by spray drying and that prepared by freeze drying by multiple orders of magnitude. The coefficients for the preparations of spray dried amorphous lactose from 10wt% and 30wt% solutions determined by Paterson and Ripberger (2011) were found to be statistically different. In contrast the values for spray dried samples including milled supertab, were not found to differ significantly (Clark, 2012). Both Clark (2012) and Paterson and Ripberger (2011) determined the coefficients of diffusion by using a mathematical model for adsorption of water into a sphere combined with the size distribution of particles being investigated and experimental sorption data, minimizing the sum of squares to estimate the diffusivity. Paterson and

Ripberger (2011) used a balance with a controlled humidity environment exposing a sample stored in a dry environment to a step change in relative humidity. Clark (2012) used a Dynamic Vapour Sorption (DVS) device to measure the mass change of a dry sample ramped from 0% RH to 40% RH. The time taken for relative humidity ramp in the DVS was suggested as the reason Clark (2012) obtained lower diffusion coefficients than those of Paterson and Ripberger (2011).

2.3.3 Amorphous Lactose Crystallization Kinetics:

It is important to determine the kinetics of amorphous lactose crystallization, particularly during drying conditions, as incomplete crystallization or the hypothesized directional crystallization can cause the product to have undesirable handling properties (O'Donnell, 1998; Paterson, 2017). The following models/methods have been used to describe the kinetics of amorphous lactose crystallization.

Avrami Model

The Avrami model describes solid phase changes under constant temperature conditions. The Avrami equation has often been used to describe crystallization kinetics, including those of amorphous lactose (Arvanitoyannis & Blanshard, 1994; Saunders et al., 2004). Equation (2-4) is the Avrami equation in a simplified form with the assumptions that nucleation rate is independent of the amount crystallized and that crystal growth rate that is linear over time. This equation has a sigmoidal dependency between the crystallized mass and elapsed time. The kinetics apply to limiting nucleation at the beginning progressing to a decreasing crystallizing concentration before completion (Palzer, 2010). The kinetics of amorphous lactose crystallization have been observed to increase not only with temperature but also moisture content (Ibach & Kind, 2007). The difference between the experimental and glass transition temperatures (T-Tg) accounts for this behaviour and has been used to model changes in the Avrami constants (Bronlund, 1997).

$$1 - Y = Y_{cr} = 1 - \exp(-((k\,t)^n)) \qquad (2\text{-}4)$$

Where:

- $1 - Y = Y_{cr}$ is the crystallized fraction or the amount of crystallized mass over the total mass able to undergo crystallization (g/g).
- k is the rate constant, containing the nucleation and growth rate (s^{-1}).
- n is the Avrami exponent, this has no clear physical interpretation and has an integer value typically between, but not limited to, 1 and 4 (Bronlund, 1997; Çelikbilek, Ersundu, & Aydın, 2012; Jena & Chaturvedi, 1992).

WLF Equation

The Williams, Landel, and Ferry (1955) developed an empirical (WLF) equation describing the temperature dependence of all mechanical and electrical relaxation processes above T_g for an amorphous polymer. Changes in viscosity by glass transition can be related to the temperature above the glass transition temperature as shown in equation (2-5). This equation can be applied for conditions where both drying and crystallization are occurring as it accounts for the dependence of the crystallization rate on the difference between the material temperature and T_g of the material.

$$\frac{\mu}{\mu_g} = \frac{-C_1(T - T_k)}{C_2 + (T - T_k)} \tag{2-5}$$

Where:

- T is the temperature of the material, greater than T_g (K).
- T_k is the a reference temperature (K).
- C_1, μ_g, C_2 are experimentally derived parameters
- μ is the viscosity at temperature T (Pas).

Differential Scanning Calorimetry was employed to investigate amorphous lactose crystallization kinetics, and the rate of crystallization was found to agree well with WLF kinetics by equation (2-6) (Roos & Karel, 1990; Roos & Karel, 1992)

$$\log_{10}\left(\frac{t_{cr}}{t_g}\right) = \frac{-17.44 * \left(T - T_g\right)}{51.6 + \left(T - T_g\right)} \tag{2-6}$$

Where:

- T is the temperature of the material (K).
- T_g is the glass transition temperature, selected as the WLF reference temperature (K).
- t_{cr} is the crystallization time, the time at which maximum heat flow occurs (s).
- t_g is the average crystallization time at T_g (s)

Avrami-Bronlund Model

A model based on the differentiated form of the Avrami equation was produced by Bronlund (1997) to describe amorphous lactose crystallization. This model is displayed as equation (2-7) which includes the WLF equation, thus accounting for viscosity changes with $T-T_g$.

$$\frac{d(1-Y)}{dt} = n_A K_A Y \left[-\frac{\ln Y}{K_A}\right]^{\frac{n_A-1}{n_A}} \quad (2\text{-}7)$$

The parameter n_A was experimentally determined to be 3, interpreted as meaning that growth was linear in 3 dimensions (Bronlund, 1997). Where nucleation is not rate limiting the rate constant K is given by equation (2-8).

$$K_A = C_3(\exp\left(-\frac{C_1}{R\left(C_2 + T - T_g\right)}\right))^3 \quad (2\text{-}8)$$

Where C_1, C_2, and C_3 are constants most recently fitted by Brooks (2000) at $3.54*10^4$, 110.9, and 2.66×10^{27}, R is the universal gas constant = 8.3144 $Jmol^{-1}K^{-1}$.

Arrhenius Model

Ibach and Kind (2007) used the Avrami equation (2-4) to model the crystallization of amorphous lactose under a range of temperature and humidity conditions (20-80%RH, 50-110°C) observed by mass change. The Arrhenius model (2-9), used to describe the effect of temperature on the reaction rate, was then fitted to these results. The pre-exponential factors and activation energies were determined for the range of water activities used 0.2 to 0.8.

$$k(T) = k_0 \exp\left[-\frac{\Delta H^*}{R\,T}\right] \quad (2\text{-}9)$$

Where:

- k is the first order rate constant (s^{-1}).
- k_0 is the pre-exponential factor (s^{-1}).
- T is the temperature (K)
- R is the universal gas constant = 8.3144 $Jmol^{-1}K^{-1}$.
- ΔH^* is the enthalpy of activation ($Jmol^{-1}$).

Activated-State Model

An activated state model was applied by Das and Langrish (2012) to water induced crystallization results for amorphous lactose at 15°C, 25°C, and 40°C all at 75%RH.

The crystallinity over time, tracked by mass changes of the sample, was modelled using a first-order kinetic model (2-10). First-order kinetic models were found to be appropriate for solid phase carbohydrate crystallization by Roos (2003).

$$\frac{dY}{dt} = kY \tag{2-10}$$

The Eyring equation (2-11) which describes the changes in reaction rate with temperature using a transition-state model was fitted using the rate constant and temperature data to obtain the entropy and enthalpy of activation with values of -156±6 $Jmol^{-1}K^{-1}$ and 39±2 $kJmol^{-1}$ respectively. The enthalpy of activation agreed well with a value of 40 $kJmol^{-1}$ determined by Ibach and Kind (2007). The equation could then be used to predict the reaction rate at different temperature conditions.

$$\ln\left(\frac{k}{T}\right) = \left[\ln\left(\frac{k_B}{h}\right) + \left(\frac{\Delta S^*}{R}\right)\right] - \left(\frac{\Delta H^*}{R}\right)\frac{1}{T} \tag{2-11}$$

- k is the fist order rate constant (s^{-1}).
- k_B is Boltzmann's constant = 1.381×10^{-23} J/g.
- h is Plank's constant = 6.626×10^{-34} Js.
- T is the temperature (K)
- R is the universal gas constant = 8.3144 $Jmol^{-1}K^{-1}$.
- ΔS^* is the entropy of activation ($Jmol^{-1}K^{-1}$).
- ΔH^* is the enthalpy of activation ($Jmol^{-1}$).

Friedman Analysis

Burnett et al. (2006) used Friedman analysis from NETZSCH Thermokinetics © software to model the crystallization of amorphous lactose under a range of temperature and humidity conditions (48-60%RH, 22-32°C) observed by mass change. The first derivative of the crystallization data showed the trials below 55%RH at 25°C or below 25°C at 51%RH occurred in two-step processes in contrast to one-step processes for the more favourable conditions. The software identified the best fitting mechanism for the one-step data to be two independent reaction sequences; the first being auto-catalysed and the second being three dimensionally diffusion limited. This was interpreted as being autocatalytic crystal nucleation

followed by diffusion of water from the bulk of the sample. The two-step process data had a poorer fit posited to be due to multiple crystalline products being formed.

Evaluation of Models

Figure 2-12 shows the analysis by Clark (2012) with the relative fits of the Bronlund-Avrami model and WLF model to literature crystallization time data. Both models are determined to be unfit for prediction above a T-T_g of 60°C, and the WLF model appears to be a generally poor fit.

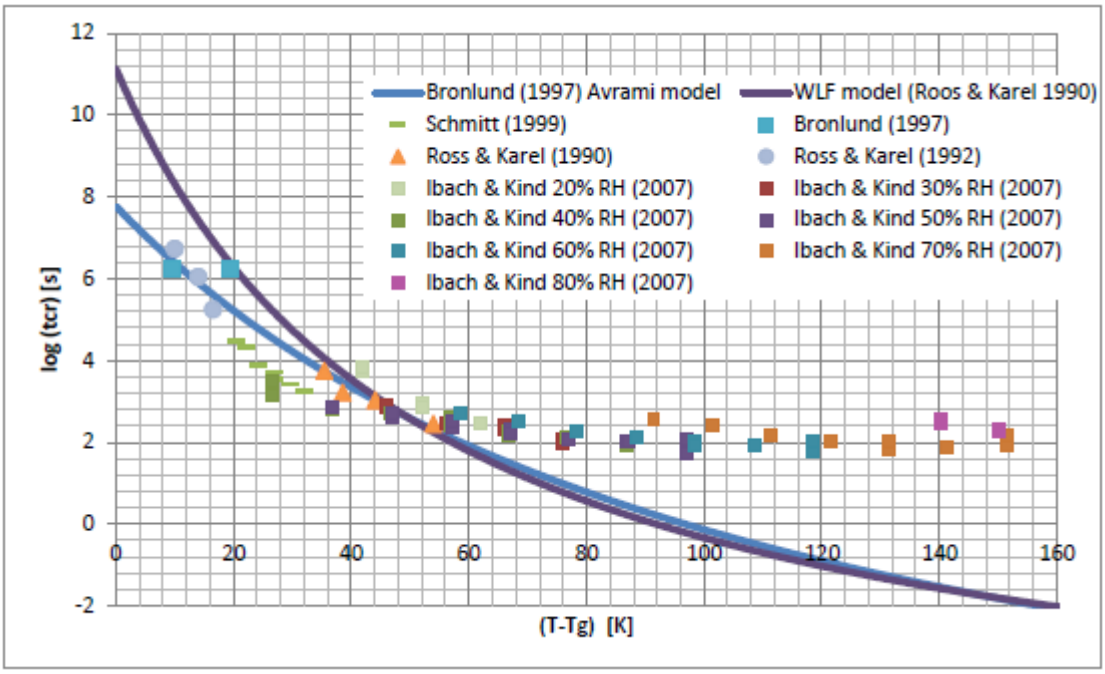

Figure 2-12: Time for 90% crystallization versus T-T_g for literature data including (Ibach & Kind, 2007). Reproduced from (Clark, 2012).

Clark (2012) also conducted one of the more recent experimental investigations into amorphous lactose crystallization kinetics. Crystallization was induced with both temperature and humidity used to manipulate T-T_g, with measurements taken for the amorphicity after a constant time at a variable T-T_g and taken over time for a constant T-T_g. The results of these trials did not show the degree of partial amorphicity predicted by the Avrami-Bronlund, with the crystallization event being described as “all or nothing”. The results also disagreed with the WLF model’s predictions for the crystallization time with crystallization occurring much earlier. The WLF predicted a T-T_g of crystallization for a given time that was higher than the experimental result. In this study the rapid crystallization process was attributed to an autocatalytic effect by either moisture release or a showering effect of nucleation. Evidence was obtained for the nucleation effect as amorphous lactose with imbedded crystalline lactose was observed crystallizing below the T-T_g required for pure amorphous lactose (Clark, 2012).

Crystallization of amorphous lactose was found to potentially involve multiple transitions by C. Kedward, W. MacNaughtan, and J. Mitchell (2000). This was hypothesized to be the result of separate crystallization of different anomers. These multiple transitions were deemed to make use of the Avrami equation unsuitable. However the Avrami equation was still considered to

be somewhat useful as it correctly described that freeze-dried amorphous lactose samples with the lowest T_g would also have the highest crystallization rate.

However some experiments have shown the Avrami equation to be suitable (Haque & Roos, 2005; Miao & Roos, 2005), although Dormeuil (2017) observed that in some cases much of the data was collected after crystallization had already occurred, leaving only a few data points available to show that the model is successful at modelling the crystallization. Another study by McIntosh, Yang, Goldup, Watkinson, and Donnan (2013) was conducted to observe real time crystallization under high humidity conditions, using terahertz pulsed spectroscopy, showing excellent agreement with Avrami kinetics.

2.3.4 Enthalpy of Crystallization

The enthalpy of recrystallization of amorphous lactose has been measured in a number of studies by using IMC. The energetic response of crystallisation by water sorption over time at a constant temperature is recorded and then the peak or peaks associated with the crystallization event are integrated (Sebhatu, Angberg, & Ahlneck, 1994). A collection of values is displayed in Table 2-7 and significant variation between them can be seen. It is important to have an accurate enthalpy of crystallization to the use of calorimetric methods for quantifying the amorphous content (Vivoda, Roškar, & Kmetec, 2011). Because of this it is necessary to understand factors which influence the value and may cause this variation.

The most important cause of error and variation is the different integration methods used between studies (Dilworth et al., 2004). Integration of the isolated crystallization peak is considered by Dilworth et al. (2004) to have poor repeatability and be inferior at predicting amorphous lactose contents when compared to net energy integration, although this is the method which has been most commonly used. The issues of isolating a crystallization peak are because of the overlap between competing processes such as endothermic desorption of moisture, and exothermic processes of crystallization and moisture adsorption.

Collapse of amorphous lactose does not affect the heat of recrystallization (Buckton & Darcy, 1996). The temperature of recrystallization, however, is known to influence the observed enthalpy of crystallization, as at higher temperatures less plasticising water is absorbed and expelled (Darcy & Buckton, 1998b; Dilworth et al., 2004). Therefore, a reference enthalpy of crystallization value of ca. 60 J/g has been suggested by Niemelä et al. (2005) for the spray-dried samples, instead of the crystallization heat, to improve IMC measurement of amorphous lactose content.

Table 2-7 gives literature values for the enthalpy of crystallization. The values of 32±1 J/g from Sebhatu et al. (1994) and 105±2 J/g from Lehto et al. (2006) in particular stand out as unusual. A likely explanation for the variation in the former value was due to the integration method applied (Dilworth et al., 2004). The latter value was determined at a different temperature than the others crystallizing at 145-170°C with little to no moisture adsorption or desorption occurring to reduce the crystallization peak (Lehto et al., 2006).

Table 2-7: Enthalpy of crystallization for amorphous lactose

Reference:	Enthalpy:	Conditions:
(Clark, 2012)	45.3 J/g	Crystallization under 53% RH, 25°C. Different quantities of pure amorphous lactose both alone and with crystalline lactose.
(Vivoda et al., 2011)	41.5 J/g	Crystallization under 100% RH, 25°C.
(Lehto et al., 2006)	48.5±0.2 J/g	Crystallization under 54% RH, 25°C. Completely amorphous spray dried particles.
(Lehto et al., 2006)	105±2J/g	Temperature induced recrystallization during DSC. Pure amorphous α-lactose.
(Dilworth et al., 2004)	45.4±3.3 J/g	Integration of crystallization peak only. 30 mg mixed samples with known amorphous content crystallized at 25°C and 53, and 75% RH.
(Darcy & Buckton, 1998b)	48 J/g	20mg crystallized at 25°C and 53, 65, 75, and 85% RH. Recrystallization of spray dried lactose.
(Chidavaenzi et al., 1997)	50 J/g	20mg crystallized at 25°C and 75% RH. Recrystallization of spray dried lactose.
(Buckton, Darcy, Greenleaf, & Holbrook, 1995)	45-50 J/g	20mg crystallized at 25°C and 53, 65, 75, and 85% RH. Recrystallization of spray dried lactose.
(Buckton, Darcy, & Mackellar, 1995)	53.9 J/g, 58.9 J/g	800mg mixed samples with known amorphous content crystallized at 25°C and 75% RH.
(Sebhatu et al., 1994)	32±1 J/g	30 mg mixed samples with known amorphous content crystallized at 25°C and 57, 75, 84 or 100% RH.

2.4 Next Steps

There is now a wealth of information on the solid-state crystallization of amorphous lactose under a variety of conditions. The models described in section 2.3.3 have not recently been fitted using experimental data and compared. A model able to describe the changes in kinetics with experimental conditions does not currently exist, but would be useful for determining the possibility of crystallization during fluid bed drying.

Several methods for observing amorphous lactose crystallization were discussed in section 2.1.2. Of these the STA method offers the advantage of combined calorimetry and gravimetry. Data was obtained for amorphous lactose crystallization with an STA method by Dormeuil (2017), but analysis was incomplete. A method of analysis developed using this data, which produces kinetic results in line with the prior work collected in Figure 2-12, would have advantages over conventional analysis methods.

The next chapter will analysis the current crystallisation kinetic data in the literature by using the alternative kinetic equations presented in the literature.

3 Modelling Analysis and Comparison

3.1 Introduction

The Avrami and William-Landel-Ferry (WLF) equations have both been popular for modelling solid-state crystallization, including that of amorphous lactose (Bronlund, 1997; Roos & Karel, 1990; Roos & Karel, 1992). While other models have been used, such as the first order model fitted by Das and Langrish (2012), these models have the advantage of being able to be fitted to data obtained via different methods.

The Avrami model has been fitted to X-ray powder diffraction (Miao & Roos, 2005), gravimetric (Schmitt, Law, & Zhang, 1999), differential scanning calorimetry (C. Kedward et al., 2000), and can also be fitted to TGA results in this case from Dormeuil (2017) transformed in the manner described in section 4.2.1. The WLF equation can be fitted based solely on the conditions of the lactose and the crystallization time. Because of their common use and flexibility these models were focused on when obtaining and producing kinetic data and fitting the models presented in this section.

As discussed in section 2.3.3 the current fit of the models for predicting the crystallization time from experimental conditions is inadequate beyond the range of conditions they were fitted for. An improved model would be valuable for predicting experimental times, and in relation to the objectives of this project, for determining whether crystallization has time to occur under set drying conditions.

3.2 Literature Crystallization Times and Avrami model Constants

Data was collected from various literature sources for the crystallization times along with the Avrami model constants for amorphous lactose crystallization. In some cases where crystallization data was presented, but not fitted to a model, the Avrami constants were fitted. Crystallization times were included when reported but if not were calculated using the fitted Avrami constants. The Avrami model is typically fitted using data below 90% crystallization and is less reliable for predicting the time required for complete crystallization data.

It is important to differentiate the induction time from the crystallization time which only includes the crystallization event. The induction time includes sorption, temperature equilibration, and structural relaxation processes, which, aside from being sparsely reported are also dependent on the sample mass. The induction time is likely to be shorter in a dryer where the temperature is high and moisture sorption processes occur more quickly (Buckton & Darcy, 1996), but it will still be significant.

Data from both spray-dried (Clark, 2012; Das & Langrish, 2012; Schmitt et al., 1999) and freeze-dried (Dormeuil, 2017; C. J. Kedward, W. MacNaughtan, & J. R. Mitchell, 2000; McIntosh et al., 2013; Miao & Roos, 2005; Roos & Karel, 1990; Roos & Karel, 1992) samples is included. The production method for the samples used by Bronlund (1997) and Ibach and Kind (2007) is unclear but suspected to be spray-drying in both cases.

The glass transition temperature value, where not reported, was calculated from the experimental conditions. The cubic fitting equation of Brooks (2000) (equation (2-2))was used for this prediction for aw <0.575, at higher water activities the equilibrium moisture content

was calculated using the isotherm constants presented by Foster (2002) (equation (2-3)) and combined with the Gordon-Taylor equation (equation (2-1)) with the constants of Brooks (2000).

The difference between the glass transitions temperature and the temperature of the sample is the driving force for crystallization in the WLF equation (equation (2-6)) and the Avrami-Bronlund model (equation (2-4)). The experimental system temperature was assumed to be the sample temperature. Figure 3-1 and Figure 3-2 show the changes in the crystallization time with T-Tg, it shortens dramatically between 0 and 40K before evening out and staying relatively constant past 80K.

Figure 3-3 shows the changes in the Avrami rate constant which behaves in an opposite manner to the crystallization time, increasing dramatically before evening out over the same ranges of T-Tg.

The second parameter of the Avrami equation, the n values, sometimes called the shape factor, does not appear to have a strong dependence on T-Tg. The value appears to generally decrease with T-Tg or experimental temperature Figure 3-4, and similarly decreases with increasing water activity. As the term shape factor indicates n largely affects the shape of the Avrami model while k determines the overall time. Because of this the most commonly reported value of 2 will be used for the calculation of crystallization time.

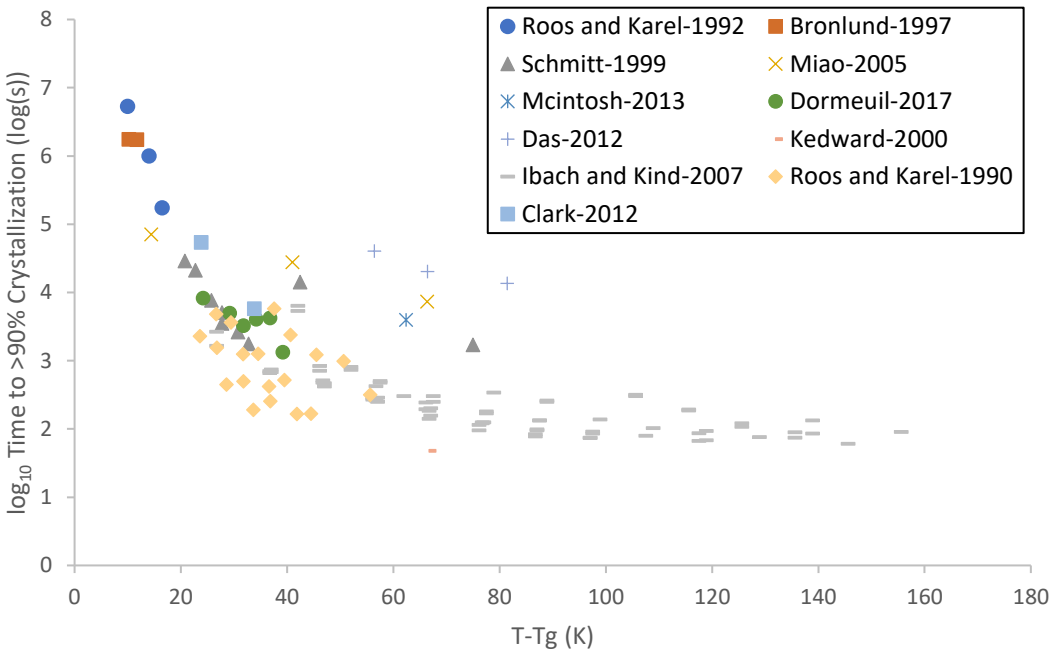

Figure 3-1: Time to 90% Crystallization versus T-Tg. Constructed using data from: from (Bronlund, 1997; Clark, 2012; Das & Langrish, 2012; Dormeuil, 2017; Ibach & Kind, 2007; C. Kedward et al., 2000; McIntosh et al., 2013; Miao & Roos, 2005; Roos & Karel, 1990; Roos & Karel, 1992; Schmitt et al., 1999)

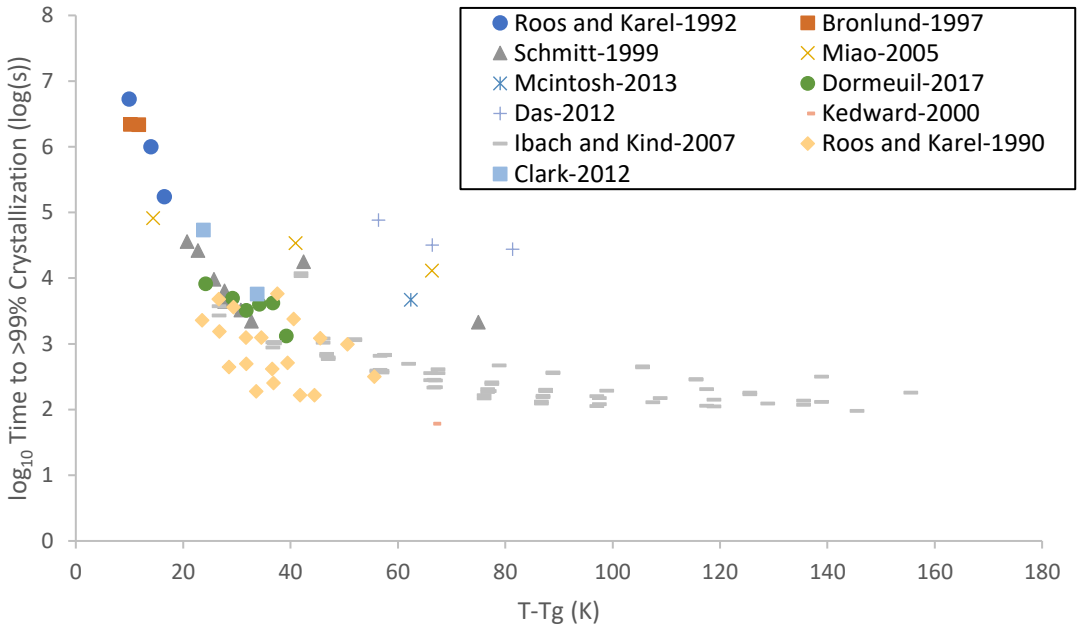

Figure 3-2: Time to 90% Crystallization versus T-Tg. Constructed using data from: from (Bronlund, 1997; Clark, 2012; Das & Langrish, 2012; Dormeuil, 2017; Ibach & Kind, 2007; C. Kedward et al., 2000; McIntosh et al., 2013; Miao & Roos, 2005; Roos & Karel, 1990; Roos & Karel, 1992; Schmitt et al., 1999)

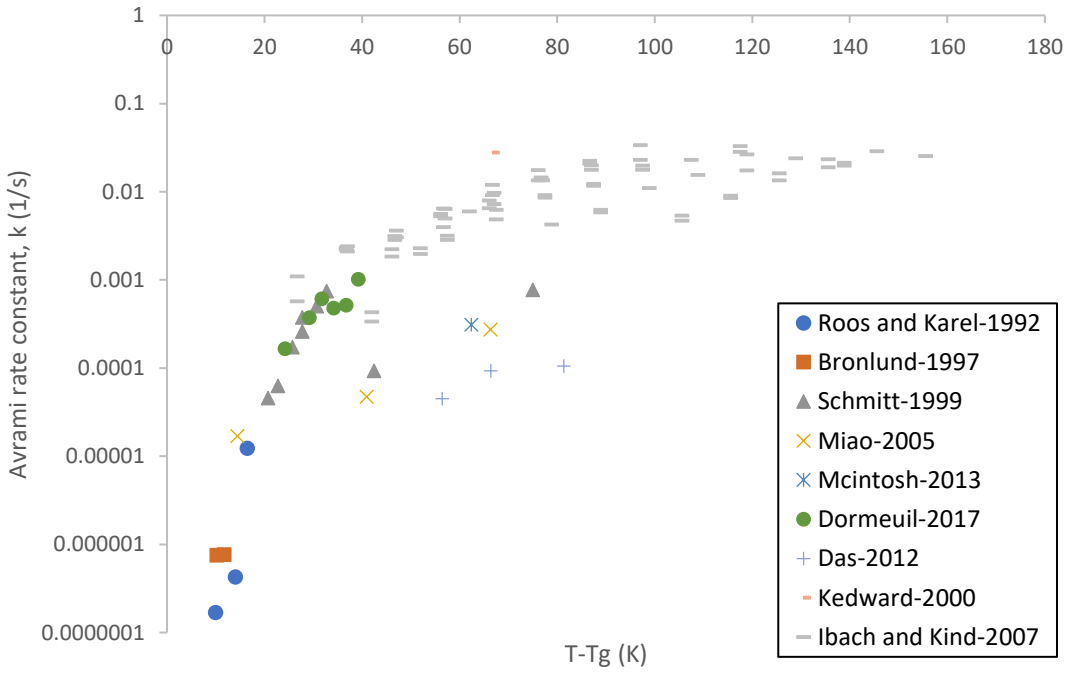

Figure 3-3: Fitted and literature Avrami rate constants on a log axis versus T-Tg. Constructed using data from: from (Bronlund, 1997; Clark, 2012; Das & Langrish, 2012; Dormeuil, 2017; Ibach & Kind, 2007; C. Kedward et al., 2000; McIntosh et al., 2013; Miao & Roos, 2005; Roos & Karel, 1990; Roos & Karel, 1992; Schmitt et al., 1999)

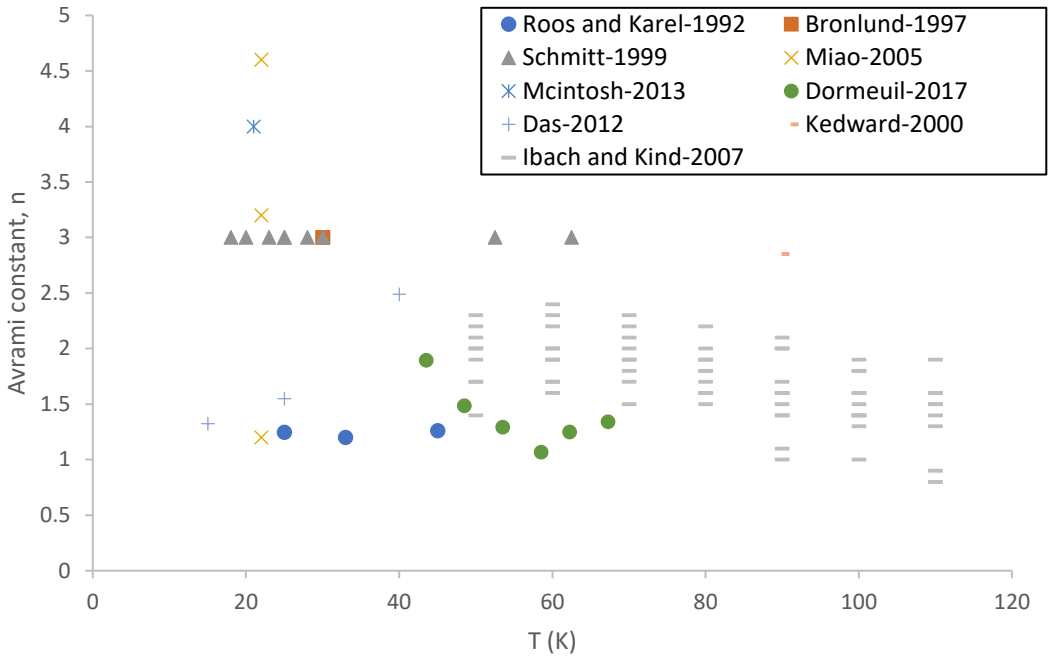

Figure 3-4: Fitted and literature Avrami constant n versus T. Constructed using data from: from (Bronlund, 1997; Clark, 2012; Das & Langrish, 2012; Dormeuil, 2017; Ibach & Kind, 2007; C. Kedward et al., 2000; McIntosh et al., 2013; Miao & Roos, 2005; Roos & Karel, 1990; Roos & Karel, 1992; Schmitt et al., 1999)

3.3 Existing Models

The two established models used for predicting the crystallization time are the WLF equation fitted by Roos and Karel (1992) and the Avrami-Bronlund model proposed by Bronlund (1997). Both models have been assessed by Clark (2012) as being unsuitable for predicting the crystallization time at high T-Tg conditions (Figure 2-12). These two models are presented with the revised literature data in Figure 3-5. The models even at low T-Tg conditions are poor predictors with calculated r^2 values of -7.788 and -6.124 for the WLF and Avrami-Bronlund models respectively.

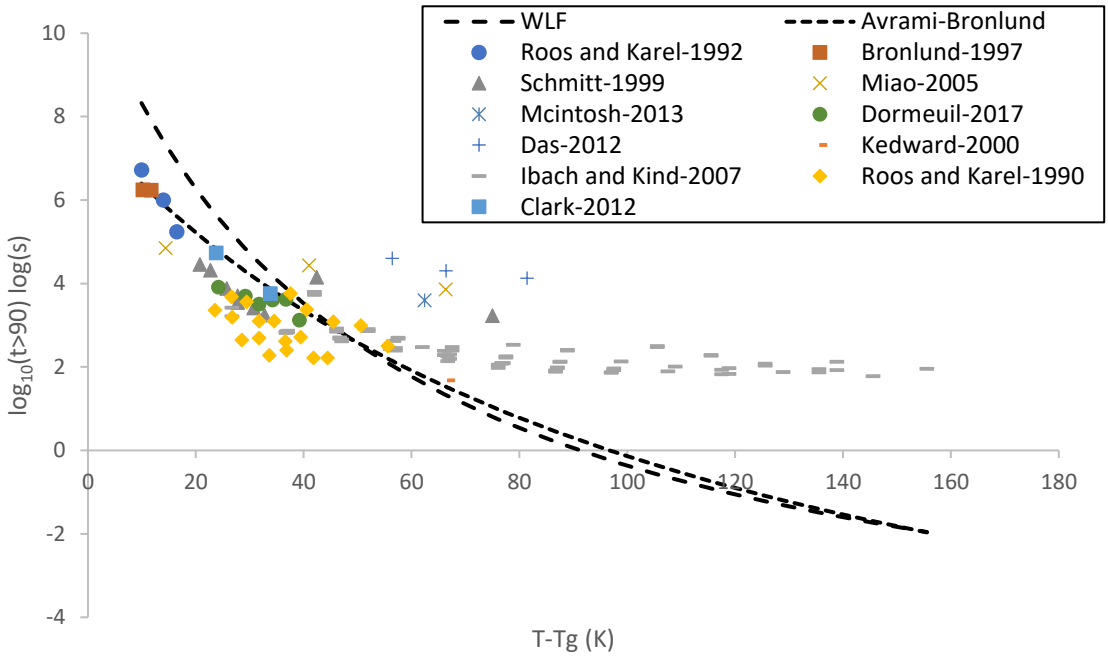

Figure 3-5: Existing crystallization time prediction models presented with revised crystallization time data.

3.4 Arrhenius Model Ibach and Kind 2007

Ibach and Kind (2007) fitted the Avrami model to gravimetric crystallization data obtained over 0.2-0.8aw and 50-110°C. They then fitted the Arrhenius equation (equation (2-9)) to the Avrami rate constants obtained at constant water activities, presenting the activation energies (E_a) and pre-exponential factor (k_0).

The constants obtained were fitted against the corresponding water activities and predicted equilibrium moisture contents by regression. The predicted equilibrium moisture (EMC) content proved the best predictor and a polynomial of the inverse EMC provided the best fit in both cases. A GAB style model as used by Das and Langrish (2012), for the prediction of constants also showed promise but ultimately did not fit the data as well.

The model for $\ln(k_0)$ used is displayed in equation(3-1) with the resulting fit shown in Figure 3-6. The standard error for the prediction is ±2.34kJ/mol.

$$\ln(k_0) = \frac{1.24 \cdot 10^{-4}}{EMC^4} - \frac{0.0213}{EMC} + 9.71 \tag{3-1}$$

Where:

- k_0 = Arrhenius pre-exponential factor (1/s)
- EMC = Equilibrium moisture content predicted from aw using (equation (2-3)) (g_{water}/g_{dry})

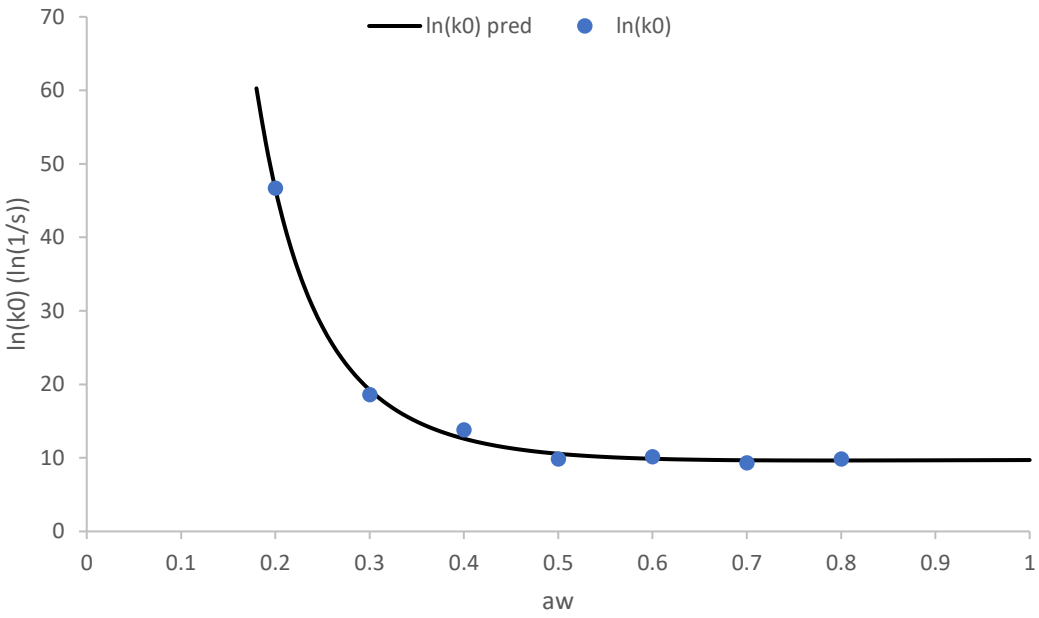

Figure 3-6: Model fitted to the pre-exponential constants k_0 versus aw of Ibach and Kind (2007)

The model for the activation energy (E_a) used is displayed in equation (3-2) with the resulting fit shown in Figure 3-7. The standard error for the prediction is ±0.808 ln(1/s).

$$E_a = \frac{3.93 \cdot 10^{-4}}{EMC^4} + \frac{0.224}{EMC} + 39.66 \quad (3\text{-}2)$$

Where:

- E_a = Arrhenius activation energy (kJ/mol)
- EMC = Equilibrium moisture content predicted from aw using (equation (2-3)) (g_{water}/g_{dry})

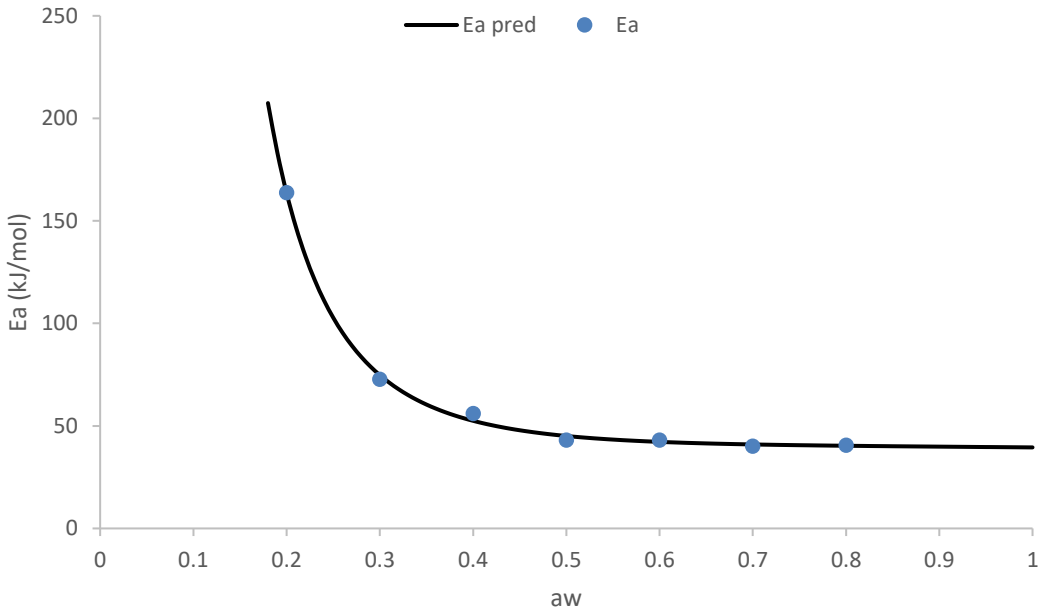

Figure 3-7: Model fitted to the activation energy E_a versus aw of Ibach and Kind (2007)

The models for activation energy and pre-exponential factor were applied to the data collected, and used to estimate the Avrami rate constant in each case (Figure 3-8) with the rate constant used to estimate the time for 90% crystallization. The resulting predictions are displayed against the collected values in (Figure 3-9).

Figure 3-8 shows that the Ibach&Kind-Arrhenius model predicts the Avrami rate constant well above a value of 0.001s^{-1} but beyond this range tends to significantly overpredict. Figure 3-9 shows that the rate constants, when used with the Avrami model, predict the crystallization time well for the data they are modelled from but provide a poor estimate for most other data. This is reflected in a calculated coefficient of determination (r^2), for the 90% crystallization time prediction, of -0.1269 which indicates the model provides a poorer fit than

a straight line at the average time. If data beyond the temperature and water activity range is excluded the fit does not improve with an r^2 of -0.2020 calculated.

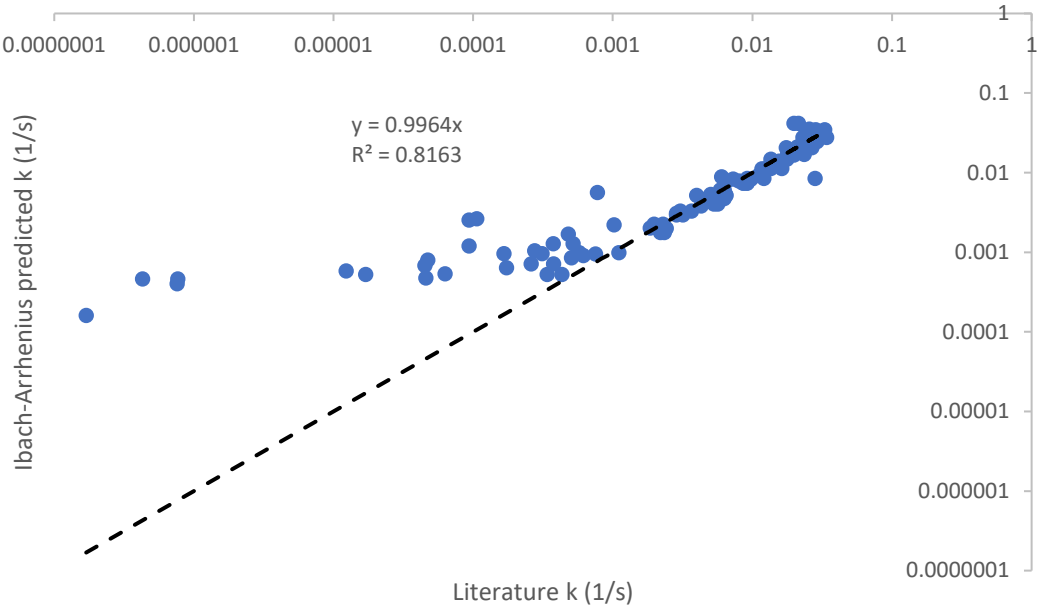

Figure 3-8: Ibach and Kind (2007) Arrhenius predicted Avrami rate constants versus Literature value both presented on a log_{10} scale

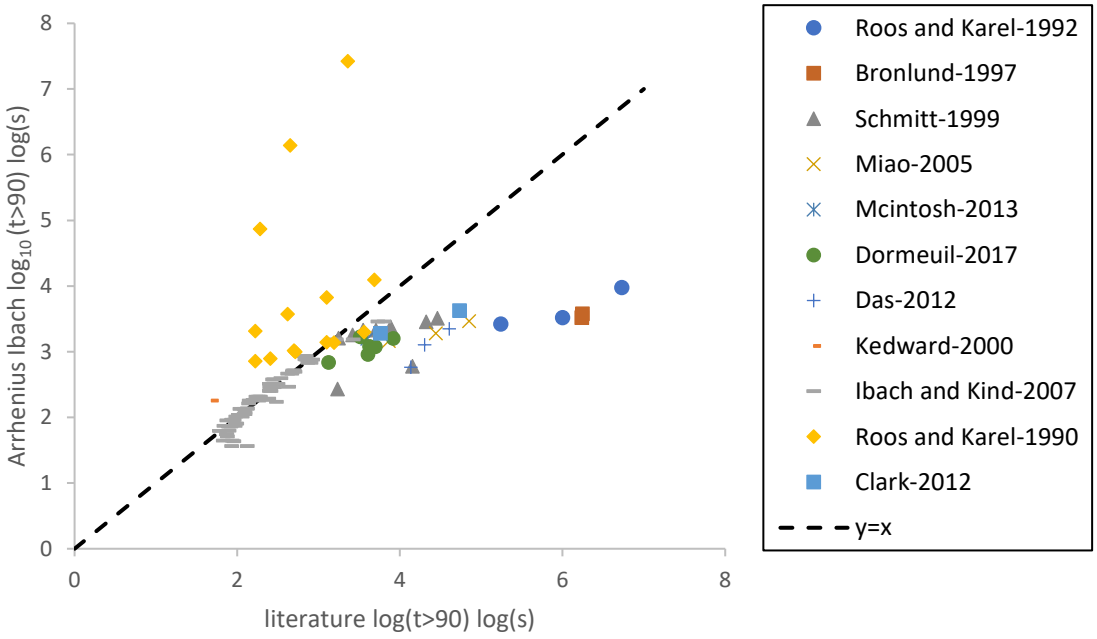

Figure 3-9: Ibach and Kind (2007) Arrhenius predicted 90% crystallization times versus Literature values.

3.5 Activated-State Model fitting

Das and Langrish (2012) fitted an activated-state model (equation (2-10)) to crystallization rate constant data from trials at different temperatures and a constant water activity.

The Avrami constant and experimental condition data collected was used to fit the two activated-state constants, enthalpy of activation ΔH and entropy of activation ΔS, for each relative humidity. These constants were then modelled based on the predicted EMC at each water activity with a polynomial model of the inverse EMC providing the best fit. Three of the sets of fitted constants, at water activities of 0.33, 0.44, and 0.575, shown in Figure 3-10 were not in-line with the other results and were excluded from the fitting. A GAB style model as used by Das and Langrish (2012) for the prediction of constants also showed promise but ultimately did not fit the data as well.

The model for ΔH used is displayed in equation(3-3) with the resulting fit shown in Figure 3-10. The standard error for the prediction is ±8770J/mol.

$$\Delta H = 0.383 \cdot EMC^{-4} + \frac{554}{EMC} + 32366 \tag{3-3}$$

Where:

- ΔH= Arrhenius pre-exponential factor (J/mol)
- EMC = Equilibrium moisture content predicted from aw using (equation (2-3)) (g_{water}/g_{dry})

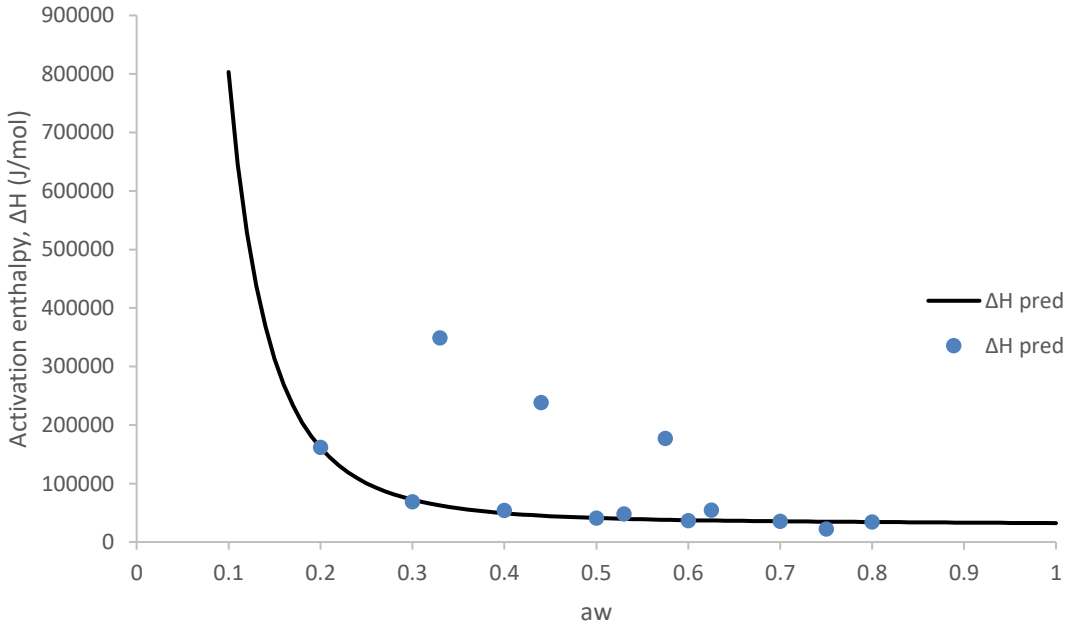

Figure 3-10: Modelled activated state activation enthalpy and fitted values versus water activity

The model for ΔS used is displayed in equation(3-4) with the resulting fit, excluding the outliers as before, shown in Figure 3-11. The standard error for the prediction is ±28.2J/molK.

$$\Delta S = -9.88 \cdot 10^{-4} EMC^{-4} - \frac{0.859}{EMC} - 209 \tag{3-4}$$

Where:

- ΔS = Arrhenius pre-exponential factor (J/molK)
- EMC = Equilibrium moisture content predicted from aw using (equation (2-3)) (g_{water}/g_{dry})

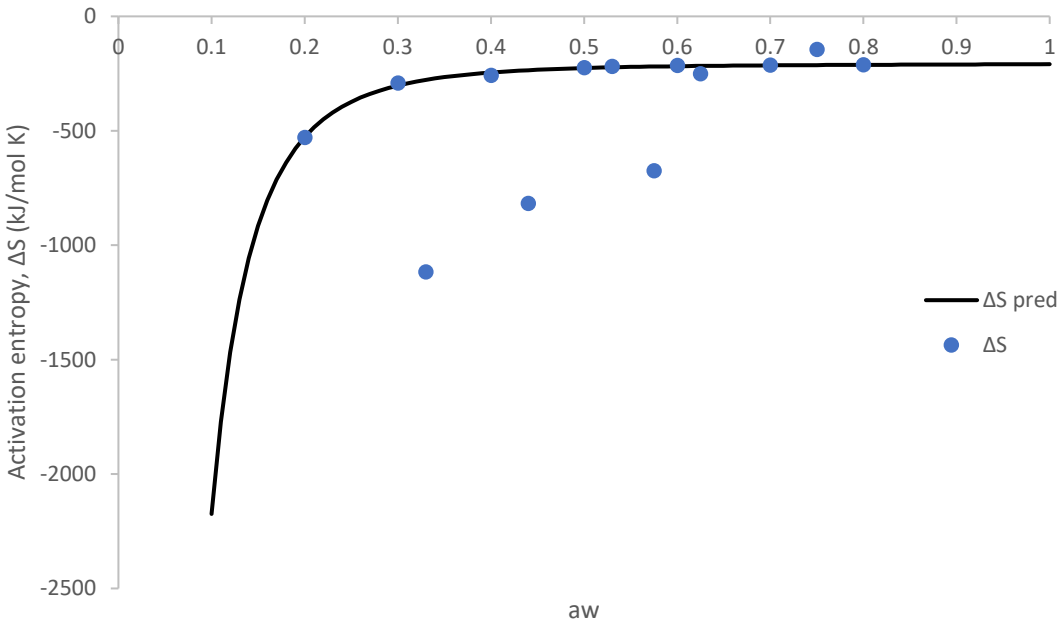

Figure 3-11: Modelled activated state activation enthalpy and fitted values versus water activity

The models for activation enthalpy and entropy were applied to the data collected in section 3.2, and used to estimate the Avrami rate constant, as shown in Figure 3-12, for the time to 90% crystallization. The resulting predictions are displayed against the collected values in Figure 3-13.

Figure 3-12 and Figure 3-13 show very similar results to Figure 3-8 and Figure 3-9 which is understandable given the similarities between the Arrhenius (equation (2-9)) and Eyring (equation (2-11)) equations.

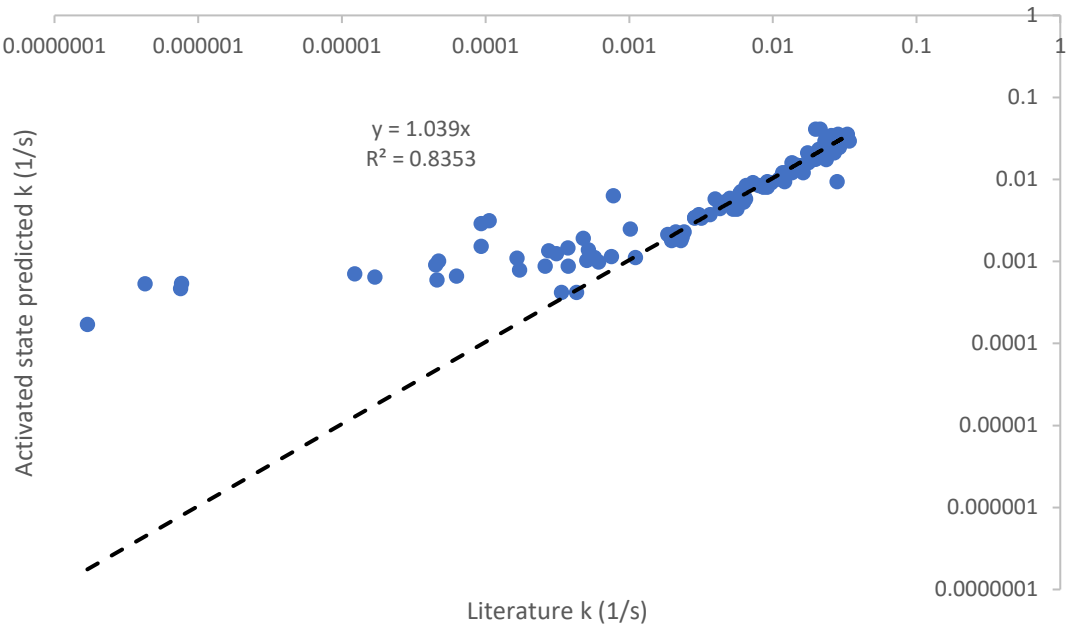

Figure 3-12: Activated state predicted Avrami rate constants versus Literature values both presented on a log_{10} scale

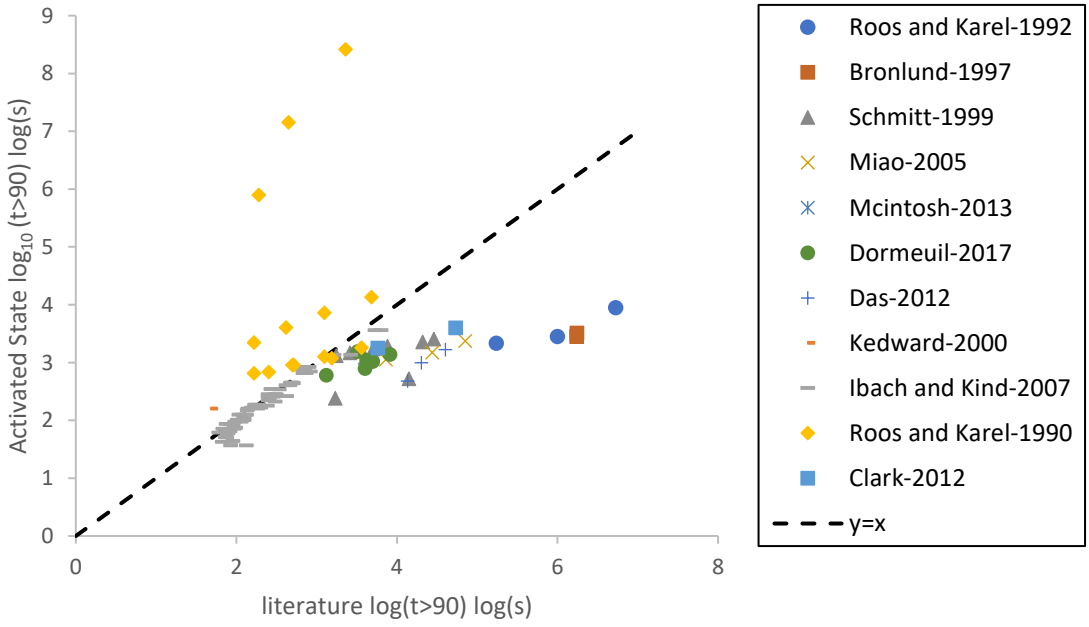

Figure 3-13: Activated state predicted 90% crystallization times versus Literature values.

3.6 Arrhenius T-Tg Model fitting

The relationship between the Avrami rate constant and the T-Tg of the crystallization conditions was investigated. An Arrhenius plot substituting T-Tg for absolute temperature was found to fit quite well (Figure 3-14); data derived from Das and Langrish (2012), McIntosh et al. (2013), and Miao and Roos (2005) was excluded to improve the fit. When the rate constants predicted by this model are plotted against the literature values (Figure 3-15) it can be seen that the data may be more scattered than those from the Arrhenius-Bach model or the activated-state model but it provides a reasonable estimate over a much wider range.

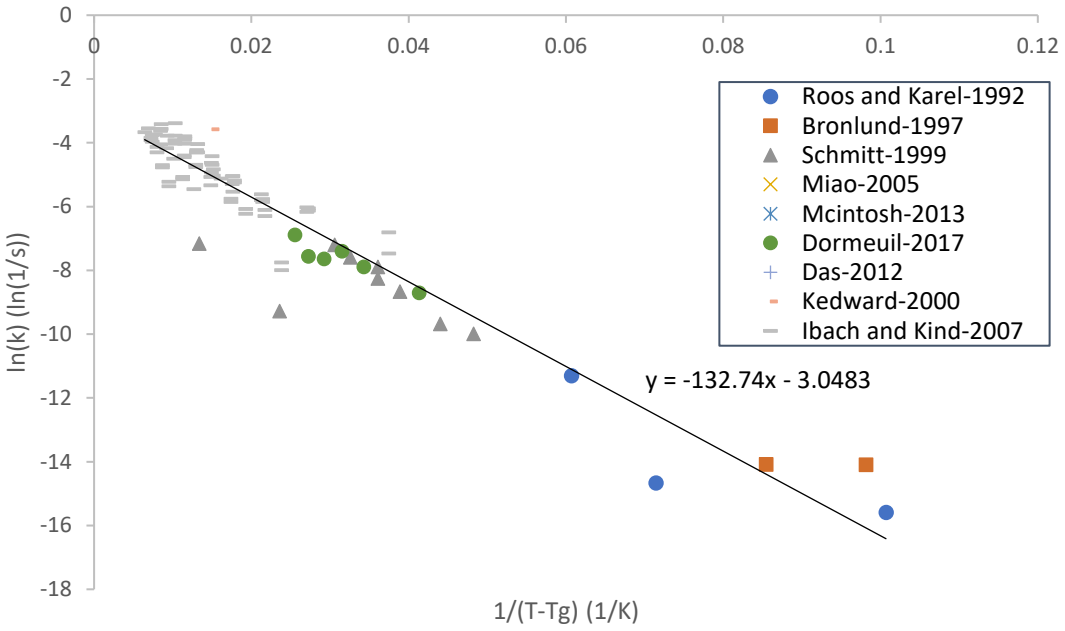

Figure 3-14: Arrhenius plot showing ln(k) versus 1/(T-Tg) with the linear fit shown.

The model for k used is displayed in equation(3-5) with the resulting fit shown in Figure 3-15. The standard error for the linear correlation is ±0.750 ln(1/s).

$$\mathrm{k} = \exp\left(-\frac{133}{T-Tg} - 3.05\right) \tag{3-5}$$

$$\ln(k) = -\frac{133}{T-Tg} - 3.05$$

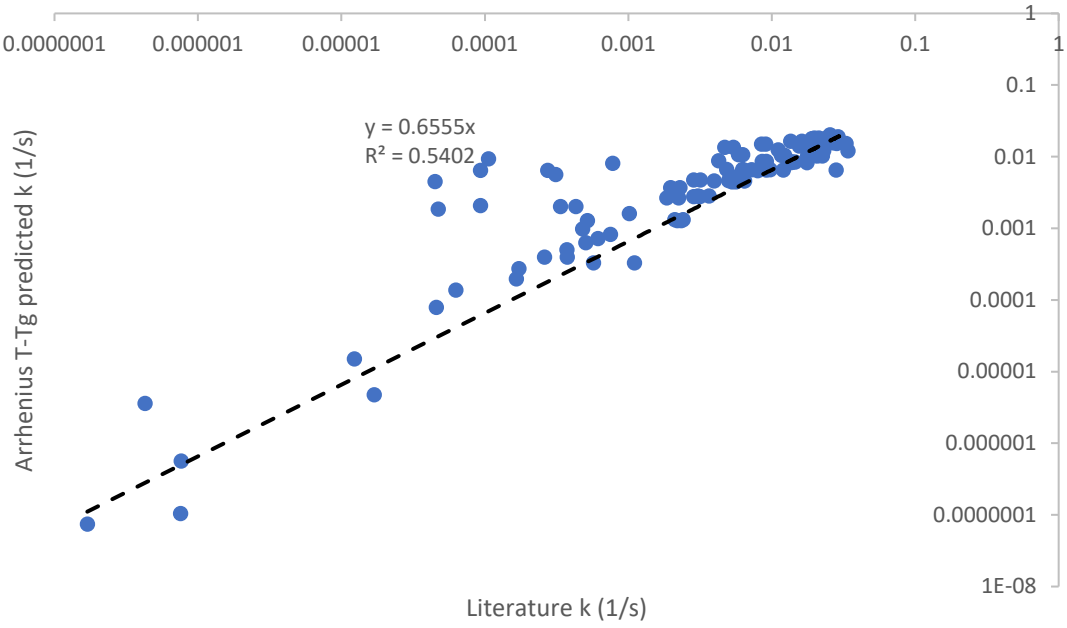

Figure 3-15: Arrhenius T-Tg model predicted Avrami rate constants versus Literature values both presented on a log_{10} scale

The modelled rate constants have then been used in the Avrami equation to predict the time to 90% crystallization in Figure 3-16. The model provides a reasonable estimate across the range of T-Tg conditions, most of the collected data lies between the standard error range. The calculated r^2 for the prediction is 0.7305 indicating a reasonable fit, this improves to 0.8596 when the data excluded for the fitting is excluded.

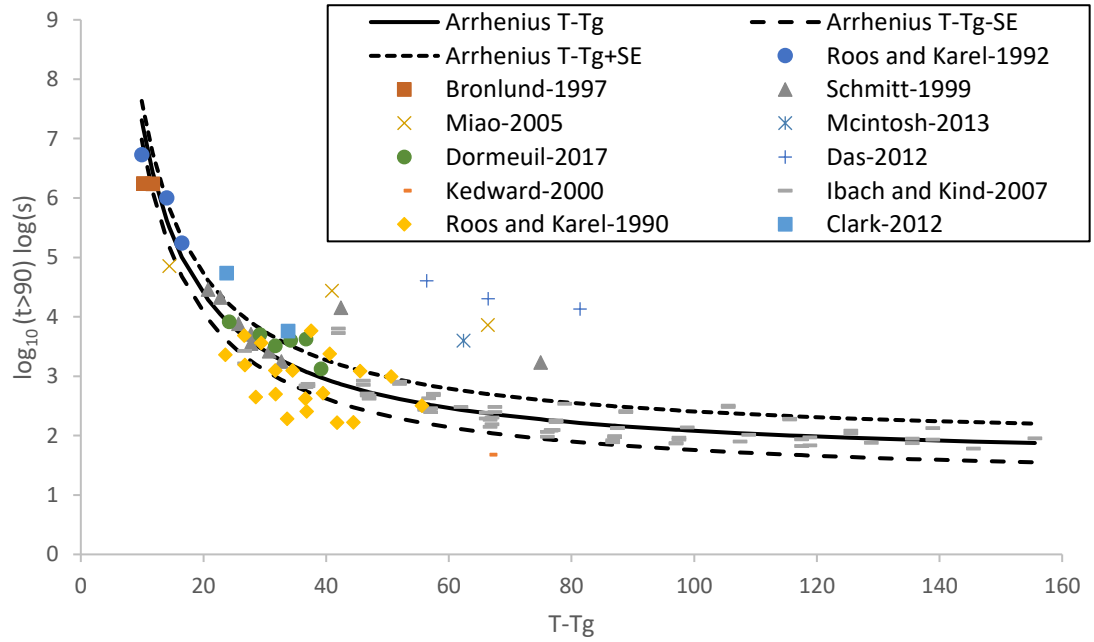

Figure 3-16: Time to 90% Crystallization versus T-Tg including predictions using Arrhenius T-Tg predicted Avrami rate constants with standard error limits.

3.7 WLF Model fitting

The William-Landel-Ferry (WLF) equation was fitted to the crystallization time versus T-T_g results by regression of the linearized form (CEAS, 2018) to obtain the four constants (of which 3 are independent). T_k was selected to off-set the data to the lowest literature calculated T-T_g. As with the Arrhenius T-Tg model, data derived from Das and Langrish (2012) and Miao and Roos (2005) was excluded to improve the fit. As the WLF equation does not rely on Avrami kinetics it was also fitted and compared to the >99% crystallization data.

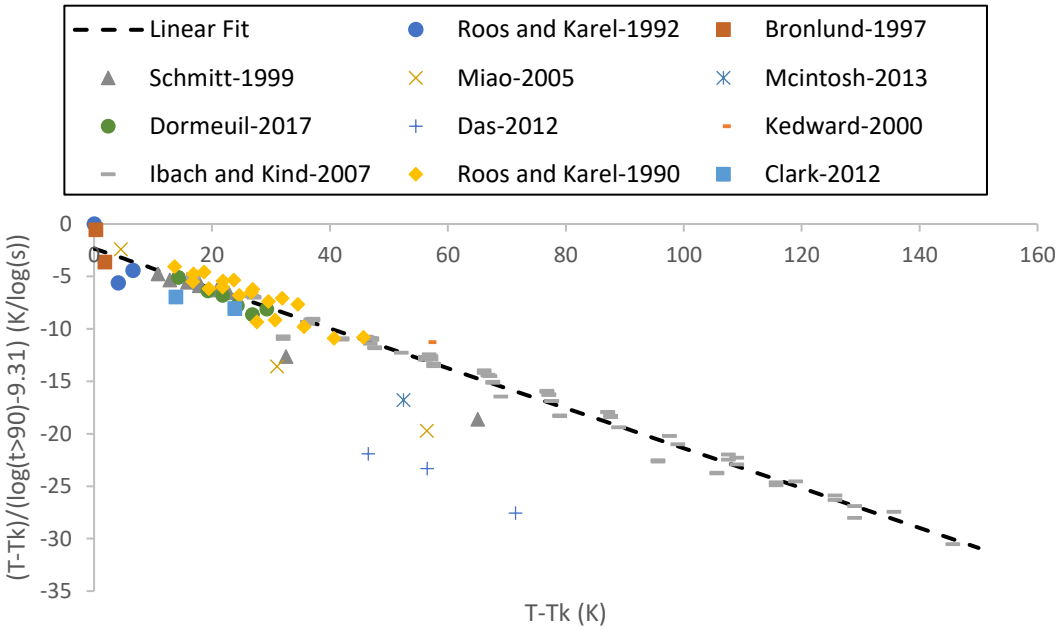

Figure 3-17: WLF fitting plot for the time to 90% crystallization and T-Tg

The WLF model and fitting constants are given below:

$$\log_{10}(t_{cr}) - \log_{10}(t_k) = \frac{-C_1 * (T - T_k)}{C_2 + (T - T_k)} \tag{3-6}$$

$$T_k = T_g + k$$

Where the optimized constants are:

- C_1 = 5.26±0.08 and 4.97±0.08 for the t_{90} and t_{99} models respectively, with standard error.
- C_2 = 12.34±0.9K (±5.5 SE of fit) and 11.24±1.0 (±5.7 SE of fit) for the t_{90} and t_{99} models respectively, with standard error.
- $\log_{10}(t_k)$ = 6.73 log10(s) is considered the log of the crystallization time at $T = T_k$.
- k= 9.31K

The standard error of the linear model affects the constant C_2 which is calculated from the intercept, this is shown in brackets along the normal standard error.

The models fit well with the crystallization time versus T-Tg data across the entire range in both cases as can be seen in Figure 3-18 and Figure 3-19. This is reflected in the calculated r^2 values of 0.7305 and 0.7310 for the 90% and 99% crystallization models respectively (improving to 0.8438 and 0.8440 when data not used to fit it is excluded). The fit for the 90% crystallization time is similar to that of the Arrhenius T-Tg model.

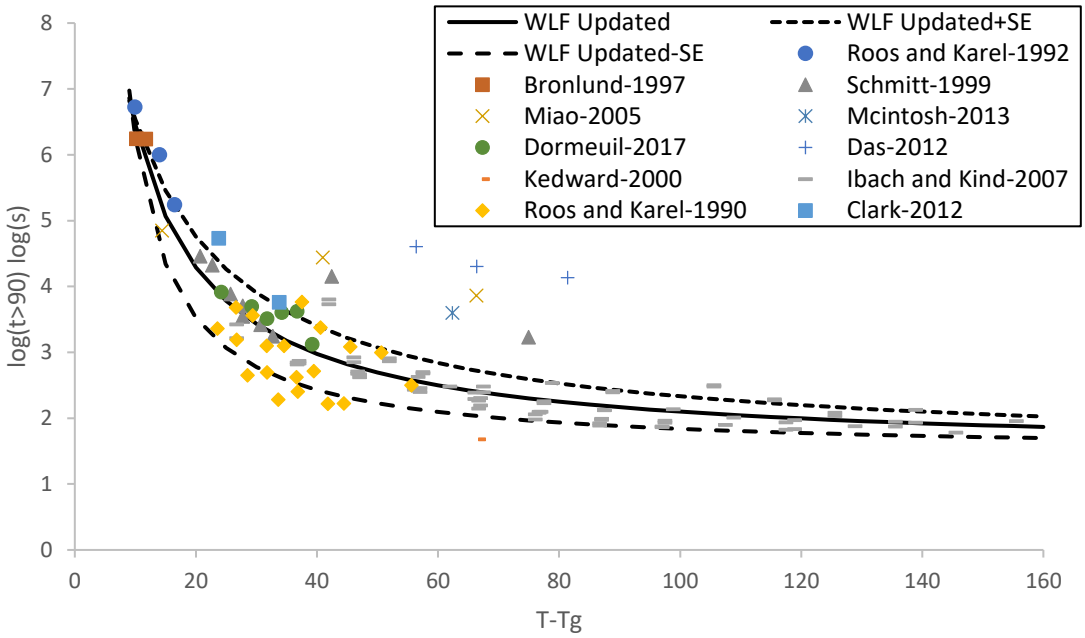

Figure 3-18: Time to 90% Crystallization versus T-Tg including predictions using WLF improved 90% constants with standard error limits.

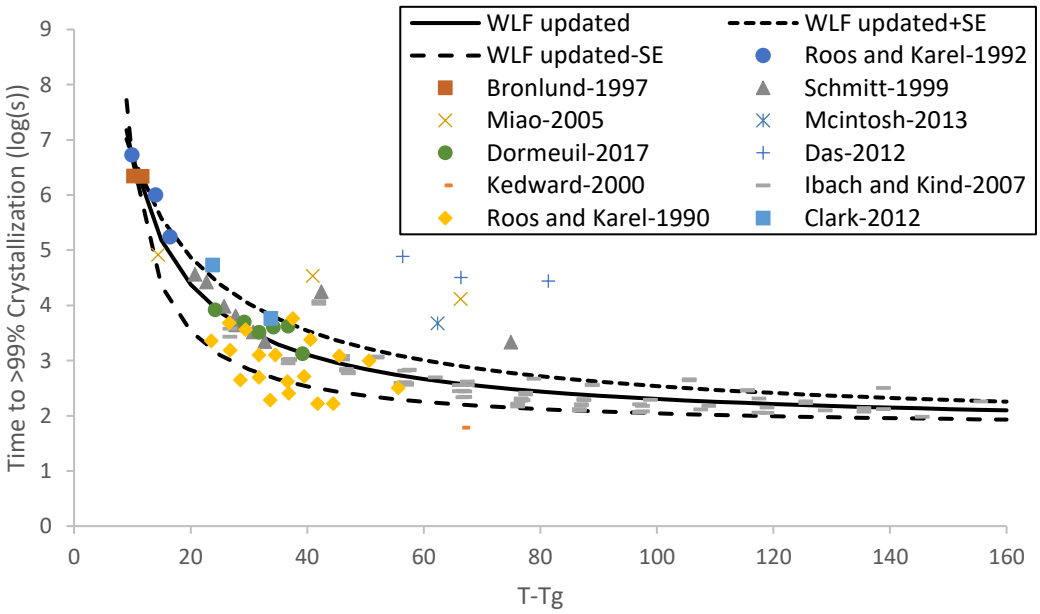

Figure 3-19: Time to 99% Crystallization versus T-Tg including predictions using WLF improved 99% constants with standard error limits.

3.8 Regions of Fit

As the activated state and Ibach&Kind-Arrhenius models have regions in which they provide a very good fit it is useful to compare them further to the WLF and Arrhenius T-T_g model.

To better compare these models and their regions of applicability for predicting the crystallization time the error in the estimates was plotted against the water activity, temperature, and T-Tg the estimate was based on. This was done using the absolute difference between the $\log_{10}$ of the predicted 90% crystallization time and that of the literature time. The difference was averaged across evenly spaced increments of each parameter (i.e. between 10 and 20°C, 20 and 30°C etc.) and plotted against the average value for that parameter. The actual error range will depend on the predicted value as the error is accounted for before the logarithm is reversed.

Figure 3-20 shows this difference from the prediction against T-Tg. The models fall into two groups; the Activated-state and Arrhenius-Ibach models which were both primarily fitted using data from Ibach and Kind (2007), and the Arrhenius T-Tg and WLF-updated models which were fitted using the data collected and calculated in section 3.2. Each group is limited in accuracy by the data it was fitted to, the previously existing models being increasingly inaccurate beyond 50K T-Tg, the activated state and Arrhenius-Ibach models becoming more accurate as the T-Tg increases, and the new T-Tg dependent models providing a good estimate across the range.

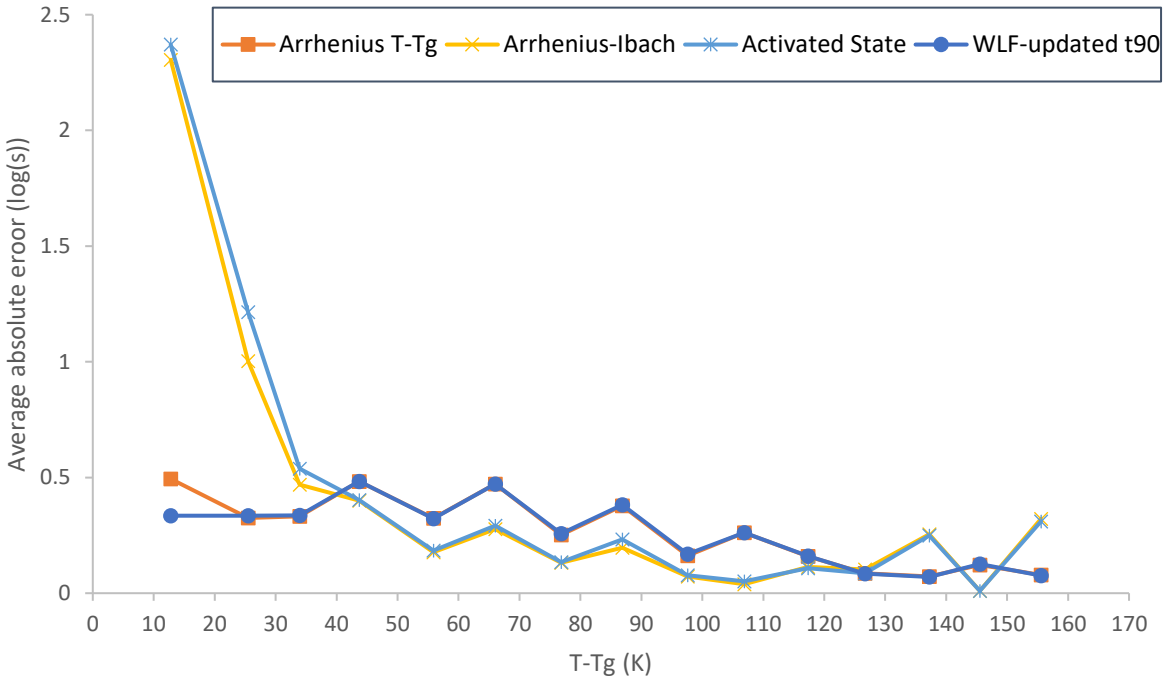

Figure 3-20: Average prediction error versus T-Tg

Figure 3-21 shows the difference from the prediction against the experimental water activity. The new T-Tg methods provide generally good predictions. The Activated-State Arrhenius-Ibach models provide a reasonable prediction at or above 0.2aw, values below this being

beyond the fitted range, becoming more accurate than the new T-Tg prediction methods above 0.7aw.

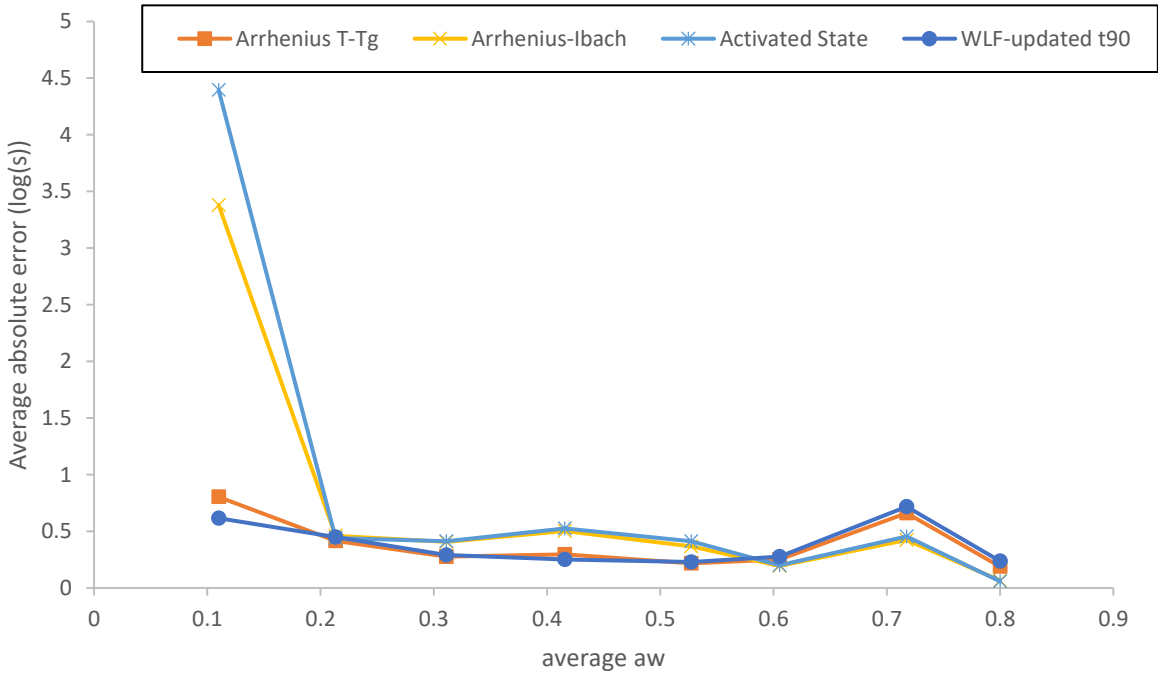

Figure 3-21: Average prediction error versus water activity

The results for the prediction error against the experimental temperature in Figure 3-22 are more scattered than the other parameters, this is thought to be because the aw conditions are not considered. All models are relatively poor below 20°C with the Arrhenius-Ibach and Arrhenius T-Tg models being the best. The Activated-state and Arrhenius-Ibach models provide estimates comparable or better than the new T-Tg models in the range of 50-80°C. The better prediction comes from the ability of the model to explain some of the variation in the crystallization time at constant T-Tg due to differing temperature and aw conditions.

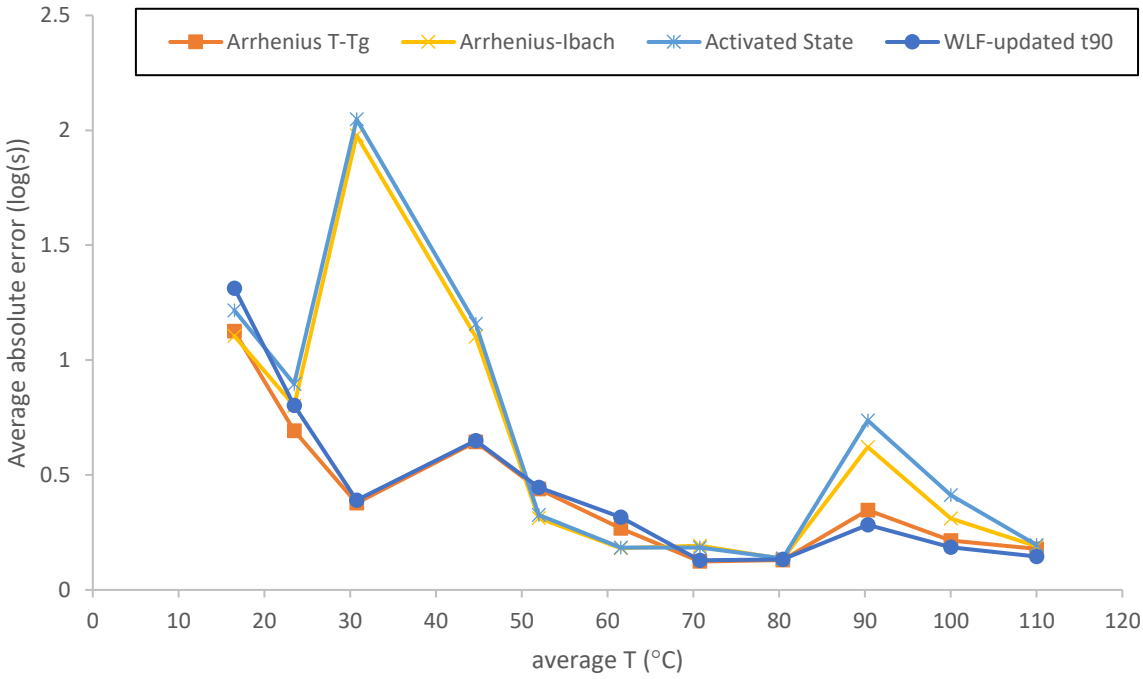

Figure 3-22: Average prediction error versus temperature

Across all three error plots (Figures Figure 3-20, Figure 3-21, Figure 3-22) the Arrhenius-Ibach model performs better than the Activated-state model.

The Arrhenius T-Tg model performs similarly to the WLF-improved model except for below 0.2aw where it is significantly poorer, above 0.7aw it is significantly better, below 30°C where it is a significant improvement and above 90°C it is significantly worse. In general terms the Arrhenius T-Tg model might be expected to perform better at low temperature high water activity conditions while the WLF-improved would provide a better prediction under low water activity high temperature conditions.

3.9 Recommendations and Implications for Project

Based on the comparisons of the predictions it is recommended that the Arrhenius T-Tg model is used to predict the Avrami rate constant. Above 0.2aw and 50°C the Arrhenius-Ibach model may also be used and the predictions compared.

For predicting the time for complete crystallization time, the WLF-improved model with the 99% fitted constants should be preferred as the Avrami model is poorer at predicting the time to achieve greater than 90% crystallization. The Arrhenius-T-Tg model may be used for comparison. In each case the standard error range provides a prediction of the time range in which crystallization is possible to very likely.

These models are useful in the context of this project for predicting whether crystallization of amorphous lactose is possible during the drying process. Figures Figure 3-23 and Figure 3-24 show the predicted time versus water activity curves produced over the temperature range present in a fluid bed drier for the Arrhenius T-Tg or WLF-updated model. Figure 3-24 is preferred as the Avrami model typically has been found to not fit well beyond 90% accomplished crystallization (see section 4.2.2). These predictions do not include induction time, so the predictions could be better considered to be if crystallization is possible rather than if it is likely.

For example, Figure 3-24 predicts that for the crystallization time to be reduced below a 15min a fluidized bed drier at 90°C needs to operate at a water activity of 0.23 or greater would be required. Between the lower and upper standard error limits it would be recommended to use the Arrhenius T-Tg model with the Avrami equation to estimate the faction of crystallization likely to occur within the desired timeframe after induction. Above the upper standard error limit complete crystallization within that timeframe after induction would be very likely.

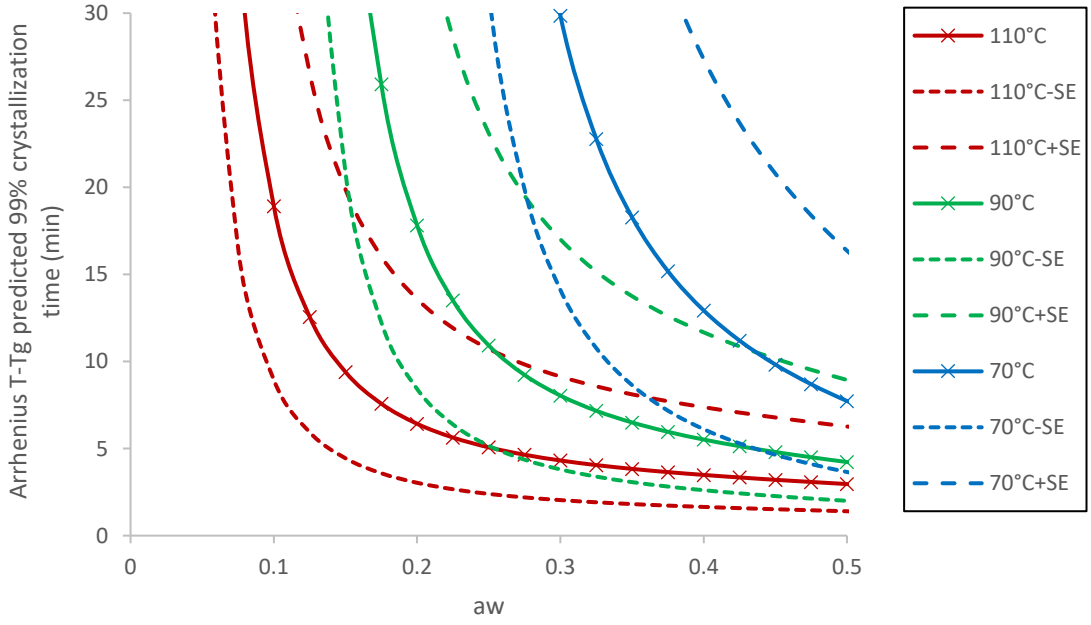

Figure 3-23: Arrhenius T-Tg model predicted 99% crystallization times versus water activity at different temperatures

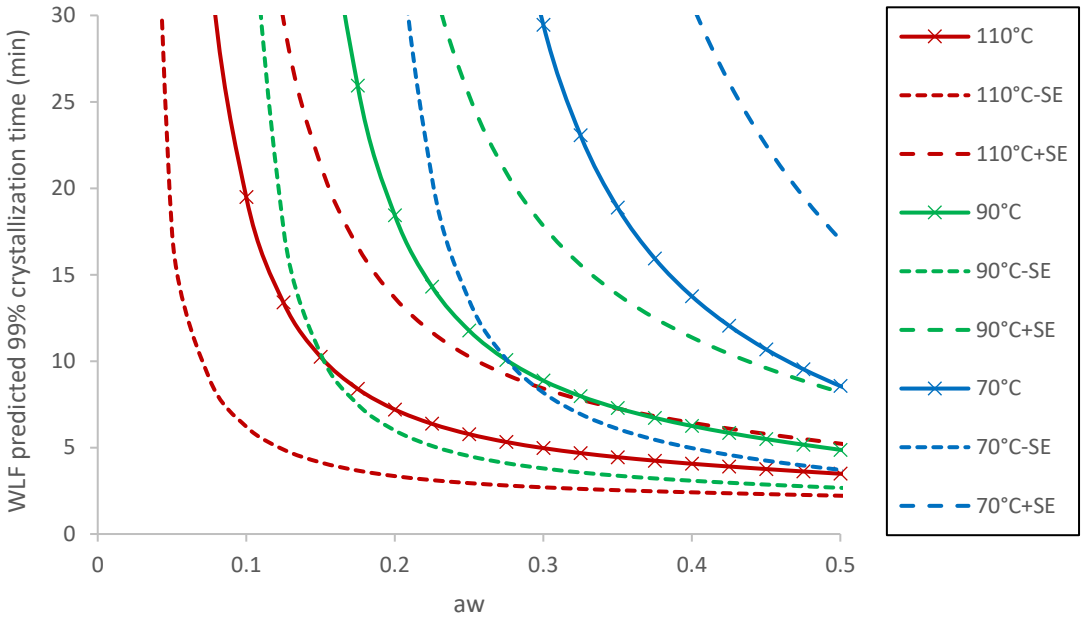

Figure 3-24: WLF-improved model predicted 99% crystallization versus water activity at different temperatures

4 Method Development

Two forms of powdered amorphous lactose were used for experimental work. They differed in the method of their production: freeze-dried and spray-dried. The spray-dried powder was used for the majority of the analysis and the freeze-dried sample was analysed to compare to the results of Dormeuil (2017). These powders were analysed to confirm their amorphicity and determine the particle size distributions.

Freeze-dried amorphous lactose was produced by Dormeuil, 2017 following the method of Clark (2012) by using burette to drop a 30wt% solution of pharmaceutical grade α-lactose from Fonterra into liquid nitrogen. The particles were then stored in a -80°C freezer for 24h before sublimation at -40°C and <0.1 millibar for 4 days in a lab-kits FD-10F-TP2 vacuum freeze drier followed by a gradual temperature increase over 3 days. The lactose was then ground to a lower particle size in a controlled-humidity glove box where the RH below 10%.

The spray-dried amorphous lactose was produced using the GEA Niro spray dryer operating with an inlet air flow of ~10.5m/s at 200°C. The feed rate was 30g/min of a 30%wt solution of pharmaceutical grade α-lactose monohydrate from Fonterra. After production the sample was dried at 105°C for 24h before being bagged (Clark, 2012).

4.1 Particle-Size Characterization

The particle size distributions of the samples were obtained using the Malvern Mastersizer 3000 with isopropan-2ol used as a dispersant. Prior to characterization the samples were sieved in a controlled humidity glove box at 3%RH to remove any agglomerated particles over 2.8 mm. The small volume sample unit was used with the stirrer set to the 1 o'clock position (Ripberger, 2010) and it was rinsed with isopropanol between measurements. A refractive index of 1.5330 was used for lactose and 1.3800 was used for the isopropanol. Each sample was characterized using 10 measurements made once an obscuration of 40-50% was reached. Blank runs without any sample confirmed that the sample unit was appropriately rinsed, and that the background was normal. This process was repeated for three trials of both spray-dried and freeze-dried lactose.

The results (Figure 4-1 and Figure 4-2) show good agreement between the trials for each sample and that the median particle size of the freeze-dried lactose is much higher at 316.7µm compared to just 13.9µm for the spray-dried sample.

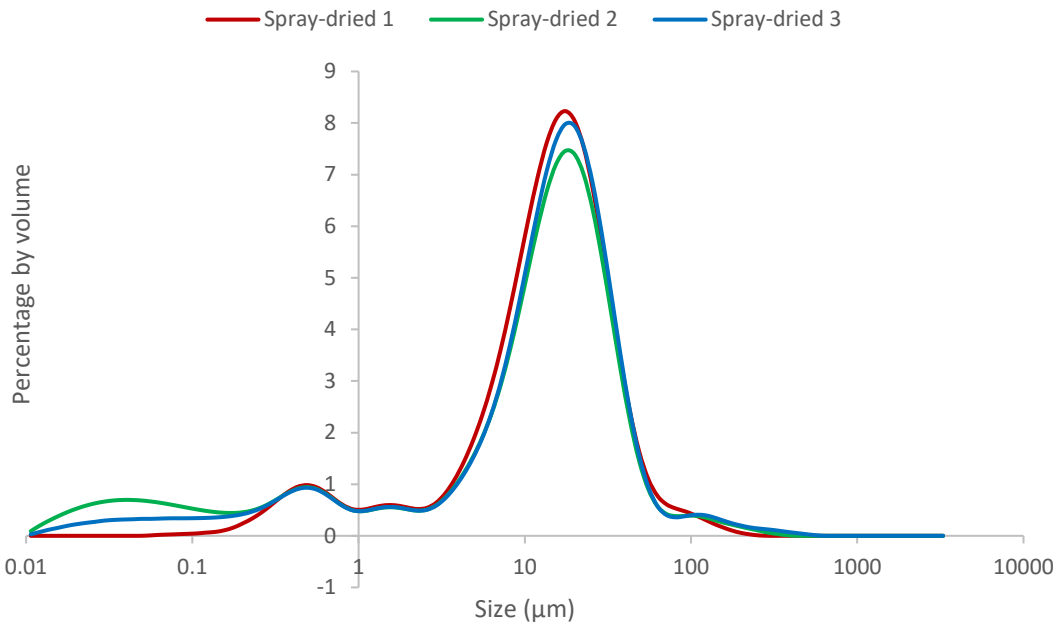

Figure 4-1: Particle size distribution for the spray-dried sample

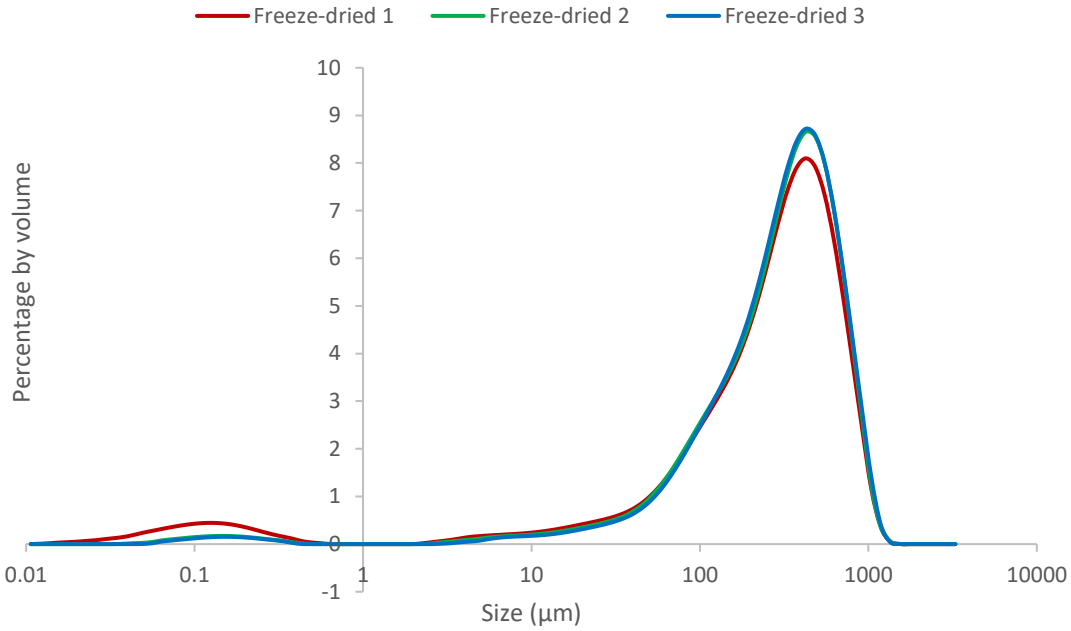

Figure 4-2: Particle size distribution for the freeze-dried sample

4.1.1 Storage and Desiccation

The samples were received having been sealed under low humidity (~0.11 aw) and once opened were stored in a desiccator over silica gel and under vacuum.

Following particle-size distribution characterization the samples were stored as a thin layer in Petri dishes over regularly replenished phosphorous pentoxide (P_2O_5) inside a desiccator. The humidity over the P_2O_5 inside the desiccator was periodically verified to remain near zero by using iButtons (Integrated, 2015).

The mass of the samples was recorded weekly during desiccation over P_2O_5 until after 3 weeks the weekly mass loss was low enough (<0.1%) to be considered stable. The weekly mass change is shown in Figure 4-3, the mass loss for the two samples is very similar which could be expected given that they had the same prior storage conditions.

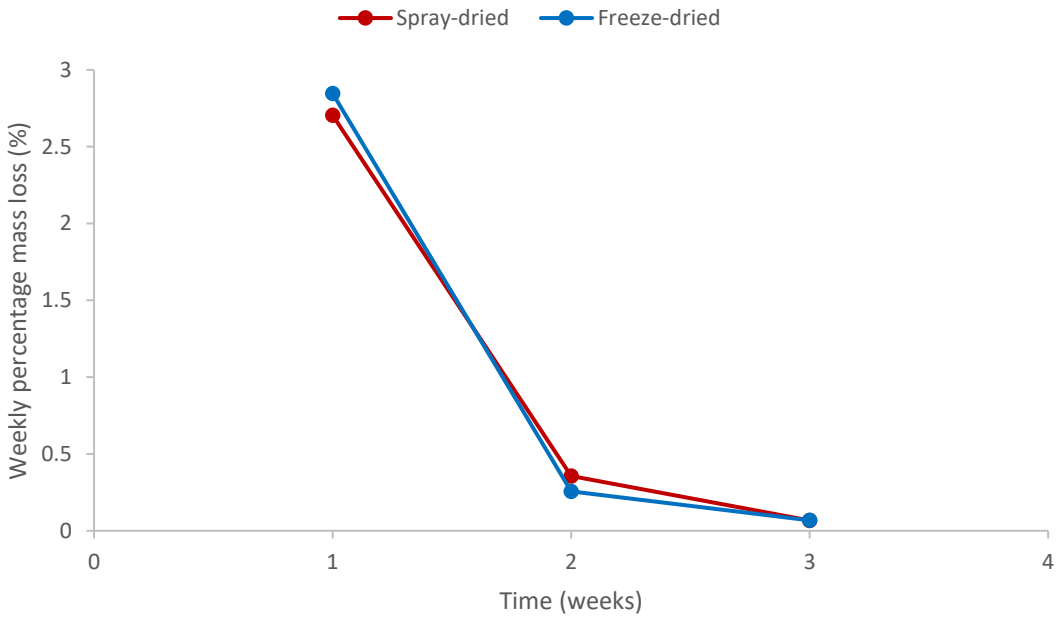

Figure 4-3: Weekly percentage mass loss for spray-dried and freeze-dried amorphous lactose desiccated above P_2O_5. Starting masses were 7.7325g for the spray-dried sample and 4.8395g for the freeze-dried sample.

Where possible the samples were transported in a desiccator and handled in a humidity-controlled glove box to prevent adsorption which could cause inconsistencies between trials or unwanted crystallization.

4.1.2 Polarized Light Microscopy

Both samples were examined along with a reference of α-lactose monohydrate, under cross-polarised light using an Olympus BX53 light microscope to confirm their amorphous nature. Photos were taken using an Olympus XC50 camera. No crystalline material was detected in either sample, example photographs are contained in appendix 9.2.1.

4.1.3 X-ray Powder Diffraction

An x-ray diffraction pattern was recorded for the spray-dried sample with a Rigaku Spider X-ray diffractometer using Cu Kα radiation -5 to 5 oscillation, and a five-minute exposure time. The pattern is shown in Figure 4-4 and no significant peaks are observed at any of the characteristic angles, such as those in Table 2-4, indicating that no crystalline lactose is present.

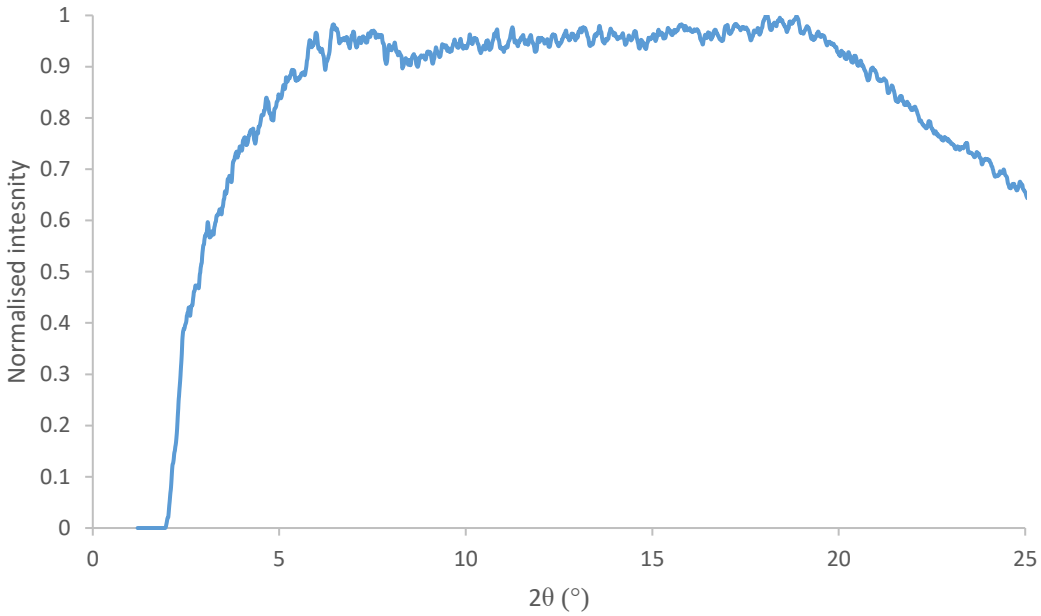

Figure 4-4: X-ray diffraction pattern for spray-dried amorphous lactose

4.2 Simultaneous Thermal Analysis (STA) Method Development

Simultaneous Thermal Analysis (STA) measures both the weight changes (TGA) and the heat flow (DSC) of a sample under a controlled atmosphere as a function of either temperature or time. Crystallization of amorphous lactose has commonly been measured by either gravimetric (Dynamic Vapor Sorption) or calorimetric (Differential Scanning Calorimetry, Isothermal Microcalorimetry) methods. Thermogravimetric analysis has been used to investigate the amorphous content (Listiohadi et al., 2009) but has not apparently been applied to crystallization kinetics.

The advantage of an STA method is that during crystallization moisture is expelled (measured by gravimetric methods) which is an endothermic process partially controlled by diffusion. The crystallization, or rearrangement of the molecules to a lower energy state, is an exothermic process (measured by calorimetry). Thus, gravimetric methods may not consider crystallization occurring where the mass loss is diffusion limited and calorimetric only record the net change in enthalpy which is a product of the exothermic molecular rearrangement and the endothermic desorption. By measuring both heat flow and mass changes simultaneously the net enthalpy change can be determined as well as the endothermic enthalpy change due to desorption can be estimated and the true enthalpy of crystallization calculated. One disadvantage of STA analysis is the small sample size able to be analysed (on the order of 10 mg).

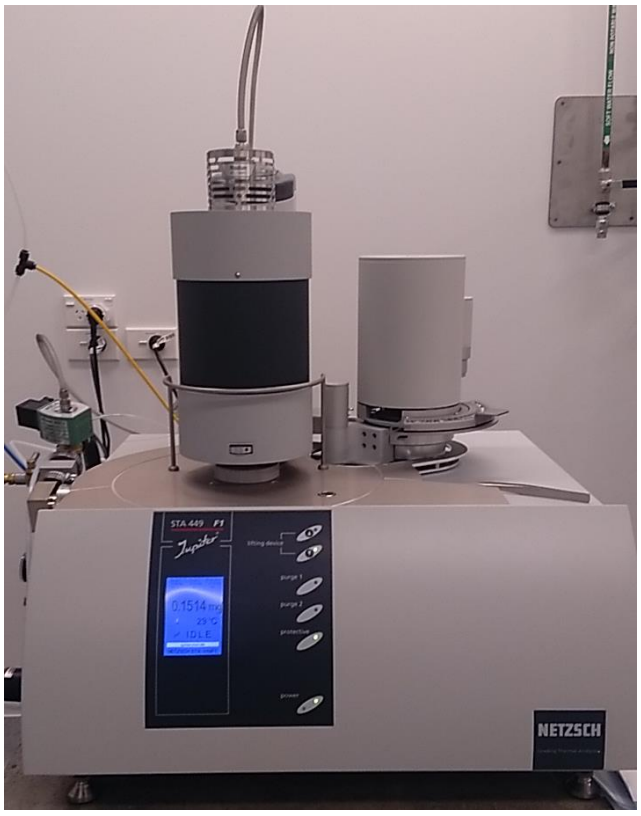

Figure 4-5: Netzsch STA 449 F3 Jupiter at Massey University

4.2.1 Examination of Dormeuil (2017) STA Results

Dormeuil (2017) used a Netzsch STA 449 F3 Jupiter to conduct simultaneous thermal analysis on the crystallization of freeze-dried lactose samples under different humidity and temperature conditions.

Temperature and humidity were controlled by using the copper furnace option for the STA 449 F3 Jupiter alongside a Prolumid (MHG32) Modular Humidity Generator and a Netzsch (TRG 004) temperature controller. The STA 449 F3 Jupiter itself allows precise control over the sample temperature over time while recording the heat flow and mass changes. The MHG32 similarly allows precise control of the humid air flow and thus humidity above the sample. The MHG32 is operated at 150ml/min air flow. The TRG 004 allows control over the temperature at which the humid air is produced. The TRG 004 also controls the temperature at the bottom of the chamber to prevent condensation in the balance. As a humidity generator was used the type E sample carrier was used along with the humidity shield. Figure 4-6 shows the relation of the air flows to the sample inside the furnace.

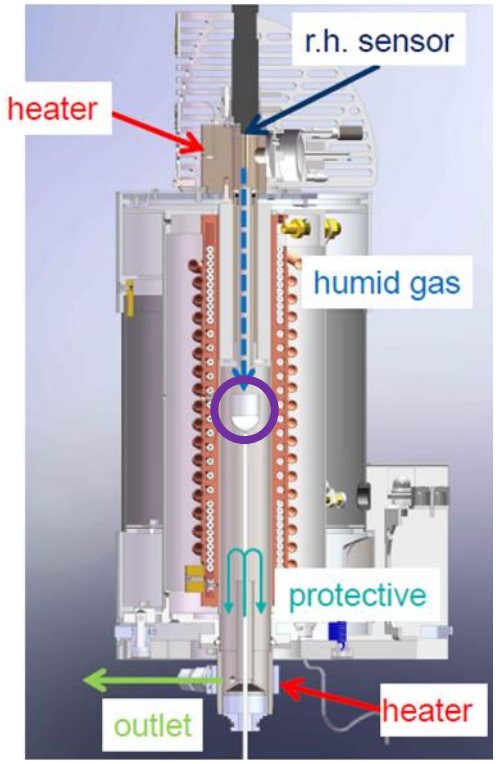

Figure 4-6: Cutaway view of the STA 449 F3 Jupiter with the humidity option showing the gas flows, the approximate location of the sample is circled in purple. Reproduced from Netzsch (2016).

The crystallization of freeze-dried amorphous lactose from section 4 was examined under constant T-Tg conditions. The samples were weighed into pre-weighed 25µl aluminium crucibles (Netzsch 6.239.2-64.5.01) with another aluminium crucible of known weight used as the reference for DSC measurement. The method used to achieve crystallization at constant conditions, controlling the theoretical T-Tg, was broadly to hold the sample at 25°C and 0%RH for 1 hour, ramp the sample to the target relative humidity, maintain the target relative humidity for an hour at 25°C, then ramp the temperature at 10K/min to the target value maintaining the target conditions until crystallization is complete before reducing the humidity to 0%RH for 15mins prior to removing the crystallized sample. This is accomplished using set

programs for the STA and TGA synchronised by an electronic trigger cable and manually increasing the set temperature for the humid air flow when the temperature increase occurs. For this method to work the desired relative humidity must not cause crystallization before the temperature is increased.

For each set of conditions, a blank run was conducted with an empty crucible to produce a correction file.

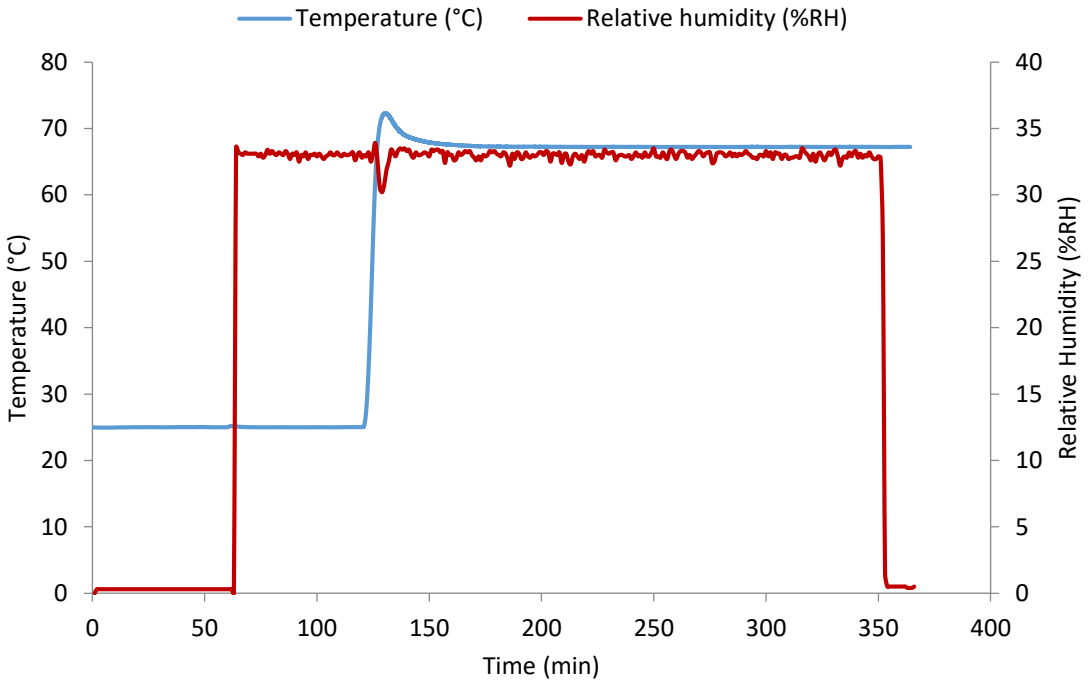

Figure 4-7: Recorded sample conditions over time for a trial at T=67.24, RH=33%, raw data from Dormeuil (2017)

The results obtained by Dormeuil (2017) were compared but not processed or modelled. To assess the suitability of the method for determining the true enthalpy of crystallization, measuring kinetics, and tracking the moisture content Dormeuil's results were analysed here. If the processed results agreed with a literature enthalpy of crystallization value for dry amorphous lactose as well as literature kinetic results it was considered that the method would be advantageous for investigating directional crystallization at dryer conditions.

For exothermic heat flows enthalpy changes are positive and endothermic changes are negative. Crystallization, the process of interest, is exothermic. Heat flow is determined relative to the initial sample mass at time 0.

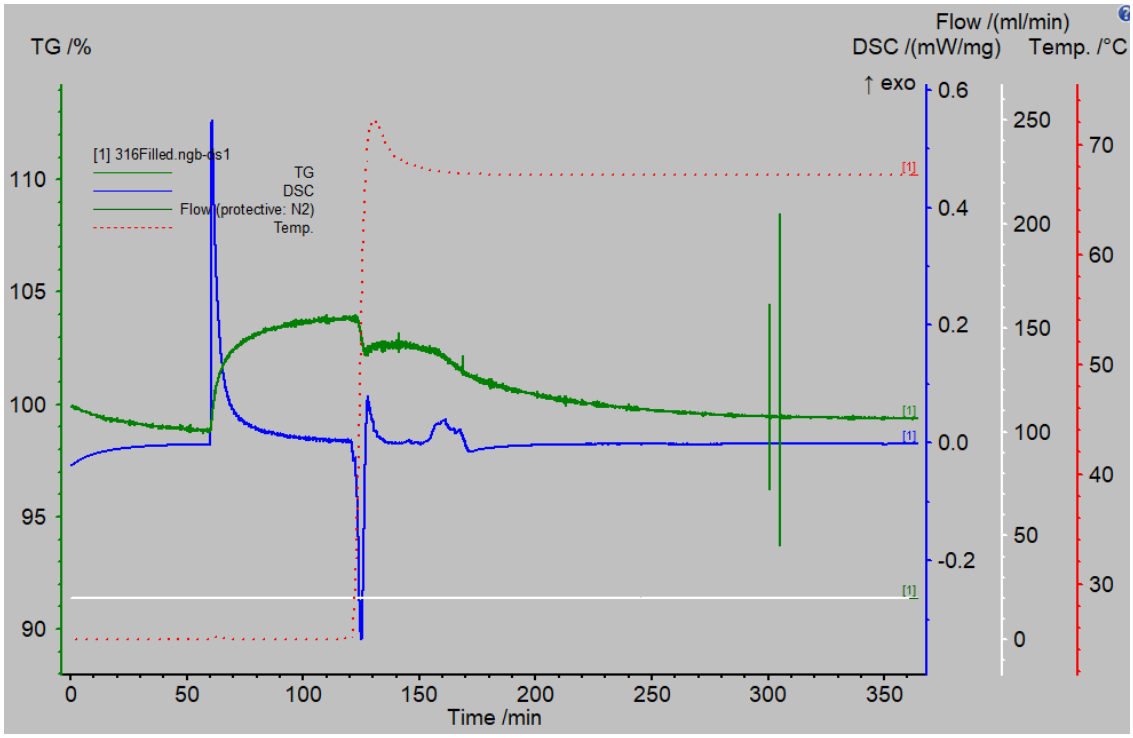

Figure 4-8: Raw STA data for a trial at T=67.24, RH=33%, raw data from Dormeuil (2017)

The following processed data was all determined as part of this project using the previously obtained results from Dormeuil (2017). All results had their associated correction file subtracted and the DSC and sample mass signals smoothed using method "4" within the NETZSCH Proteus Thermal Analysis software. Smoothing was required due to large amounts of noise in the mass signal and method "4" was found to consistently provide reasonable smoothing without loss of information. The corrected and smoothed data (e.g Figure 4-9) was then exported to excel for processing.

Figure 4-9 clearly shows an exothermic heat flow and the start of mass loss at 154min. These are both indications of crystallization, and the changes are used independently to monitor crystallization in calorimetric and gravimetric methods. Of the two indicators the point of mass loss is considered the time at which crystallization is induced (t_0) and the difference between this time and the time at which the conditions were changed is the induction time (t_{ind}). The mass loss was chosen as it consistently prominent across the trials. t_0 is later used to zero the processed crystallization data.

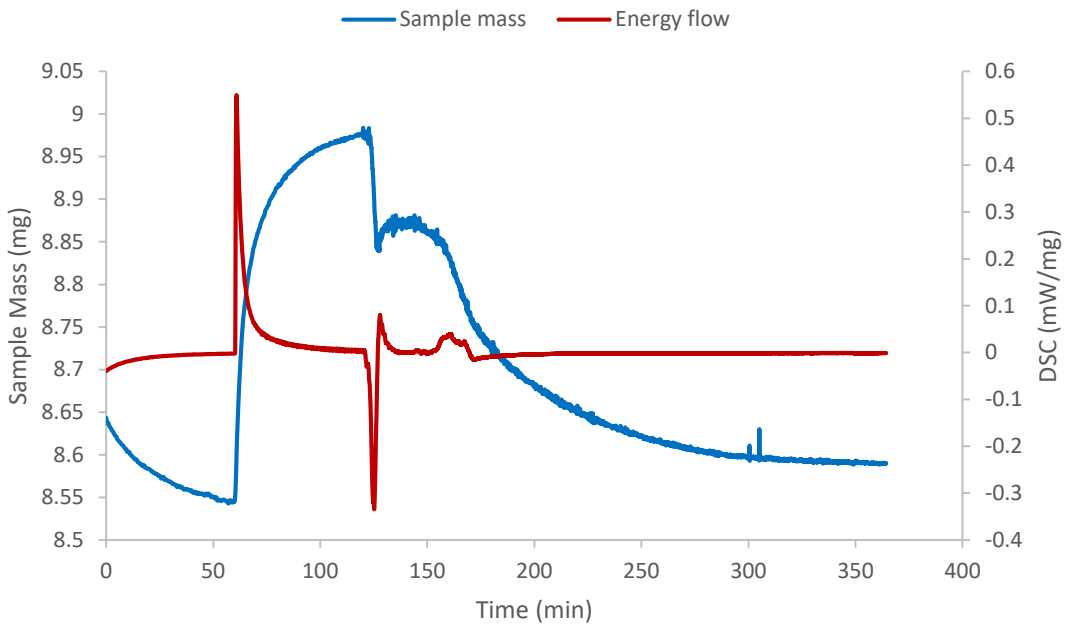

Figure 4-9: Corrected and smoothed mass and heat flow results over time for a trial at T=67.24, RH=33%, raw data from Dormeuil (2017)

Once corrections are applied the STA data is processed to isolate the enthalpy change due to crystallization. This is broken into four stages; integration of the DSC signal, calculation of the enthalpy of vaporization, subtraction of the enthalpy of vaporization from the integrated DSC, and correction of the result. The STA data is recorded every 3s during isothermal stages and every 0.6s during dynamic stages. Calculations were made for each time interval and then summed for the cumulative or net change over time.

Integration of the DSC signal

The DSC signal was integrated each time step using the trapezoidal rule approximation (equation (4-1)) which was found to give comparable results to Simpson's rule when compared for one trial.

$$[\Delta h_{DSC}]_{t_n}^{t_{n+1}} = \int_{t_n}^{t_{n+1}} DSC(t)\, dt \approx 0.5(DSC_{n+1} + DSC_n) \cdot (t_{n+1} - t_n) \quad (4\text{-}1)$$

- Δh_{DSC} is the enthalpy change of the sample recorded by the DSC signal on an initial mass basis (J/g_0)
- DSC is the recorded heat flow from the sample (mW/mg_0)
- t_n is the time at the start of the period being integrated (s)
- t_{n+1} is the next recorded time following t_n (s).

Calculation of latent heat of vaporization

It is assumed that all mass change is due to moisture loss/gain. This is considered to be a realistic assumption as the STA balance is enclosed, the gases used are humidified instrument air and nitrogen, and the temperatures are too low for any decomposition to occur. The

enthalpy change due to the latent heat of vaporization for the water loss/gain was calculated using equation (4-2).

$$\left[\Delta h_{vap}\right]_{t_n}^{t_{n+1}}, \Delta h_{vap}\ for\ t_n\ to\ t_{n+1}\ = \frac{L(T_{t_{n+1}})\left(m_{t_{n+1}} - m_{t_n}\right)}{m_0} \tag{4-2}$$

- Δh_{vap} is the enthalpy change of the sample calculated using the latent heat of vaporization on an initial mass basis (J/g_0)
- $L(T_{t_{n+1}})$ is the specific latent heat of vaporization (Moran, Shapiro, Boettner, & Bailey, 2010) at the temperature at t_{n+1} (J/g_{water})
- m_{t_n} is the mass at the start of the period being integrated on a wet basis (mg_{wet})
- $m_{t_{n+1}}$ is the mass at the next recorded time following t_n on a wet basis (mg_{wet})
- m_0 is the sample mass at the start of the measurement on a wet basis (mg_0)

Subtraction

The enthalpy of vaporization is subtracted from the integrated DSC over each interval (equation (4-3)) the cumulative change or net change in enthalpy at a given time is calculated using equation (4-4).

$$\Delta h_{net}\ for\ t_n\ to\ t_{n+1}\ = [\Delta h_{DSC}]_{t_n}^{t_{n+1}} - \left[\Delta h_{vap}\right]_{t_n}^{t_{n+1}} \tag{4-3}$$

$$\Delta h_{net}(t_x)\ = \sum_{n=0}^{n=x-1} [\Delta h_{DSC}]_{t_n}^{t_{n+1}} - \left[\Delta h_{vap}\right]_{t_n}^{t_{n+1}} \tag{4-4}$$

- $\Delta h_{net}(t_x)$ is the difference between the recorded enthalpy change and the calculated latent heat of vaporization of the sample at t_x (J/g_0)
- t_x is the xth recorded time value (s)

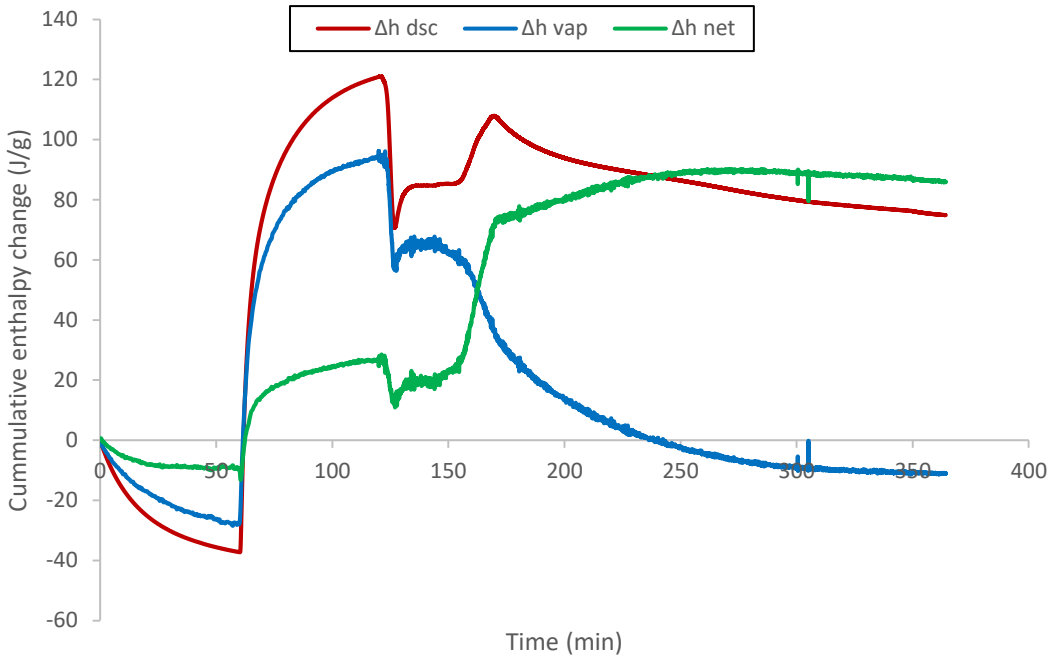

Figure 4-10: Calculated $\Delta h_{DSC}, \Delta h_{vap}, and\ \Delta h_{net}$ over time for a trial at T=67.24, RH=33%. Raw data from Dormeuil (2017)

Correction

Unexplained changes in Δh_{net} during the desorption and adsorption segments were noted across all trials (shown in Figure 4-10). They needed to be accounted for to calculate the enthalpy of crystallization. A potential explanation considered was a net isosteric heat of sorption (q_{st}) effect, described in section 2.1.1.

$$q_{st} = \Delta h_{sorption} - L \tag{4-5}$$

- q_{st} is the net isosteric heat of sorption (J/g_{water})
- $\Delta h_{sorption}$ is the observed enthalpy change during the sorption process occurring between t_1 and t_2 (the beginning and end time of the sorption process); $\Delta h_{sorption} = [\Delta h_{DSC}]_{t_1}^{t_2} \times \frac{m_0}{m_{t2} - m_{t1}}$ (J/g_{water})
- L is the specific latent heat of vaporization (Moran et al., 2010) at the given temperature (J/g_{water})

To model this effect and remove it to isolate the enthalpy changes not due to sorption effects, such as crystallization, the q_{st} value was calculated for the periods of adsorption and desorption without crystallization, as well as the mass change over that period.

Zuo, Rhim, and Lee (2015) modelled the net isosteric heat of sorption in terms of the moisture content of the sample by an exponential function. A model based on the moisture content would allow the prediction of the q_{st} and the isolation of the enthalpy of crystallization (Δh_{cr}).

To determine the moisture content the dry mass of the samples was individually estimated. The estimations were based on an extended drying run at 0%RH and 25°C which went to

equilibrium. For that run 85% of the mass loss occurred within the first hour and for which was used in equation (4-6) to estimate the dry sample masses. This dry mass was used to estimate the moisture content over time for each trial and reasonable agreement was found with moisture contents predicted using the isotherm of Brooks (2000).

$$m_{dry} = m_0 + \frac{\Delta m_{1hr}}{0.85} \tag{4-6}$$

- m_{dry} is the estimated dry mass at 0aw, not accounting for bound moisture (mg_{dry})
- Δm_{1hr} is the recorded change in mass after one hour at 25°C and 0%RH (mg_{water})

$$MC(t) = \frac{(m_t - m_{dry})}{m_{dry}} + 0.01 \tag{4-7}$$

- $MC(t)$ is the moisture content at time t on an absolute dry basis, including 1% bound moisture from Brooks (2000) (g/g_{dry})
- m_t is the sample mass at time t on a wet basis (mg_{wet})

The calculated q_{st} values are shown in Figure 4-11 against the moisture content before the sorption process. The plot shows no clear relationship such as the expected exponential dependence (Zuo et al., 2015). The net isosteric heat of sorption can be estimated from isotherms at different temperatures using the Clausius-Clapeyron equation. For amorphous lactose there are conflicting reports of whether isotherms vary significantly with temperature between the work of Bronlund (1997), Fan and Roos (2015).

Because of this, it was decided to treat the difference between the enthalpy change of the sample due to sorption as an error and model this based on the change in moisture content occurring, this provided a strong linear fit (Figure 4-12). This correlation proved effective for reducing the effects of sorption processed on the calculated enthalpy change. The exact cause of the error was not determined and the net isosteric sorption of the sample could be a partial explanation but the consistently larger than expected DSC response could be the result of equipment error.

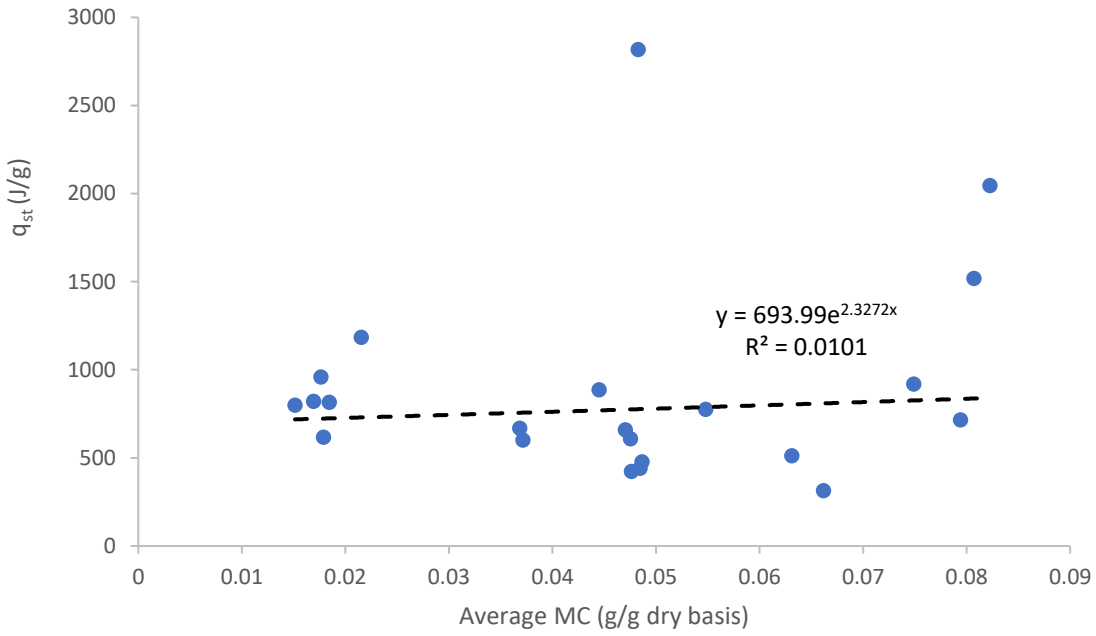

Figure 4-11: The calculated net isosteric heat of sorption versus the pre-ad/desorption process. Raw data from Dormeuil (2017)

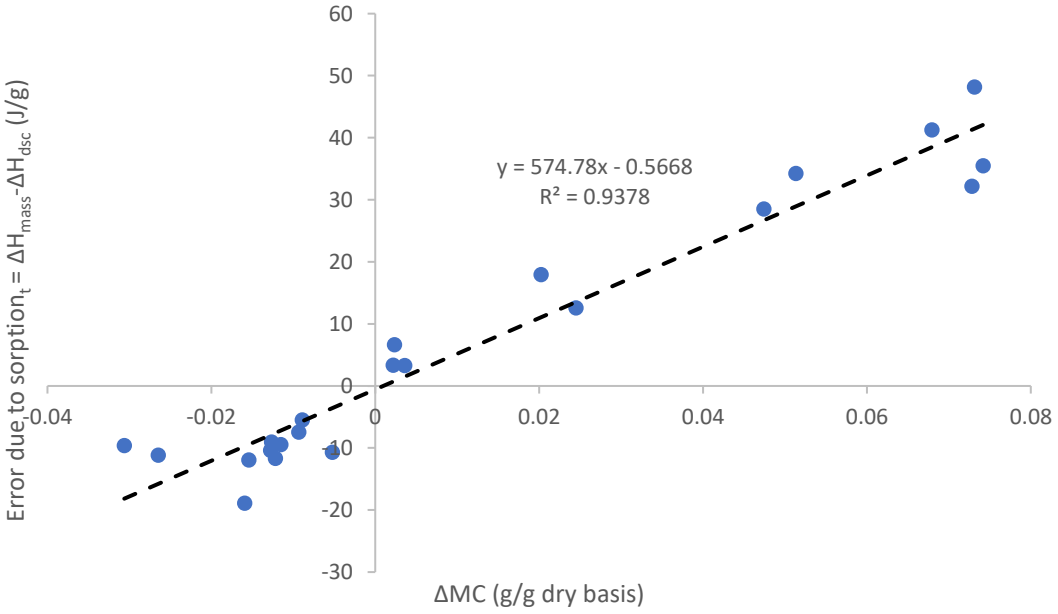

Figure 4-12: Observed error due to sorption versus estimated moisture content change. Raw data from Dormeuil (2017)

$$\Delta h_{error}(t_x) = \sum_{n=0}^{n=x-1} 574.8\left(\frac{m_{t_{n+1}} - m_{t_n}}{m_{dry\ est}}\right) - 0.5668 \quad (4\text{-}8)$$

- $\Delta h_{error}(t_x)$ is the predicted error in the Δh_{net} calculated at (t_x) (J/g_0)

Isolated Enthalpy of crystallization

With the error calculated for each time interval the corrected enthalpy change can be calculated, equation (4-9).

$$\Delta h_{corr}(t_x) = \Delta h_{net}(t_x) - \Delta h_{error}(t_x) \quad (4\text{-}9)$$

$\Delta h_{corr}(t_x)$ has removed much of the unexpected enthalpy changes and is shifted so that the point of induction occurs at 0 J/g (Δh_{zeroed}) allowing easier determination. Figure 4-13 shows the corrections applied to the example trial which has a calculated enthalpy of crystallization of 89.1 J/g_0.

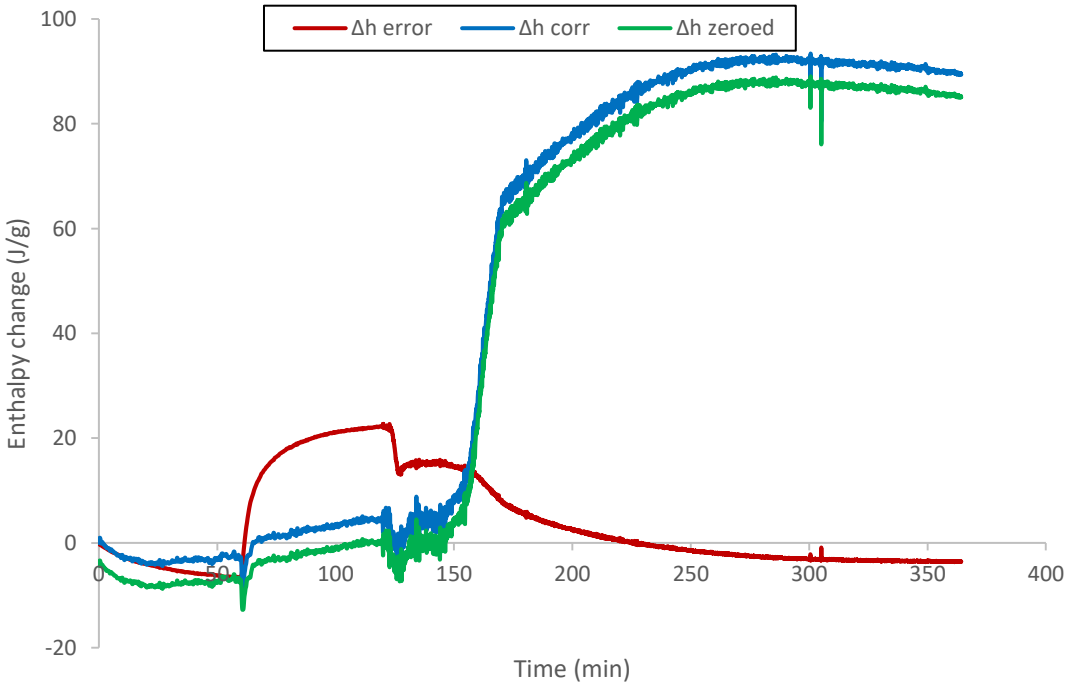

Figure 4-13: Calculated $\Delta h_{error}, \Delta h_{corr}, and\ \Delta h_{zeroed}$ over time for a trial at T=67.24, RH=33%. Raw data from Dormeuil (2017)

Δh_{zeroed} is considered the enthalpy change solely due to crystallization, Δh_{cr}. This is on a wet initial mass basis and was converted to a dry mass basis using equation (2-2).

$$\Delta h_{cr,dry\ basis} = \frac{\Delta h_{cr,\,m_0\ basis}}{1 - MC_0} \quad (4\text{-}10)$$

- MC_0 is the initial moisture content calculated using equation (4-8) for t=0 (g/g_{dry})

Modelling of Processed Data

It was assumed that each sample crystallized fully for the purposes of modelling, with complete crystallization having been achieved at the point where the maximum heat of crystallization was obtained. It was also assumed that the extent of crystallization which was directly proportional to the cumulative heat flow that drives crystallization.

$$Y_{cr} = \frac{\Delta h_{cr}(t_x)}{\Delta h_{max}} \tag{4-11}$$

- Y_{cr} is the fraction of the sample which has crystallized (g/g cr)
- Δh_{max} is the maximum observed Δh_{cr} (J/g_{dry})

The transformed crystallization data could then be used to determine the time for complete and 90% crystallization (t_{100} and t_{90} respectively). The time was zeroed so that $t_{avrami}=t-t_{ind}$ removing the induction time.

The Y_{cr} versus t_{avrami} data were used to construct Avrami plots (see Figure 4-14) with the Avrami model (equation (2-4)) fitted based on the t_{50} for 0.05< Y_{cr} <0.9 as described by Çelikbilek et al. (2012). The root mean square error (RMSE) between the model predicted and experimental $Y_{cr}$was then calculated. An example of experimental data and the fitted model is shown in Figure 4-15.

The Avrami plot (Figure 4-14) shows some non-linearity which is reflected in the fitted model, with regions of poor fit (Figure 4-15). Comparing the Y_{cr} calculated by enthalpy and that calculated by mass alone (appendix 9.2.2) the fit is poorer when also considering heat flow. There appear to be two distinct stages of crystallization. This could be related to the steps proposed by Burnett et al. (2006) with the first being auto-catalysed and the second being three-dimensionally diffusion limited.

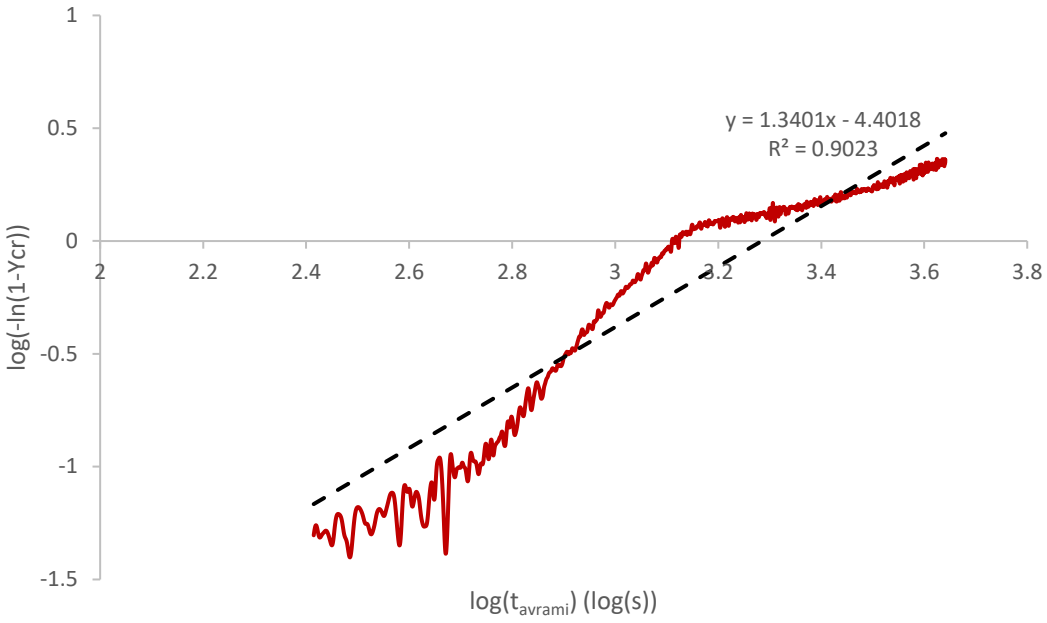

Figure 4-14: Avrami fitting plot for a trial at T=67.24°C, RH=33%. Raw data from Dormeuil (2017).

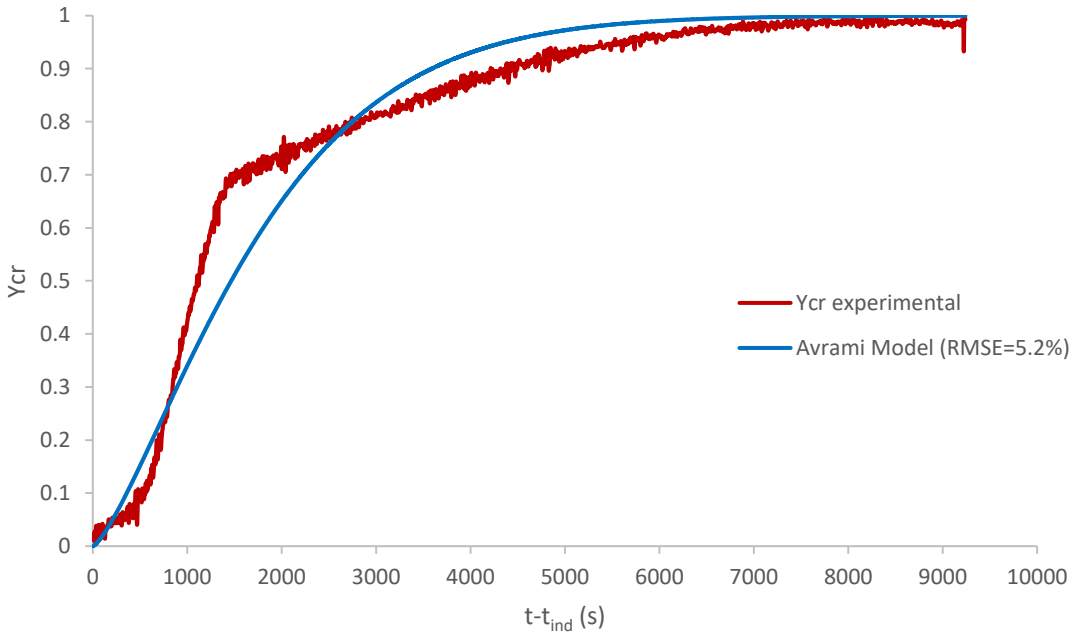

Figure 4-15: Y_{cr} experimental and Avrami-predicted ($k= 5.19 \cdot 10^{-4}\ s^{-1}$, $n= 1.340$) versus $t\text{-}t_{ind}$ data for a trial at T=67.24°C, RH=33%. Raw data from Dormeuil (2017).

4.2.2 Results Summary for Prior Work

Table 4-1 summarizes the experimental conditions and analysis results calculated from the data of Dormeuil (2017). Several general trends are observed with relation to the T-Tg of the experimental conditions at 0.44aw. The induction and duration of crystallization both reduce as the conditions become more favourable. For the fitted Avrami constants the constant n decreases with an increase in T-Tg and the rate constant appears to generally increase.

The calculated Δh_{cr} values are consistent for 0.44aw and with an average value of 99±3J/g_{dry} (StdDev). Δh_{cr}=99J/g_{dry} agrees reasonably with the result obtained by Lehto et al. (2006) of 105J/g for temperature induced crystallization of dry amorphous α-lactose. Other enthalpies of crystallization from 30-60 J/g from Table 2-7 were determined under humidity by DSC only so would not account for enthalpy changes due to moisture loss.

At 0.33aw however the Δh_{cr} values are significantly lower than the average which could indicate incomplete crystallization. The sample mass at 0.33aw and 67.2°C can be seen to have reached equilibrium or near-equilibrium before the end of the trial (Figure 4-9), at 62.2°C the sample mass did not equilibrate (appendix 9.2.2) and it is presumed that complete crystallization did not occur. By assuming Δh_{max}= 99J/g_{dry} the Avrami equation was refitted for the data and used to predict the t_{90} and t_{100} as Y_{cr} now only reached 0.75. The uncorrected values are shown with the new fitted and predicted values underlined below them. If these experiments were repeated and extended to ensure that crystallization was completed and confirm these results.

Table 4-1: Summary of experimental conditions and analysis results, predicted values underlined. Raw data from Dormeuil (2017).

T_{cr}	aw_{cr}	$(T-Tg)_{cr}$	m_{dry}	MC_0	t_{ind}	t_{90}	t_{100}	Δh_{cr}	n_{avrami}	k_{avrami}	$RMSE_{avrami}$
°C	-	K	mg_{dry}	g/g_{dry}	min	min	min	J/g_{dry}	-	s^{-1}	%cr
58.5	0.44	39.2	5.265	0.020	2	22	23	99.2	1.066	$1.02\cdot10^{-3}$	11.2
53.5	0.44	34.2	7.460	0.025	25	67	87	99.6	1.293	$4.80\cdot10^{-4}$	3.7
48.5	0.44	29.2	7.140	0.030	56	83	305	101.3	1.484	$3.74\cdot10^{-4}$	3.0
43.5	0.44	24.2	9.950	0.025	84	137	178	94.8	1.893	$1.66\cdot10^{-4}$	3.0
67.2	0.33	36.7	8.535	0.023	27	70	154	91.1	1.340	$5.19\cdot10^{-4}$	5.2
62.2	0.33	31.7	11.500	0.022	260	54	85	74.0	1.248	$6.13\cdot10^{-4}$	5.6
						<u>260</u>	<u>130</u>	<u>98.7</u>	<u>1.003</u>	<u>$2.94\cdot10^{-4}$</u>	<u>5.2</u>

4.3 High Temperature Amorphous Lactose Isotherms

4.3.1 Background

It has been hypothesized that during flash drying of alpha lactose monohydrate crystals a layer of amorphous lactose is formed (Paterson, 2017). During the subsequent fluid bed drying, depending on the conditions, this layer may then crystallize in one of two ways; inside-out or outside-in. Inside-out crystallization is theorized to cause a stable dry product, whereas outside-in crystallization traps moisture which slowly diffuses in storage and causes handling issues.

With a small sample, such as that required for the STA, a temperature gradient is difficult to maintain long enough for induction to take place. Furthermore, the TGA signals can be unreliable for a period during temperature increase. Because of this it was decided to control the direction of crystallization using a moisture gradient induced once the target temperature was reached.

To ensure outside-in crystallization it is necessary that adsorption continues until crystallization is induced. This maintains a higher moisture content at the surface, with a greater molecular freedom making nucleation more likely.

To ensure that inside-out crystallization occurs two conditions are required: desorption needs to occur prior to induction of crystallisation creating a moisture gradient, and the outer surface moisture content must be low enough that crystallization there is unlikely. To achieve these conditions a greater understanding is required of the sorption and crystallization behaviour of amorphous lactose under the higher temperatures present in a fluid bed dryer. The models produced in section 3 are useful for prediction of crystallization time, but the confidence intervals are quite broad, and specific data for the sample to be used was desired.

Existing isotherms (section 2.1.1) only cover temperatures up to 45°C. Higher temperature isotherms showing the water activity at which crystallization occurs at each temperature would aid experimental design while also clarifying the currently conflicting information on temperature dependence. The STA set-up with the sensitive balance, precise control over temperature and humidity, and the direct applicability to other STA trials is ideal for this application. The equipment used was that described in section 4.2.

4.3.2 Conditions and Method

Temperatures of 110°C and 95°C were selected as temperatures likely to exist in a fluid bed drier and 30°C was selected for comparison. Relative humidity conditions at 95°C and 110°C were selected up to one at which crystallization was considered very likely and then spaced evenly below that. Relative humidity conditions at 30°C were spaced up to 50%RH. The TRG-004 which heats the humidified air is limited to 95°C and is more accurate at 90°C or below. As such, the required relative humidity at 90°C (for the humidity program) to achieve the desired relative humidity once the air is heated to 110°C in the furnace was calculated using the Arden-Buck equation (Buck, 1981). The humidity was increased from 0%RH every 6h for the high temperature trials and every 8h for the 30°C trial to account for the slower adsorption. An additional stage was added to the temperature program for the 30°C isotherm for reasons discussed in section 4.3.3.

Experimental Steps

1. The MHG was pre-set to produce 0%RH and allowed to equilibrate.
2. The temperature and humidity programs were setup for the trial. The humidity program was generated and set to wait for the temperature program and record to a logfile. The temperature program was completed besides the sample weight. The STA furnace was opened.
3. Approximately 10mg of the P_2O_5 desiccated spray-dried amorphous lactose sample (section 4) was weighed into the NETZSCH aluminium crucible with the weight recorded and put into the temperature program.
4. Immediately after being weighed the sample containing crucible was carefully positioned on the sample carrier along with the reference crucible, and the furnace was closed.
5. The temperature program was started, with the STA recording the sample mass and temperature data, and the MHG recording the relative humidity conditions. Once complete the sample was removed and transported in a desiccator to be sealed in a controlled humidity glove box.
6. The process was then repeated with the same conditions using an empty crucible to produce the correction file, and then for the next sample at a different temperature and set of relative humidity conditions.

Once collected all results had their associated correction file subtracted and the sample mass signal smoothed using method "A" within the NETZSCH Proteus Thermal Analysis software. Smoothing was required due to severe noise in the mass signal and method "A" was found to consistently provide the best smoothing. After this the 95°C and 110°C trials required further manual correction to correct for a known error where an unexpected gradual decrease in sample mass is recorded at constant conditions. The moisture content was then calculated.

4.3.3 Results and Discussion

Following the increase in temperature at ~0%RH very rapid desorption was observed to a stable mass which was used as the dry mass (Figure 4-16 & Figure 4-17). This dry mass is considered to be without any bound moisture. Brooks (2000) estimated the bound moisture by oven drying at 120°C and an unknown aw for 24h, at 110°C and ~0aw equilibrium was observed after just 3h (likely less because of the error described in section 4.3.2). Comparing the isotherm results at 95°C and 110°C the percentage drop in the mass was similar with a greater relative mass drop recorded at 95°C. Because both isotherms used the same sample stored under the same conditions the initial moisture content should be reasonably consistent. Therefore, it is assumed that 95°C and ~0%RH was also sufficient to remove bound moisture.

Noticeable yellowing of the crystallized sample from the 110°C isotherm occurred, as could be expected given the duration, but not for the 95°C sample. To avoid any potential complication of non-enzymatic browning as described by Ranger et al. (2017) on future results the temperature was limited to 95°C.

Based on these two observations, to allow proper comparison in terms of moisture content, the temperature of the sample was raised to 95°C under 0%RH and held for 6 hours before being allowed to cool to 30°C for 8hours.

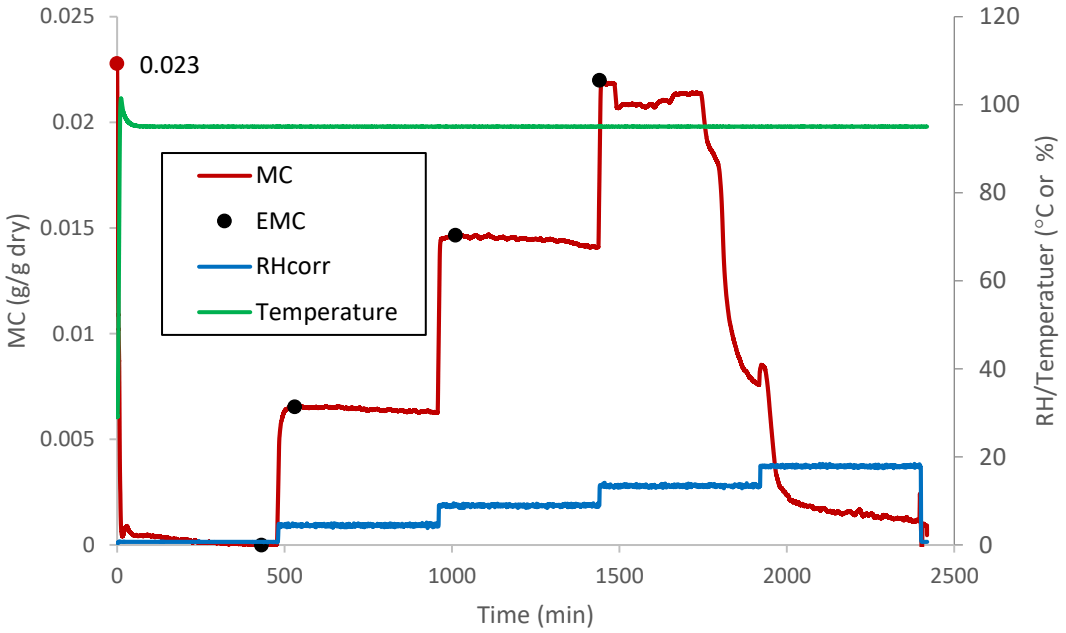

Figure 4-16: Experimental conditions and results with calculated EMCs for the isotherm trial at 95°C.

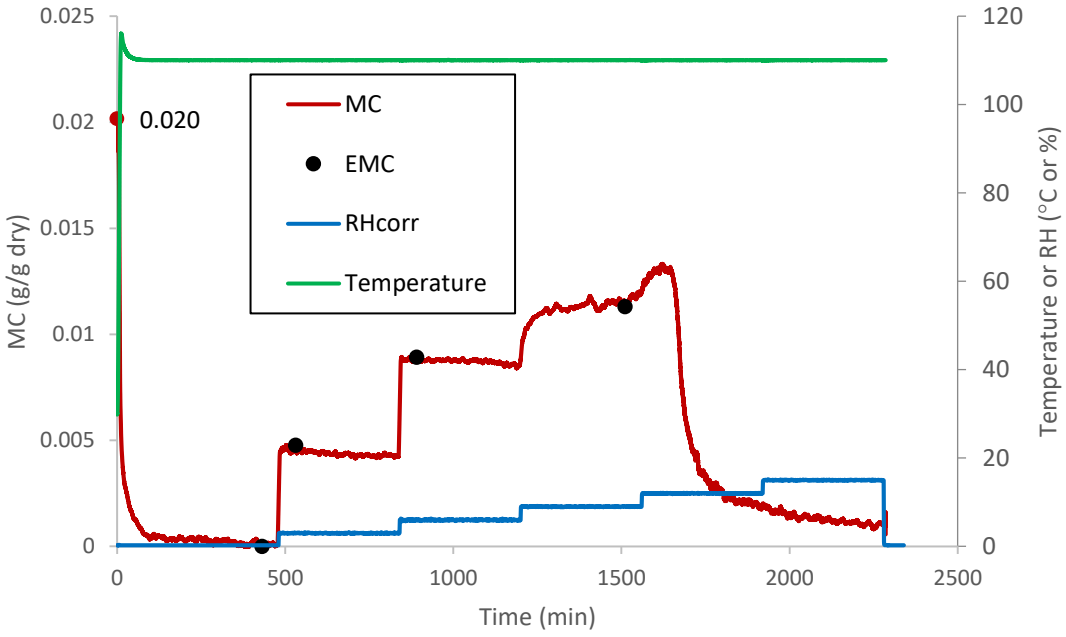

Figure 4-17: Experimental conditions and results with calculated EMCs for the isotherm trial at 110°C.

For the 30°C isotherm (Figure 4-18) the sample mass did not reach equilibrium at 15%RH or 25%RH. At 15%RH equilibration appears close. The sorption data for these conditions was modelled using an inverse relationship model which provided a good fit. The inverse model was extrapolated out to the estimated equilibration time of 10h and 12h for 15%RH and 25%RH respectively.

One clear difference is that sorption occurs more rapidly in the high temperature isotherms than the 30°C isotherm.

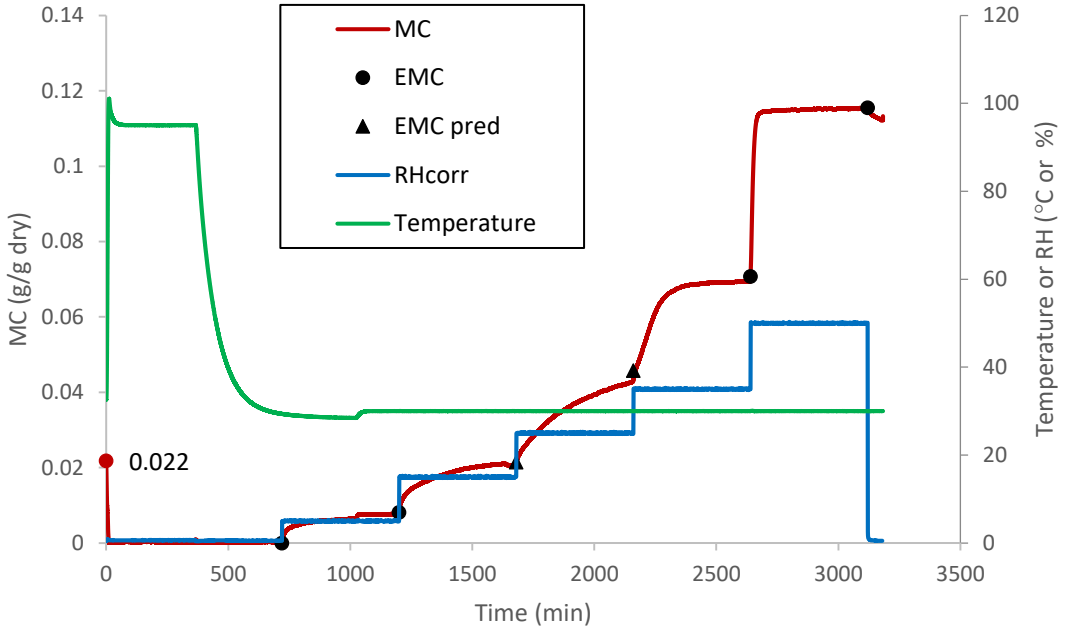

Figure 4-18: Experimental conditions and results with calculated and predicted EMCs for the isotherm trial at 30°C.

When comparing the equilibrium moisture content (EMC) results versus water activity they were found to follow a very similar trend with no clear indication of temperature dependence. As a result the GAB model (equation (2-3)) was fitted to the data using the method described by Samaniego-Esguerra, Boag, and Robertson (1991) obtaining the following constants: w'_m = 0.0637 (g water/g dry), K = 1.22, C = 1.92. The collected data points and fitted model are shown in Figure 4-19, with the model appearing to provide a reasonable prediction for all EMCs.

The GAB model was also fitted to the maximum estimated EMCs (w'_m = 0.0107 (g water/g dry), K = 0.96, C = 1.55) and the minimum estimated EMCs (w'_m = 0.0429 (g water/g dry), K = 1.41, C = 2.25). These models were used to get a measure of the uncertainty of the EMC prediction at a given water activity.

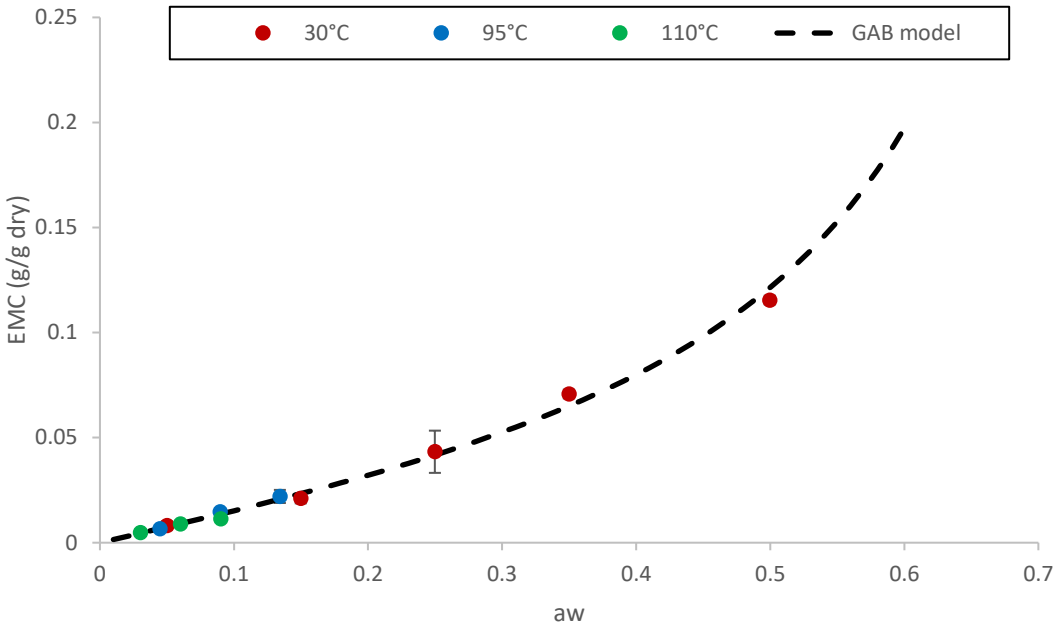

Figure 4-19: Collected calculated and predicted EMC values versus aw. Error bars represent the maximum potential error of calculation or prediction.

The equilibrium moisture content at which crystallization was induced within 6 hours was 0.0220g/g dry at 95.0°C for a Gordon-Taylor predicted T-Tg (equation (2-1)) of 13.0K and 0.0131g/g dry at 110.0°C for a T-Tg of 16.0K.

4.3.4 Aside: Source of Experimental Noise

Experimental noise for the sample mass recorded by the STA was a significant issue throughout for all trials but was especially noticeable for the 110°C isotherm trial. The data from this trial was used to quantify the experimental noise. Noise was taken as the absolute difference in the sample mass, from mass averaged for the five minutes around it. This noise was averaged around each local whole hour, and plotted against the corresponding wind speed from 12:00pm 12/03/18 and 12:00am 14/03/18 from Metroblue (2018) in Figure 4-20. The weather seems to be very likely to be the cause of the experimental noise and not an aspect of the procedure.

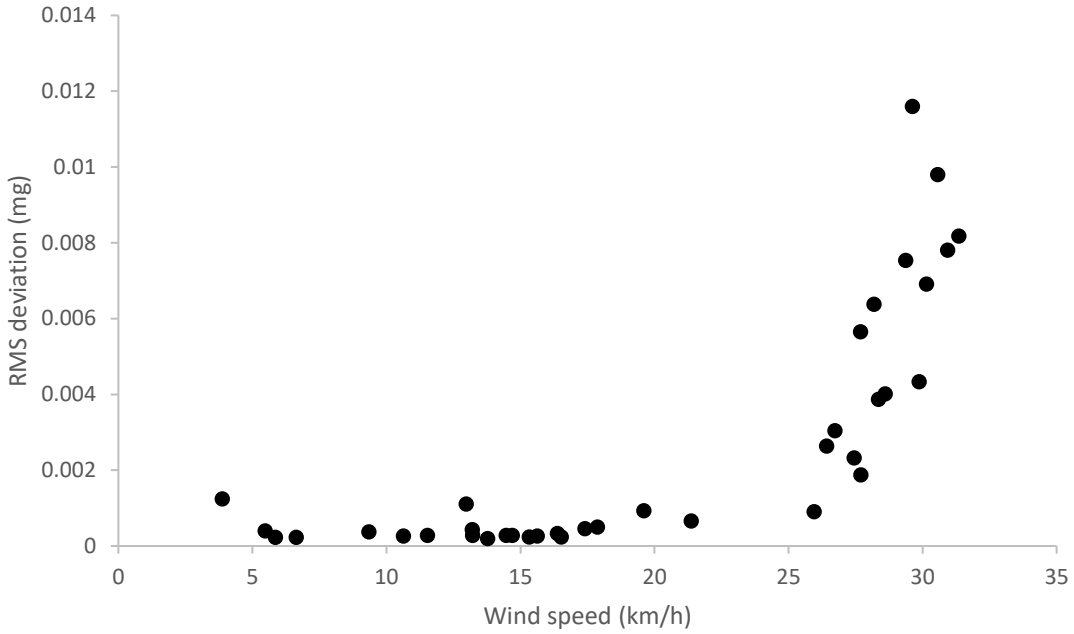

Figure 4-20: Hourly averaged RMS noise from 110°C isotherm versus Palmerston North wind speed. For 12:00pm 12/03/18 and 12:00am 14/03/18 (Metroblue, 2018).

5 Directional Crystallization Method

The following section describes the development of a method to achieve inside-out and outside-in crystallization, observe the crystallization kinetics, monitor the release of moisture from the two groups of samples, and determine possible sources of moisture.

Spray-dried amorphous lactose sample was selected early on for use in the design of the directional crystallization trials and the trials themselves. Amorphous lactose, if formed during flash drying, would have been formed due to the rapid removal of moisture from a solution forming a solid layer. This is process is more like spray-drying than freeze drying where the moisture is sublimed from a frozen solution leaving a porous solid. The STA set-up was found in section 4 to be suitable for the purposes of precisely controlling the conditions of crystallization and providing detailed information on the crystallization process. The STA was largely used as described in section 4.2 with the following changes:

Minimum Temperature

The temperature at which the sample was equilibrated before it was ramped to the crystallization temperature was increased to 30°C. This was necessary as the STA does not have active cooling and the ambient temperature during the trials went above 25°C but not above 30°C.

STA Temperature Control

In the STA program, for each segment, there is the option for sample temperature control (STC). STC maintains the sample temperature at the setting during isothermal sections and was used for all such segments. During temperature ramp segments active STC provided rapid control with some temperature overshoot, inactive STC provided slower control with no overshoot.

Modular Humidity Generator (MHG) Operation and Temperature Control

The MHG was set to control the humidity, by varying the flow of water to the mixing valve, at the inlet temperature of the heated air entering the furnace. This temperature is controlled separately from either the STA or the MHG by using the TRG-004.

To achieve a reproducible relative humidity above the sample as the furnace temperature increased, the humidified air temperature had to be increased to match it. The flange heater temperature, also controlled by the TRG, was kept at the same setting as the humidified air to prevent condensation on the balance. The TRG settings were increased manually in 5K increments. As the setting took some time to be achieved it was maintained above the sample temperature. To best match the temperatures the TRG was increased from the sample temperature by 1-15K depending on the sample temperature. The sample temperature ranges and increase for, the TRG setting (in brackets) were: 30→31°C (+1K), 31→35°C (+4K), 35°C → 65°C (+10K), >65°C (+15K) with a maximum TRG setting of 90°C.

At a sample temperature of >90°C the humidity was maintained or varied solely by the RH setting in the MHG program. The setting was calculated by the Arden-Buck equation using the desired relative humidity and temperature data obtained using the same temperature program to be used. This was required as the rate of the temperature increase in the STA was

not constant. Similarly following each trial, the humidity above a sample was calculated using the logged humidity and temperature results.

Removal of Samples

The samples were deemed to be at equilibrium after crystallization when the mass change over 60 minutes was less than 0.003%. Waiting for an extended equilibrium was considered undesirable as the theoretically trapped free moisture would have been removed during this period. Once at equilibrium the sample was removed from the STA to be measured for moisture release. As described in section 5.2 it was thought that measurement of humidity would give a better understanding of the presence of free moisture. If it was driven off by drying in small amounts it may have been difficult to distinguish by the DSC signal from desorption.

5.1 Experimental Steps

- The MHG was pre-set to produce 0%RH and allowed to equilibrate.
- The temperature and humidity programs were setup for the trial. The humidity program was generated and set to wait for the temperature program and record to a logfile. The temperature program was completed awaiting the sample weight. The STA furnace was opened.
- Approximately 10 mg of the P_2O_5 desiccated spray-dried amorphous lactose sample (section 4) was weighed into the NETZSCH aluminium crucible. Both the sample and crucible weights were recorded and put into the temperature program.
- Immediately after being weighed the sample containing crucible was carefully positioned on the sample carrier along with the reference crucible, and the furnace was closed.
- The temperature program was started, with the STA recording the sample mass and temperature data, and the MHG recording the relative humidity conditions.
- After 1180 min the temperature ramp started and the TRG settings were manually changed as described in section 5.
- The sample mass signal was then monitored periodically; firstly, to ensure that equilibrium did not occur before crystallization: and secondly, to determine when the mass was at equilibrium.
- Once complete, the sample was removed and transported in a desiccator to be sealed in a controlled humidity glove box.

The process was then repeated using the same programs using an empty crucible to produce the correction file, as well as repeated for two more samples. The blank trials were completed immediately after the first trial of each kind, to ensure similar ambient conditions. Once the method was finalized the order of the repeat trials was randomized.

Once collected all results had their associated correction file subtracted the sample mass signal was smoothed using method “A” within the NETZSCH Proteus Thermal Analysis software. Smoothing was required due to noise in the mass signal and method “A” was found to consistently provide the best smoothing.

5.2 Moisture Release Measurement

The hypothesis of moisture being trapped by inside-out crystallization and slowly released raising the water activity of the bagged product. To test this the samples had to be monitored determine whether this occurred. The STA equipment can be used to achieve and verify inside-out or outside-in crystallization but is poorly suited for extended monitoring due to limited availability, and regularly required maintenance. During the crystallization process inside the STA, the sample moisture content can be determined from the recorded mass data. Continuing to measure the mass changes once the sample is removed from the STA was considered. This method had the advantage of continuing to measure the moisture content. Unfortunately, the facilities to continuously measure the mass of multiple samples were not readily available. Manually measuring the weight change over time would have required additional handling of the sample all of which would have been required to be done under controlled humidity.

Logging the humidity was ultimately considered to be better due to the greater sensitivity, ease of continuous monitoring, and reduced handling of the sample. Greater sensitivity is achieved because, given a low enough volume of air, even a very small amount of moisture can raise the humidity considerably. With the small sample masses, a very sensitive balance would be required, and the dry mass would need to be determined, potentially by oven-drying. The suspected cases of inside-out crystallization recorded by O'Donnell (1998) and Chavda (2009) were indicated by a higher than expected water activity after drying, and a lower than expected increase in water activity during crystallization respectively.

I-buttons have been used previously by Clark (2012) and Chavda (2009) to log humidity over time. They are ideal for this purpose due to their small size, which allows for the change in a small volume of air to be measured. The iButtons used were “DS1923: iButton Hygrochron Temperature/Humidity Logger with 8KB Datalog Memory” produced by Maxim Integrated (Integrated, 2015). The activated buttons were set to log temperature and relative humidity every 10minutes with a resolution of 0.04%RH and 0.5°C respectively. Each iButton was checked for accuracy by the equilibrium humidity reading over saturated salt solutions of lithium chloride (11.3±0.27%RH) and magnesium chloride (32.78±0.16%RH)(OMEGA, 2018).

5.2.1 Method Description

The proposed moisture release measurement by humidity relies on the increase in humidity, recorded by an activated iButton, in the volume of air above the sample. The sample was removed from the STA only once the heat flow and mass are at equilibrium following crystallization. If crystallization was not complete when the sample was sealed, then water expelled due to crystallization would cause a humidity increase and make any release of trapped moisture difficult to distinguish. Once it was removed from the STA the sample was transported and handled under low humidity, preferably at or below the relative humidity at which it was crystallized, to prevent any adsorption. The sample was sealed, in a controlled humidity glove box below 10%RH, in a jig which holds the activated iButton above the sample. Prior to sealing the jig was equilibrated inside the controlled humidity glove box to ensure it is not a source of moisture. The humidity at which the sample was sealed was noted as well as the time, the jig containing the sample is stored in a desiccator above phosphorous pentoxide for one week. Another activated iButton measured the conditions in the desiccator. By storing the jig in the desiccator at ~0%RH any leak could be detected by a drop in the humidity instead

of the expected plateau or rise. In the case of a leak, adsorption was also prevented. After a week the sample was removed from the jig in the humidity-controlled glove box and bagged below 15%RH for further analysis, the logged temperature and data from the iButton was downloaded.

5.2.2 IButton Jig

The jigs used to clamp the iButton over the sample consisted of two cylindrical pieces of acetyl plastic held together using four bolts and wingnuts. The bottom section has two concentric chambers milled out to hold the sample in the crucible and locate the iButton so the measurement opening of the iButton is directly above the crucible. Similarly the top piece has a depression to help locate the iButton. A seal is achieved by the rubber washer between the iButton and the pocket holding the sample, with a secondary o-ring seal between the acetyl parts.

The estimated volume of air between the sample and the iButton was 251mm^3. This is based on a combined volume for the crucible and sample of 15mm^3 (using a typical weight of 23mg for the crucible and 10mg for the sample along with the respective densities) and ignoring compression of the neoprene washer.

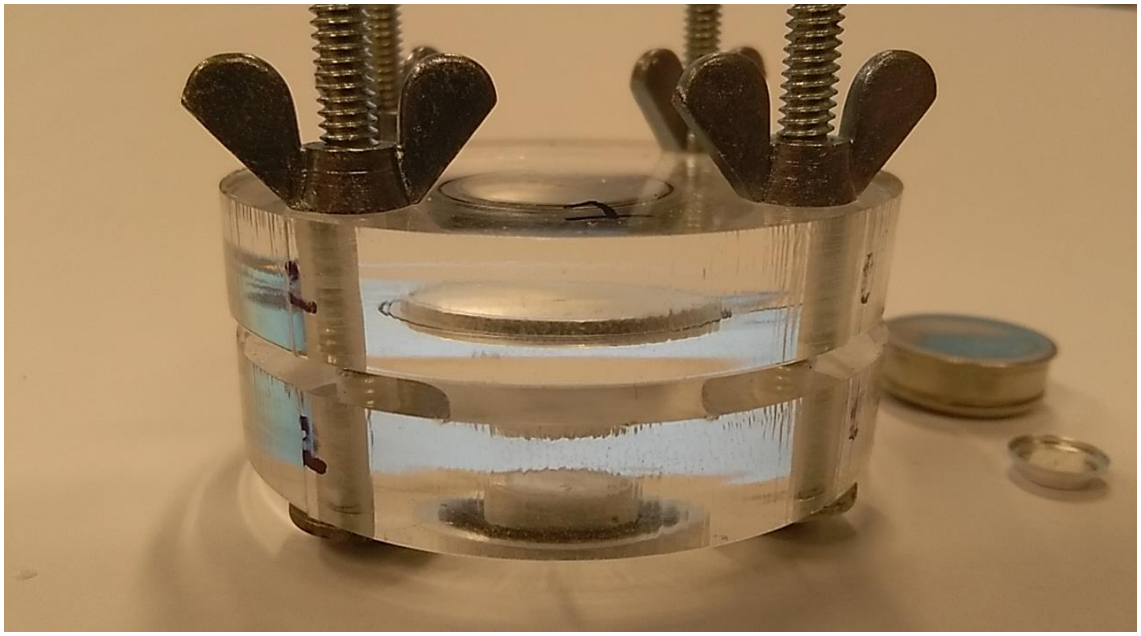

Figure 5-1: Photo showing the assembled jig. To the right is a crucible containing crystallized amorphous lactose and behind that an iButton.

5.3 Isothermal Amorphous Determination Methodology

Following moisture release and XRD analysis of the samples an investigation into any remaining amorphous lactose was conducted using the STA. As with all STA trials, the general steps described in section 4.2 were followed. The conditions used were 30°C and 0%RH for 30mins before the humidity was ramped to 75% and held for 4 hours. The relative humidity of 75% was selected as it was commonly used in isothermal micro-calorimetry and dynamic vapour sorption methods (section 2.1.2). A correction run as well as trials for pure samples of α-lactose monohydrate and amorphous spray-dried sample were made for comparison.

Amorphous content was estimated using the area of the exothermic DSC peak (associated with adsorption and crystallization both of which are proportional to the amorphous content) and the percentage mass gain.

5.4 Preliminary Trials

5.4.1 Desorption

It was important to estimate the dry mass of the samples prior to crystallization to track the moisture content.

The method used in section 4.2.1 gave reasonable predictions for the dry mass and moisture content for freeze-dried samples. Desorption is known to occur more slowly for spray-dried amorphous lactose than for freeze-dried samples (Ripberger, 2010), therefore desorption rate data had to be obtained for the spray-dried sample.

A drying trial was conducted using the STA under conditions of 30°C, 0%RH for 16h followed by a temperature ramp to 250°C at 5K/min (appendix 9.3). An equilibrium was reached after 14h, and ~1% moisture was removed during the heating up to the range of 110-120°C with melting and decomposition thereafter. The >14h required to estimate the dry mass with bound moisture was unable to be accommodated in each trial. Instead drying at 0%RH, 30°C for 4h was selected as the point where over 80% (85.8%) of the mass loss was accomplished in the extended trial. The period of drying was extended to 6h as this could be accommodated in the schedule.

$$m_{dry} = m_0 + \frac{\Delta m_{4hr}}{0.858} \tag{5-1}$$

- m_{dry} is the estimated dry mass at 0 aw, not accounting for bound moisture (mg_{dry})
- Δm_{4hr} is the recorded change in mass after four hours at 30°C and 0%RH (mg_{water})

The moisture content accounting for bound moisture could then calculated using equation (4-7).

5.4.2 Inside-out Conditions Selection

A relative humidity of 22% was known to cause rapid induction of crystallization at 95°C and so this was used as a starting point from which desorption could occur. After the 6h of drying at 30°C and ~0%RH the relative humidity was increased to 22%RH for 13.7h which, in practice, was slightly below the time required for equilibration.

The humidity program for desorption was more challenging to determine. The program was required to generate a moisture gradient which would allow rapid induction on the interior of the particle but not on the surface. It was known from the isotherm trials (section 4.3) that at 95°C and above adsorption and removal of bound moisture occurs rapidly. It was desirable to have crystallization occur at the lowest relative humidity possible to reduce the chance of crystallization being first induced at the surface.

The first trial used the program shown in Figure 5-2 resulting in rapid desorption to an equilibrium moisture content without crystallization occurring as seen in Figure 5-3.
The failure to achieve crystallization was confirmed as when the sample was examined it was still in amorphous powder form. The set points were selected at 0%RH to allow dry mass estimation, then 26%RH followed by 6%RH to establish a moisture gradient across the sample

prior to the temperature being increased. These humidities were selected as at 95°C they would induce rapid crystallization (26% RH) and not allow crystallization to occur (6%RH) respectively as seen in the isotherm trials (section 4.3).

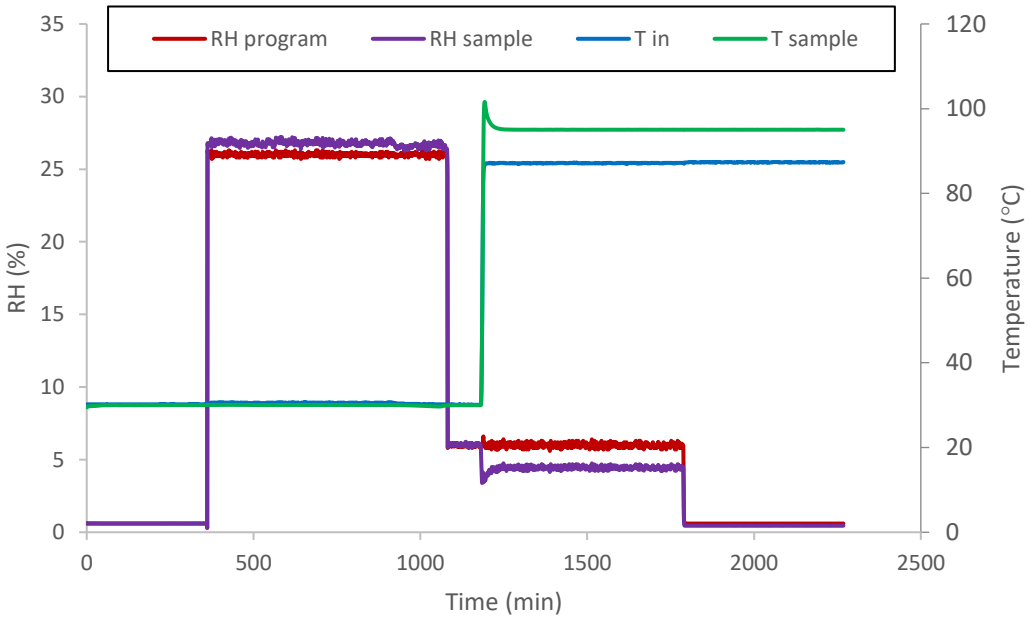

Figure 5-2: Experimental conditions for the first unsuccessful inside-out crystallization trial.

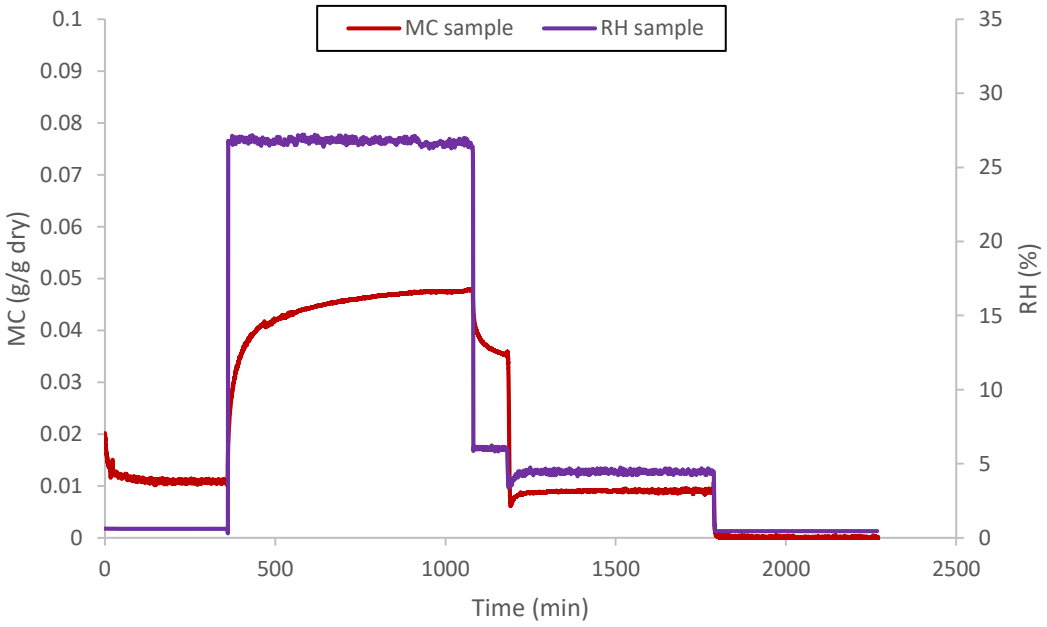

Figure 5-3: Sample moisture content and relative humidity results for the first unsuccessful inside-out crystallization trial.

The relative humidity setting was increased from 6%RH to 16%RH for the next trial but the result was the same, with equilibration occurring too rapidly. This humidity was used as it was known to take upwards of 12h for induction of crystallization to occur at 11%RH and 95°C.

A gradual change in the effective relative humidity above the sample, calculated based on previous experimental sample temperature data using the Arden-Buck equation, was trialled next. This was accomplished by several ramp changes in the humidity program to a final value of 16%RH (11%-12% above sample) over 40mins as shown in Figure 5-4. Again, desorption was too rapid for induction of crystallisation to take place prior to equilibration.

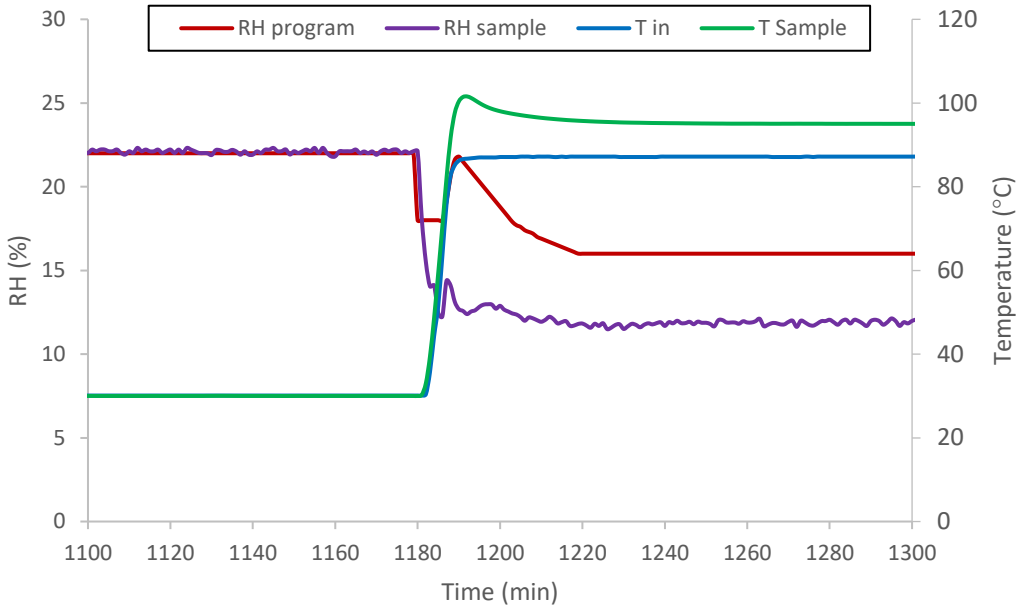

Figure 5-4: Experimental conditions during the temperature ramp for the third unsuccessful inside-out crystallization trial.

At this point it was identified that much of the mass loss was occurring during the temperature increase. Of particular concern was a dip was observed in the moisture content/mass when the sample temperature peaked before decreasing to the set value. It was therefore decided to turn off STC for the temperature ramp section and use a modified version of the gradual humidity ramp program, with the set humidities increased slightly. This resulted in a more variable humidity above the sample during desorption, see Figure 5-5, but extended the period of desorption enough that crystallization was induced before equilibration occurred (Figure 5-6).

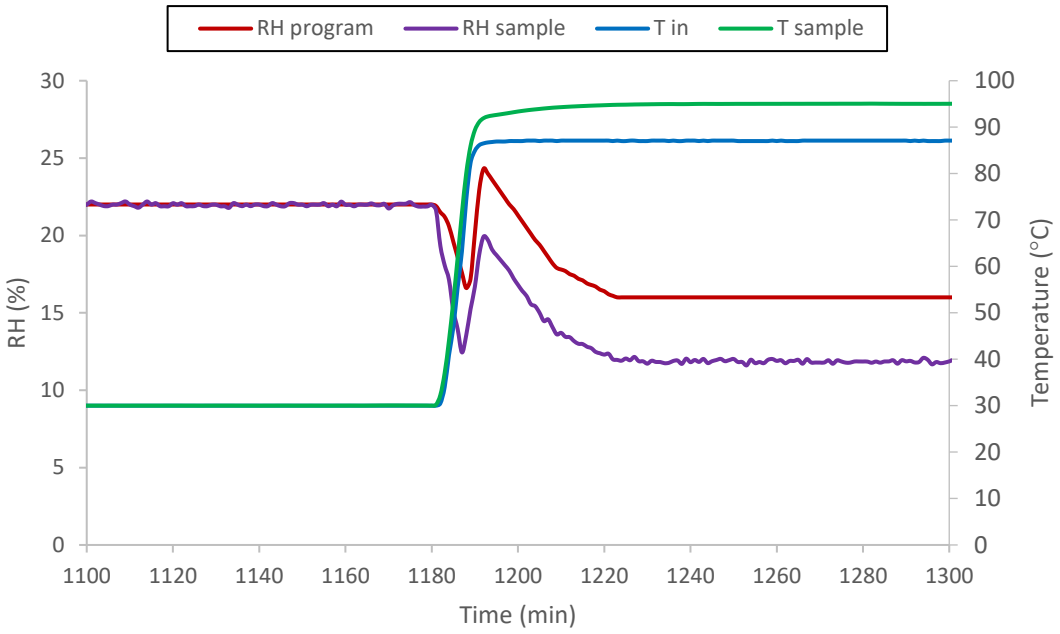

Figure 5-5: Experimental conditions during the temperature ramp for the first successful inside-out crystallization trial (IO1)

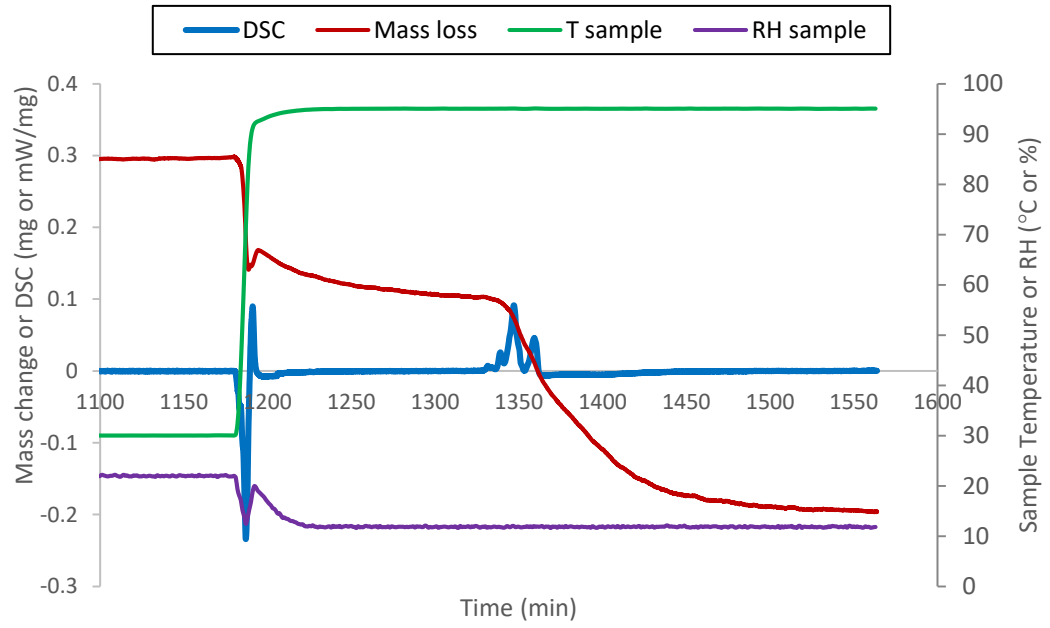

Figure 5-6: Corrected and smoothed results with experimental conditions for IO1. Mass change is with respect to the initial sample mass.

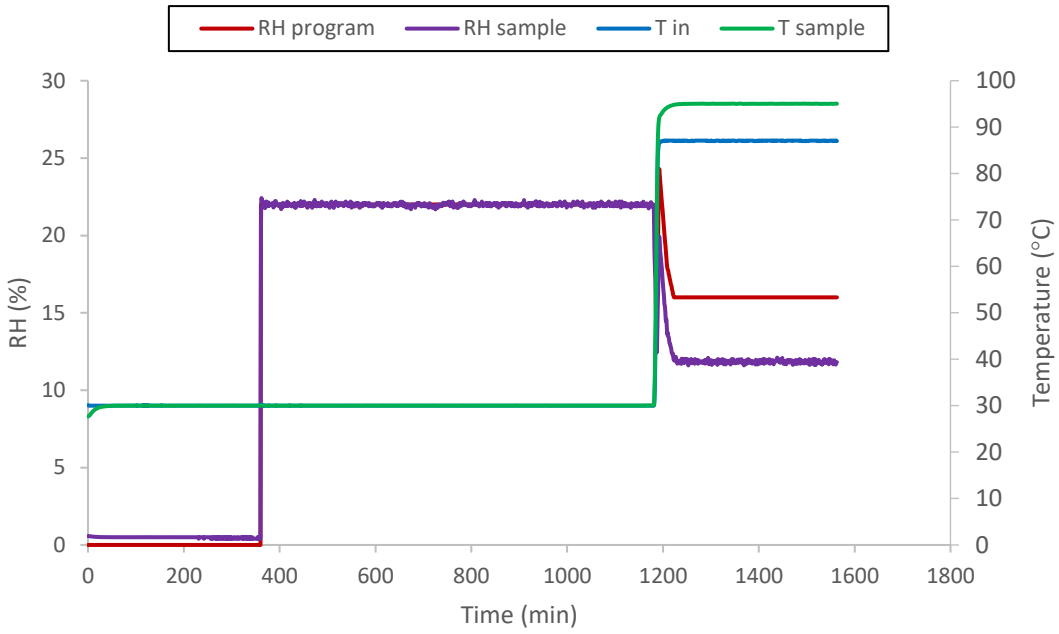

Figure 5-7: Experimental conditions during the full range of the first successful inside-out crystallization trial (IO1)

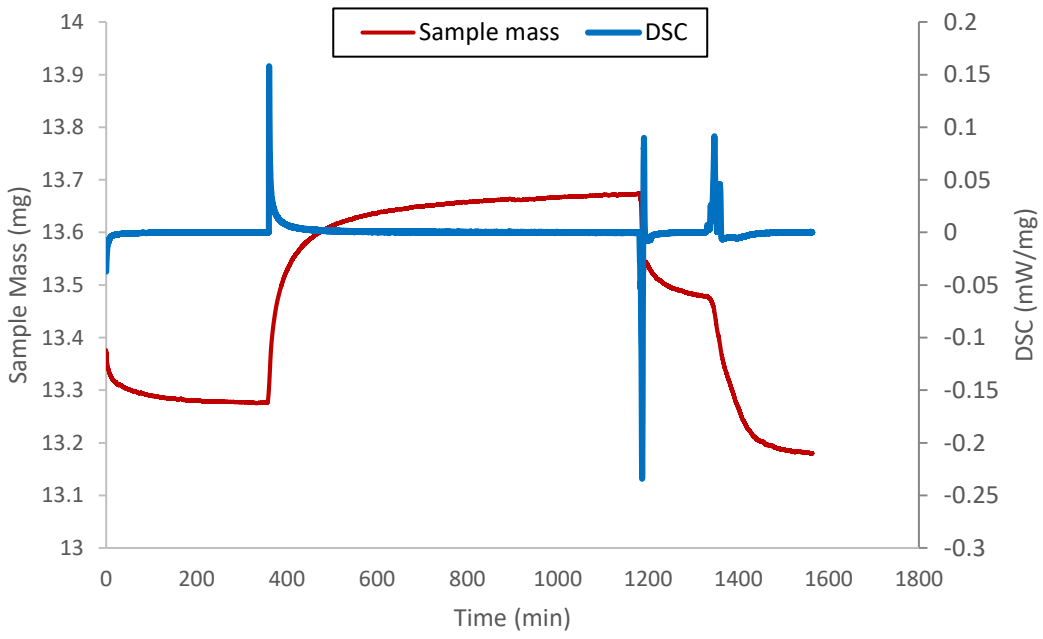

Figure 5-8: Full corrected and smoothed results for IO1.

The full experimental conditions results for the first inside-out trial are shown in Figure 5-7 and Figure 5-8 respectively. The conditions used were repeatable and met the criteria of crystallization occurring following desorption. This ensured that an inside-out gradient and an external RH condition too low for rapid induction existed for this trial and the subsequent repeats (IO2 and IO3 see appendix 9.4.1). The STA provided allowed for the sample conditions to be precisely set despite this it was still difficult to achieve inside-out crystallization, requiring

multiple trials and fine changes to the temperature control. It is suggested that deliberately targeting these conditions for an industrial fluid be dryer may not be practical.

5.4.3 Outside-in Conditions Selection

The conditions required for isothermal outside-in crystallization induced by adsorption are thought to be just that a significantly large outside-in moisture gradient exists. A relative humidity of 11% was known to cause extremely delayed induction of crystallization at 95°C so was used as a starting point from which adsorption could occur. After the 6h of drying at 30°C and ~0%RH the relative humidity was increased to 11%RH for 13.7h allowing the sample to equilibriate. The temperature was then raised with the relative humidity controlled to try and maintain 11%RH above the sample. Once a constant relative humidity and temperature condition above the sample was achieved, the relative humidity produced by the MHG was ramped up to an effective relative humidity of 22%RH, which is known to cause rapid induction of crystallisation. As before, the Arden-Buck equation was used to calculate the humidity above the sample from the sample temperature, and the temperature and relative humidity of the air entering the STA.

The conditions used are shown in Figure 5-9 which were successful as shown in Figure 5-10 crystallization was induced before equilibrium was reached.

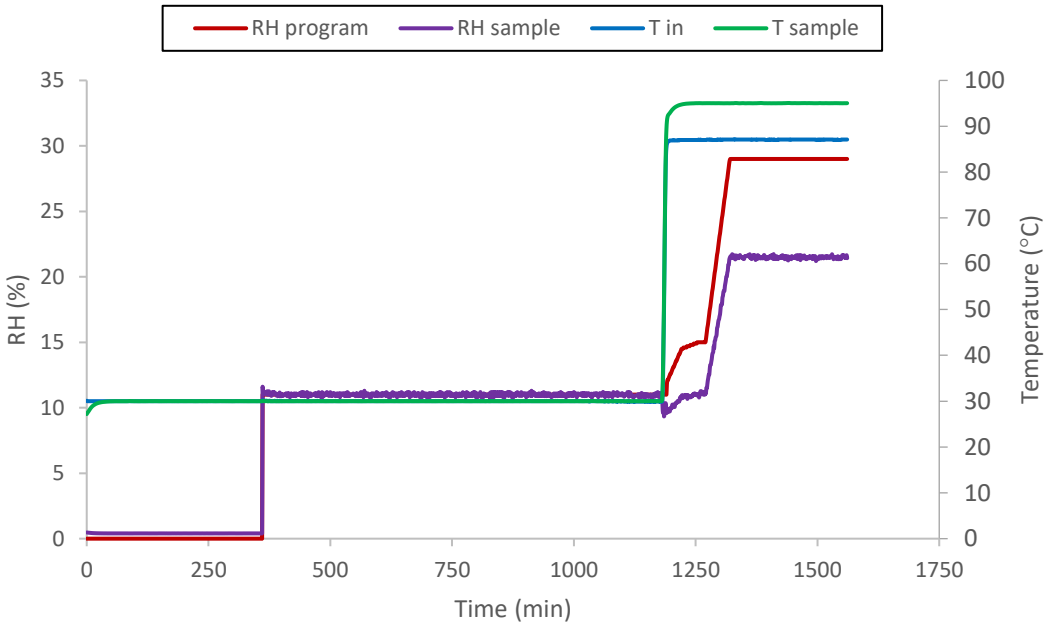

Figure 5-9: Experimental conditions for the first (successful) outside-in trial (OI1)

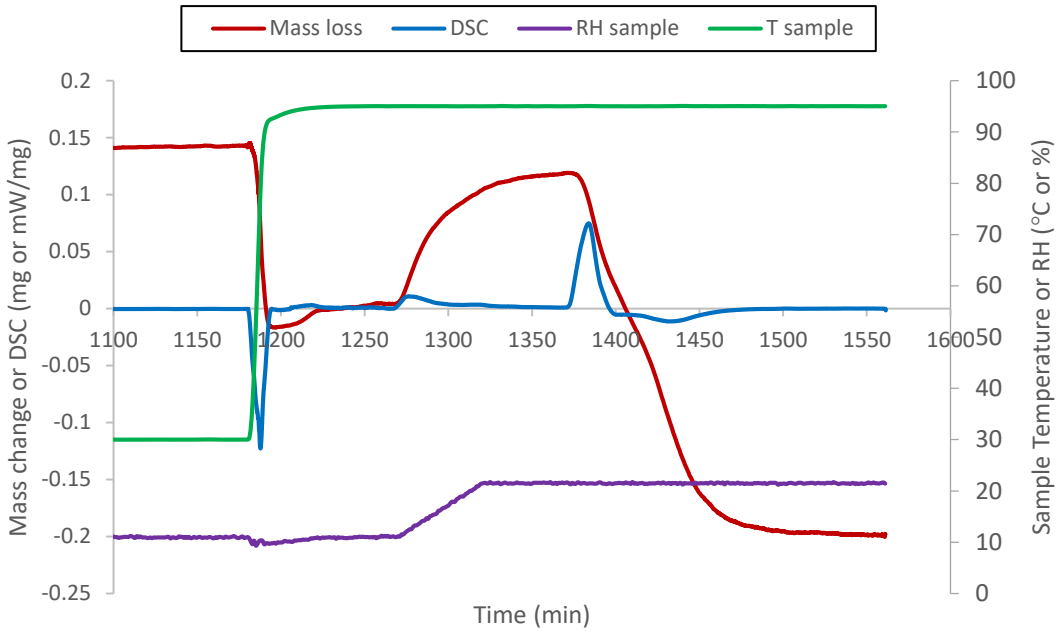

Figure 5-10: Sample conditions and corrected+smoothed results following the temperature ramp for sample OI1. Mass change is with respect to the initial sample mass.

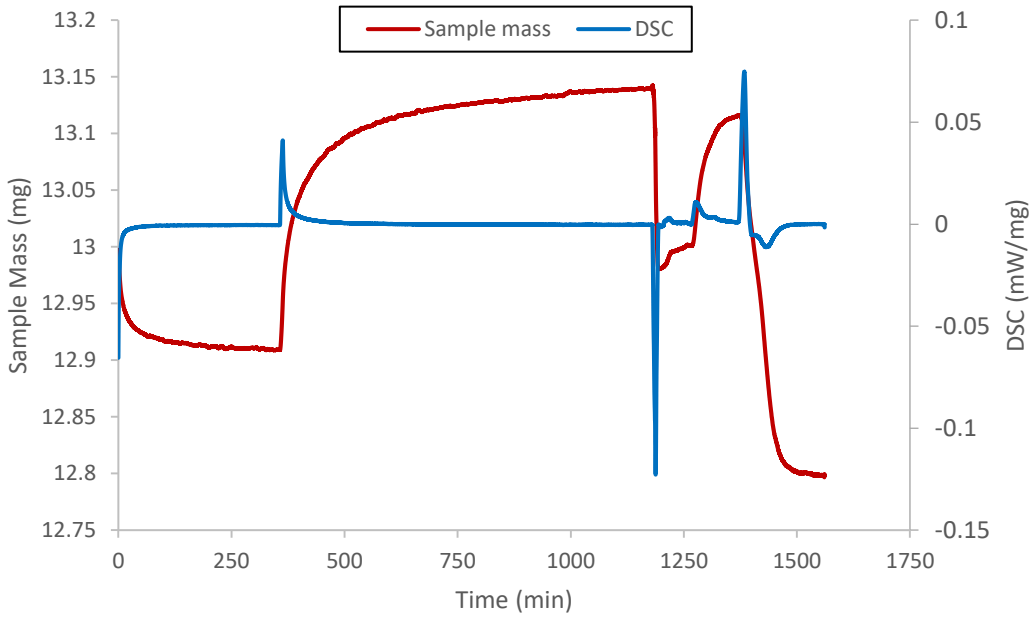

Figure 5-11: Full corrected and smoothed STA results for sample OI1

The full results for the first inside-out trial are shown in Figure 5-11. The conditions used were repeatable and met the criteria of crystallization occurring following adsorption from a MC too low for rapid induction for this and subsequent trials (OI2 and OI3 see appendix 9.4.1).

All corrected, smoothed data from the successful inside-out/outside-in trials was processed as described in section 4.2.1. The only change was the different calculation of the moisture

content as described in section 5.4.1. The correction method fitted using the freeze-dried errors in section 4.2.1 was found to still work well.

6 Directional Crystallization Results

6.1 Processed STA Results

The STA results were processed to allow better comparison between the trials. Important information collected was the moisture content changes of the sample, the observed enthalpy change due to crystallization, as well as the induction and crystallization times.

6.1.1 Inside-out

Using the calculated dry mass, the moisture content at the key stages in the trials was determined. Figure 6-1 shows that while the initial moisture content of the samples varied, potentially due to different times of desiccation, crystallization was induced at a consistent moisture content and the moisture content at which the sample was removed was consistent.

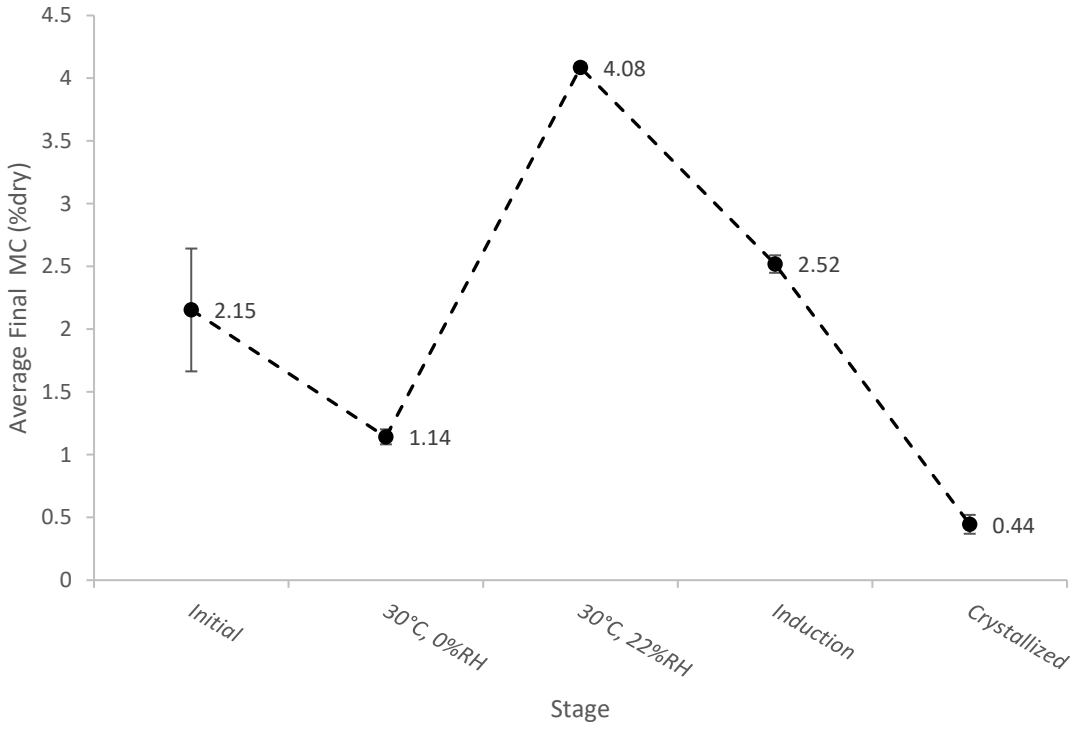

Figure 6-1: Inside-out crystallization trials averaged moisture content at each stage, error bars represent 1 s.d.

The conditions, kinetic data, and fitted models are shown in Table 6-1 and Table 6-2. The Δh_{obs} and Y_{cr} results indicate that complete crystallization was not achieved even though the enthalpy value stopped increasing and the mass was at/near equilibrium (appendix 9.4.1). The unfavourable conditions at the surface of the sample could have been such that crystallization occurred until the moisture content decreased below a critical value. Models were fitted assuming crystallization finished during the STA run. Variation in the sample mass occurred as the dry sample had to be transferred to the crucible quickly to avoid exposure to the humid atmosphere. This effect of this variation is not expected to be major due to the consistency of the moisture contents at induction, and the end of the trial, between the samples.

Table 6-1: Conditions and derived kinetic data for the inside-out trials.

Trial	T_{ind}	aw_{ind}	m_{dry}	MC_0	MC_{ind}	MC_f	$T\text{-}Tg_{GT1}$	t_{90}	t_{100}	Δh_{obs}
-	°C	-	mg_{dry}	g/g_{dry}	g/g_{dry}	g/g_{dry}	K	min	min	J/g_{dry}
IO1	95.0	0.11	13.141	0.018	0.025	0.004	18.7	71	233	89.7
IO2	95.0	0.11	10.281	0.020	0.024	0.005	16.9	39	217	70.6
IO3	95.0	0.11	9.089	0.027	0.025	0.005	17.9	70	273	76.6
Av	-	-	10.837	0.022	0.025	0.004	17.8	61	242	79.0

- T_{ind} is the temperature at which crystallization was induced (°C).
- aw_{ind} is the water activity at which crystallization was induced.
- m_{dry} is the initial dry mass (mg)
- MC_0 is the initial moisture content (g/g_{dry}).
- MC_{ind} is the moisture content at induction (g/g_{dry}).
- MC_f is the final moisture content (g/g_{dry})
- $T\text{-}T_{g\,GT1}$ is the $T\text{-}T_g$ calculated using the Gordon Taylor equation with the constants derived by Brooks (2000) and MC_{ind} (K)
- t_{90} is the time for 90% of the change in Δh_{obs} to occur.
- t_{100} is the time for 100% of the change in Δh_{obs} to occur.
- Δh_{obs} is the calculated observed change in enthalpy of the sample due to crystallization calculated as per section 4.2.1 (J/g).

Table 6-2: Model fitting parameters for the inside-out trials.

Trial	Y_{cr}	$T\text{-}Tg_{Brooks}$	$T\text{-}Tg_{GT2}$	n_{Avrami}	k_{Avrami}	$RMSE_{Avrami}$
-	g/g	K	K	-	s^{-1}	%cr
1	0.825	28.7	6.4	1.590	$5.05\cdot10^{-4}$	5.2
2	0.649	28.7	6.4	2.560	$6.67\cdot10^{-4}$	3.5
3	0.704	28.7	6.4	0.968	$4.08\cdot10^{-4}$	3.4

- Y_{cr} is the fraction crystallized calculated as Δh_{obs}/ (Δh_{cr}=108J/g). Δh_{cr} is calculated using $\Delta h_{obs\,max}$=107J/g to achieve 99.2% crystallization per section 6.3.1
- $T\text{-}Tg_{Brooks}$ is the $T\text{-}T_g$ calculated using the polynomial fitted by Brooks (2000) and aw_{ind} (K)
- $T\text{-}Tg_{GT2}$ calculated using the Gordon Taylor equation with the constants derived by Brooks (2000) and EMC_{ind} (K)
- n_{Avrami} is the Avrami shape constant fitted to the enthalpy change data.
- k_{Avrami} is the Avrami rate constant fitted to the enthalpy change data (s^{-1}).
- $RMSE_{Avrami}$ is the root mean square error of the Avrami model fitted to the enthalpy change data (%).

6.1.2 Outside-in

Using the calculated dry mass, the moisture content at the key stages in the trials was determined. Figure 6-2 shows crystallization was induced at a consistent moisture content and the moisture content at which the sample was removed was consistent. Equilibrium is believed to have been reached, between the temperature ramp and subsequent humidity ramp, at 0.0182g/g_{dry} 95°C and 11%RH the decrease from the equilibrium at 30°C of 0.028 g/g_{dry} is approximately the 0.01g/g_{dry} bound moisture loss expected (Brooks, 2000).

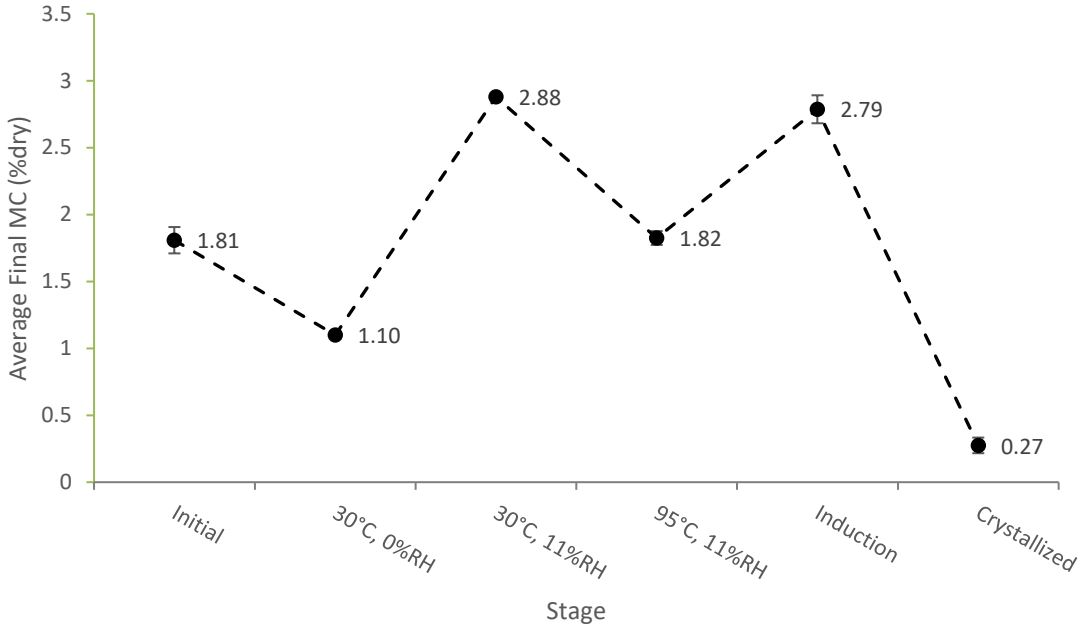

Figure 6-2: Outside-in crystallization trials averaged moisture content at each stage, error bars represent 1 s.d.

The conditions, kinetic data, and fitted models are shown in Table 6-3 and Table 6-4. The Δh_{obs} and Y_{cr} result for trial OI2 indicate that complete crystallization may not have been achieved even though the enthalpy value stopped increasing and the mass was at/near equilibrium (appendix 9.4). This was unexpected due to the consistent method used for the outside-in trials and could be attributed to the Δh_{cr} value being inapplicable to all data. The Δh_{obs} for trial OI3 is unusually high compared to those previously calculated using the same method. Models were fitted assuming crystallization finished during the STA run.

Table 6-3: Conditions and derived kinetic data for the outside-in trials.

Trial	T_{ind}	aw_{ind}	m_{dry}	MC_0	MC_{ind}	MC_f	$T\text{-}Tg_{GT}$	t_{90}	t_{100}	Δh_{obs}
-	°C	-	mg_{dry}	g/g_{dry}	g/g_{dry}	g/g_{dry}	K	min	min	J/g_{dry}
OI1	95.0	0.22	12.767	0.018	0.027	0.002	20.1	71	188	100.5
OI2	95.0	0.22	10.810	0.017	0.028	0.003	21.1	88	246	98.3
OI3	95.0	0.22	9.040	0.019	0.029	0.002	22.7	74	201	107.1
Av	-	-	10.872	0.018	0.028	0.003	21.3	77	212	101.9

- All parameters are as described in section 6.1.1

Table 6-4: Model fitting parameters for the outside-in trials.

Trial	Y_{cr}	$T\text{-}Tg_{Brooks}$	$T\text{-}Tg_{GT}$	n_{Avrami}	k_{Avrami}	$RMSE_{Avrami}$
-	g/g	K	K	-	s^{-1}	%cr
OI1	0.924	50.2	31.0	1.020	4.19E-02	6.5
OI2	0.904	50.2	31.0	1.036	3.42E-02	5.7
OI3	0.984	50.2	31.0	0.831	4.85E-02	6.0

- All parameters are as described in section 6.1.1

6.1.3 Further Analysis

Moisture Content Change and Δh_{obs}

The best predictor for the Δh_{obs} was the change in moisture content of the sample from induction to the final value. This can be expected as the correction and latent heat of vaporization used to calculate Δh_{obs} are dependent on the change in sample mass (section 4.2.1).

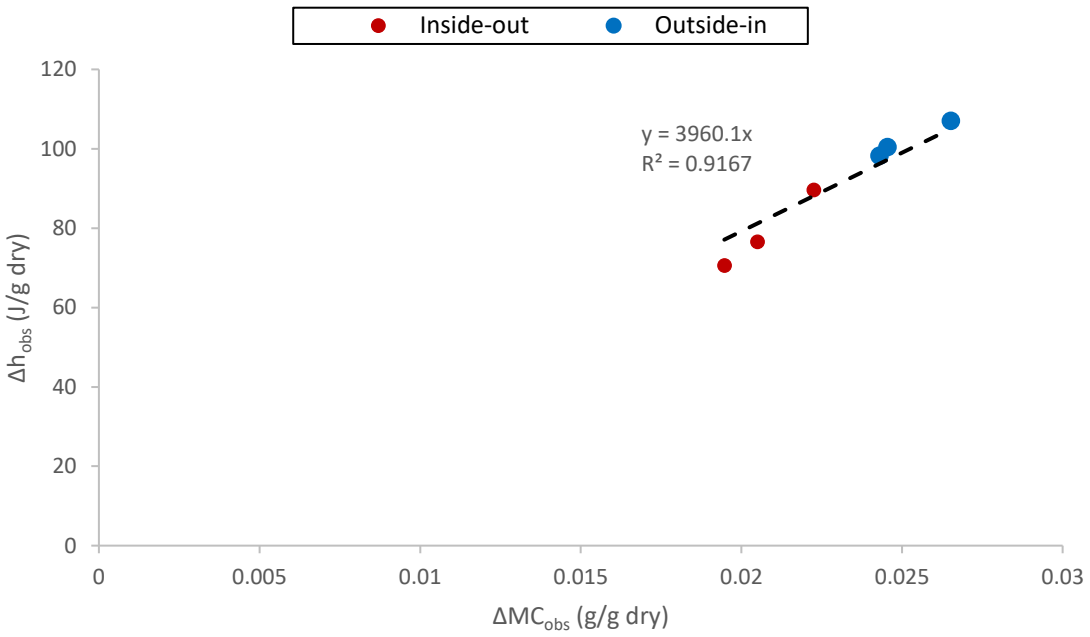

Figure 6-3:Observed enthalpy change attributed to crystallization versus the observed change in moisture content from induction to the end of the trial.

Final Moisture Content and Amorphous Content

The amorphous content of the sample can also be estimated from the final STA moisture content MC_f. If this moisture is not trapped as free moisture, it is adsorbed into the remaining amorphous lactose in the sample, as crystalline lactose does not adsorb water significantly (Bronlund, 1997). The trials were stopped when the mass was believed to have reached equilibrium so the amorphous lactose would be at the equilibrium moisture content (EMC_{AL}) at the final RH. The amorphous fraction at equilibrium, $X_{af\ EMC}$ can be calculated using equation (6-1). This equation neglects the possibility of trapped moisture, which if present would reduce the amount of the total moisture in the amorphous lactose, so represents a limit for the amorphous fraction.

It has been found that the moisture content of the crystalline component,$m_{dry}EMC_{\beta}(aw_{cr})$, should have included the mass fraction of the crystal $(1 - X_{af})$ in all calculations. This has not significantly affected the calculations as the dry mass (m_{dry}) samples were confirmed to be largely crystalline by several methods (see Figure 6-4), and the moisture associated with the crystal is so small that the error introduced is less than 1% (for example the lowest measured moisture content is .002g/g_{dry} and the error introduced in the crystalline moisture content would be below 0.00002g/g_{dry}).

$$X_{af\ EMC} = \frac{MC_f m_{dry} - m_{dry} EMC_{\beta}(aw_{cr})}{EMC_{AL}(aw_{cr}) m_{dry}} \tag{6-1}$$

- MC_f is the estimated final moisture content from Table 6-1 and Table 6-2 (g/g_{dry})
- aw_{cr} is the average water activity above the sample during crystallization; 0.11 for IO trials, 0.22 for OI trials.
- m_{dry} is the estimated dry mass from section Table 6-1 and Table 6-2 (g/g_{dry})
- $EMC_{\beta}(aw_{cr})$ is the equilibrium moisture content of β-lactose at aw_{cr} from the isotherm of Bronlund (1997) (g/g_{dry})
- $EMC_{AL}(aw_{cr})$ is the equilibrium moisture content of amorphous lactose at aw_{cr} from the isotherm in section 4.3 (g/g_{dry})

In the directional crystallization trials mass change was occurring immediately prior to induction, and equilibrium was not achieved. Because of this the actual amorphous moisture content would be higher for the inside-out samples (where desorption was occurring) and lower for the outside-in samples (where adsorption was occurring). The moisture content at induction (MC_{ind}) is considered to be a practical lower (for inside-out trials) and upper (for outside-in trials) limit to the final moisture content of any remaining amorphous lactose. Subsequently the amorphous content calculated using the moisture content at induction ($X_{af\ MCind}$) calculated from equation (6-2) represents a limit for the amorphous fraction if not at equilibrium.

$$X_{af\ MCind} = \frac{MC_f m_{dry} - m_{dry} EMC_{\beta}(aw_{cr})}{MC_{ind} m_{dry}} \tag{6-2}$$

- MC_{ind} is the moisture content at induction from Table 6-1 and Table 6-2 (g/g_{dry})

The results for equations (6-1) and (6-2) are shown alongside the calculated $X_{af\ h} = (1\text{-}Y_{cr})$ values below in Figure 6-4. The remaining amorphous contents calculated by enthalpy are mostly between the limits of the two predictions with the exception of trials IO2 and OI3.

Trial OI3 had the highest calculated enthalpy change at 107J/g from which the Δh_{cr} was estimated. From Figure 6-4 to explain $X_{af\ h}$ being below $X_{af\ EMC}$ either the Δh_{cr} used must be inappropriate or the moisture must be not located in the amorphous lactose.

Trial IO2 has a calculated $X_{af\ h}$ above the calculated limits. This seems unlikely as the only explanation would be for the moisture content to be below EMC. This result casts further doubt in the accuracy of using the Δh_{obs} to directly compare the final amorphicity of samples.

For the results to make sense Δh_{cr} would have to be significantly lower than 108J/g for trial IO2 and therefore different to the Δh_{cr} for trial OI3. This is not accounting for the formation of different crystal forms which would have an effect as discussed in section 2.3.4. XRD results in section 6.4 found the potential presence of α-lactose monohydrate in the sample IO2, which was absent from the patterns of other trials.

Assuming the Δh_{cr} is applicable to all trials, except IO2 and OI1 for the reasons discussed above, Figure 6-4 shows that in trials IO3, OI1 and OI2 it was likely that all remaining moisture was located in the amorphous lactose and that in trial IO2 there could have been bound moisture. If the $X_{af\ h}$ value lies within the error-inclusive range of $X_{af\ EMC}$ and $X_{af\ MC\ ind}$ then it is possible that all of the moisture at the end of the trial was held within the remaining amorphous lactose predicted using the enthalpy results.

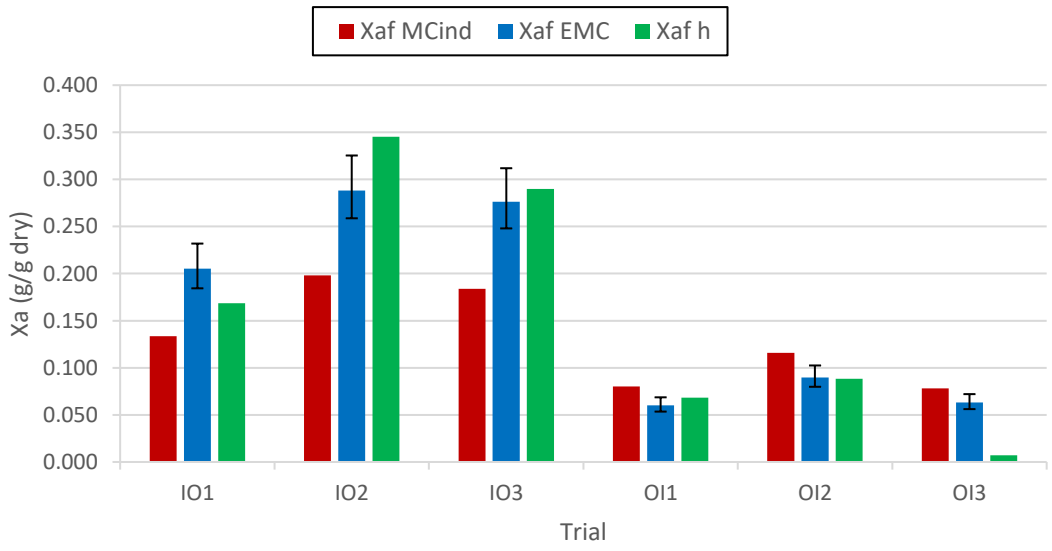

Figure 6-4: The calculated $X_{af\ EMC}$ and $X_{af\ MC\ ind}$ values for each trial alongside the $X_{af\ h}$ values (calculated from the $X_{cr\ h+}$ in Table 6-2 and Table 6-4. Error bars represent the uncertainty of the EMC_{al} prediction made using equation (2-3) and the parameters from section 4.3.3.

6.1.4 Conclusions

The observed enthalpy change associated with crystallization (Δh_{obs}) is proportional to the extent of crystallization determined gravimetrically. This was expected due to the apparent equilibrium at the end of each run meaning that desorption should have "caught up" to the crystallization event.

A comparison of amorphous contents calculated using the sample conditions at the end of the trial and the observed enthalpy change was inconclusive for determining the moisture distribution. While the majority of the trials show that it was likely a majority of the moisture was located in the remaining amorphous, the others cast doubt on the applicability of a single Δh_{cr} value despite the consistent relationship between Δh_{obs} and the moisture content change.

With the inside-out and outside-in crystallization cases achieved, the hypothesis of trapped moisture needed to be tested. This was done following the method described in section 5.2. If the sample was observed to release moisture this could then be compared to the STA results to assess the cause.

6.2 Moisture Release Results

After successful directional crystallization in the STA the samples were used to test the hypothesis of "trapped" moisture being slowly released if outside-in crystallization had occurred. This was achieved by using i-buttons to log the humidity above the sample as described in section 5.2.

6.2.1 Inside-out

The moisture release over time results for the inside-out trials are shown below. In each case the RH increases above the sealing RH shown at t=0 and the relative humidity at induction (11%RH), as moisture was released. The source of this could not be solely desorption from the amorphous lactose as the sample was at/near equilibrium at 11%RH, and certainly below equilibrium at 22%RH.

This was unexpected as it was hypothesized that inside-out crystallization would avoid the trapping of free water, and with the mass signal at apparent equilibrium crystallization was thought to have finished. Although it is likely that there was amorphous lactose remaining, based on the final enthalpy change (section 6.1), moisture would not be trapped in amorphous lactose. The crystals identified were anhydrous and non-absorbent (section 6.4).

Therefore, the moisture release could only come from hypothesized "trapped" free water, moisture released from continuing crystallization, or a combination of the two. The reasoning and relative merit of these two scenarios is discussed further in section 6.5.

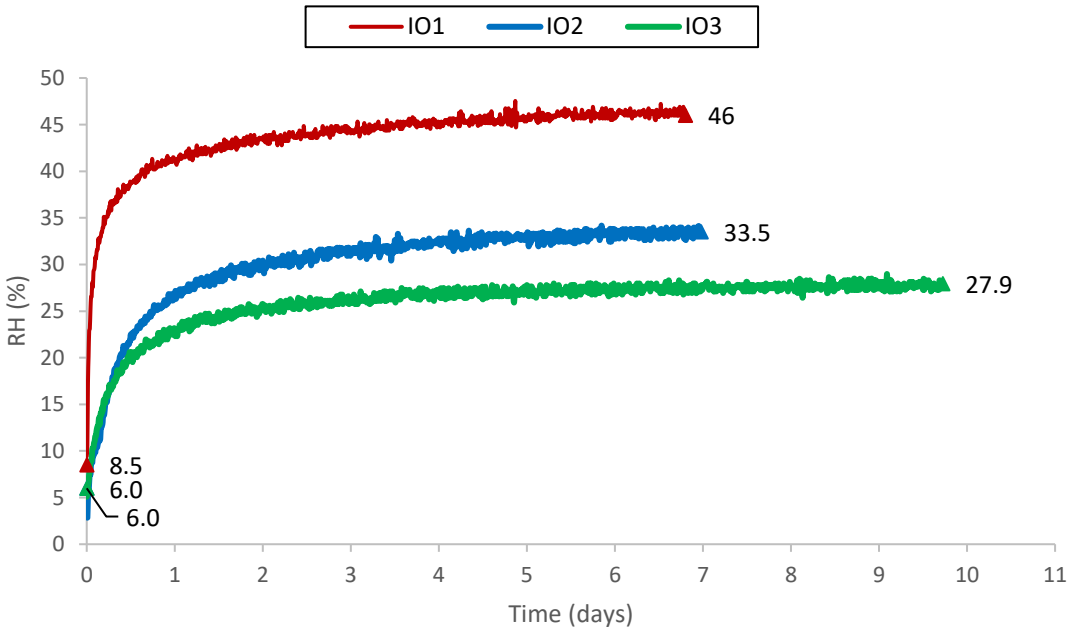

Figure 6-5: Relative humidity above sample over time results for inside-out crystallized samples.

6.2.2 Outside-in

The moisture release over time results for the inside-out trials are shown below. In each case the RH increases above the sealing RH shown at t=0 and the relative humidity at induction

(22%RH), as moisture was released. The source of this could not be solely desorption from the amorphous lactose as the sample was adsorbing to near equilibrium at 22%RH.

Although it is possible some the samples may have been partially amorphous based on the final enthalpy change (section 6.1), moisture would not be trapped in amorphous lactose. The samples were determined to consist of anhydrous and non-absorbent crystalline lactose forms in section 6.4.

Therefore, the moisture could only come from hypothesized trapped free water, moisture released from continuing crystallization, or a combination of the two. The reasoning and relative merit of these two scenarios is discussed further in section 6.5.

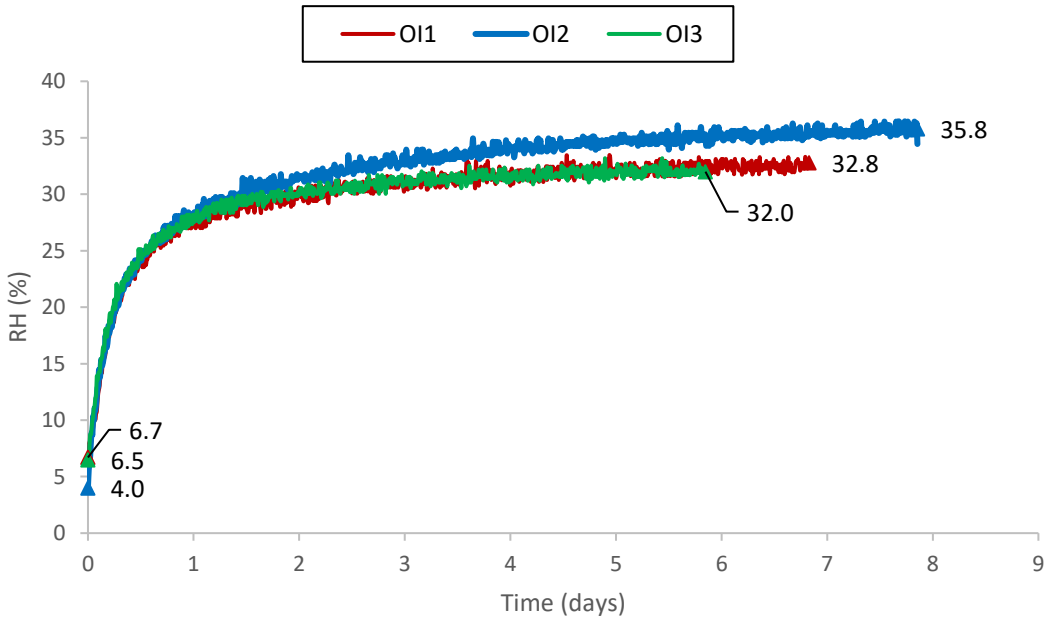

Figure 6-6: Relative humidity above sample over time results for outside-in crystallized samples.

6.2.3 Analysis

The volume of air above the sample is very small ($2.51 \cdot 10^{-7} m^3$) and the moisture capacity in the storage temperature range of 20-30°C is very low (17.3-30.4g/m^3 (Moran et al., 2010)) with a maximum capacity of 7.63µg of water. For desorption of free moisture to not cause saturation of the air the balance must be contained elsewhere. As lactose crystals have a very low absorbency (<0.000344g/g EMC (Bronlund & Paterson, 2004)) the balance would need to be contained in amorphous lactose. The final moisture content for each trial is known and the equilibrium moisture content at the final relative humidity can be used to estimate the required amorphous fraction to balance the moisture within the system by equation (2-2).

$$X_{af\ required} = \frac{MC_f m_{dry} - V_{air} MC_{air} - m_{dry} EMC_\beta(aw_f)}{EMC_{AL}(aw_f) m_{dry}} \quad (6\text{-}3)$$

- MC_f is the estimated final moisture content from section 6.1 (g/g_{dry})
- aw_f is the average water activity above the sample for the last recorded hour from Figure 6-5 and Figure 6-6.
- m_{dry} is the estimated dry mass from section 6.1 (g/g_{dry})
- V_{air} is the volume of air between the sample and the iButton, calculated in section 5.2, $2.51 \cdot 10^{-7} m^3$
- MC_{air} is the moisture capacity of the air at the average ambient temperature of 25°C 24 g/m^3 (Moran et al., 2010)
- $EMC_\beta(aw)$ is the equilibrium moisture content of β-lactose at aw_f from the isotherm of Bronlund (1997) (g/g_{dry})
- $EMC_{AL}(aw)$ is the equilibrium moisture content of amorphous lactose at aw_f from the isotherm in section 4.3 (g/g_{dry})

Equation (2-2) assumes that equilibrium was reached at the end of the STA trial and the subsequent moisture release trial and that the moisture content remained the same. In actuality some moisture was likely lost in the dry air box during the sealing process which took up to 15 minutes, and true equilibrium appears not to have been reached for most trials. The effect of this would be that the calculated amorphous content is likely higher than the actual value.

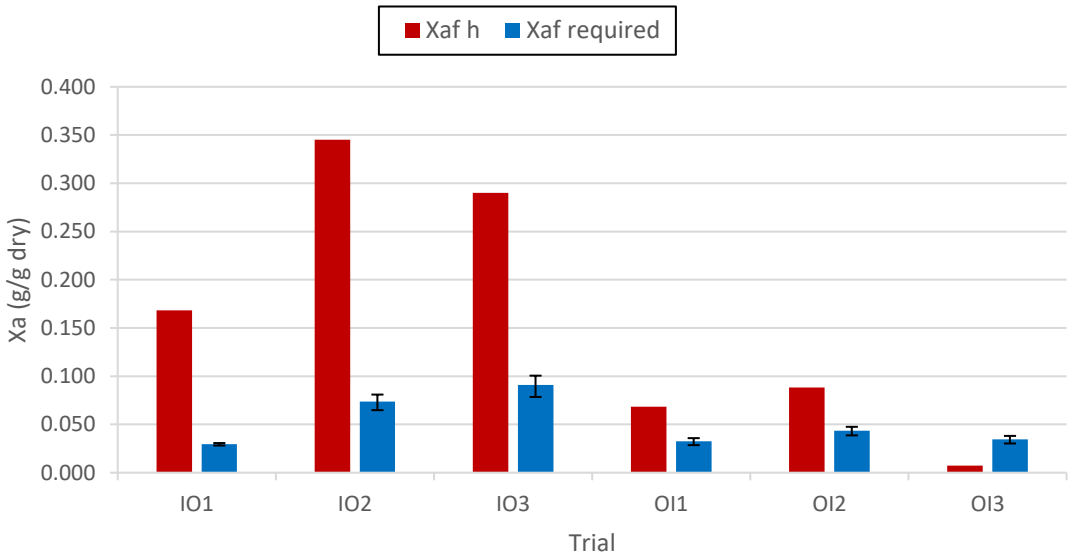

Figure 6-7: The calculated $X_{af\ required}$ values for each trial alongside the $X_{a\ h}$ values (calculated from the $X_{cr\ h+}$ in Table 6-2 andTable 6-4. Error bars represent the uncertainty of the EMC_{al} predictions.

Figure 6-7 shows that the required amorphous content calculated using equation (2-2) is significantly below that calculated using the observed enthalpy change for all but the last trial.

The discrepancy for the outside-in crystallization trial 3 indicates that the reference Δh_{cr} at 108J/g may have been too low in that case. This calls into question whether the calculation

method for Δh_{obs} is consistent enough from trial to trial that the same Δh_{cr} can be used. The uncertainty in the Δh_{cr} value however would not be expected to be large enough to explain the difference in the inside-out trials. The calculation of Δh_{cr} relied upon smoothed and corrected values, any error in the smoothing or offset of the correction file could cause some of the inconsistency.

The difference between the $X_{a\,h}$ and the $X_{af\ required}$ values for the inside out trial is especially significant and, if the assumptions made are correct, would indicate that crystallization occurred while the sample was sealed.
This crystallization would be a source of the free moisture which was released as seen in Figure 6-7. For the outside in trials it is unclear whether the difference is significant.

6.2.4 Conclusions

The amorphous lactose contents calculated from the STA and moisture release analysis disagree, with the STA determined content often higher. This could indicate crystallization occurred after STA analysis finished or that the observed enthalpy change was not a reliable measure of crystallinity.

The results of both the STA and moisture release analysis indicated there was amorphous lactose remaining in the samples. It was important to confirm and quantify the amorphous lactose quantity for comparison with the different estimates. The method selected for this was recrystallization in the STA by isothermal adsorption.

6.3 Amorphous Confirmation Results

To confirm the presence of amorphous lactose in the samples following the detection by enthalpy change (section 6.1) and X-ray diffraction (section 6.4) some samples were able to be recrystallized in the STA using the method in section 5.1. These samples were incomplete as for XRD a portion of the sample had to be broken off and mounted for examination, this portion was no longer suitable for STA analysis. The two samples excluded from this analysis (IO3 and OI1) were used for an unsuccessful microscopic investigation.

6.3.1 Results

The raw STA results were processed in the Proteus Analysis software to obtain the percentage mass changes and DSC areas for the samples, α-lactose monohydrate, and spray-dried amorphous powder (appendix 9.4.2). The corrected data and calculated amorphous contents are summarized below in Table 6-5:

Table 6-5: Amorphous content of the remaining samples calculated from recrystallization at 0.75aw

Sample	X_{meas}	A_{peak}	$X_{af\ peak}$	A_{full}	$X_{af\ full}$	TG_a	$X_{af\ ad}$	TG_d	$X_{af\ de}$	$X_{af\ av}$
-	g/g_{dry}	J/g	g/g_{dry}	J/g	g/g_{dry}	%	g/g_{dry}	%	g/g_{dry}	±Stdv
IO1	0.952	9.3	0.028	10.16	0.066	0.18	0.015	0.15	0.016	0.03±0.02
IO2	0.809	25.3	0.077	16.68	0.108	1.02	0.084	0.67	0.070	0.09±0.02
OI2	0.987	1.2	0.004	7.31	0.047	-0.12	0	-0.20	0	0.01±0.02
OI3	0.990	0.6	0.002	5.04	0.033	-0.08	0	-0.20	0	0.01±0.02
A	-	331	1	154.70	1	12.08	1	9.61	1	1
α-LM	-	0	0	0	0	0	0	0	0	0

- X_{meas} is the percentage of the sample which was reanalysed for the amorphous content; the balance was used for XRPD or lost when transferring to a new crucible (g_{dry}/g_{dry})
- A_{peak} is area of the exothermic DSC peak, corrected using the results of a blank STA run under the same conditions, associated with adsorption/crystallization of amorphous lactose (J/g), this was used to calculate $X_{af\ peak}$ ($g_{amorphous}/g_{dry}$).
- A_{full} is the corrected net area of the DSC signal during the 2h the sample was exposed to 75%RH (J/g), this was then used to calculate $X_{af\ full}$ ($g_{amorphous}/g_{dry}$).
- TG_a is the corrected peak percentage mass increase (%) this was used to calculate $X_{af\ ad}$ ($g_{amorphous}/g_{dry}$).
- TG_a is the corrected percentage mass decrease from the peak value (%) this was used to calculate $X_{af\ de}$ ($g_{amorphous}/g_{dry}$).
- $X_{af\ av}$ is the average of the other calculated amorphous contents ($g_{amorphous}/g_{dry}$).

6.3.2 Prediction for Whole sample

The portion of the sample not analysed can be assumed to be either all crystalline, all amorphous, or of the same composition as the analysed sample. In the case of the inside-out sample, where the amorphous is expected to be located in smaller particles (see section 6.4), the amorphous assumption may be valid. In the case of outside-in crystallized samples where

the amorphous is expected to be located on the interior or bottom of the particle the assumption of only crystalline lactose being lost may be valid.

For the trials analysed the range of possible amorphous contents based on the known amount of missing sample and the uncertainty in the measured $X_{af\ measured}$ value from the different prediction methods.

1. Maximum: The sample lost was entirely amorphous and the $X_{a\ full}$ value was the most accurate.

$$X_{af\ measured\ max} = \frac{X_{a\ full} + (1 - X_{meas})}{(X_{meas} - X_{a\ full})} \tag{6-4}$$

2. Minimum: The sample lost was entirely crystalline and the $X_{a\ de}$ value was the most accurate.

$$X_{af\ measured\ min} = \frac{X_{a\ de}}{2 - X_{meas}} \tag{6-5}$$

3. Average: The amorphous fraction of the particle is even at $X_{a\ av}$, the sample lost was of the same composition.

$X_{af\ measured\ av}$ was calculated for each sample and plotted (with error bars showing the range from $X_{af\ measured\ max}$ to $X_{af\ measured\ min}$) alongside $X_{af\ required}$ from section 6.2.3 in Figure 6-8. The ranges overlap for all samples, with the average value for the inside-out sample, and the maximum value for the outside in samples, matching well with that calculated previously.

If the assumptions made in the calculations of $X_{af\ required}$ are correct then the $X_{a\ measured}$ value, measured afterwards, could not be higher. This could be explained by:

- The sensitivity of the STA to the low amount of amorphous lactose as found in the OI samples being poor. The detection limit for STA is estimated at 1% (Listiohadi et al., 2009; Smith et al., 1981) and quantities close to this limit may not be detected accurately.
- Amorphous lactose located on the base of the outside-in samples being lost. Following incomplete outside-in crystallization it would be expected that the region least exposed to the humid air, the base of the sample, would have a lower moisture content and would be most likely to remain amorphous. During the transfer of the sample to a new crucible some of the amorphous lactose could have remained adhered to the old crucible.
- A more even distribution of remaining amorphous lactose in the inside out sample than thought based on the observations during X-ray diffraction.

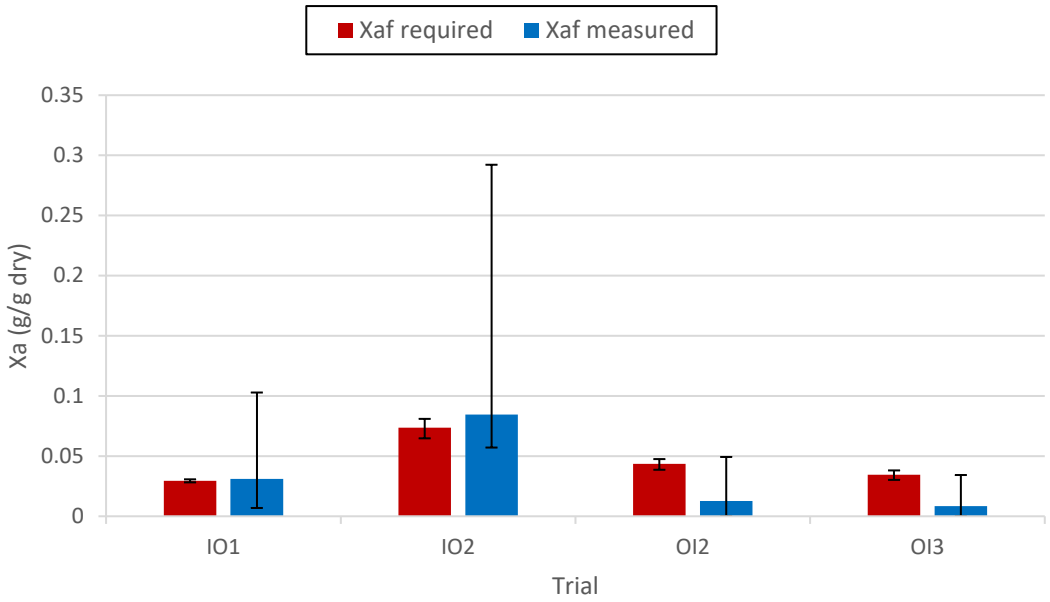

Figure 6-8: The calculated $X_{af\ measured}$ values for each trial alongside the $X_{af\ required}$ values (calculated in section 6.2.3). Error bars represent the minimum and maximum possible value calculated using equations (6-4) and (6-5).

6.3.3 Conclusions

The large error due to the incomplete samples makes a definitive statement difficult beyond that amorphous lactose was likely present in all samples. The quantities determined for the inside-out trials are likely lower than would be expected given the Δh_{obs} results, agreeing with the observations of section 6.2.3.

To determine whether the estimated moisture content for section 9.4.1 includes water of crystallization presence of α-lactose monohydrate in the samples had to be determined. This was done by X-ray powder diffraction to identify the forms of crystalline lactose present in the samples non-destructively.

6.4 XRD Results

Once all the samples had been analysed for moisture release they were analysed by X-ray powder diffraction (XRPD) to determine the crystal forms present.

XRPD patterns were obtained for the directional crystallization samples using the same equipment and method as described in section 4.1.3.

Pure laboratory grade α-lactose monohydrate and β-lactose powders were run first to obtain reference patterns. These patterns were compared with literature patterns from Buma and Wiegers (1967) and found to agree well (appendix 9.4.3).

As the samples were brittle solids; in contrast with the amorphous powder, it was decided to break small fragments off to be mounted on the 0.25mm loop. The full sample would be much too large to mount itself.

The appearance of the samples was that of several lumps of different sizes which were largely fused together. This is thought to be due to uneven distribution of the powder in the crucible as the sample collapsed and began to flow. The outside-in samples were more evenly spread, while the inside-out samples had more discreet lumps.

To preserve the samples as much as possible the fragments were initially taken from smaller "lumps" of the sample. This method was varied, with fragments taken from larger areas of sample, for reasons discussed later.

6.4.1 Data Processing

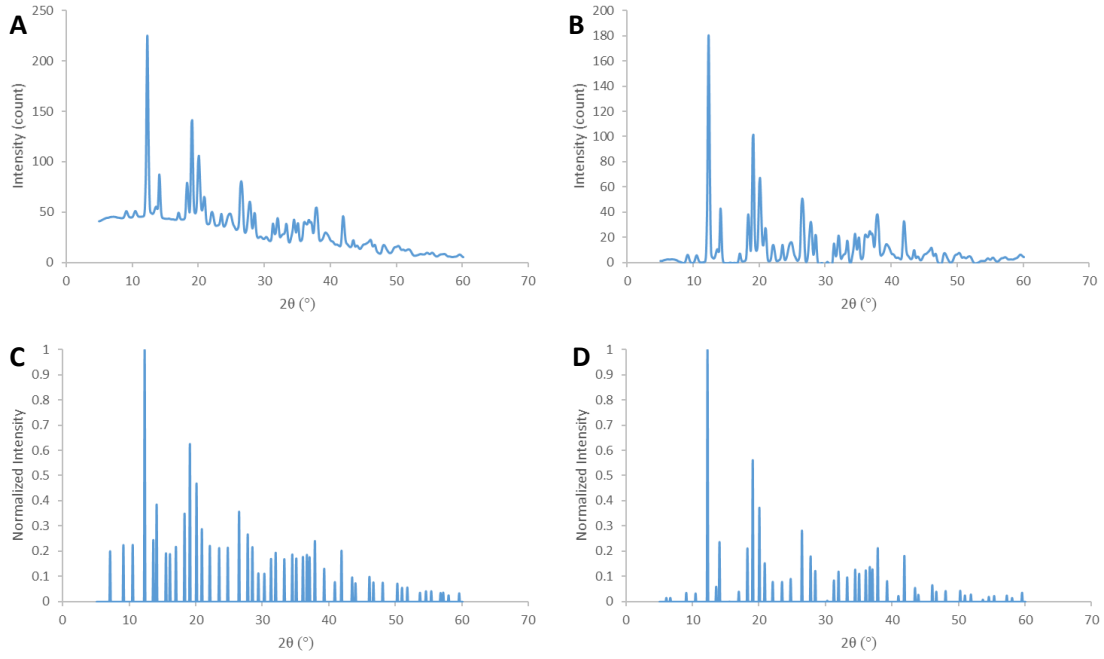

Figure 6-9: Figure showing the progression for an XRPD pattern obtained for a fragment from sample IO1, A is the pattern obtained using the software, B is the same pattern with the background removed, C shows the peaks identified and normalized from the raw pattern, D shows the peaks identified and normalized from the background corrected pattern.

The data was processed to determine the location of the peaks and their relative intensity. First the background was removed by modelling the minima of the data with a polynomial and subtracting the result, seen in Figure 6-9 A to B. The background corrected data was then used for peak identification as local maxima, and these peaks were normalized against the greatest observed intensity (Figure 6-9 D). Figure 6-9 C shows the normalized peaks determined from the uncorrected data. Comparing this with plot D, many of the peaks are overemphasized.

Following the processing the peaks were compared against literature diffraction patterns for α-lactose monohydrate, α-lactose anhydrous unstable, α-lactose anhydrous stable, β-lactose, α:β 5:3 mixed crystal, and α:β 4:1 mixed crystal (Buma & Wiegers, 1967; Simpson et al., 1982). The characteristic peaks collected in Table 2-4 were also used for identification. Of note is that in some instances the only pattern which provided a match had characteristic peaks slightly offset by 0.1°, this was considered acceptable given the variation in reported characteristic angles.

6.4.2 Inside-out

The first two XRPD patterns were made using fragments from smaller discrete lumps of the inside-out samples. The result was two highly amorphous patterns, lacking strong peaks associated with crystallinity shown in Figure 6-10. The only identifiable characteristic peaks were at 18.3° for IO1 and 18.3°, 19°, and 20° for IO2, both potentially indicating α:β 5:3 mixed crystal.

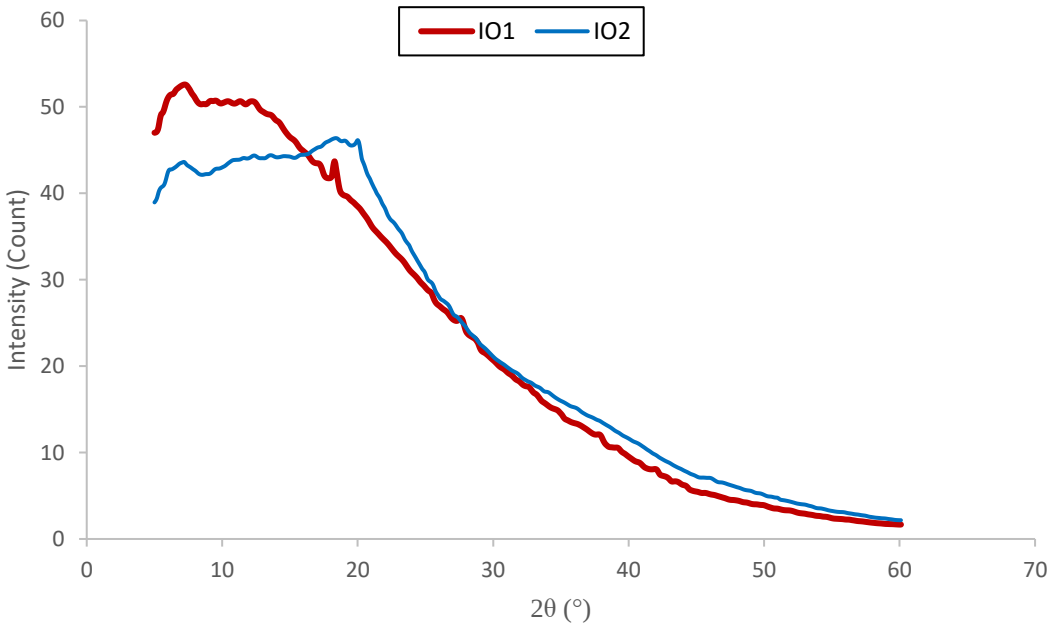

Figure 6-10: Amorphous patterns of fragments taken from small "lumps" of IO2 and IO3.

The sampling method was changed for the next runs for the IO1 and IO2 samples and IO3 sample. Instead of taking a fragment from a smaller "lump" they were taken from the largest continuous area of the sample. The resulting patterns for these were highly crystalline with a low level of background compared to the peaks, the processed peaks are shown in Figure 6-11. Characteristic peaks at 19.1°, 20.1°, 18.3°, and 22.1° were present for all of the samples

indicating the presence of α:β 5:3 mixed crystal. IO1 and IO2 also had peaks at 10.5° and 21.0° characteristic of β lactose.

The strong peak at 12.3° for IO1 and IO2 could not be clearly attributed to a crystal form. 12.3° is not far from 12.5° a characteristic peak for α-lactose monohydrate although only IO2 had another peak near 16.4°, the other characteristic peak. As such IO2 may have contained some α-lactose monohydrate.

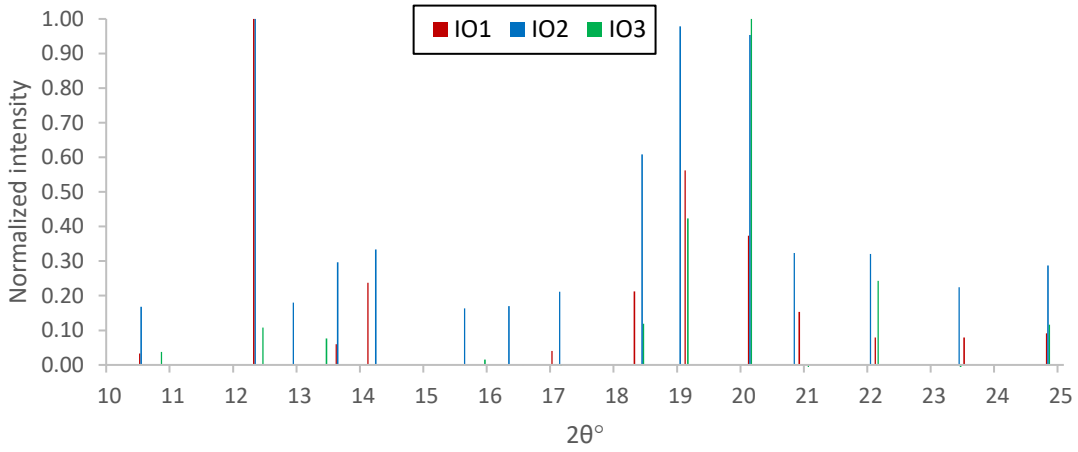

Figure 6-11: Identified XRD peaks for inside-out crystallized sample fragments versus 2ϑ.

6.4.3 Outside-in

The outside-in crystallized samples lacked the discrete lumps of the inside-out samples so the fragments analysed were taken at random. The resulting patterns were all highly crystalline with clear peaks. The processed peak data is displayed in Figure 6-12. All samples agreed well with characteristic peaks at/near 19.1°, 20.1°, 18.3°, and 22.1° indicating α:β 5:3 mixed crystal. IO1 and peaks at 10.5° and 21.0° indicating β lactose.

The peaks of OI1 and OI2 were slightly offset from the literature by ±0.1 and this is attributed to the smoothing method used to obtain the data.

Again a peak was present at 12.3° for all samples but without a peak in the region of 16.4° so no significance was assigned to it.

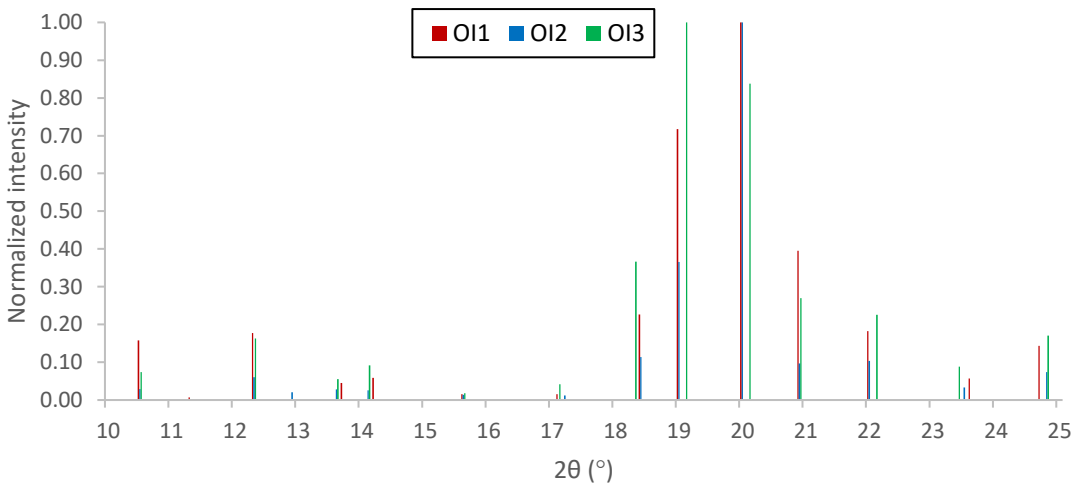

Figure 6-12: Identified XRD peaks for outside-in crystallized sample fragments versus 2θ.

6.4.4 Conclusions

The formation of anhydrous β lactose and α:β mixed crystal was expected given the conditions under which crystallization took place (A. Paterson, personal communication, June 20, 2018).

The presence of amorphous lactose could also be expected for the inside-out crystallized samples as the trials showed a lower enthalpy associated with the crystallization than the outside-in trials and previous results.

An important result was that the fragments found to be amorphous were taken from smaller discrete “lumps” of the sample. These were rounded in shape and no-longer a powder indicating at least partial collapse had taken place. Previous failed attempts at inside-out crystallization, where desorption occurred too rapidly, had resulted in the sample remaining as a fine powder.

A theory was developed for why these smaller unconnected pieces of sample were amorphous where the bulk of the sample was crystalline. Because of the gradual decrease in the relative humidity the lumps were able to begin glass transition. Because of the smaller mass and critical dimension when compared with the bulk of the sample however desorption was faster for this component, and much of it dried to a moisture content which would not allow the rapid crystallization observed elsewhere. Figure 6-13 shows the theorized process from the amorphous sample (1) to the partially crystalline product (2) as the moisture gradient is developed. It is suggested that maintaining an even gradient across the sample would require better control of particle size and agglomeration. This could be accomplished with a single large particle of amorphous lactose produced by freeze-drying, which would also provide a greater cross section for a moisture gradient to occur through.

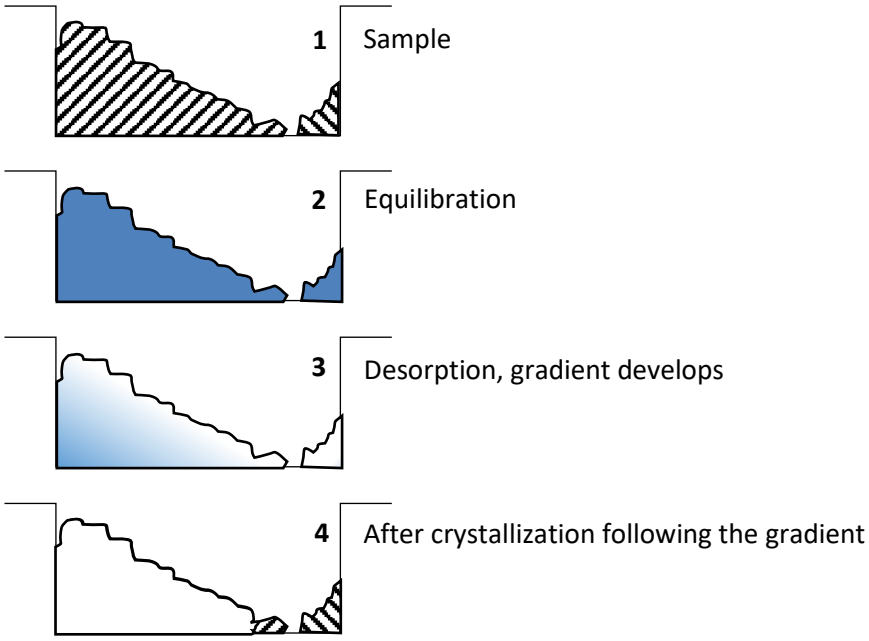

Figure 6-13: Cross section view of a crucible showing the theorized changes to an inside-out crystallized sample. 1: purely amorphous, 2: equilibrated at the maximum RH, 3: moisture gradient develops the small particle on the right desorbs more quickly, 4: crystallization occurs where the moisture content is sufficient.

6.5 Source of Moisture

The results from the moisture release section clearly show that moisture is released from both sets of samples. The analysis of the results from sections 6.1, 6.2, and 6.3 provide conflicting estimates of the amorphous content of the sample meaning that crystallization after the STA measurement is a possibility. Determining the source of this moisture is important in testing the hypothesis of trapped free water in the particle. Due to the methods used to transport and seal the sample described in section 5.2 external moisture seems unlikely to be the cause. The only exposure a sample had to environmental humidity conditions would have been in the few seconds it took to transfer the sample from the STA to a desiccator.

Forms of Moisture

The final moisture content of each sample has been estimated and there are four forms which this moisture could take:

Free Water

This is the form in which water is hypothesised to be trapped in the inside out case, diffusing slowly from a crystalline particle and raising the water activity of the surroundings.

Water of Crystallization

This is water bound within the crystalline structure and is only known to occur in α-lactose monohydrate. The XRPD results showed the samples from both trials are a highly crystalline mix of anhydrous β and β:α 5:3 lactose. Trace amounts of α-lactose monohydrate may have existed, but this would not be a significant portion of the sample moisture content.

Water Adsorbed to the Crystal Fraction

Bronlund (1997) measured sorption isotherms for both α-lactose monohydrate and β-lactose anhydrous. Both had very low (<0.01% dry) equilibrium moisture contents below 0.6aw. Water would be expected to be adsorbed to the crystal but in a nearly insignificant quantity.

Water Adsorbed to the Amorphous Fraction

Amorphous lactose in contrast to the crystalline fraction has a high affinity for moisture. The mass of the sample was at or near equilibrium when the sample was removed from the STA. Any amorphous fraction would therefore be expected to be at the equilibrium moisture content for the final experimental conditions (i.e. 95°C 11% or 22%RH.

Incomplete crystallization, resulting in an amorphous fraction, can be considered likely for all inside-out results and possible for the outside-in results from the enthalpy analysis. XRPD patterns for fragments of two inside-out samples showed high amorphicity. The results from the amorphous confirmation also showed that there was some amorphous lactose remaining in all the samples tested. The amount measured agreed with that required at the final water activity above the sample.

Possible Cases for These Samples

The moisture remaining inside the particle at the end of the trial could be either: located solely within the amorphous lactose, or both in the amorphous lactose and as free moisture. For the

moisture within the amorphous lactose to be released and raise the water activity above the sample higher than the equilibrium water activity, crystallization must occur.

Relative Strength of X_a Predictors

- Δh_{obs}: The enthalpy change result has a considerable potential error. The mass and DSC signals, from which it was calculated it, both had significant noise and errors. Because of this considerable smoothing and correction was required as detailed in section 4.2.1. This processing may have introduced considerable error in the value. When used to track crystallization this precision is not as important as when comparing the values between trials. However, the consistent relationship between Δh_{obs} and the change in moisture content supports it as a useful measure of the extent of crystallization.
- Δh_{cr}: The enthalpy of crystallization for amorphous lactose was calculated from the maximum Δh_{obs} so has the associated error described there. From section 6.1.4 the amorphous contents calculated using the value of 108J/g do not always agree with the moisture content range.
- MC_f: The final moisture content at the end of the STA run is considered quite accurate. The sample mass at the end of the trial is from the smoothed and corrected STA data set, and the dry mass was predicted using equation (5-1). Despite the prediction of the dry mass having some associated error it gives results consistent with the isotherms in section 4.3.3.
- RH_f: The relative humidity over the sample at the end of approximately 1 week is considered accurate. As discussed in section 5.2 the iButtons were confirmed to be accurate and leaks should not have occurred.
- EMC: The equilibrium moisture content calculated from the isotherm in section 4.3.3 varies in precision depending on the water activity. In the region of 0.14 to 0.5aw there could be a significant amount of error as the fit in this region was made using predicted values.
- $X_{a\ measured}$: The amorphous contents calculated in section 6.3 have the largest potential for inaccuracy. The samples were measured following XRPD and were not "complete" compared to what came out of the STA and error is introduced by the missing material. The analysis by integration of the DSC signal and observing the mass change separately is valid for detection but with lower masses of amorphous present noise and experimental error are significant.

Having compared the reliability of the results obtained, the next thing to be considered was the potential explanations for both the crystallization and no-crystallization cases during the moisture release experiments.

Crystallization

The most plausible explanation for crystallization to occur at room temperature is a sufficient local moisture content to allow crystallization in a portion of the amorphous fraction. This uneven distribution of moisture could exist prior to sealing or be the result of moisture movement following sealing. Once the moisture content was sufficient for crystallization to occur the crystal has a lower equilibrium moisture content and water is driven out. This released moisture could increase the local moisture content of nearby amorphous lactose, causing crystallization. For crystallization at ambient temperature of 25°C a moisture content of the most likely crystalline product α-lactose monohydrate. Using the updated WLF model in section 3.7 and the Gordon-Taylor equation with the constants derived by Brooks (2000) an

estimated amorphous moisture content of 0.12-0.13g/g dry would be required for crystallization to occur at 25°C within 7 days. This is 3.35 and 7.14 times the respective EMCs at the end of the STA runs for the inside-out and outside-in trials.

The concentration of moisture within the remaining amorphous lactose could be due to:

- Trapped free moisture: Crystallization could occur due to the movement of free water trapped in the crystal structure. As the free moisture diffuses it could be adsorbed by the hygroscopic amorphous lactose. At the increased moisture content (>0.12g/g dry) crystallization could occur at room temperature.
- Ongoing crystallization: in this case crystallization is still occurring as the experiment ends but at a much slower rate. Moisture is still released and diffuses being concentrated in some amorphous areas causing crystallization. Alternatively, the moisture distribution is uneven.

Another potential explanation is that the remaining amorphous lactose has collapsed, and the reversal of this process is slow enough for crystallization to occur.

If crystallization occurred due to moisture movement it would make sense that the inside-out trials would be have a higher final amorphous content ($X_{af\ required}$) than the outside-in samples. This is due to theorized uneven drying: that smaller “lumps” of collapsed amorphous lactose which dried too quickly to crystallize, would be not adsorb moisture from the rest of the crystallizing sample.

No-Crystallization

Because of the experimental design crystallization during the humidity readings was considered unlikely due to several factors:

- Before removal from the STA sample mass was checked to have been stable with less than a 0.03% mass change in the past hour. This was taken to mean that crystallization had ceased.
- Because of the low sample masses, they would cool to room temperature within the time it took to seal them. The moisture content of any amorphous component would be too low at room temperature to allow crystallization.
- The exposure of the samples at atmospheric humidities was minimized by transporting the samples in desiccators and only handling them in the controlled humidity glove box. This would not be expected to be a source of moisture inside the sample.
- The water activity above the samples never reached a high enough level for crystallization at room temperature to be possible.

If crystallization did not occur during the moisture release measurements then; as shown in Figure 6-14, for Δh_{obs} to agree with the estimated Y_{cr} (Y_{cr} =1-$X_{af\ required}$ from section 6.2.3) Δh_{cr} cannot be constant. Instead it would have to vary between 76 and 111J/g. If so, such a wide variation would be unexpected despite the sources of uncertainty. Furthermore, the variation of the required Δh_{cr} value appears to be strongly dependent on Δh_{obs} (see Figure 6-15), in which case samples releasing less heat during partial crystallization are also expected to require less heat to fully crystallize which could not be plausibly explained. If $X_{af\ required}$ is the

actual amorphous content at the end of crystallization, then Δh_{cr} is not a valid measure of crystallinity.

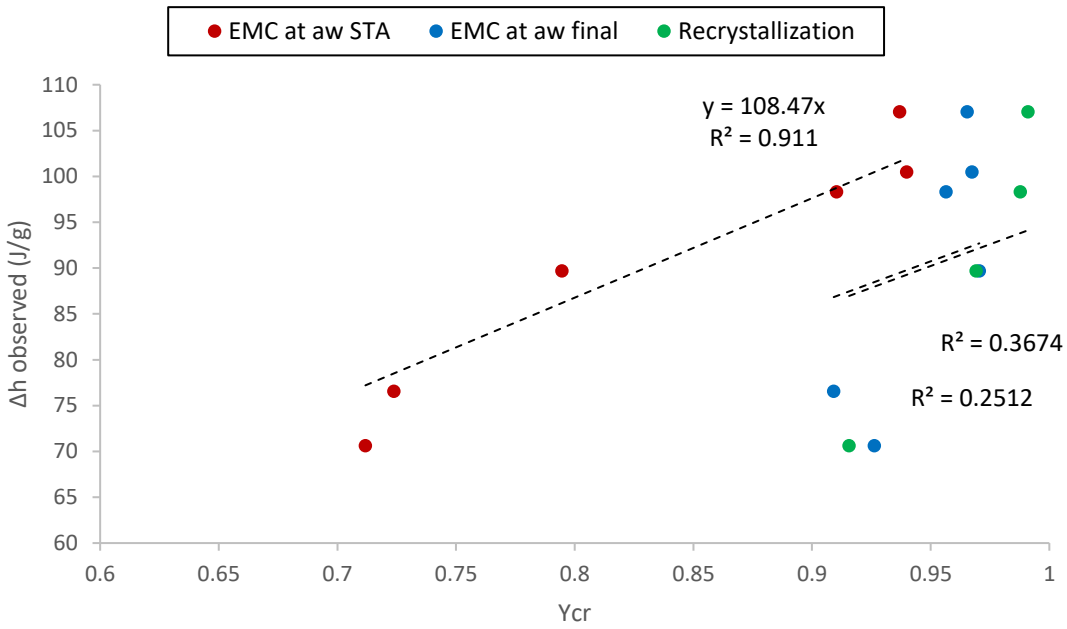

Figure 6-14: Δh_{obs} versus Y_{cr} calculated from the final water activity during crystallization (Section 6.1.3), the final water activity above the sample during moisture release (Section 6.2.3), and the average from the recrystallization trials (Section 6.3.1). Trendlines are fitted for Δh_{obs} =0 at Y_{cr}=0.

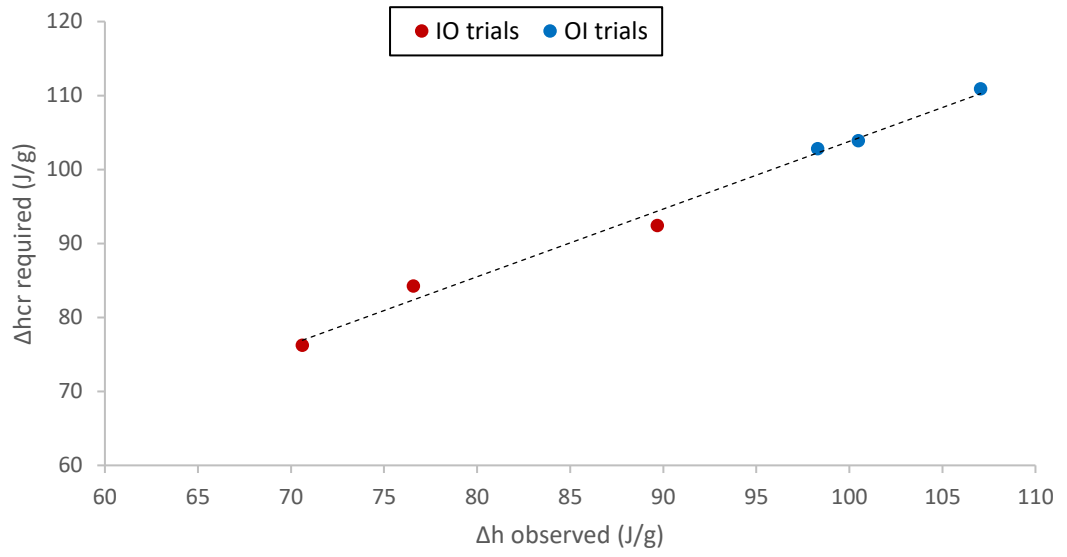

Figure 6-15: $\Delta h_{required}$ for the $X_{af\ required}$ results to agree with the enthalpy results versus Δh_{obs}.

The theoretical trapped moisture content for each sample along with the equilibrium water activity is shown in Figure 6-16. For the moisture to be trapped crystallization would have to significantly out-pace desorption from the sample. Trapped moisture would be considered less likely to occur in the inside-out crystallization cases where desorption was occurring prior to

crystallization. This conflicts with the significantly higher theoretical mass of water trapped in the samples of 0.036±0.005 (±stdv) mg for the inside-out crystallized samples compared to the 0.016±0.012mg (±stdv) for the outside-in crystallized samples.

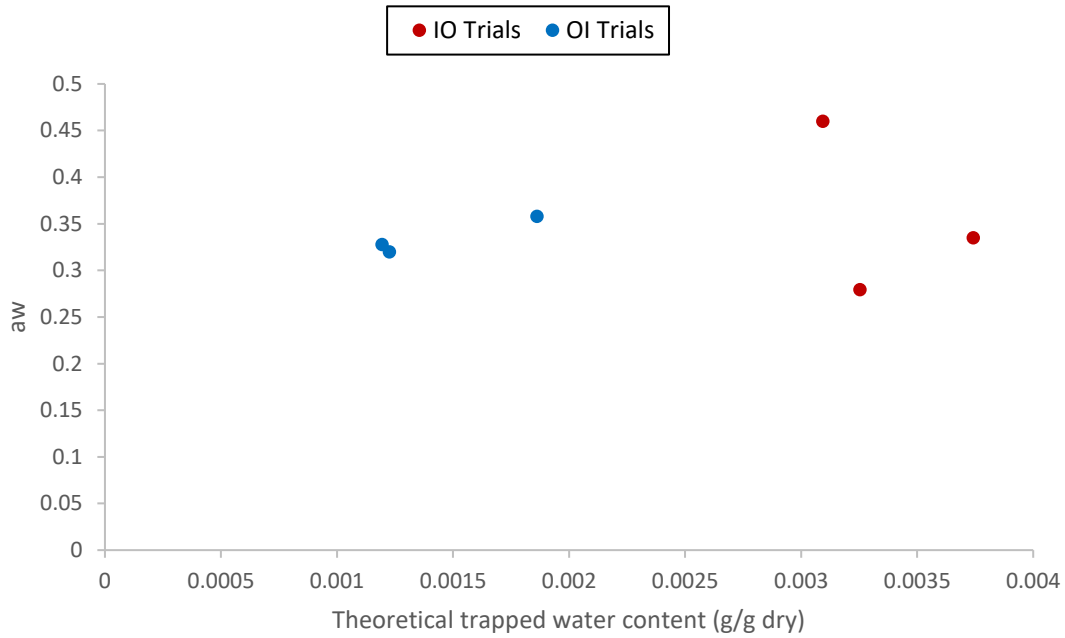

Figure 6-16: Theoretical trapped moisture content at the end of the STA measurement, assuming no crystallization, versus final water activity recorded above sample from section 6.2.

Conclusion

The source of the moisture in the i-button headspace cannot be definitively determined with the current information. Crystallization seems unlikely due to the unfavourable conditions but cannot be completely discounted if the moisture content was not evenly distributed.

What can be conclusively stated is that the samples were partially amorphous and that all released a significant amount of free moisture over time after crystallization looked to be complete in the STA trials. This raised the water activity above them indicating that further crystallization occurred or another mechanism such as the release of “trapped” moisture occurred.

Trapped moisture inside the crystal structure seems more likely under the conditions in which the rise was observed. However, this has not been documented before. Furthermore, the possibility of trapped moisture disagrees with the observed enthalpy change of the samples.

This can be applied to the hypothetical case of bulk crystalline lactose powder on which a layer of amorphous lactose formed then recrystallized, during the drying process. The increase in the water activity above this product as it is stored could cause the handling issues described in section 1. Whether the increase in water activity is due to trapped moisture, ongoing crystallization, or a combination; it would not occur if the amorphous layer had not crystallized. Based on these observations the operation of a dryer to achieve directional crystallization, or in fact crystallization at all would not be recommended. Instead it would be recommend to operate the fluid bed dryer under conditions for which crystallization is

unlikely, using the models fitted in section 3, and that the resulting product is stored below 0.25 aw as determined by Bronlund (1997).

7 Conclusions and Suggestions for Future Work

The William-Landel-Ferry (WLF) and Arrhenius type kinetic models were compared and found to fit well with literature data for amorphous lactose crystallization, and are valid over a wider range of conditions than prior models. The WLF type model is recommended for use in determining the crystallization time, the Arrhenius type model recommended for predicting the crystallization kinetics. Based on predictions from these models it is believed that crystallization of amorphous lactose could take place under fluid bed drying conditions.

The method developed for isolating the enthalpy changes in amorphous lactose from isothermal simultaneous thermal analysis data shows promise for observing the crystallization process. The resulting kinetic data did not follow the Avrami model with two clear regimes of crystal growth visible. This method was found to be potentially unsuitable for low-level amorphous lactose quantification because of disagreement with subsequent measurements.

The sorption behaviour of amorphous lactose was investigated and no evidence of temperature dependence was found. The presence of bound moisture in desiccated amorphous lactose was confirmed.

Methods developed to achieve inside-out and outside-in are believed to have successfully achieved the moisture gradient required for directional crystallization to have occurred. These methods were unsuccessful in achieving complete crystallization and testing the theory of trapped moisture. Achieving complete crystallization while maintaining a gradient of the conditions would be unlikely unless a much larger particle size was used. Given the complexity in achieving these conditions experimentally with a fully amorphous sample it would be hard to deliberately achieve them industrially.

The samples crystalized under both outside-in and inside-out conditions increased the relative humidity of the air above samples when stored over an extended period of time compared to the water activity at which they were equilibrated. The source of the moisture could not be clearly distinguished between ongoing crystallization and moisture diffusing through a crystal barrier formed at the surface. This rise in water activity would not be expected from a fully amorphous lactose sample or pure lactose crystals.

Based on these results it is recommended that lactose crystal fluid bed driers are operated under conditions below those required for the induction of amorphous lactose crystallization. Conditions under which crystallization is unlikely could be estimated using the WLF or Arrhenius kinetic models fitted in this work.

8 References

Affertsholt-Allen. (2007). *Market developments and industry challenges for lactose and lactose derivatives.* Paper presented at the IDF Symposium "Lactose and its Derivatives.

Angberg, Nyström, & Castensson. (1991). Evaluation of heat-conduction microcalorimetry in pharmaceutical stability studies. III. Crystallographic changes due to water vapour uptake in anhydrous lactose powder. *International Journal of Pharmaceutics, 73*(3), 209-220.

Arvanitoyannis, & Blanshard. (1994). Rates of crystallization of dried lactose-sucrose mixtures. *Journal of Food Science, 59*(1), 197-205.

Asano, Aoki, & Yamazaki. (1978). Method of producing beta-lactose: Google Patents.

Barham, & Hodnett. (2005). In Situ X-ray Diffraction Study of the Crystallization of Spray-Dried Lactose. *Crystal Growth & Design, 5*(5), 1965-1970. doi:10.1021/cg050237c

Bell. (1930). Some Methods of Prepaing Quickly Soluble Lactose. *Industrial & Engineering Chemistry, 22*(1), 51-54. doi:10.1021/ie50241a015

Bolhuis, Kussendrager, & Langridge. (2004). Spray-Dried Lactose.

Bronlund. (1997). *The modelling of caking in bulk lactose.* (Ph.D.), Massey University, Palmerston North, New Zealand.

Bronlund, & Paterson. (2004). Moisture sorption isotherms for crystalline, amorphous and predominantly crystalline lactose powders. *International Dairy Journal, 14*(3), 247-254.

Brooks. (2000). *The sticking and crystallisation of amorphous lactose.* (M.E.), Massey University, Palmerston North, New Zealand.

Brum, & Burnett. (2011). Quantification of Surface Amorphous Content Using Dispersive Surface Energy: the Concept of Effective Amorphous Surface Area. *AAPS PharmSciTech, 12*(3), 887-892. doi:10.1208/s12249-011-9655-5

Buck. (1981). New equations for computing vapor pressure and enhancement factor. *Journal of applied meteorology, 20*(12), 1527-1532.

Buckton, & Darcy. (1995). The use of gravimetric studies to assess the degree of crystallinity of predominantly crystalline powders. *International Journal of Pharmaceutics, 123*(2), 265-271. doi:http://dx.doi.org/10.1016/0378-5173(95)00083-U

Buckton, & Darcy. (1996). Water mobility in amorphous lactose below and close to the glass transition temperature. *International Journal of Pharmaceutics, 136*(1–2), 141-146. doi:http://dx.doi.org/10.1016/0378-5173(96)04503-6

Buckton, Darcy, Greenleaf, & Holbrook. (1995). The use of isothermal microcalorimetry in the study of changes in crystallinity of spray-dried salbutamol sulphate. *International Journal of Pharmaceutics, 116*(1), 113-118. doi:https://doi.org/10.1016/0378-5173(94)00322-V

Buckton, Darcy, & Mackellar. (1995). The use of isothermal microcalorimetry in the study of small degrees of amorphous content of powders. *International Journal of Pharmaceutics, 117*(2), 253-256. doi:https://doi.org/10.1016/0378-5173(94)00421-Z

Buckton, Yonemochi, Hammond, & Moffat. (1998). The use of near infra-red spectroscopy to detect changes in the form of amorphous and crystalline lactose. *International Journal of Pharmaceutics, 168*, 231-241.

Buma, & Wiegers. (1967). X-ray powder patterns of lactose and unit cell dimensions of ß-Lactose. *Neth. Milk and Dairy J., 21*.

Burnett, Malde, & Williams. (2009). Characterizing amorphous materials with gravimetric vapour sorption techniques. *Pharmaceutical Technology Europe, 21*(4), 41-45.

Burnett, Thielmann, Sokoloski, & Brum. (2006). Investigating the moisture-induced crystallization kinetics of spray-dried lactose. *International Journal of Pharmaceutics, 313*(1), 23-28. doi:https://doi.org/10.1016/j.ijpharm.2006.01.012

Bushill, Wright, Fuller, & Bell. (1965). The crystallisation of lactose with particular reference to its occurence in milk powder. *Journal of the science of food and agriculture, 16*, 622-628.

Cal, Iglesias, Souto, Concheiro, Gómez-Amoza, & Martinez-Pacheco. (1996). Effects of hydration on the properties of a roller-dried β-lactose for direct compression. *International Journal of Pharmaceutics, 129*(1-2), 253-261.

Carpin, Bertelsen, Dalberg, Roiland, Risbo, Schuck, & Jeantet. (2017). Impurities enhance caking in lactose powder. *Journal of Food Engineering, 198*, 91-97. doi:10.1016/j.jfoodeng.2016.11.013

Carter, & Norton. (2007). *Ceramic materials: science and engineering*: Springer Science & Business Media.

CEAS. (2018). The Williams Landau Ferry (WLF) equation and Time Temperature Superposition. Retrieved from http://www.eng.uc.edu/~beaucag/Classes/Characterization/DMA%20Lab/WLF.pdf

Çelikbilek, Ersundu, & Aydın. (2012). Crystallization kinetics of amorphous materials *Advances in crystallization processes*: InTech.

Chavda. (2009). *Quantification of low level of amorphous lactose in alpha lactose monohydrate.* (Postgraduate Diploma in Food technology).

Chen, Bates, & Morris. (2001). Quantifying amorphous content of lactose using parallel beam X-ray powder diffraction and whole pattern fitting. *Journal of Pharmaceutical and Biomedical Analysis, 26*(1), 63-72. doi:https://doi.org/10.1016/S0731-7085(01)00346-6

Chidavaenzi, Buckton, Koosha, & Pathak. (1997). The use of thermal techniques to assess the impact of feed concentration on the amorphous content and polymorphic forms present in spray dried lactose. *International Journal of Pharmaceutics, 159*(1), 67-74. doi:https://doi.org/10.1016/S0378-5173(97)00272-X

Clark. (2012). *Amorphous lactose crystallisation kinetics.* (M.E. M.E.), Massey University, Palmerston North.

Clarke. (2002). *The Production of a New Lactose Crystal in a Super-Heated Steam Environment*. Retrieved from Palmerston North:

Darcy, & Buckton. (1998a). Crystallization of Bulk Samples of Partially Amorphous Spray-Dried Lactose. *Pharmaceutical Development and Technology, 3*(4), 503-507. doi:10.3109/10837459809028632

Darcy, & Buckton. (1998b). Quantitative assessments of powder crystallinity: Estimates of heat and mass transfer to interpret isothermal microcalorimetry data. *Thermochimica Acta, 316*(1), 29-36. doi:https://doi.org/10.1016/S0040-6031(98)00300-1

Das, & Langrish. (2012). An activated-state model for the prediction of solid-phase crystallization growth kinetics in dried lactose particles. *Journal of Food Engineering, 109*(4), 691-700. doi:https://doi.org/10.1016/j.jfoodeng.2011.11.024

Dhanjee, & Paterson. (2000). *A new lactose crystal*. Retrieved from

Dilworth, Buckton, Gaisford, & Ramos. (2004). Approaches to determine the enthalpy of crystallisation, and amorphous content, of lactose from isothermal calorimetric data. *International Journal of Pharmaceutics, 284*(1), 83-94.

Domovs, & Freund. (1960). Methanol-soluble complexes of lactose and of other carbohydrates. *Journal of Dairy Science, 43*(9), 1216-1223.

Dormeuil. (2017). *A Novel Method for Investigating Amorphous Lactose Crystallization*. Internship Report. Massey University.

Downton, Flores-Luna, & King. (1982). Mechanism of stickiness in hygroscopic, amorphous powders. *Industrial & Engineering Chemistry Fundamentals, 21*(4), 447-451. doi:10.1021/i100008a023

Drapier-Beche, Fanni, Parmentier, & Vilasi. (1997). Evaluation of Lactose Crystalline Forms by Nondestructive Analysis. *Journal of Dairy Science, 80*(3), 457-463. doi:10.3168/jds.S0022-0302(97)75957-5

Durham. (2009). Modern approaches to lactose production. In M. Corredig (Ed.), Dairy-Derived Ingredients: Food and Nutraceutical Uses (pp. 103-144): Elsevier Science. Retrieved from https://books.google.co.nz/books?id=cI2kAgAAQBAJ.

Durham, Hourigan, & Sleigh. (2007). *New approach for high purity lactose - utilising the by-products from whey*.

Earl, & Parrish. (1983). A cross-polarization—magic-angle sample spinning n.m.r. study of several crystal forms of lactose. *Carbohydrate Research, 115*, 23-32. doi:https://doi.org/10.1016/0008-6215(83)88131-2

Ecroyd. (2003). *Production of a New Lactose Crystal in Superheated Steam*. Retrieved from Palmerston North:

Fan, & Roos. (2015). X-ray diffraction analysis of lactose crystallization in freeze-dried lactose–whey protein systems. *Food Research International, 67*, 1-11. doi:https://doi.org/10.1016/j.foodres.2014.10.023

Figura, & Epple. (1995). Anhydrous α-lactose A study with DSC and TXRD. *Journal of thermal analysis and calorimetry, 44*(1), 45-53.

Fix, & Steffens. (2004). Quantifying low amorphous or crystalline amounts of alpha-lactose-monohydrate using X-ray powder diffraction, near-Infrared spectroscopy, and differential scanning calorimetry. *Drug development and industrial pharmacy, 30*(5), 513-523.

Foster. (2002). *The prediction of sticking in dairy powders.* (Ph.D.), Massey University, Palmerston North, New Zealand.

Fox. (2009). Lactose: Chemistry and Properties. In P. McSweeney & P. F. Fox (Eds.), *Advanced Dairy Chemistry: Volume 3: Lactose, Water, Salts and Minor Constituents* (pp. 1-15). New York, NY: Springer New York.

Gänzle, Haase, & Jelen. (2008). Lactose: crystallization, hydrolysis and value-added derivatives. *International Dairy Journal, 18*(7), 685-694.

Garnier, Petit, & Coquerel. (2002). Dehydration Mechanism and Crystallisation Behaviour of Lactose. *Journal of thermal analysis and calorimetry, 68*(2), 489-502. doi:10.1023/a:1016087702409

Gordon, & Taylor. (1952). Ideal copolymers and the second-order transitions of synthetic rubbers. I. Non-crystalline copolymers. *Journal of Chemical Technology and Biotechnology, 2*(9), 493-500.

Gustafsson, Lennholm, Iversen, & Nyström. (1998). Comparison of solid-state NMR and isothermal microcalorimetry in the assessment of the amorphous component of lactose. *International Journal of Pharmaceutics, 174*(1), 243-252. doi:https://doi.org/10.1016/S0378-5173(98)00272-5

Haque, & Roos. (2005). Crystallization and X-ray diffraction of spray-dried and freeze-dried amorphous lactose. *Carbohydrate Research, 340*(2), 293-301. doi:https://doi.org/10.1016/j.carres.2004.11.026

Hardy, Scher, & Banon. (2002). Water activity and hydration of dairy powders. *Lait, 82*(4), 441-452.

Hargreaves. (1995). *Characterisation of lactose in the liquid and solid state using nuclear magnetic resonance and other methods.* Massey University, Palmerston North, New Zealand.

Harjunen, Lehto, Koivisto, Levonen, Paronen, & Järvinen. (2004). Determination of Amorphous Content of Lactose Samples by Solution Calorimetry. *Drug development and industrial pharmacy, 30*(8), 809-815. doi:10.1081/DDC-200030302

Hockett, & Hudson. (1931). A novel modification of lactose. *Journal of the American Chemical society, 53*(12), 4455-4456.
Hogan, & Buckton. (2001). The Application of Near Infrared Spectroscopy and Dynamic Vapor Sorbtion to Quantify Low Amorphous Contents of Crystalline Lactose. *Pharmaceutical Research, 18*(1), 112-116.
Holsinger. (1988). Lactose, in fundamentals of dairy chemistry: Van.
Hourigan, Lifran, Vu, Listiohadi, & Sleigh. (2012). Lactose: Chemistry, Processing, and Utilization. In G. W. Smithers & M. A. Augustin (Eds.), Advances in Dairy Ingredients (pp. 21-41): John Wiley & Sons, 2012.
Hudson. (1908). FURTHER STUDIES ON THE FORMS OF MILK-SUGAR. *Journal of the American Chemical society, 30*(11), 1767-1783.
Ibach, & Kind. (2007). Crystallization kinetics of amorphous lactose, whey-permeate and whey powders. *Carbohydrate Research, 342*(10), 1357-1365.
Ihli, & Paterson. (2015). Effect of galacto-oligosaccharide concentration on the kinetics of lactose crystallisation. *International Dairy Journal, 41*, 26-31. doi:https://doi.org/10.1016/j.idairyj.2014.09.001
Integrated. (2015). iButton DS1923 Spec Sheet.
J. Lloyd, Dong Chen, & B. Hargreaves. (2003). *Glass transition and caking of spray-dried lactose* (Vol. 31).
Jena, & Chaturvedi. (1992). *Phase transformation in materials*: Prentice Hall.
Jenness, & Walstra. (1984). *Dairy chemistry and physics*: Wiley.
Jones. (1956). "Glass". *Methuen: London*.
Jouppila, Kansikas, & Roos. (1997a). Glass Transition, Water Plasticization, and Lactose Crystallization in Skim Milk Powder. *Journal of Dairy Science, 80*(12), 3152-3160. doi:10.3168/jds.S0022-0302(97)76286-6
Jouppila, Kansikas, & Roos. (1997b). Glass transition, water plasticization, and lactose crystallization in skim milk powder. *Journal of Dairy Science, 80*, 3152-3160.
Jouppila, & Roos. (1994). Water sorption and time-dependent phenomena of milk powders. *Journal of Dairy Science, 77*(7), 1798-1808.
Kedward, MacNaughtan, & Mitchell. (2000). Crystallization Kinetics of Amorphous Lactose as a Function of Moisture Content Using Isothermal Differential Scanning Calorimetry. *Journal of Food Science, 65*(2), 324-328. doi:doi:10.1111/j.1365-2621.2000.tb16001.x
Kedward, MacNaughtan, & Mitchell. (2000). Crystallization kinetics of amorphous lactose as a function of moisture content using isothermal differential scanning calorimetry. *Journal of Food Science, 65*(2), 324-328.
Kellam. (2005-2017). The Manufacture of Lactose. Retrieved from http://nzic.org.nz/ChemProcesses/dairy/3F.pdf
Kirk, Dann, & Blatchford. (2007). Lactose: A definitive guide to polymorph determination. *International Journal of Pharmaceutics, 334*(1), 103-114. doi:https://doi.org/10.1016/j.ijpharm.2006.10.026
Kussendrager, & Andreae. (1986). Process for preparing lactose products: Google Patents.
Lehto, Tenho, Vähä-Heikkilä, Harjunen, Päällysaho, Välisaari, . . . Järvinen. (2006). The comparison of seven different methods to quantify the amorphous content of spray dried lactose. *Powder Technology, 167*(2), 85-93.
Lerk, Andreae, De Boer, De Hoog, Kussendrager, & Van Leverink. (1984). Transitions of lactoses by mechanical and thermal treatment. *Journal of Pharmaceutical Sciences, 73*(6), 857-859.
Levine, & Slade. (1986). A polymer physico-chemical approach to the study of commercial starch hydrolysis products (SHPs). *Carbohydrate Polymers, 6*(3), 213-244.
Lifran, Sleigh, Johnson, Steele, Hourigan, & Dalziel. (2001). Method for purification of lactose: Google Patents.

Lim, & Nickerson. (1973). Effect of methanol on the various forms of lactose. *Journal of Dairy Science, 56*(7), 843-848.
Listiohadi. (2000). Modifications of sugars by extrusion. *MSc. thesis, University of Western Sydney*.
Listiohadi, Hourigan, Sleigh, & Steele. (2005). Properties of lactose and its caking behaviour. *Australian journal of dairy technology, 60*(1), 33.
Listiohadi, Hourigan, Sleigh, & Steele. (2008). Moisture sorption, compressibility and caking of lactose polymorphs. *International Journal of Pharmaceutics, 359*(1–2), 123-134. doi:http://dx.doi.org/10.1016/j.ijpharm.2008.03.044
Listiohadi, Hourigan, Sleigh, & Steele. (2009). Thermal analysis of amorphous lactose and alpha-lactose monohydrate. *Dairy Science and Technology, 89*(1), 43-67.
Majd, & Nickerson. (1976). Effect of alcohols on lactose solubility. *Journal of Dairy Science, 59*(6), 1025-1032.
McIntosh, Yang, Goldup, Watkinson, & Donnan. (2013). Crystallization of amorphous lactose at high humidity studied by terahertz time domain spectroscopy. *Chemical Physics Letters, 558*(Supplement C), 104-108. doi:https://doi.org/10.1016/j.cplett.2012.12.044
Metroblue. (2018). Weather history download Palmerston North. Retrieved from https://www.meteoblue.com/en/weather/archive/export/palmerston-north_new-zealand_2185018?daterange=2018-03-08+to+2018-03-15&params=&params%5B%5D=32%3B10+m+above+gnd%3B31%3B10+m+above+gnd&params%5B%5D=32%3B900+mb%3B31%3B900+mb&utc_offset=13&aggregation=hourly&temperatureunit=CELSIUS&windspeedunit=KILOMETER_PER_HOUR
Miao, & Roos. (2005). Crystallization Kinetics and X-ray Diffraction of Crystals Formed in Amorphous Lactose, Trehalose, and Lactose/Trehalose Mixtures. *Journal of Food Science, 70*(5).
Moran, Shapiro, Boettner, & Bailey. (2010). *Fundamentals of engineering thermodynamics*: John Wiley & Sons.
Netzsch. (2016). Copper furnace with humidity option.
Newell, Buckton, Butler, Thielmann, & Williams. (2001). The use of inverse phase gas chromatography to study the change of surface energy of amorphous lactose as a function of relative humidity and the processes of collapse and crystallisation. *International Journal of Pharmaceutics, 217*(1), 45-56. doi:https://doi.org/10.1016/S0378-5173(01)00589-0
Newman, & Zografi. (2014). Critical Considerations for the Qualitative and Quantitative Determination of Process‐Induced Disorder in Crystalline Solids. *Journal of Pharmaceutical Sciences, 103*(9), 2595-2604. doi:10.1002/jps.23930
Niemelä, Päällysaho, Harjunen, Koivisto, Lehto, Suhonen, & Järvinen. (2005). Quantitative analysis of amorphous content of lactose using CCD-Raman spectroscopy. *Journal of Pharmaceutical and Biomedical Analysis, 37*(5), 907-911. doi:https://doi.org/10.1016/j.jpba.2004.09.027
Nieuwmeyer, Damen, Gerich, Rusmini, van der Voort Maarschalk, & Vromans. (2007). Granule Characterization During Fluid Bed Drying by Development of a Near Infrared Method to Determine Water Content and Median Granule Size. *Pharmaceutical Research, 24*(10), 1854-1861. doi:10.1007/s11095-007-9305-5
Nijdam, Ibach, Eichhorn, & Kind. (2007). An X-ray diffraction analysis of crystallised whey and whey-permeate powders. *Carbohydrate Research, 342*(16), 2354-2364. doi:https://doi.org/10.1016/j.carres.2007.08.001
O'Donnell. (1998). Conditioning of lactose. *Masterate Thesis, Massey University, Palmerston North, New Zealand*.
Olano. (1978). Treatment of forms of lactose with dilute alcoholic solutions of sodium hydroxide. *Journal of Dairy Science, 61*(11), 1622-1623.

Olano, Bernhard, & Nickerson. (1977). Alteration in the ratio of α-to β-lactose co-crystallized from organic solvents. *Journal of Food Science, 42*(4), 1066-1068.
Olano, Corzo, & Castro. (1983). Studies on beta-lactose crystallization. *Milchwissenschaft*.
Olano, & Rios. (1978). Treatment of lactose with alkaline methanolic solutions: production of beta-lactose from alpha-lactose hydrate. *Journal of Dairy Science, 61*(3), 300-302.
OMEGA. (2018). Equilibrium Relative Humidity Saturated Salt Solutions. Retrieved from https://www.omega.com/temperature/z/pdf/z103.pdf
Otsuka, Ohtani, Kaneniwa, & Higuchi. (1991). Isomerization of lactose in solid-state by mechanical stress during grinding. *Journal of pharmacy and pharmacology, 43*(3), 148-153.
Otsuka, Ohtani, Otsuka, & Kaneniwa. (1993). Effect of humidity on solid-state isomerization of various kinds of lactose during grinding. *Journal of pharmacy and pharmacology, 45*(1), 2-5.
Palzer. (2010). The relation between material properties and supra-molecular structure of water-soluble food solids. *Trends in Food Science & Technology, 21*(1), 12-25. doi:https://doi.org/10.1016/j.tifs.2009.08.005
Parrish, & Brown. (1982). Solid state transformations of α-lactose monohydrate in alcoholic media. *Journal of Dairy Science, 65*(9), 1688-1691.
Parrish, Ross, & Valentine. (1980). Formation of β-lactose from the stable forms of anhydrous α-lactose. *Journal of Food Science, 45*(1), 68-70.
Paterson. (2009). Production and Uses of Lactose. In P. McSweeney & P. F. Fox (Eds.), *Advanced Dairy Chemistry: Volume 3: Lactose, Water, Salts and Minor Constituents* (pp. 105-120). New York, NY: Springer New York.
Paterson. (2017). Lactose processing: From fundamental understanding to industrial application. *International Dairy Journal, 67*, 80-90. doi:http://dx.doi.org/10.1016/j.idairyj.2016.07.018
Paterson, Brooks, Bronlund, & Foster. (2005). Development of stickiness in amorphous lactose at constant T− T g levels. *International Dairy Journal, 15*(5), 513-519.
Paterson, & Ripberger. (2011). *Measurement of the effective diffusion coefficient of water in spray dried amorphous lactose particles.(EPF665).* Paper presented at the 11th International congress on engineering and food; Food process engineering in a changing world. , Athens, Greece.
Paterson, Ripberger, & Bridges. (2015). Measurement of the viscosity of freeze dried amorphous lactose near the glass transition temperature. *International Dairy Journal, 43*(0), 27-32. doi:http://dx.doi.org/10.1016/j.idairyj.2014.11.005
Pazesh, Gråsjö, Berggren, & Alderborn. (2017). Comminution-amorphisation relationships during ball milling of lactose at different milling conditions. *International Journal of Pharmaceutics, 528*(1-2), 215-227. doi:10.1016/j.ijpharm.2017.05.043
Pazesh, Lazorova, Berggren, Alderborn, & Gråsjö. (2016). Considerations on the quantitative analysis of apparent amorphicity of milled lactose by Raman spectroscopy. *International Journal of Pharmaceutics, 511*(1), 488-504. doi:https://doi.org/10.1016/j.ijpharm.2016.07.001
Pharma (Producer). (2017a). Amorphous lactose, origins and measurement.
Pharma (Producer). (2017b). Lactose: Some basic properties and characteristics.
Ranger, Paterson, & McLeod. (2017). The effect of temperature on the development of browning of amorphous and crystalline lactose. *International Dairy Journal, 73*, 63-67. doi:10.1016/j.idairyj.2017.05.005
Ripberger. (2010). *Mechanism of viscous droplet/solid stickiness during impact investigation of the diffusivity and viscosity of amorphous lactose.* (German Diploma Thesis), Massey University, Palmerston North.

Roos. (2003). Thermal analysis, state transitions and food quality. *Journal of thermal analysis and calorimetry, 71*(1), 197-203.
Roos. (2012). Phase and State Transitions and Related Phenomena in Foods *Food Materials Science and Engineering* (pp. 136-150): Wiley-Blackwell.
Roos, & Karel. (1990). Differential scanning calorimetry study of phase transitions affecting the quality of dehydrated materials. *Biotechnology Progress, 6*(2), 159-163.
Roos, & Karel. (1991). Plasticizing effect of water on thermal behavior and crystallization of amorphous food models. *Journal of Food Science, 56*(1), 38-43.
Roos, & Karel. (1992). Crystallization of amorphous lactose. *Journal of Food Science, 57*(3), 775-777.
Rückold, Isengard, Hanss, & Grobecker. (2003). The energy of interaction between water and surfaces of biological reference materials. *Food Chemistry, 82*(1), 51-59. doi:https://doi.org/10.1016/S0308-8146(02)00541-1
Saleki-Gerhardt, Ahlneck, & Zografi. (1994). Assessment of disorder in crystalline solids. *International Journal of Pharmaceutics, 101*(3), 237-247. doi:https://doi.org/10.1016/0378-5173(94)90219-4
Samaniego-Esguerra, Boag, & Robertson. (1991). Comparison of regression methods for fitting the GAB model to the moisture isotherms of some dried fruit and vegetables. *Journal of Food Engineering, 13*(2), 115-133. doi:https://doi.org/10.1016/0260-8774(91)90014-J
Saunders, Podluii, Shergill, Buckton, & Royall. (2004). *The potential of high speed DSC (Hyper DSCTM) for the detection and quantification of small amounts of amorphous content in predominantly crystalline samples* (Vol. 274).
Schmitt, Law, & Zhang. (1999). Nucleation and Crystallization Kinetics of Hydrated Amorphous Lactose above the Glass Transition Temperature. *Journal of Pharmaceutical Sciences, 88*(3), 291-296.
Sebhatu, Ahlneck, & Alderborn. (1997). The effect of moisture content on the compression and bond-formation properties of amorphous lactose particles. *International Journal of Pharmaceutics, 146*, 101-114.
Sebhatu, Angberg, & Ahlneck. (1994). Assessment of the degree of disorder in crystalline solids by isothermal microcalorimetry. *International Journal of Pharmaceutics, 104*(2), 135-144. doi:http://dx.doi.org/10.1016/0378-5173(94)90188-0
Sharp. (1934). Method of preparing lactose: Google Patents.
Sharp. (1943). Stable crystalline anhydrous alpha lactose product and process: Google Patents.
Simpson, Parrish, & Nelson. (1982). Crystalline forms of Lactose Produced in Acidic Alcoholic Media. *Journal of Food Science, 47*, 1948-1954.
Singh, & Shah. (1992). Characterisation of lactose crystallised in acidified aqueous ethanol. *Journal of the science of food and agriculture, 58*(1), 161-164.
Smith, Hussain, Bukhari, & Ermolina. (2015a). Quantification of residual crystallinity in ball milled commercially sourced lactose monohydrate by thermo-analytical techniques and terahertz spectroscopy. *European Journal of Pharmaceutics and Biopharmaceutics, 92*(Supplement C), 180-191. doi:https://doi.org/10.1016/j.ejpb.2015.02.026
Smith, Hussain, Bukhari, & Ermolina. (2015b). Quantification of residual crystallinity of ball-milled, commercially available, anhydrous β-lactose by differential scanning calorimetry and terahertz spectroscopy. *Journal of thermal analysis and calorimetry, 121*(1), 327-333. doi:10.1007/s10973-015-4469-4
Smith, Mannheim, & Gilbert. (1981). Water Sorption Isotherms of Sucrose and Glucose by Inverse Gas Chromatography. *Journal of Food Science, 46*(4), 1051-1053. doi:10.1111/j.1365-2621.1981.tb02989.x

Strachan, Rades, Newnham, Gordon, Pepper, & Taday. (2004). Using terahertz pulsed spectroscopy to study crystallinity of pharmaceutical materials. *Chemical Physics Letters, 390*(1), 20-24. doi:https://doi.org/10.1016/j.cplett.2004.03.117

Strachan, Taday, Newnham, Gordon, Zeitler, Pepper, & Rades. (2005). Using Terahertz Pulsed Spectroscopy to Quantify Pharmaceutical Polymorphism and Crystallinity. *Journal of Pharmaceutical Sciences, 94*(4), 837-846. doi:https://doi.org/10.1002/jps.20281

Tadapaneni, Yang, Carter, & Tang. (2017). A new method to determine the water activity and the net isosteric heats of sorption for low moisture foods at elevated temperatures. *Food Research International, 102*(Supplement C), 203-212. doi:https://doi.org/10.1016/j.foodres.2017.09.070

van 't Land. (2011a). Continuous Fluid-Bed Drying *Drying in the Process Industry* (pp. 67–97): Wiley.

van 't Land. (2011b). Flash drying *Drying in the Process Industry* (pp. 117-131): Wiley.

van 't Land. (2011c). Spray Drying *Drying in the Process Industry* (pp. 133–162): Wiley.

Van Leverink. (1981). Extrusion process for the preparation of anhydrous stable lactose: Google Patents.

Vivoda, Roškar, & Kmetec. (2011). The development of a quick method for amorphicity determination by isothermal microcalorimetry. *Journal of thermal analysis and calorimetry, 105*(3), 1023-1030.

Vollenbroek, Hebbink, Ziffels, & Steckel. (2010). Determination of low levels of amorphous content in inhalation grade lactose by moisture sorption isotherms. *International Journal of Pharmaceutics, 395*(1), 62-70. doi:https://doi.org/10.1016/j.ijpharm.2010.04.035

Walstra. (1999). *Dairy technology: principles of milk properties and processes*: CRC Press.

Williams, Landel, & Ferry. (1955). The temperature dependence of relaxation mechanisms in amorphous polymers and other glass-forming liquids. *Journal of the American Chemical society, 77*(14), 3701-3707.

Würsch, Rosset, Köllreutter, & Klein. (1984). Crystallization of beta-lactose under elevated storage temperature in spray-dried milk powder. *Milchwissenschaft*.

Yazdanpanah, & Langrish. (2011). Fast crystallization of lactose and milk powder in fluidized bed dryer/crystallizer. *Dairy Science & Technology, 91*(3), 323-340. doi:10.1007/s13594-011-0015-8

Zuo, Rhim, & Lee. (2015). Moisture Sorption and Thermodynamic Properties of Vacuum-Dried Capsosiphon fulvescens Powder. *Preventive Nutrition and Food Science, 20*(3), 215-220. doi:10.3746/pnf.2015.20.3.215

9 Appendices:

9.1 Literature Review:

Expanded list of references for Figure 2-3:

0 (Walstra, 1999)

1 (Listiohadi, Hourigan, Sleigh, & Steele, 2005)

2 (Holsinger, 1988)

3 (Sebhatu et al., 1994)

4 C. J. Kedward et al. (2000)

5 (Newell et al., 2001)

6 (Lerk et al., 1984)

7 (Bushill et al., 1965)

8 (Würsch, Rosset, Köllreutter, & Klein, 1984)

9 (Hudson, 1908)

10 (Bell, 1930)

11 (Sharp, 1934)

12 (Asano, Aoki, & Yamazaki, 1978; Listiohadi, 2000; Van Leverink, 1981)

13 (Olano, 1978)

14 (Singh & Shah, 1992)

15 (Lifran et al., 2001)

16 (Listiohadi et al., 2008)

17 (Cal et al., 1996)

18 (Sharp, 1943)

19 (Buma & Wiegers, 1967)

20 (Figura & Epple, 1995)

21 (Hockett & Hudson, 1931)

22 (Domovs & Freund, 1960)

23 (Olano, Bernhard, & Nickerson, 1977)

24 (Jouppila et al., 1997b)

25 (Listiohadi et al., 2005)

26 (Garnier, Petit, & Coquerel, 2002)

27 (Kussendrager & Andreae, 1986)

28 (Otsuka, Ohtani, Otsuka, & Kaneniwa, 1993)

29 (Otsuka, Ohtani, Kaneniwa, & Higuchi, 1991)

30 (Parrish, Ross, & Valentine, 1980)

31 (Olano, Corzo, & Castro, 1983)

32 (Majd & Nickerson, 1976)

33 (Angberg, Nyström, & Castensson, 1991)

34 (Olano & Rios, 1978)

36 (Drapier-Beche et al., 1997)

37 (Parrish & Brown, 1982)

38 (Lim & Nickerson, 1973)

9.2 Method Development

9.2.1 Sample Microscope Photos

The following photos were taken to confirm the amorphicity of the samples used, a reference of alpha lactose monohydrate was used for comparison.

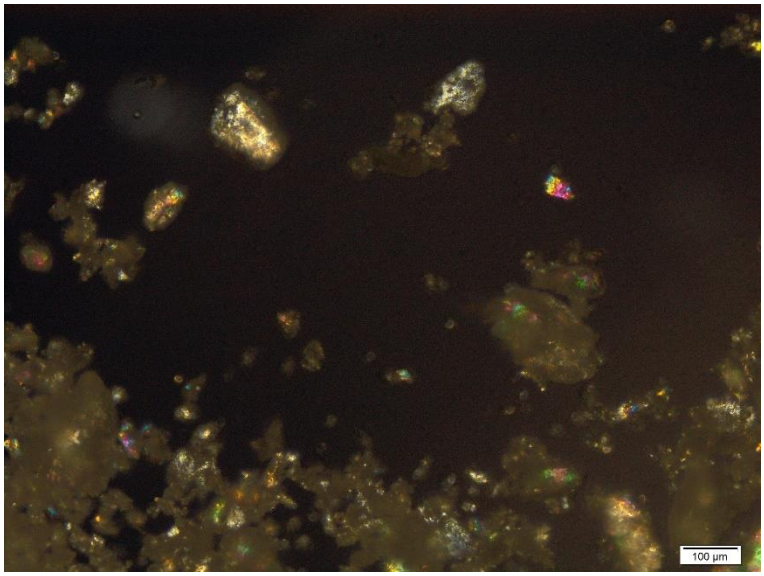

Figure 9-1: An example microscope photo of α-lactose monohydrate viewed under cross polarized light

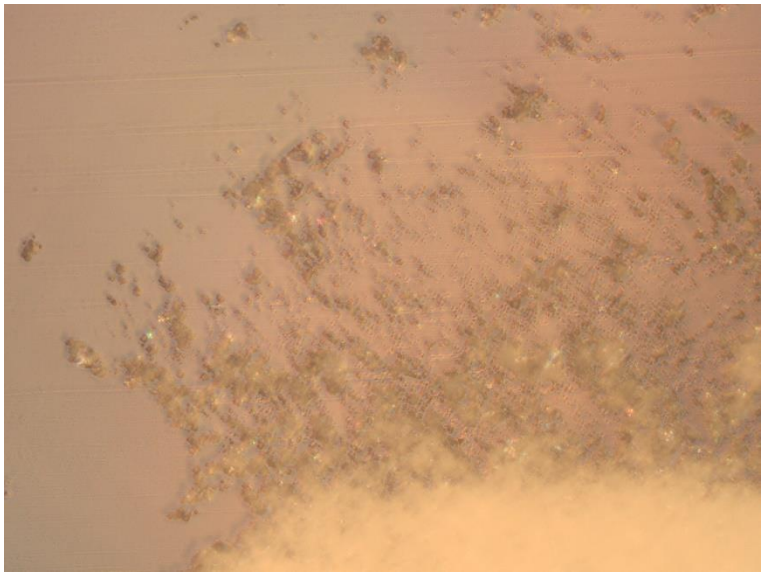

Figure 9-2: An example microscope photo of a spray-dried amorphous lactose sample viewed at 10x magnification.

Figure 9-3: An example microscope photo of a spray-dried amorphous lactose sample viewed at 10x magnification under cross polarised light. The lack of any visible diffraction confirms the sample's amorphicity.

9.2.2 Avrami Model Fitting

The following figures provide additional detail on factors affecting the fitting of the Avrami model as well a data set referenced in the text where crystallization did not appear to go to completion.

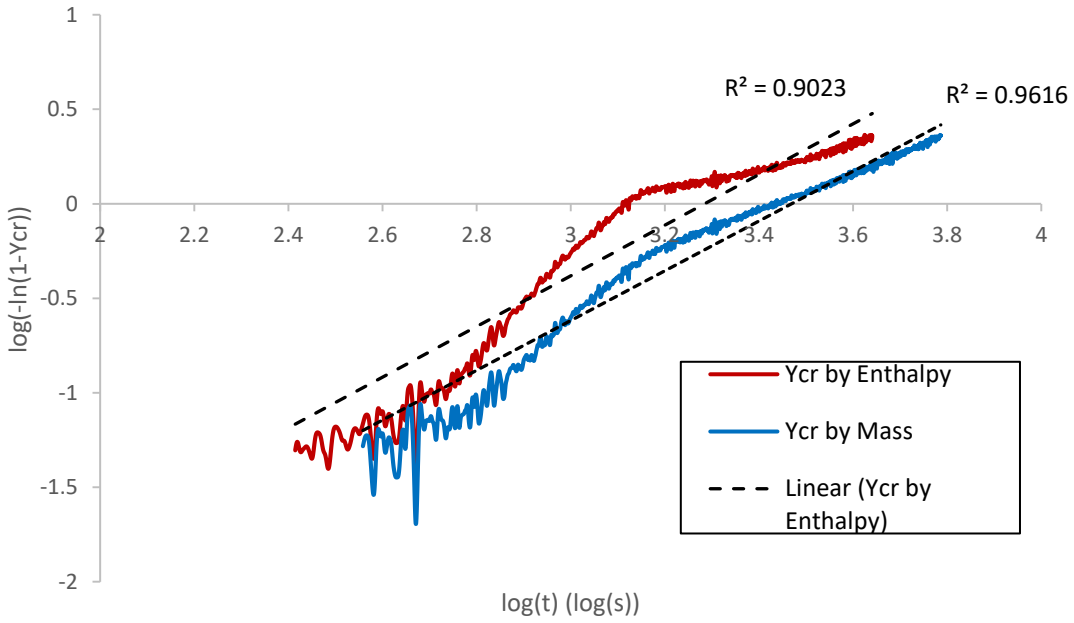

Figure 9-4: Effect of Ycr calculation method (by calculated enthalpy change or by mass change) on the linearity of the Avrami fitting plot for a trial at T=67.24°C, RH=33%. Raw data from Dormeuil (2017).

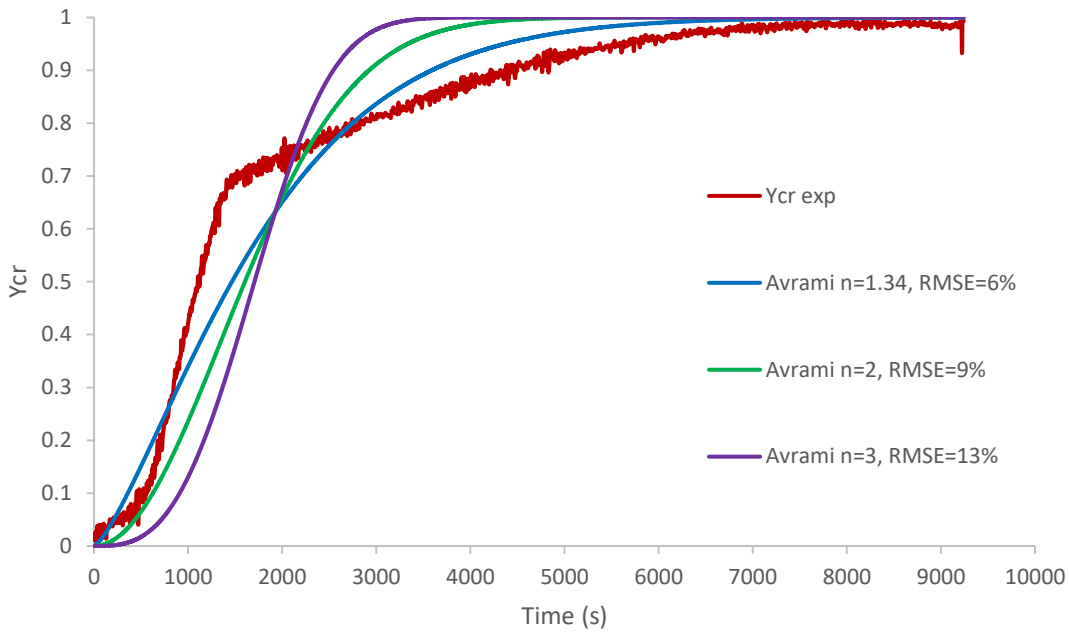

Figure 9-5: Example of the effects of changing the Avrami n constant on the model predictions for a trial at T=67.24°C, RH=33%. Raw data from Dormeuil (2017).

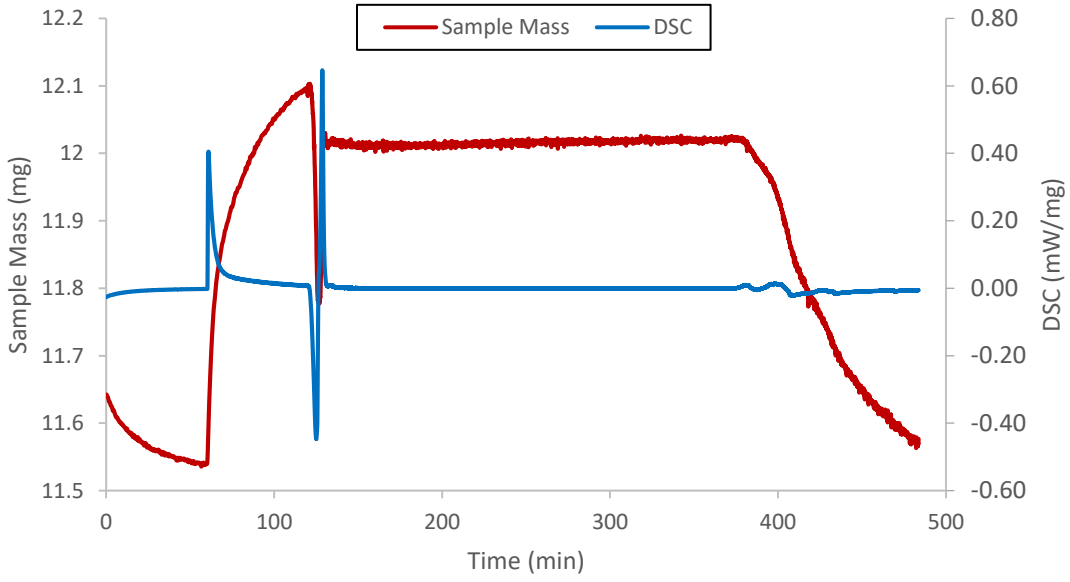

Figure 9-6: Corrected and smoothed mass and heat flow results over time for a trial at T=62.24°C, RH=33%, raw data from Dormeuil (2017).

9.2.3 Isotherm Trial Predictions

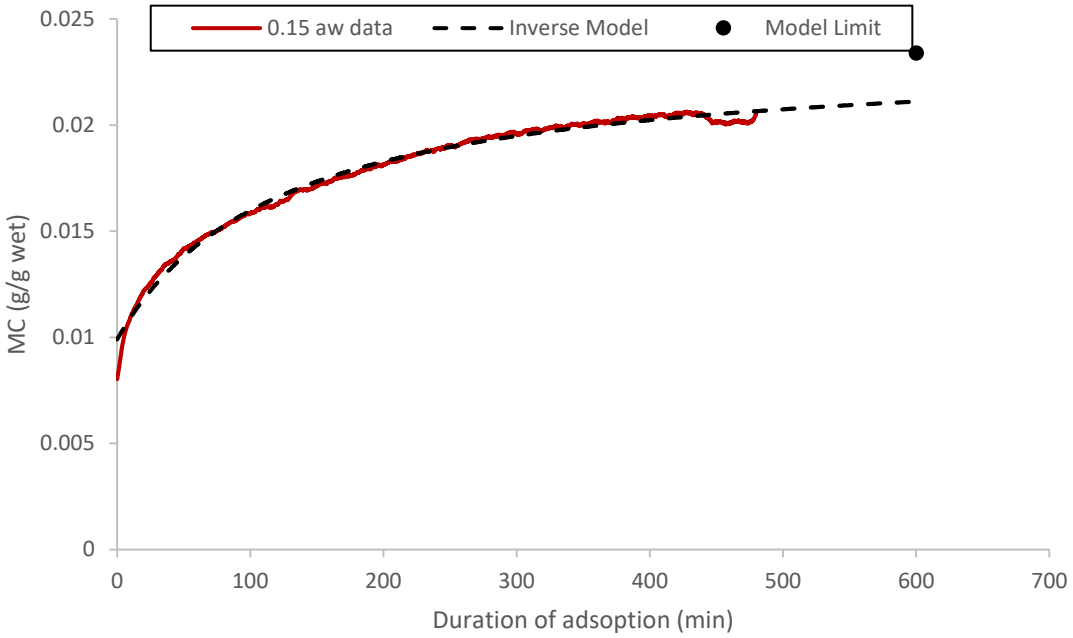

Figure 9-7: Prediction of 0.15aw EMC for 30°C isotherm using an inverse function model.

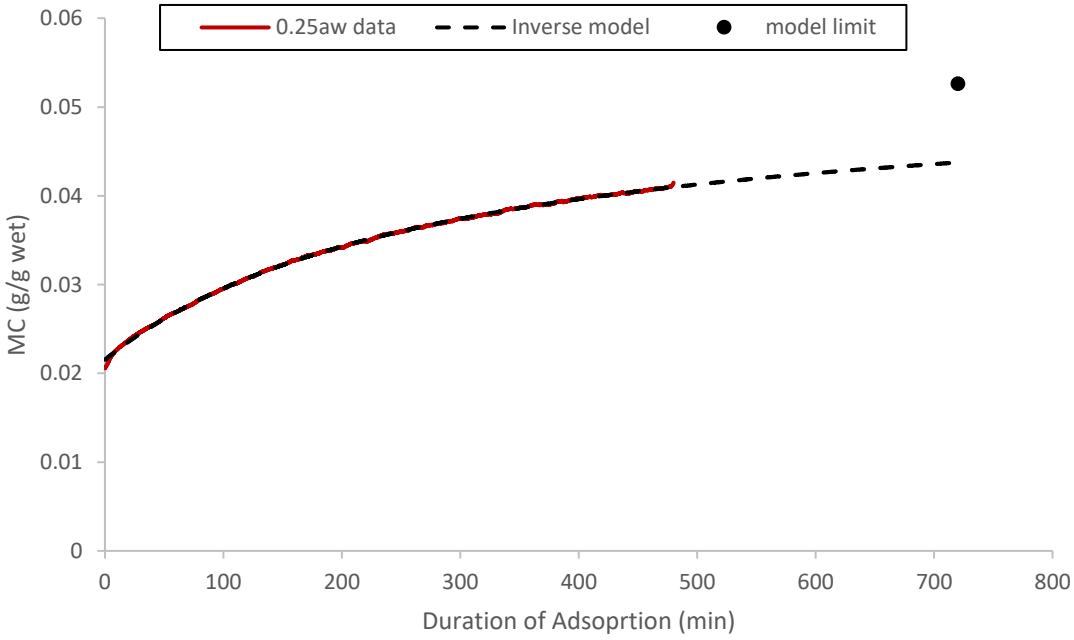

Figure 9-8: Prediction of 0.25aw EMC for 30°C isotherm using an inverse function model.

9.3 Directional Crystallization Method

9.3.1 Extended Drying Trial

The following extended drying trial was used to help estimate the dry sample mass for the directional crystallization STA results.

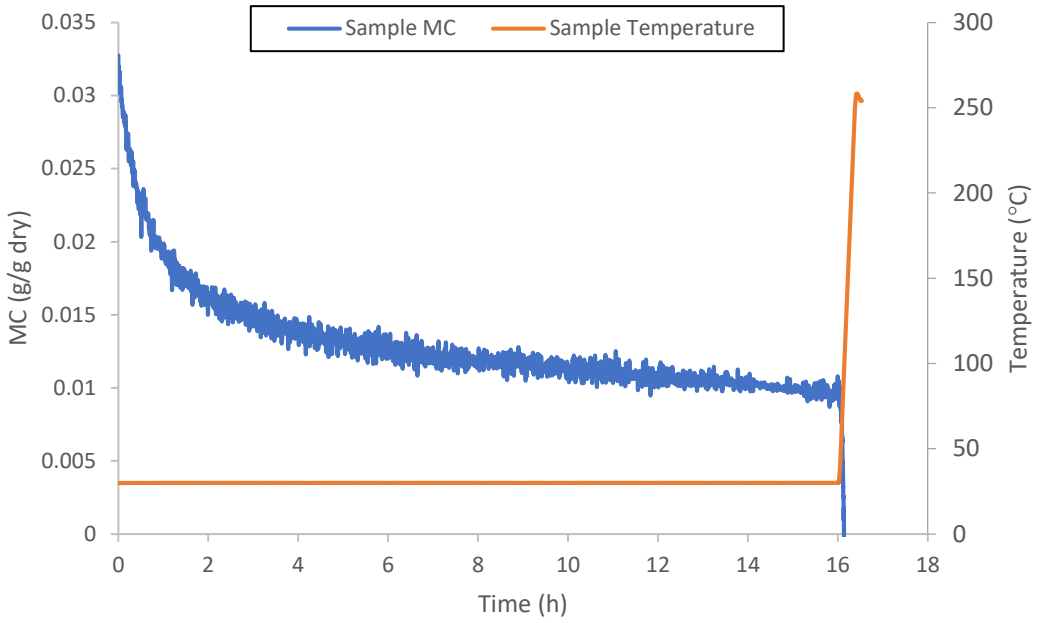

Figure 9-9: Extended drying trial for spray-dried sample at ~0%RH, with temperature ramp of 10K/min at the end.

9.3.2 I-Button Jig Components

The i-button jig designed for this project was made using the following designs:

Each i-Button jig consisted of:

- 1x 1.5mm neoprene washer 16mm OD 8mm ID
- 4x 5/32” 38mm long galvanized bolts wingnuts and washers
- 1x 17.3x2.4mm n70 o-ring
- 1x each of the parts detailed in Figure 9-10 and Figure 9-11 in clear acetyl plastic.

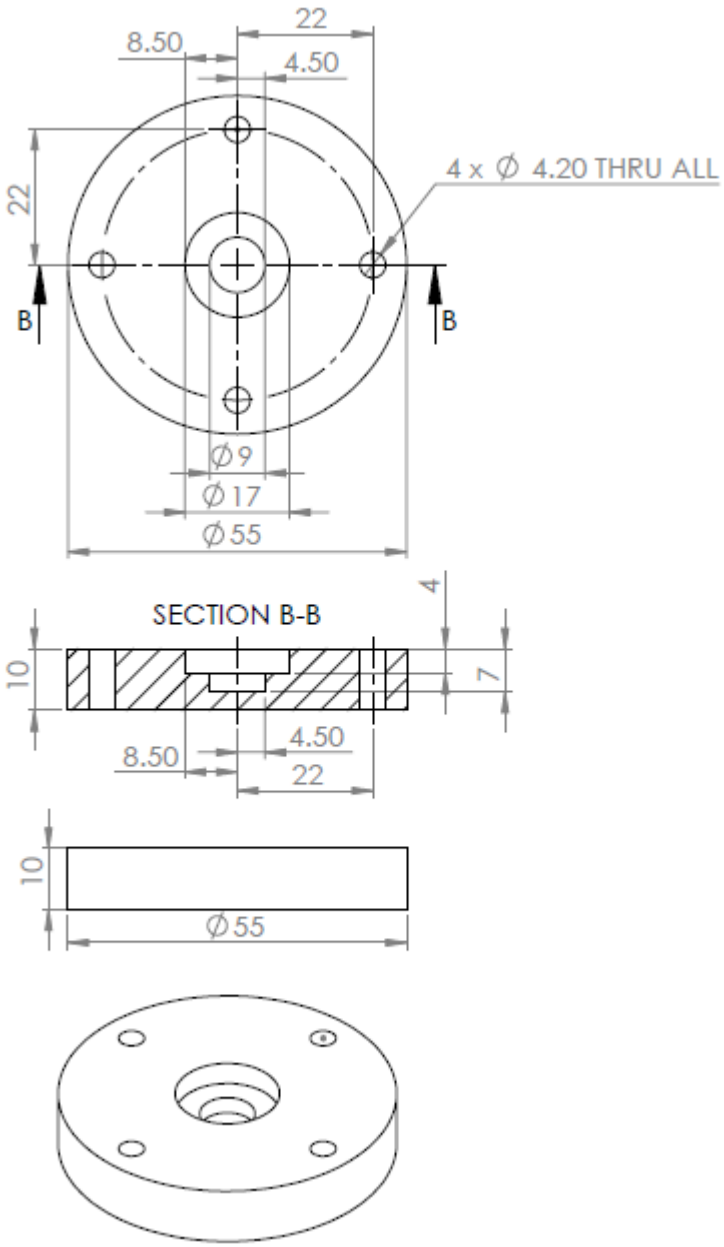

Figure 9-10: i-Button jig bottom section plans, all dimensions in mm.

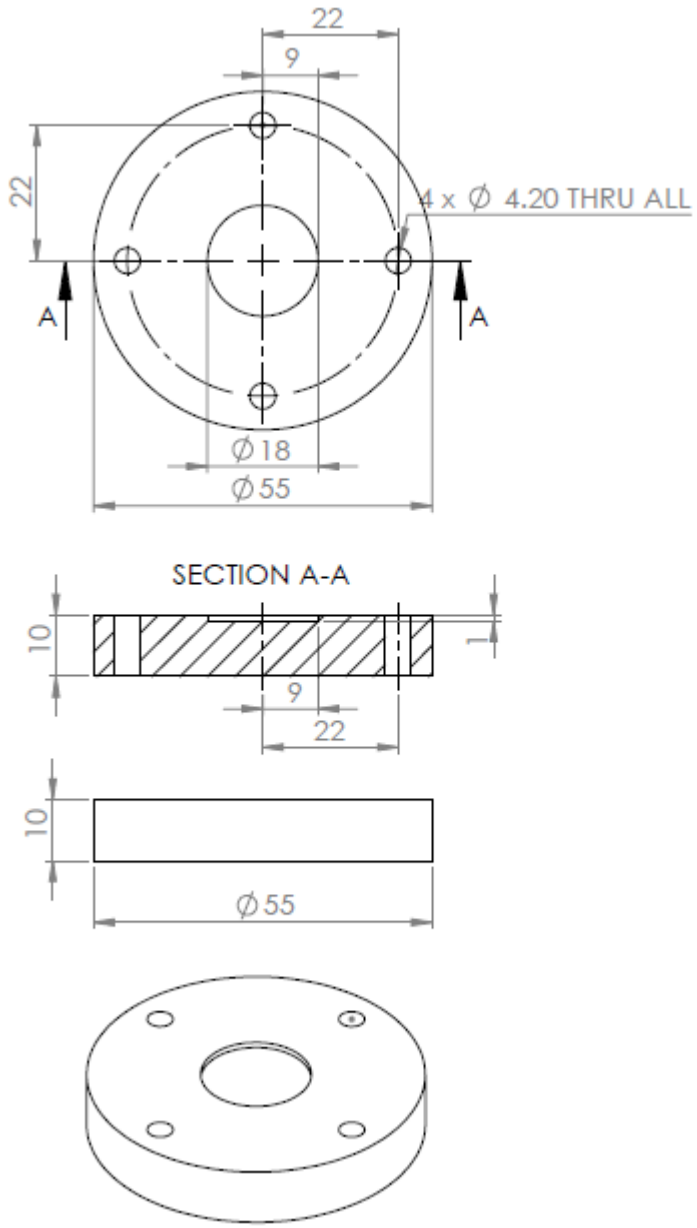

Figure 9-11: i-Button jig top section plans, all dimensions in mm.

9.4 Directional Crystallization Results

9.4.1 STA Results

Shown below are the full smoothed and corrected STA results and corresponding enthalpy evolution and Avrami fitting results for all directional crystallization trials.

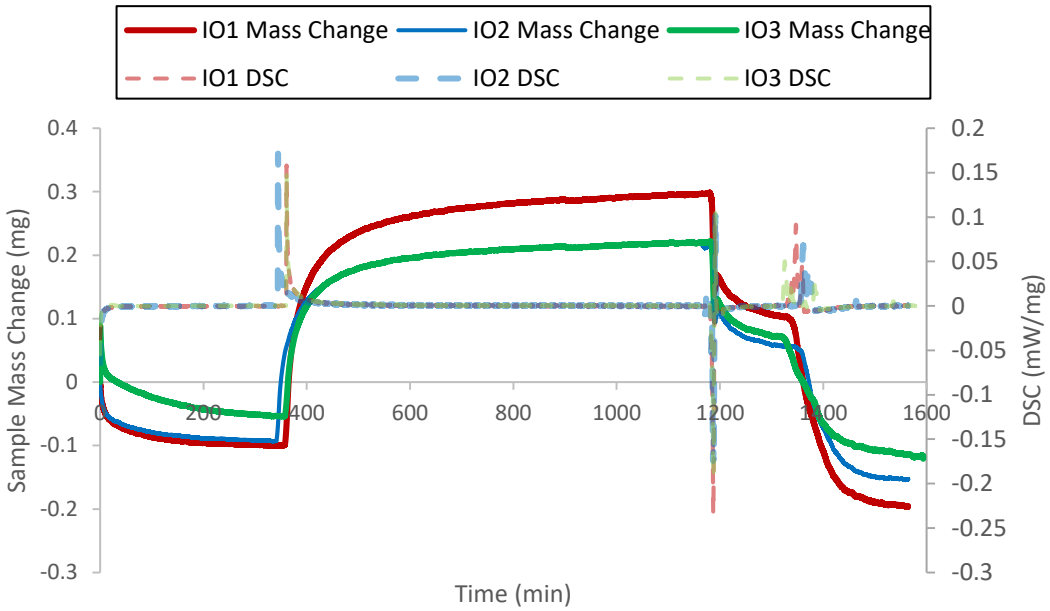

Figure 9-12: Corrected, smoothed STA results for inside-out directional crystallization trials IO1, IO2, and IO3. All trials had the same experimental conditions as detailed in section 5.4.2.

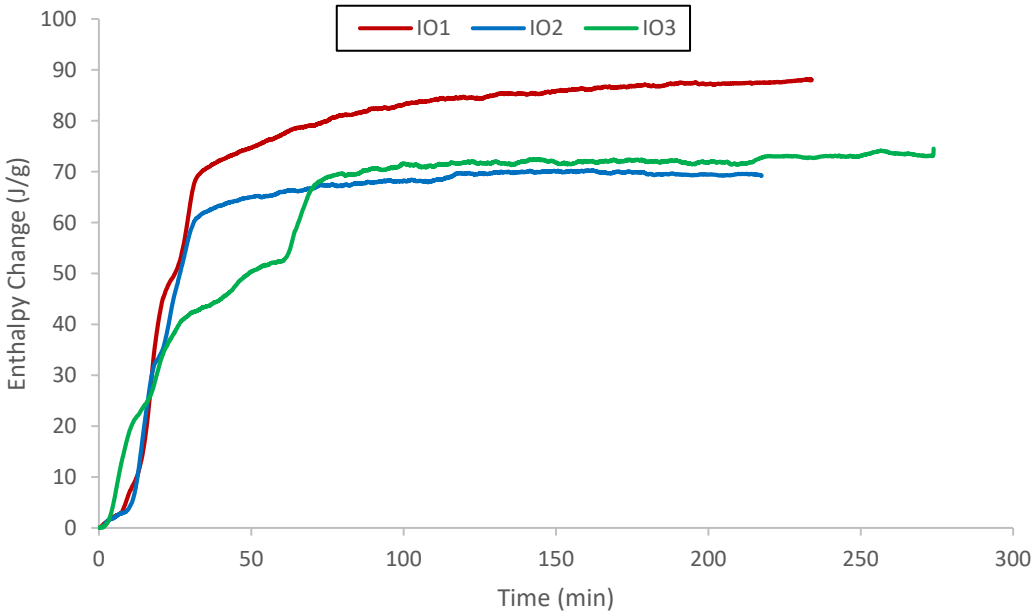

Figure 9-13: Calculated enthalpy evolution results for inside-out directional crystallization trials IO1, IO2, and IO3. All trials had the same experimental conditions as detailed in section 5.4.2.

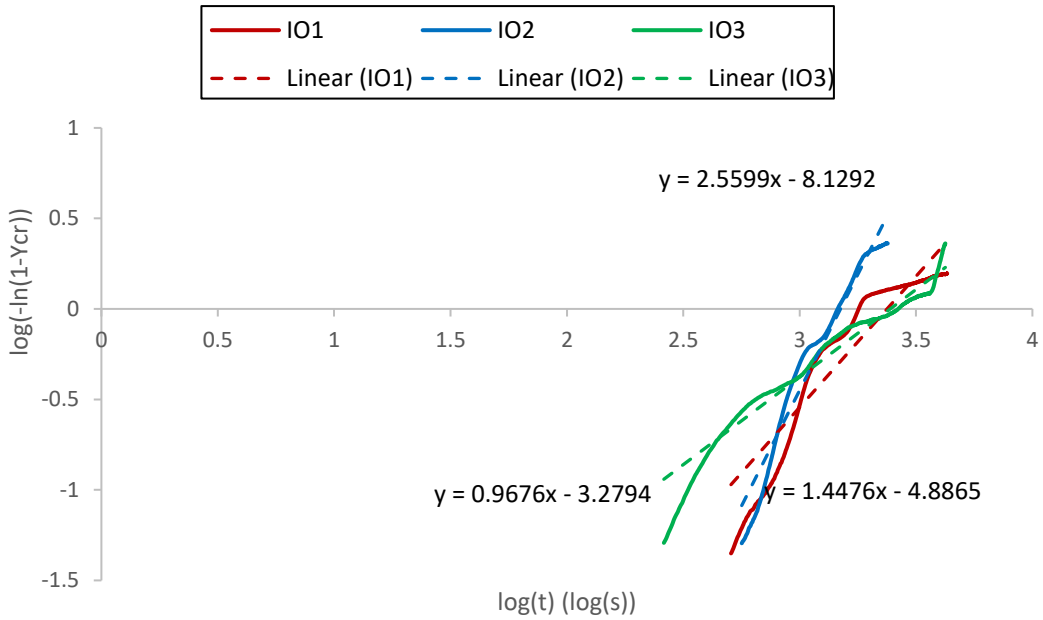

Figure 9-14: Avrami fitting plots for inside-out directional crystallization trials IO1, IO2, and IO3. All trials had the same experimental conditions as detailed in section 5.4.2.

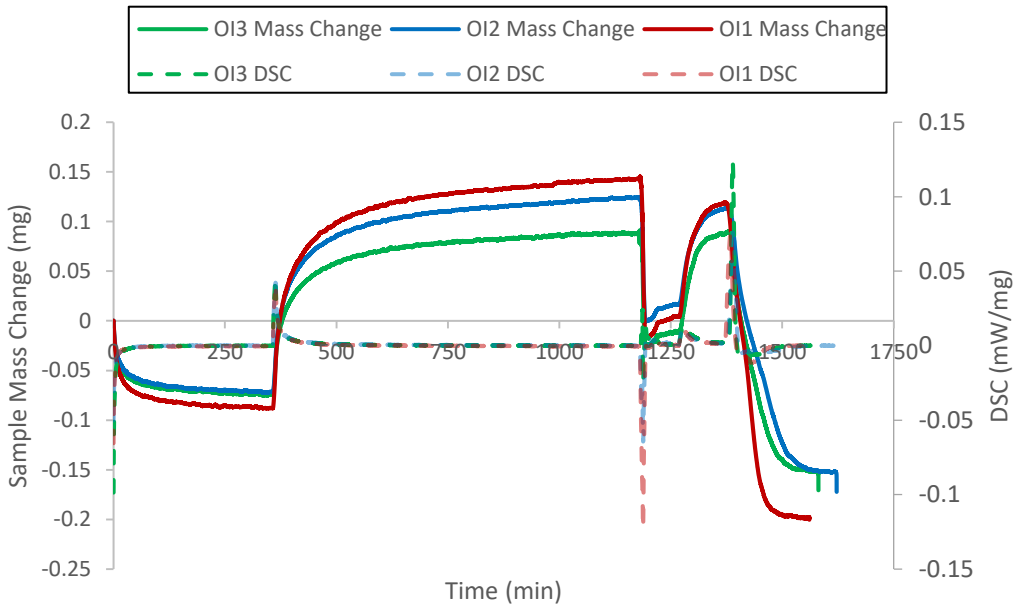

Figure 9-15: Corrected, smoothed STA results for outside-in directional crystallization trials OI1, OI2, and OI3. All trials had the same experimental conditions as detailed in section 5.4.3.

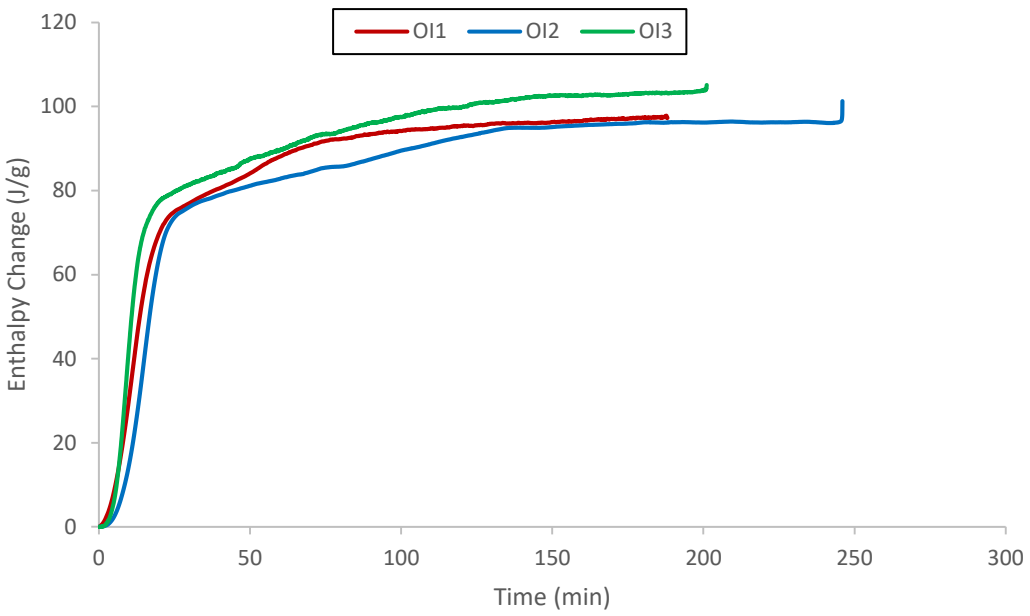

Figure 9-16: Calculated enthalpy evolution results for outside-in directional crystallization trials OI1, OI2, and OI3. All trials had the same experimental conditions as detailed in section 5.4.2.

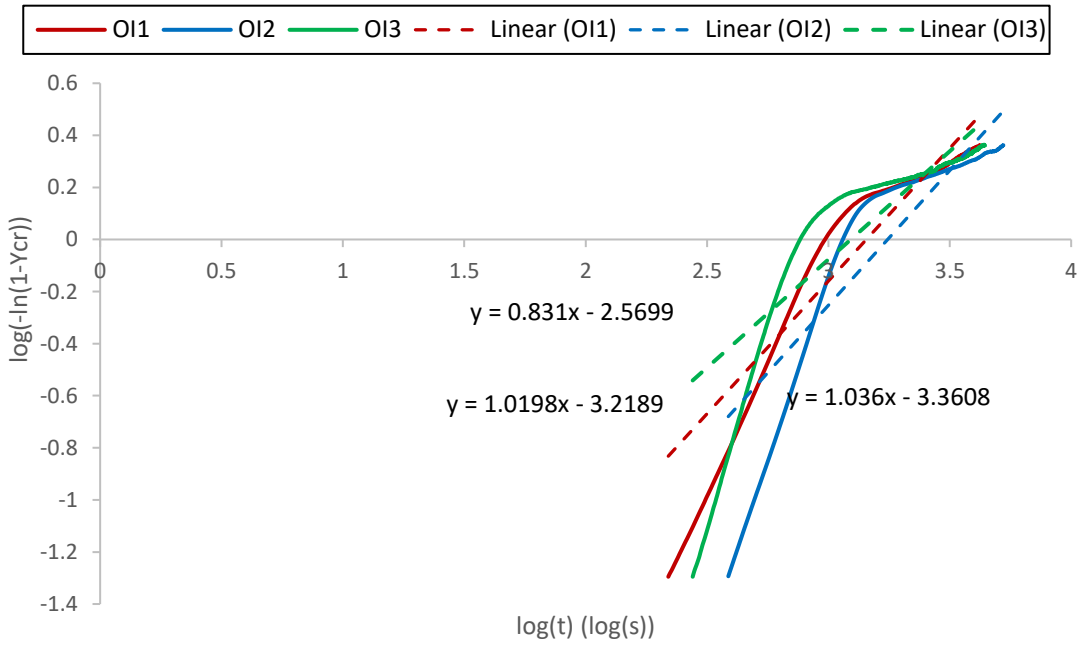

Figure 9-17: Avrami fitting plots for outside-in directional crystallization trials OI1, OI2, and OI3. All trials had the same experimental conditions as detailed in section 5.4.2.

9.4.2 A-Test Results

Shown below are the raw STA results used to estimate the remaining amorphous content of the samples following moisture release and XRD analysis.

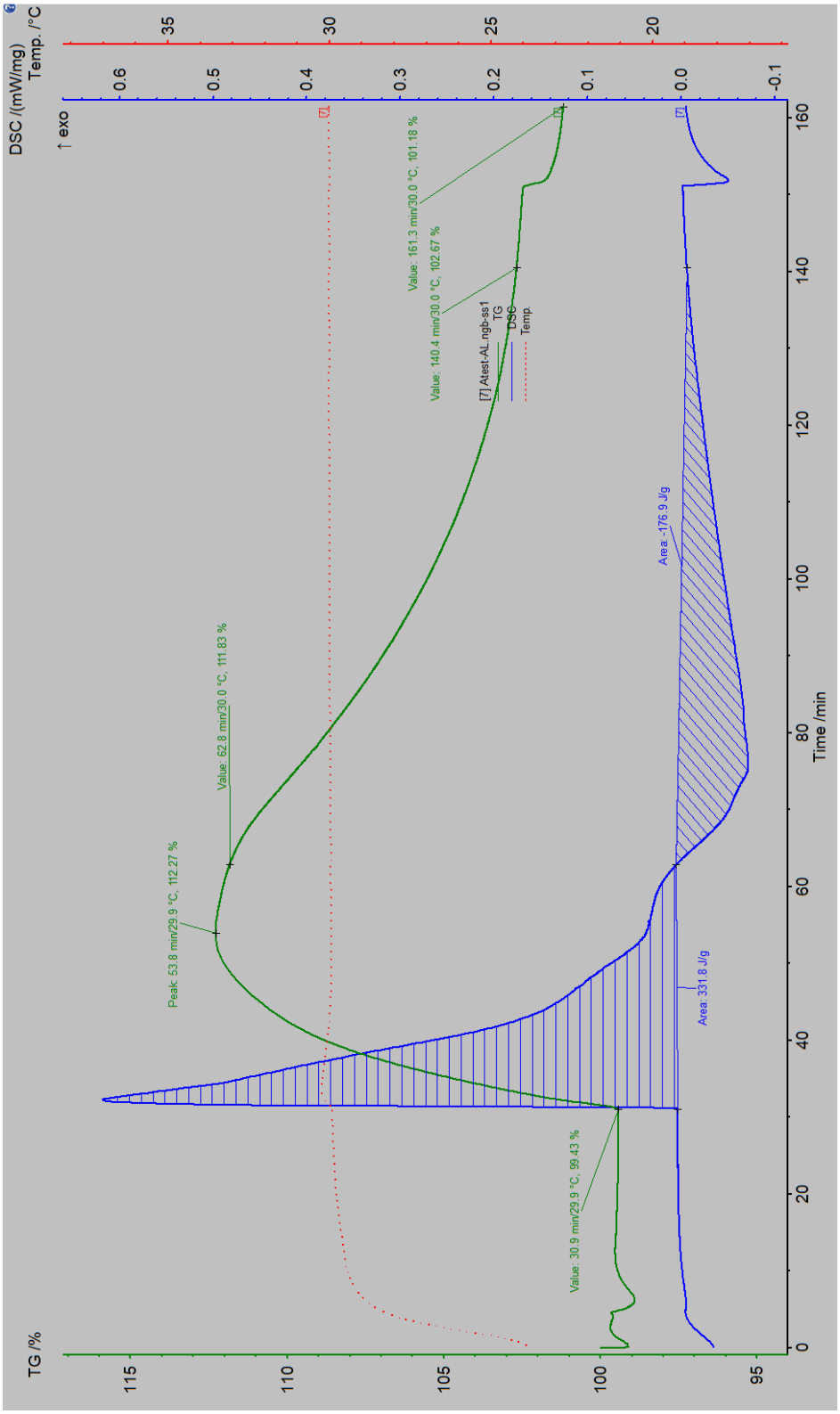

Figure 9-18: Uncorrected STA amorphous determination trial for spray-dried amorphous lactose sample

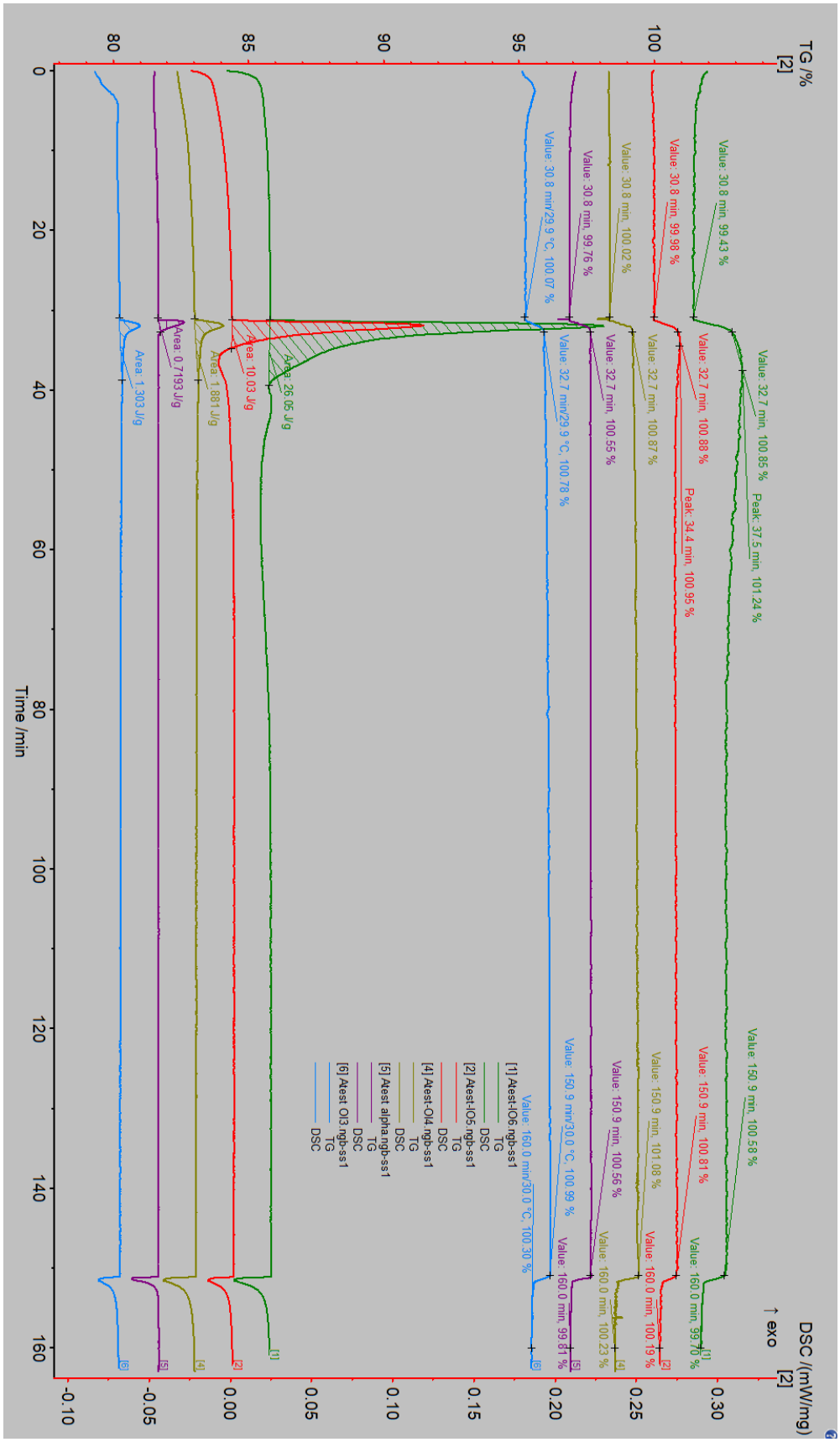

Figure 9-19: Uncorrected STA amorphous determination trial for all samples and α-lactose monohydrate

9.4.3 XRD Results

Below are some of the reference patterns used for the XRD analysis these consist of a literature pattern displayed with one obtained experimentally using the same compound.

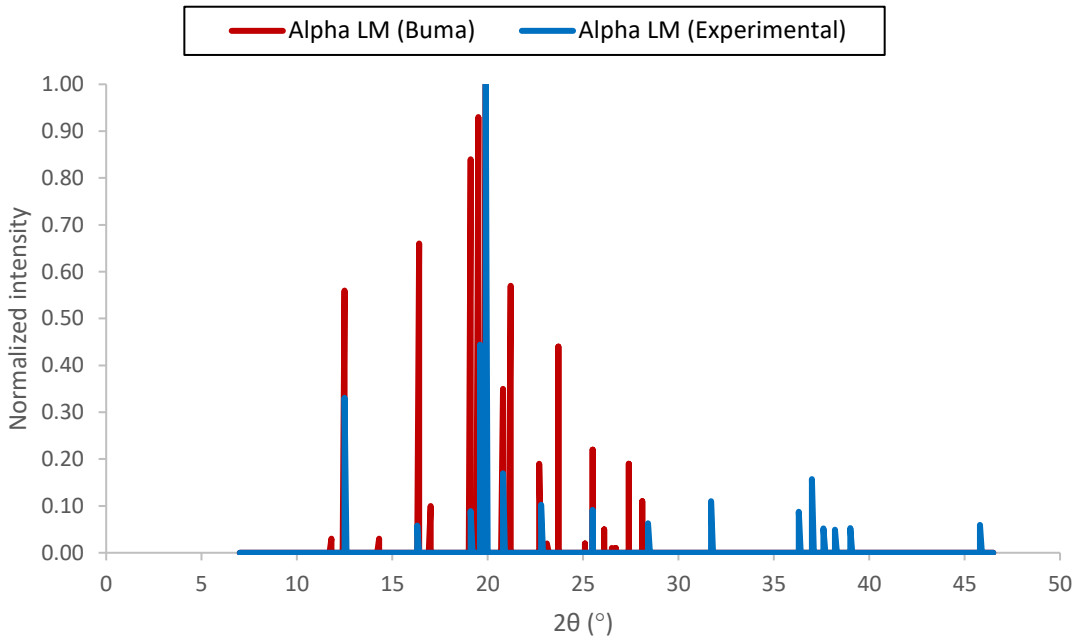

Figure 9-20: Experimental XRPD pattern for pharmaceutical grade α-lactose monohydrate alongside pattern published in (Buma & Wiegers, 1967).

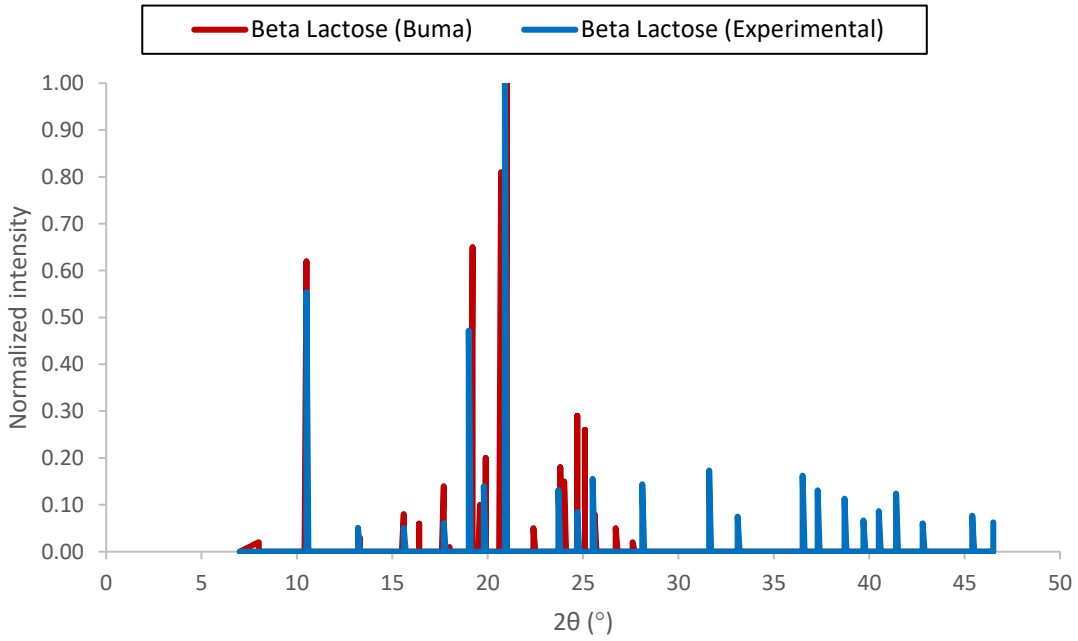

Figure 9-21: Experimental XRPD pattern for laboratory grade β-lactose alongside pattern published in (Buma & Wiegers, 1967).